STUDIES ON PHYSICO-CHEMICAL CHARACTERISTICS OF SELECTED CATIONIC DYES AND THEIR INTERACTIONS WITH SMECTITE AND ZEOLITE

THESIS SUBMITTED FOR THE DEGREE OF
DOCTOR OF PHILOSOPHY (SCIENCE)
OF THE
UNIVERSITY OF NORTH BENGAL
1996

[illegible]
University Library
[illegible]

By
SHAMSUZZAMAN AHMED, M. Sc.

DEPARTMENT OF CHEMISTRY
UNIVERSITY OF NORTH BENGAL
DARJEELING, WEST BENGAL
INDIA

ST - VERF

Ref.
547.3412
S 528/s

116651

23 JUN 1997

STOCK TAKING - 2011

-: ACKNOWLEDGEMENT :-

I take this opportunity to express my heartfelt gratitude to my supervisor Dr. S.K. Saha, Senior lecturer in Chemistry, University of North Bengal for his active and valuable guidance, continued interest and incessant encouragement throughout the entire period of work .

I thankfully acknowledge the award of a teacher fellowship by the University Grant Commission, New Delhi, for completion of this work and appreciate the authority of the University of North Bengal for extending the required laboratory and other facilities.

I extend my sincere thanks and gratitude to Dr. T.Kurucsev, Department of Chemistry , University of South Australia, for providing the FORTRAN version of non-linear least square program DATAFIT and generous help in analysing some spectroscopic data. Thanks are also due to Dr. J.L.Dye, Department of Chemistry, Michigun State University, USA, for sending his well known general non-linear weighted least square program KINFIT on request and to Dr.T.D. Smith, Department of Chemistry, Monas University, Australia, for the gift sample ZSM-5 used in this study.

The co-operation and help from the Head of the department, teachers, officers, research fellows and other staff members of

the Department of Chemistry, University of North Bengal, are thankfully acknowledged. I am thankful to Palas Bera, Senior Research Fellow of this laboratory, for his good gesture and generous help. Thanks are also due to Dr.S.Pal and R.Adhikary for their kind cooperation.

I express my best regards to my parents for their ceaseless blessings and thanks to my younger brothers and other family members for their inspiration. Finally, I would like to thank my wife, Seri, for her constant encouragement and moral support under all circumstances.

Shamsuzzaman Ahmed

(SHAMSUZZAMAN AHMED)

Department of Chemistry,
University of North Bengal
Darjeeling ; West Bengal
India

-: CONTENTS :-

		PAGE
	: ACKNOWLEDGEMENT	I
	: CONTENTS	III
CHAPTER 1	: INTRODUCTION	1
CHAPTER 2	: SCOPE AND OBJECT	15
CHAPTER 3	: STUDIES ON AGGREGATION OF DYES IN AQUEOUS AND AQUEOUS - ETHANOLIC MEDIA	20
SECTION		
3.1.1.	: INTRODUCTION AND REVIEW OF THE PREVIOUS WORK	20
3.1.2.	: THE MOLECULAR EXCITON MODEL	27
3.1.3.	: SPECTRAL PROPERTIES OF DIMER IN TERMS OF EXCITON THEORY	40
3.1.4.	: VIBRONIC EXCITON MODEL	44
3.2.	: EXPERIMENTAL	51
3.3.	: RESULTS AND DISCUSSION	54
3.3.1.	: STUDIES ON MONOMER-DIMER EQUILIBRIA OF THE DYES	54
3.3.2.	: ANALYSIS OF DIMER SPECTRA IN TERMS OF MOLECULAR EXCITON MODEL	87
3.3.3.	: ANALYSIS OF DIMER SPECTRA IN TERMS OF VIBRONIC EXCITON MODEL	95

PAGE

CHAPTER 4 : ELECTROCHEMICAL STUDIES OF THE DYES ON CLEAN AND MODIFIED ELECTRODES 101

SECTION

4.1. : INTRODUCTION AND REVIEW OF THE PREVIOUS WORK 101

4.2. : EXPERIMENTAL 111

4.3. : RESULTS AND DISCUSSION 113

4.3.1. : ELECTROCHEMICAL STUDIES ON CLEAN ELECTRODE 113

4.3.2. : ELECTROCHEMICAL STUDIES ON MODIFIED ELECTRODE 131

4.3.3. : STUDIES ON THE HOMOGENEOUS REACTIONS OF THE LEUCODYES WITH Fe(III) IONS : CATALYTIC REGENERATION MECHANISM 139

CHAPTER 5 : INTERACTION OF DYES WITH MONTMORILLONITE AND ZEOLITE (ZSM-5) : SORPTION AND METACHROMASY 148

SECTION		PAGE
5.1.	: INTRODUCTION AND REVIEW OF THE PREVIOUS WORK	148
5.2.	: EXPERIMENTAL	164
5.3.	: RESULTS AND DISCUSSION	166
5.3.1.	: STUDIES ON SORPTION	166
5.3.2.	: STUDIES ON METACHROMASY	170

CHAPTER 6 : SUMMARY AND CONCLUSIONS 175

REFERENCES 186

CHAPTER 1

INTRODUCTION:

In recent years there has been an increasing interest in systems which enable the conversion of solar energy into electrical or chemical energy (1-4). Many types of systems have been proposed and studied experimentally, the fundamentals of which extend from solid state physics to photo-electrochemistry. For most of the systems considered excitation of an electron by absorption of a photon is followed by charge separation at an interface. It follows that the different fields involved (photovoltaics, photo-electrochemistry, photogalvanics, etc.) have several essential aspects in common. Although photo-electrochemical studies commenced with the observation of Becquerel (5) in 1839, the mechanism of photovoltage generation in photosensitive electrode / electrolyte systems are still at an early stage of development.

A mumber of analyses of the general thermodynamic and kinetic aspects of the electrical output of photogalvanic cells (PG) have been published (6,7). It is inconvenient to separate such analyses completely from devices specifies. After the discovery over sixty years ago (8,9) that thionine is reversibly photoreduced by Fe^{+2} in acidic aqueous solution, Robinowitch (10) explored the possibility of utilizing the system in the construction of a photogalvanic cell for the solar energy conversion. In the "primitive beaker" cell the electrodes are

identical with one illuminated and the other in the dark. The open circuit voltage is ideally the difference in the reversible potentials at the two electrodes. For the iron-thionine system, the concentration of the leuco-thionine is negligible at the dark electrode so that the exchange current is determined entirely by the iron couple. The potential at the dark electrode is given by the Nerst expression,

$$E_{dark} = E^{\emptyset}_{Fe} + 0.058 \log ([\ Fe^{+3}\ ]/\ [\ Fe^{+2}\ ])_{dark} \qquad (1)$$

Where $E^{\emptyset}_{Fe}$ is the standard reduction potential of the $[Fe^{+3}]/[Fe^{+2}]$ couple and the terms in the square brackets represents the activities of the species. The potential at the illuminated electrode is a complex function and depends on the concentrations of all the redox species at the electrode (11). The expression for this potential can be simplified for an ideal electrode by assuming that the electron transfer rate constants for all the redox species are the same and further simplified by assuming that the photostationary concentration of the half reduced dye, semithionine, is negligible. The result is equation 2, where f = F/RT, F is the faraday in columbs, E_{light} is the potential of the illuminated electrode, $E^{\emptyset}_{Fe}$ is the standard reduction potential of the $Fe^{+3}/\ Fe^{+2}$ couple.

$2Fe^{+2} + 2H^{+} +$ 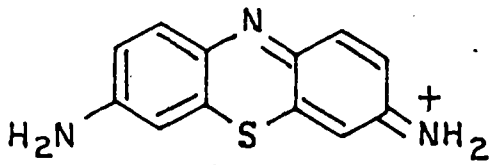 $\underset{\text{dark}}{\overset{h\nu}{\rightleftharpoons}}$

Thionine, T

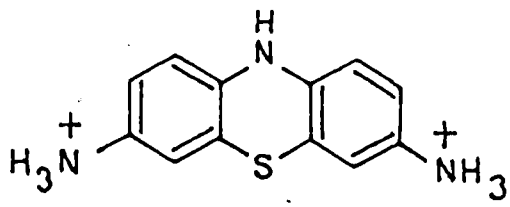 $+ 2Fe^{+3}$

Leucothionine, L

$+$ 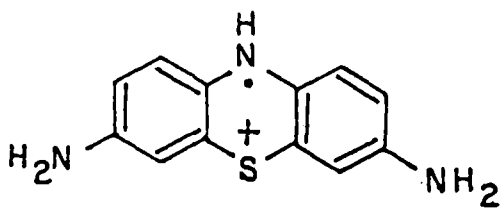

Semithionine, S

$E^{\emptyset}_{T \rightarrow S}$ is the standard potential for the one electron reduction of thionine, and $E^{\emptyset}_{S \rightarrow L}$ is the standard potential for the one electron reduction of the semithionine. The terms in the square brackets represent the activities of the various species in the photostationary state.

$$\exp(fE_{light}) = \frac{[Fe^{+3}]\ \exp(fE^{\emptyset}_{Fe/2}) + 2[T]\ \exp(fE^{\emptyset}_{T \rightarrow S}/2)}{[Fe^{+2}]\ \exp(-fE^{\emptyset}_{Fe/2}) + 2[L]\ \exp(-fE^{\emptyset}_{T \rightarrow S}/2)} \qquad (2)$$

The potential of the PG cell under the open circuit

photostationary condition is equal to the $E_{dark} - E_{light}$ as calculated from equation 1 and 2. The current produced by such PG cell with ideally reversible electrodes depends on the composition of the bulk solution in the photostationary state under the short circuit or the other conditions of current withdrawal and on the rate of diffusion of charge carriers to the electrodes. This current is related to various system parameters by equation 3, where n is the number of redox equivalents per mole of a given charge carrier, F is the Faraday,

$$i = nFADC/\delta \qquad (3)$$

A is the electrode area, D is the diffusion coefficient of a given charge carrier, C is the concentration of given chagre carrier in bulk solution under photostationary conditions and δ is the thickness of the diffusion layer. The crucial figure of merit in evaluating the efficiency of solar energy conversion is sun light engineering efficiencies (S.E.E) as defined in equation 4, for conversion to electrical power or energy

$$S.E.E. = \frac{\text{Electrical power or energy delivered to load}}{\text{Incident Sun light power or energy}} \times 100 \qquad (4)$$

The totally illuminated thin layer (TI-TL) PG cell was first

described by Clark and Eckert (12) and a number of stydies of the behaviour of the iron-thionine (11, 13-18) photoredox system in such cells have been reported. In TI-TL cells, atleast one electrode is selective; ideally, a selective electrode completely blocks one redox couple while it is completely reversible to the other. Greatest efficiency would be achieved with TI-TL cell in which each electrode was perfectly selective for a different couple . Unfortunately, in homogeneous solution, thermal back reaction of electron transfer also takes place. This dissipation of free energy constitutes a considerable problem in the use of iron-thionine cell for practical purposes. However, the following reaction scheme adequately summerizes the whole process, including the relevant recombination reaction :

Solution :

$$\text{Thionine (A)} + \text{Fe(II) (Z)} \rightleftharpoons \text{Leucothionine (B)} + \text{Fe(III) (Y)}$$

Photochemistry :

$$\text{Thionine (A)} \xrightarrow{h\nu} \text{Semithionine (A*)}$$

$$\text{Semithionine (A*)} + \text{Fe(II) (Z)} \longrightarrow \text{Leucothionine (B)} + \text{Fe(III) (Y)}$$

Electrochemistry :

At the illuminated electrode :

$$\text{Leucothionine (B)} - e \longrightarrow \text{Thionine (A)}$$

At the dark electrode :

$$\text{Fe(III) (Y)} + e \longrightarrow \text{Fe(II) (Z)}$$

For an efficient cell it is obvious that one must avoid the thermal back reaction of B and Y. Hence one of the problems with this type of device is that the honmogeneous kinetics may destroy the energetic species B and Y. A crucial requirement for the PG cell is that the illuminated electrode should be selective. If the illuminated electrode is not selective between B and Y then we will have

$$B \pm e \longrightarrow A$$

and

$$Y \pm e \longrightarrow Z$$

$$B + Y \longrightarrow A + Z$$

The beastly electrode is merely an efficient catalyst for the back reaction.

The Electrode Kinetics :

At the illuminated electrode, we need the A,B couple to be reversible so that B is easily converted to A, but we also require that, as far as possible, the conversion of Y to Z is blocked. The electrode will then be close to the standard electrode potential of the A,B couple, $E_{A,B}$. Very little B reaches the dark electrode because the illuminated electrode is close to the region where B is generated as opposed to the dark electrode being far away. This means that the dark electrode has merely to convert the photo-generated Y back to Z at a potential close to the standard electrode potential of the Y,Z couple, $E_{Y,Z}$. In fact if there is little concentration polarization , and if the Y,Z couple is reversible, the dark electrode potential will shift very little when the cell is illuminated. The change in voltage on illumination occurs at the illuminated electrode from the many fold increase in the concentration of B.

The problem with thionine as a constituent of a photogavanic cell is that although its kinetics of reaction has a satisfactory value, its solubility is far too low to achieve an optimum result. Thus it is impossible , using thionine, to achieve the necessary optimum conditions. Attempts have been made to overcome these problems using non-aqueous organic solvents. Even so, the solubility is not sufficient. Various substitution in the thionine molecule may increase the solubility to a great extent. Moreover,

there is another problem that thionine forms dimers and higher aggregates at concentration above 10^{-5} M. These dimers are inactive from the point of view of the photoredox system, the energy is lost by internal quenching in the dimer.

Self Quenching :

A problem with increasing concentration of the dye is that there may be self quenching of thionine* by thionine . Moreover, dimer and higher aggregates of the dye are shown to undergo efficient internal quenching. As a result, absorption of light by ground state thionine dimer resulted in little, if any, transduction to electricity in a totally illuminated thin layer acidic iron- thionine cell with water as solvent and with a 1.2×10^{-3}M stoichiometric concentration of thionine (19). Thus, the most effective materials for use as solar harvesters will be those that absorb strongly in the visible and near UV region of the spectrum. Even if all the other characteristics of photogalvanic cells employing thionine were perfectly efficient, such cells would be limited by the fraction of the solar output absorbed by the solution. It is, therefore, necessary to improve the absorption characteristics of the medium as well. Molecular modification of thionine to methylene blue results in a substantial shift of λ_{max} from 595 nm to 660 nm ($\epsilon_{thionine} = 6.16\times10^{4}$, $\epsilon_{methyleneblue} = 7.2\times10^{4}M^{-1}Cm^{-1}$) (chapter 3)

In most cases, the intense visible absorption bands and those further to the blue are separated by region of significantly lower absorbance. In order to utilize those solar photons, sensitizers can be employed to absorb light and transfer energy from the excited state of the sensitizer to the photochemically active species. The requirement is for the energy of the excited state of the donor to be higher than the energy required to reach the populated excited state of the acceptor.

Electrode Selectivity :

We now turn from the processes occuring in the bulk of the solution to the kinetics of the eletrode reactions. Regardless of the type of the ptotogalvanic cell, efficient electron transfer must occur between photochemically generated separate charge carriers and appropriate elctrodes.

If practical photogalvanic cells are ever achived, it appears likely that electrodes selective to particular redox couples will be employed. Selectivity is not, however, the only requirement. In addition, the electrode must not catalize back reaction of charge carriers on its surface. Such back reaction is equivalent to shorting a circuit in parallel with load. It is vital that the illuminated electrode should discriminate between the photogenerated products, B and Y (page.6) in general, or in

particular leucothionine and Fe (III). Thus, in the PG cells the selective electrodes separate both B and Y and prevent their recombination. That is why, it is a vital part of the cell. For example, the SnO_2 electrode is more selective to the thionine / leucothionine couple rather than the Fe^{+3}/Fe^{+2}couple, as shown by Clark and Eckert (12). Investigations, with different carbon materials as light electrodes have also shown that although the leucothionine oxidation is fast on all types of carbon materials (reticulated vitreous carbon, carbon paste, glassy carbon, pyrolytic graphite and carbon cloth), the Fe^{+3}/ Fe^{+2} electron transfer is slow (20). Electrode modification is another approach. Albery and coworkers (21) have found that Pt and SnO_2 electrodes modified with coatings of thionine of upto 20 monolayers could discriminate between photogenerated leucothionine and Fe^{+3} and hence are suitable for an iron-thionine PG cell. Murthy and Reddy (22) have shown that poly pyrrole modified elctrodes are more selective to Fe^{+3}/ Fe^{+2} rather than to thionine/leucothionine couple. Moreover, molecular modification of thionine must also affect the thermal back reaction to a great extent. The rate constants for the methylene blue system are always larger than those for the thionine system and the PG outputs for the Fe^{+2}-methylene blue system are less than those from the Fe^{+2}-thionine system. The additon of Triton X-100 micelles also suppressed the back reactions increasing the power of the cell by a factor of five (20).

Dye Incorporated Modified Electrode :

Not satisfied with electrode surfaces that passively accept or provide electrons or content with elctrode surfaces that actively accelerate or hinder certain elctron transfer reactions chemists in the last 20 years have turned to designing chemical structures on electrode surfaces that redefine the chemical and physical microenvironment in which heterogeneous electron transfer reactions occur (23). Inherent in many inorganic materials (e.g. clay, zeolite etc.) are pores, channels, or layer spacings of molecular dimensions. These molecular gateways impart a selective screen, so that differentiation results on the basis of molecular size or shapes of solutes. Further discrimination arises if fixed charged sites are part of the inorganic lattice, producing an ionic filter as well. In these senses, the inorganic layer can "act" as a passive discriminator, allowing, e.g., preconcentration of an analyte or reactant (24).

Kamat (25) successfully incorporated thionine in the clay films cast on SnO_2 and Pt electrodes. Though the sunlight engneering efficiency of the PG cell employing thionine incorporated clay modified electrode in the present case was very poor (10^{-4}%), such a modified electrode possesses several attractive features :

(i) a high concentration of the photoactive dye species can be achieved at the electrode surface.

(ii) because of the small thickness of the film, the incident photons are efficiently absorbed by the dye molecules present near the electrode surface.

If the electrochemical experiment is carried out at a modified electrode, the area of the conductive channel can play an important role in defining the type of diffusion behaviour observed. For example, all the parameters accessible to the electrochemist depend upon the competitive exchange reaction as shown for a trivalent/monovalent exchange reaction.

$$A^{3+} + 3\ NaX = A^{3+}X_3 + 3\ Na^{+} \qquad (5)$$

Where A^{+3} is an exchanging trivalent species, NaX is a single clay (smectite) site containing a Na^{+} counter ion, and $A^{3+}X_3$ is the clay exchanged with trivalent species. The selectivity coefficient for the exchange is,

$$K_{III} = [\ Na^{+}]^3\ [\ Al^{3+}\ X_3\ ]\ /\ [\ A^{3+}]\ [\ NaX\ ]^3 \qquad (6)$$

The magnitude of the diffusion coefficient D is directly dependent on the distance (d) between equilibrium sites, and exponentially dependent on -E/RT, where E is the activation energy necessary to leave the equilibrium site (26). E is related to K_{III}, or analogously, to K_{II}, for a divalent species. As the energy of interaction between a site and an intercalated molecule

increases, the diffusion coefficient diminishes. Also, as the number of sites increases the distance between the sites decreases, so that the distance travelled in any one "hop" is small and the observed diffusion coefficient decreases. The magnitude of concentration C, in modified layer, and formal potential $E^{\emptyset}$, for any bathing solution are also determined by the value of the selectivity coefficient. Finally, cobining expressions for divalent and trivalent exchange with the Nerst equation yield an expression for the shift (ΔE) in the observed formal potential in the film ($E^{\emptyset}_{app}$) with respect to the solution formal potential ($E^{\emptyset}_{solution}$) of the couple

$$\Delta E = E^{\emptyset}_{app} - E^{\emptyset}_{solution}$$

$$= (RT/nF) \ln (K_{II}/K_{III}) [NaCl]) + (RT/nF) \ln C_{Na} \qquad (7)$$

where, [NaCl] is the number of exchange sites occupied by the Na^+ and C_{Na} is the analytical concentration of Na^+, which approximates the equilibrium concentration of Na^+ if the bulk solution volume is large with respect to the volume of the film on the surface of the electrode. If the clay modified electrode is exposed to a solution containing only the Na^+ electrolyte and a trivalent exchanging complex, the potential shifts positive as a function of the analytical concentration of the trivalent complex, and the total number of exchange sites, if C_{Na} is

constant. The shift in potential is a function of the magnitude of the trivalent / Na^+ exchange constant.

The preliminary study of the clay modified electrode has indicated the feasibility of dye incorporated clay films in the photogalvanic conversion of light enrgy into electricity. Recent reviews on the material science aspects of zeolites and the use of clays and zeolites to coat electrodes have included the discussions on the use of and interest in zeolite layers on electrodes too. However, better understanding of the interaction between the dye and both clay and zeolite is necessary in order to improve their performances viz, PG transducers (25)

116651

23 JUN 1997

University Library

CHAPTER 2

SCOPE AND OBJECT :

During the last few years, there has been an increasing awareness of the importance of photochemical and electrochemical effects of dyes due to their interesting role in solar energy conversion and for providing convenient means of probing electrodic processes. It is commonly believed that the primary processes which lead to photovoltage generation in a photogalvanic (PG) cell do not occur at the electrode electrolyte interface, but are results of photochemical reactions in the bulk of the solution, which are followed by the diffusion of electrodically active photoproducts to the electrode surface where electron transfer takes place. Knowledge of the association properties of the photogalvanic solution is thus important because the aggregates produce greater reabsorption and quenching, decreasing quantum yield and residence time of the first singlet excited state of the dye. The electrochemical rate constant, mass transfer etc. of PG cell are important because they precisely determine whether the species are likely to react on the electrode or lost by diffusing away or reacting in the bulk of the solution. Since thionine is known to be photoreduced reversibly by Fe(II) ions in acidic aqueous solution, many workers have been trying to explore the possibilities of utilizing the system in the construction of PG cell for solar

The efficiency of such a cell is, however, severely influenced by the degree of solubilities of the dye. Various alkyl substitutions in thionine seem to influence not only the solubilities but also certain physicochemical properties which in turn must influence the phenomena occuring in the cell. Since above system is most successful to date for solar energy conversion, almost all the previous workers emphasized that aggregation properties, mass transfer processes, and electrode kinetics must be studied separately in order to understand the factors that limit the performance of the cell. Keeping these in view the object of the present study has been chosen.

Progressively alkylated thiazine dyes, viz.,thionine, azure C (monomethyl thionine), azure A (dimethyl thionine), azure B (trimethyl thionine) and methylene blue (tetramethyl thionine) have been selected for the present study. Self aggregation of these dyes have been investigated in aqueous and aqueous-ethanolic solution of various compositions. The systematic study of the aggregation characteristics of dyes from spectroscopic data is also useful for other important aspects too e.g., its possible application in understanding phenomena such as energy transfer in biological systems, metachromasia, hypochromism, conformation of polypeptides and staining properties of dyes for biological specimens. Structural aspects of progressively alkylated thiazine dye aggregates are also studied. The interpretation of the absoption spectra by means of exciton theory allows the determination of the

geometrical disposition of the monomers in all the aggregates. From the changes produced by the dimerization process on some thermodynamic functions, the nature of bonding in the aggregates has also been investigated.

Another aspect covering the present investigation is the electrochemical study which includes redox behaviour of the thiazine dyes at stationary elèctrode surface in cyclic voltammetry, mechanism of electrode processes and heterogeneous rate constant of electron transfer at the elctrodes. Dissipation of free energy due to thermal back reaction of electron transfer in a PG cell constitutes a major problem in the use of Fe(II)/ thionine system for any practical purposes. In view of these an electrochemical technique has been adopted to study thermal back reaction of progressively alkylated thiazine leucodyes with Fe(III) ions. Effect of hydrophobic interaction, if any, in such a reaction will also be examined.

Moreover, electrode surface modified with clay minerals possesses several attractive features: a high concentration of the photoactive dye species can be achieved at the elctrode surface and due to the small thickness of the film, the incident light is efficiently absorbed by the dye molecule, present near the electrode. Pores, channels and interlayer spacing of molecular dimensions in clay minerals and zeolites can form molecular gateways which impart a selective screen so that differentiation results on the basis of molecular sizes and

shapes of the solutes. Differential electrode kinetics at two electrodes is another way of differentiation among various species in PG cell. Such discrimination is crucial because otherwise reverse electron transfer often takes place causing dissipation of energy as already mentioned. A preliminary work has been undertaken on the electrochemical characteristics of the five thiazine dyes at the smectite (montmorillonite) and zeolite (ZSM-5) modified elctrode using cyclic voltammetric technique.

If the electrochemical experiment is carried out at a modified layer, the same relationships as those of a clean bare elctrode hold, except that the area of the conductive channel can now play an important role in defining the type of diffusion behaviour observed. Experiment in the situation can be considered to be a normal electrochemical experiment with a new medium. All parameters accessible to the electrochemist would depend precisely upon the competitive exchange reaction of dye and counter ion. Selectivity coefficients of various ions toward clay minerals explain the above phenomena quantitatively and also influence tha extent of dye loading process from an equilibrium solution. Therefore, a chapter of the present thesis contains the study of physicochemical aspects of ion exchange equilibria of the five thiazine dyes onto the montmorillonite and zeolite exchanger in fundamental detail not only because of their involvement in the electrochemistry of clay and zeolite modified electrode but also with a view of deriving some insight into the factors that govern and influence the ion

exchange process, in general. Moreover, adsoption of dyes by clay minerals often results in significant spectral changes, specially in the electronic spectrum. Little is known, however, about the adsorption interactions which cause these alterations. There is much controversy about the origin of this metachromasy as to whether this is due to the aggregation of the dye in layered space or due to π electron interaction between the oxygen planes of montmorillonite and the aromatic ring of the dye. To understand the nature of interaction of the dye molecules with montmorillonite and zeolite (ZSM-5) in further detail the present study has been extended to the investigation of metachromasy of the five thiazine dyes by clay minerals. It may be mentioned that being structurally similar with like charge delocalization and chemical properties, present dyes differ from each other only in molecular weight and alkyl substitution. This fact provides an excellent opportunity for studying the effect of molecular size on the adsorption of the dye and metachromasy phenomena.

CHAPTER 3

STUDIES ON AGGREGATION OF DYES IN AQUEOUS AND AQUEOUS-ETHANOLIC MEDIA

3.1.1. INTRODUCTION AND REVIEW OF THE PREVIOUS WORK :

Spectral changes on increasing concentration of an aqueous solution of many dyes which have large planar hydrophobic skeleton with hydrophilic substituents have been known for a long time (27). It is now well accepted that these spectral changes are mainly due to the aggregation of such molecules. Aggregation can bring about drastic changes in physical and chemical properties of the dyes specially their photophysics. The photophysics and photochemistry of dyes in general are of considerable interest in the appreciation of various phenomena such as fluorescence, phosphorescence, long range and short range excitation energy transfer and electron transfer and other modes of quenching, as probes for liquid structure in mixed solvents and various relaxation process in solution (28). Certain concentration effect is also observed during the study of photochemical and photoelectrochemical properties of the thiazine dyes, which leads one to enquire into the molecular states of these dyes in solution (29).

The strength of dye aggregation is strongly dependent on the structure of the dye molecules, nature of the solvent and temperature. A number of physical descriptions of this phenomenon have been proposed to account for the changes in the dye specrtum

but none is found to be superior than others. In this chapter attempts have been made to understand the nature of dye-dye aggregation, the effect of progressive alkylation of dye molecule and the solvent polarity on aggregation, the type of interaction in terms of exciton theory, the probable structure of the dye aggregates and the thermodynamics of dye aggregation in aqueous and aqueous-ethanolic media.

Formation Constant and Thermodynamics of Aggregation of Dyes :

Most of the basic dyes in solution show deviations from the Beer's law at higher concentrations. This behaviour has been attributed to the formation of dimers and higher aggregates of the dyes (30,32,33). In general, the dimerization constants are in the range of 100-10000, corresponding to free energies $\sim$ 8-22KJ mol^{-1}. These are of the order of the magnitude of formation of hydrogen bonds (34), as well as, of other types of interactions such as hydrophobic (35,36), vander waals or π-π interactions dispersion forces (31,36), all of which are presumed to be present when dyes undergo self aggregation in solution. Remarkable changes in the spectral characteristics with increasing concentrations, and the effect of temperature on this have been studied to unravel the nature of the forces involved in dye aggregation. Aggregates of the above type, are also formed at lower concentration in the presence of some natural or synthetic

polymers (37,38) or polyelectrolytes (39,40). In these cases the equilibrium constants are, atleast, a factor 10 higher, so that aggregation can be observed at concentration which are well behaved in the absence of the additives (41). Bergman and O'Konski (42) described a spectroscopic study of methylene blue sorbed on Na-bentonite. Spectral changes were found to follow changes in the amount of methylene blue sorbed on the clay surface. Due to the fact that these changes are similar to the specrtal shifts accompanying dimerization and polymerization of MB in aqueous solution, these shift also attributed to dye-dye interaction on the surface of the montmorillonite and the corresponding dimer dissociation constant was determined as 1.7×10^{-4} mol lit^{-1} at 25^{0}C. West and Pearce (43) examined the dimeric state of cyanine dyes and showed that the stability of the dimers, as measured by the free energy of dimerization, increase steadily with chain length. Authors showed that if a solution in which 95% of the dye is present as monomer is regarded as tolerable approximation to a solution of the pure monomer, the concentration at which this conditions prevailed was found to vary from 2.8×10^{-5} (for $K = 10^{-3}$) to 2.8×10^{-8}M (for $K = 10^{-6}$)

Baranova and levshin reported that rhodamine 6G forms aggregates upto dimerization stage at concentration below 2×10^{-3} M, but higher aggregates are formed at higher concentration (44). The change in the spectrum of an aqueous solution of 3,6 diamino

acridine dye with the increase in concentration was not very large, reliable results could not be obtained by Mataga (45). However, the degree of aggregation and log K_n were determined by means of Zanker's method (46). Hida and sanuki opined that the maximum slope method for evaluating dimerization parameters was more reliable over some other methods (47) viz. Zanker's method. These authors also found the dependence of dimerization constants of a number of dyes in neutral salt concentrations. In 1972, Selwyn and Steinfeld persented a very convincing and detailed account of the absoption spectra of laser active dyes rhodamine B, rhodamine 6G and acridine red in aqueous, ethanolic and EPA (2 parts ethanol: 5 parts isopentane: 5 parts ethylether by volume) solutions as a function of concentration and temperature (48). The observed absorbance of the aqueous solutions of rhodamine B and rhodamine 6G was analysed in terms of a monomer-dimer equilibrium. The dissociation constants, $K = C^2_{monomer}/C_{dimer}$ were 6.8×10^{-4} and 5.9×10^{-4} mol/lit. at 22^0C for aqueous rhodamine B and rhodamine 6G solutions respectively. The absorption spectra of pure monomer and dimer were obtained for these two systems. Acridine red in H_2O was shown to be monomeric upto 3.38×10^{-5} M. Rhodamine B in ethanol formed dimers for which the equilibrium constant for dissociation was 1.1×10^{-4} mol/lit. at 62^0C and 4.9×10^{-5} mol/lit at 22^0C. Calculation of the thermodynamic function for the process gives $\Delta H \cong 16.8$ KJ/mol and $\Delta S_{315}^0 \cong -6$ eu. At -78.5^0C higher aggregates are formed in ethanolic

rhodamine B solutions but rhodamine 6G solutions ($2x10^{-4}$ M) show no evidence for the formation of aggregates in ethanol, even at -78.5^{0}C. Small amount of dimer were noted in acridine red-ethanol solution under the same conditions. Solutions of rhodamine B in EPA are totally dimeric at -196^{0}C. At 22^{0}C the equilibrium constant was $6.2x10^{-5}$ mol/lit.; at -78.5^{0}C it was $3.1x10^{-5}$mol/lit. The low value of ΔH (3.36 KJ/mol) in this solvent gives a strong support to the hypothesis that hydrogen bonding is important in dimer formation. Rhodamine 6G-EPA failed to aggregate even when cooled to -196^{0}C. Acridine red-EPA is predominantly monomeric at 22^{0}C; at -78.5^{0}C an equilibrium constant for the dissociation of dimer of $4.4x10^{-4}$ mol/lit. was calculated. James and Robinson studied the self-aggregation of N(10) alkyl derivative of acridine orange and their interactions with cationic and anionic surfactants (49). The dimerization of the dyes in aqueous solution was enhanched relative to acridine orange when the alkyl substituent has more than six carbon atoms. A temperature jump study of the dimerization equilibrium of the octyl and dodecyl derivatives shows the greater stability of the dimer which is reflected in lower rate constant for dissociation. This study further shows a variation of dimerization constant of acridine orange derivatives from $1.05x10^{4}$ to $(79\pm52)x10^{4}$ lit/mol for variation of the number of carbon atoms in the alkyl group from 0 to 16. Kamat and Litchin examined the electron transfer in the quenching of protonated triplet methylene blue by ground

state molecule of the dye (19). They determined the extent of dimerization of methylene blue (s_0) spectrophotometrically and found to be negligible in solvents containing 50% (vol/vol) or more organic component. Association was found to be significant in neat water and they had taken the value of dimerization constants at 25^0C with μ < 0.001M, as $2.5x10^3$ lit/mol from the work of Zadoroznnaya et al.(50). From these data, monomer present in a solution with $[MB^+]_{stoich}$ = 200 μM was calculated as ~ 83% . Arbeloa found changes in the shapes of visible absorption spectra of the fluorescein dianion when the concentration was increased, due to the formation of aggregates (51). The absorption spectra of dilute dye solutions did not change remarkably with temperature. The variation produced in the spectra of the concentrated solutions with an increase in temperature were due to the dissociation of aggregates. The author applied an iterative method in computing the formation constants of aggregation of the dyes. In the concentration range between $5x10^{-6}$ and ca. 10^{-1}M, the dimerization constant (K_d) does not change appreciably. At the higher concentrations the K_d value increases due to the non-negligible existence of other aggregates. The average dimerization constant at 20^0C for concentration upto 10^{-1} M was 5.0± 0.2 (Standard concentration 1 mol lit^{-1}) The dimer formation enthalpy (ΔH_d), entropy change (ΔS_d), and Gibbs potential (ΔG_d), were determined to be - 28±1 KJ mol^{-1},- 82±5 J $mol^{-1}K^{-1}$ and - 3.9±0.1 KJ mol^{-1} respectively. At

higher concentrations, possibility of trimer formation was considered and examined in considerable detail. Recently, Arbeloa and Rohatgi-Mukherjee determined the formation constants and absorption spectra of the dimer and trimer of phenosafranine in aqueous solutions (52). Using two different iterative methods (43,51), the two average dimerization constants at room temperature ($28^{\circ}C$) with solutions of concentration smaller than 4×10^{-3} M were calculated as 42 ± 2 and 44 ± 2.lit mol^{-1} respectively. Thermodynamic functions for the dimerization process have also been determined. The enthalpy of dimerization, ($\Delta H_{\circ}$), was found to be -17 ± 1 KJ mol^{-1}. The standard free energy change and entropy variations of the dimer formation were -9.4 ± 0.1 KJmol^{-1} and -25 ± 5 J $mol^{-1}K^{-1}$ respectively, at $28^{\circ}C$. The calculated enthalpy change was smaller than the usual values found for hydrogen bond i.e. about -20 KJ mol^{-1}. It has been proposed that besides the possible participation of hydrogen bond, contribution of Vander waals and London forces, which are temperature dependent to some extent, were also important in the dimer formation. The formation constant and absoption spectrum of the trimer were determined assuming that the trimer hypochromism H_t is equal to H_d^2. The average trimerization constant at $28^{\circ}C$, thus calculated was 65 ± 10 lit/mol, which is greater than the dimerization constant. $\Delta G_{\circ}$, $\Delta H_{\circ}$ and $\Delta S_{\circ}$ values were of -9.4 ± 0.1, -17 ± 1 and -25 ± 5 KJ/mol, respectively for trimerization process suggest that the forces responsible for aggregation are changing from an enthalpy

directed one to an entropy directed one. The contribution of hydrogen bonding in the association process is decreased and that of the Vander waals force is increased. The increased hydrophobic interactions justify the sustantial increase in the entropic contribution in higher aggregates presumably due to the breaking of water structure. Neumann et al. examined the formation of mixed dimers in solutions of basic dyes (53). Mixed dimer equilibrium constants for various dyes were estimated to be between 1.4×10^{2} and 4.9×10^{4} lit/mol. However, the mixed dimer formation equilibrium constant are in general, larger than those for self dimers. These are ascribed to a charge transfer contribution to the interaction as a result of the difference in the electron densities of the different dyes.

3.1.2 THE MOLECULAR EXCITON MODEL :

The molecular exciton model offers a theoretical method for treating the resonance interaction of excited states of weakly coupled composite systems (54). The types of problems which have been dealt with on the basis of molecular exciton model among other include spectra of dimers and polymers consisting of molecules held together by weak intermolecular forces (hydrogen bond, Vander waals forces etc.) and the electronic transitions of composite molecules (polyenes, parapolyphenyles and others)

considered as resulting from the interaction of excited unit chromophores. In the weakly coupled composite systems for which the molecular exciton model offers a satisfactory approximation for the treatment of excited states, intermolecular (or interchromophore) eletron overlap and electron exchange are negligible. In such systems the optical electrons associated with individual component molecules (or chromophoric units) are considered localized, and the molecular units (or chromophoric units) preserve their individual characteristics in the composite (aggregate) system, with relatively slight perturbation. The mathematical formalism then takes the form of a state interaction theory, with the omission of details of atomic orbital composition usual in molecular electronic theories. The electronic states of the aggregate are then expressed in terms of the electronic states of the component light absorbing units.

Thus, the spectral properties of a molecular aggregate are related to the spectral properties of the component molecules by theoretical expressions involving observable experimental parameters: intermolecular distance, mutual intermolecular orientation and geometry, and intensity (oscillator strengh) of light absorption by component molecules. Although the spectral effects of aggregation are small enough to satisfy the use of a quantum mechanical perturbation method, nevertheless these effects are extremely characteristics and may be understood on the basis of the quantum mechanical resonance of excited states.

Thus, blue shifts, red shifts, or spectral splittings may be observed, depending on the geometry of the aggregate, accompanied by characteristics changes in polarization properties. Spectral absorption intensity changes may also be observed for the aggregate, and luminescence properties may be affected profoundly compared with those for the component molecules.

The exciton concept was introduced by Frenkel in 1931 in connection with the theory of transformation of electromagnetic radiation into heat in argon crystal. In 1948, Davydov applied the molecular exciton model to the problem of electronic states of naphthalene crystals. Since then, a host of researches have appeared exploring all aspects of the model. Davydov's "Theory of Molecular Excitons" (55) summerizes his results, and contains bibliographies of the research literature in this field. Simpson explores underlying elements of the model under the title " Independent Systems Approach" in his "Theories of Electrons in Molcules" (56). McClure's review (57) on the interpretation of the spectra of molecular crystals on the basis of exciton theory is a standard reference. Kasha, on the other hand, emphasized in applications of the molecular exciton model to non crystalline molecular aggregate systems. In a first paper, the distinction between atomic excitons and molecular excitons was stressed, together with the non conductive nature of exciton bands (58). In a second paper, diverse spectral effects for various coupling strengths were described, the quasi-classical electrostatic

vector model was developed as an aid in understanding exciton band formation, and various mechanisms of excitation migration were elaborated on (59).

Molecular Exciton Wave Functions :

The starting point of the molecular exciton model treatment will be singlet electronic energy states and their corresponding electronic state wave functions for a component molecule of the aggregate. It is assumed that the electronic singlet state energies E_0, E_1 ,E_2 ..... and wave functions ψ_0 ,ψ_1, ψ_2....are known, satisfying the individual molecule Schrödinger equation:

$$H_n \psi_n = E_n \psi_n \qquad (8)$$

In general, each problem will involve only a pair of states and wave functions, so these may be designated as G and E for ground and excited singlet state energy, and ψ_u and $\psi_u^\dagger$ for corresponding state wave functions for molecule u. It is a very great abstraction to represent an entire molecule in an electronic state by ψ_u or $\psi_u^\dagger$. But these are the starting states for the model.

Molecular dimers :

The ground state wave function for a molecular dimer consisting of two identical molecules will be (Fig.1)

$$\Psi_G = \psi_u \psi_v$$

Where, ψ_u and ψ_v are wave functions associated with molecule u and v respectively. This is the unique ground state wave function of the dimer; it is totally symmetric with respect to all symmetry operations of the dimer.

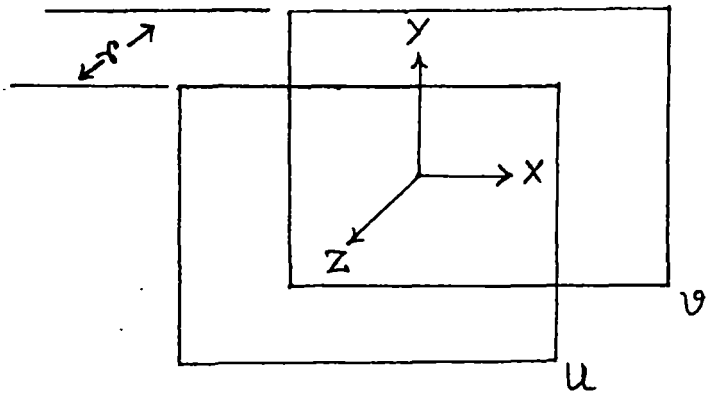

Fig. 1 Structure and co-ordinate of parallel or card-pack dimer.

The first excited state of the dimer can be described equally well by two possible wave functions,

$$\phi_1 = \psi_u \psi_v^{\dagger} \quad \text{and} \quad \phi_2 = \psi_u^{\dagger} \psi_v$$

These are degenerate and do not describe stationary states of the system. The correct zeroth order wave functions are,

$$\Psi_I = 1/\sqrt{2}\ (\phi_1 + \phi_2) = 1/\sqrt{2}\ (\psi_u\ \psi_v^\dagger + \psi_u^\dagger\ \psi_v)$$
$$\Psi_{II} = 1/\sqrt{2}\ (\phi_1 - \phi_2) = 1/\sqrt{2}\ (\psi_u\ \psi_v^\dagger - \psi_u^\dagger\ \psi_v) \qquad (9)$$

interchange of molecular levels u,v indicates that the first function is totally symmetric and the second is antisymmetric. In both of the stationary exciton states Ψ_I, Ψ_{II} the excitation is on both molecules, u and v, i.e., the excitation is collective or delocalized. The node corresponding to minus sign in the exciton wave function is an excitation node not an electron orbital node. At an excitation node the phase relation between transition moments on the respective molecular centres changes sign.

The Intermolecular Perturbation Potential :

The energy states and wave functions of molecular aggregate are determind by adding to the total Hamiltonian for the collection of unperturbed molecules a term $\Sigma_{1,k<l} V_{kl}$ where V_{kl} is the intermolecular interaction operator acting between molecules k and 1, and the summation is carried over all pairs of

molecules. This is essentially an intermolecular coulmbic potential term, giving the interactions between charged particles (electron and nuclei) on the two molecules. However, the use of an exact coulmbic potential, V_{coul}, would involve $1/r_{kl}$ as an operator (r_{kl} is the kl intermolecular distance), which would make simplification of the interaction integrals impossible. Accordingly, a point-multipole expansion can be used :

$$V_{coul} = V_{mono-mono} + V_{mono-di} + V_{di-di} + \ldots\ldots\ldots\ldots \quad (10)$$

For neutral total charge distribution the monopole interactions are zero. For allowed electric-dipole transitions, the dipole-dipole potential term becomes the leading one and higher multipoles are neglected. Thus, for strong absorption bands, corresponding to allowed electric dipole transitions

$$V_{coul} \cong V_{dipole-dipole} = -\frac{e^2}{r_{kl}^3} \sum_{ij} (2z_k^i z_l^j - x_k^i x_l^j - y_k^i y_l^j) \quad (11)$$

where in the classical dipole-dipole potential r_{kl}, is the distance between the point dipoles in molecules k and l, and x_k^i is the x coordinate of the ith electron on molecule k, x_l^i is the x coordinate of the jth electron on molecule l, and so forth, the coordinate system being chosen with the z axis parallel to the

line of molecular centres, and the summation is over all electrons in each molecule. Thus, an approximation may be introduced, which allows the physical interpretation that the excited state resonance splitting comes about from the electrostatic interaction of transition electric dipoles on neighbouring or nearly neighbouring molecules (the interaction falling off as the inverse cube of the intermolecule distance). Moreover, in most cases electron displacement along only one cooprdinate is effected by light wave causing the excitation at a particular frequency, so that in general only one term in the dipole-dipole interaction may remain, e.g., for the upper state of an x-polarized transition in a dimer consisting of two molecules u and v, whose transition moments are both parallel to the x-axis, the perturbation potential reduces to

$$V_{uv} = \frac{e^2}{r_{uv}^3} \sum_{ij} (x_u^i \, x_v^j) \qquad (12)$$

Exciton Splitting in a simple Dimer :

The application of the quantum mechanical molecular exciton formalism to the problem of spetral properties of Vander Waals dye aggregates was made by Simpson et al. for the case of pyridocyanine parallel or card-pack dimers (60). The application to dimers of diverse geometries, especially for hydrogen bonded

molecular pairs (61,62) was made by El-Bayoumi and Kasha. The application to benzoic acid dimers was made by Nagakura and co-workers (63) Considering the parallel card-pack dimer of Fig.1 to understand the spectral properties of such a molecular dimer, we must evaluate the excited state interaction energy to measure the exciton splitting, and the transition moment in order to determine the selection rules.

The Exciton Band Width :

In evaluating the excited state interaction energy we shall examine merely the exciton splitting for simplicity. The energy of interaction will be given by the expectation value of the interaction potential with respect to the degenerate excited states of the dimer.

$$\mathcal{E} = \int\int \psi_u \, \psi_v^{\dagger} \, V_{uv} \, \psi_u^{\dagger} \, \psi_v \, d\tau_u \, d\tau_v \qquad (13)$$

Where V_{uv} is the intermolecular interaction operator acting between molecules u and v. Inserting the form of V_{uv} appropriate to an X-polarized electric-dipole transition in molecules u and v (cf. Fig. 1)

$$\mathcal{E} = \frac{e^2}{r_{uv}^3} \int\int \psi_u \, \psi_v^{\dagger} \left(\sum_{ij} x_u^i \, x_v^j \right) \psi_u^{\dagger} \, \psi_v \, d\tau_u \, d\tau_v \qquad (14)$$

Where x_u^i is the x co-ordinate of the ith electron on molecule u and x_v^j is the x co-ordinate of the jth electron on the molecule v. Because of the form of V_{uv}, this equation may be factored to yield.

$$\mathcal{E} = \frac{1}{r_{uv}^3} \left[\int \psi_u \left(\sum_i ex_u^i \right) \psi_u^\dagger \, d\tau_u \right] \left[\int \psi_v^\dagger \left(\sum_j ex_v^j \right) \psi_v \, d\tau_v \right] \quad (15)$$

Where r_{uv} is the distance between the point dipoles in molecules u and v. We recognize immediately that each of the integrals is now precisely the transition moment integral for the excitation of the individual (monomer) molecules u and v,

$$M_u = \int \psi_u \left(\sum_i ex_u^i \right) \psi_u^\dagger \, d\tau_u \quad (16)$$

At this point an arbitrary feature regarding the phase factor of the transition moment enters the picture. We must choose a phase relationship such that a lowering of energy or stabilization of the dimer excited state occurs for the exciton stationary state wave function Ψ_I chosen to lie lowest (cf. Fig.2)

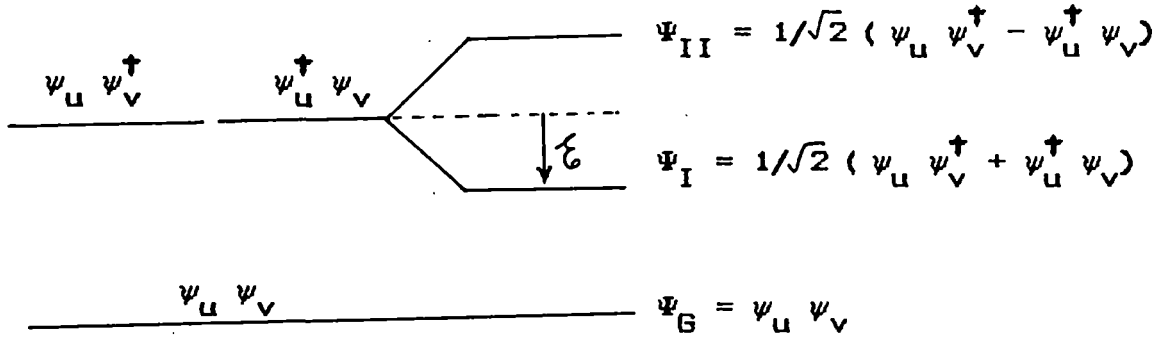

Fig.2 schematic energy level diagram showing exciton splitting in molecular dimers (Displacement term omited)

Thus, in order to make the exciton stationary state wave function Ψ_I correspond to a lowering of energy $\mathcal{E}$, we can choose the phase factors so that

$$M_u = - M_v \qquad (17)$$

This phase factor is an entirely arbitrary one. If we choose to define $M_u = + M_v$, then the stationary state exciton function Ψ_{II} of Fig. 2 would lie lowest for the parallel dimers of Fig. 1. The expression for the energy lowering or interaction energy for the parallel dimer of Fig.I becomes

$$\mathcal{E} = - \frac{M_u^2}{r_{uv}^3} \qquad (18)$$

The exciton band width will be twice this value or $2\mathcal{E}$.

Thus, we see that the energy lowering for the simple dimer case at hand (Fig. 1) is given by the monomer transition moment squared i.e., is proportional to the probability or intensity of the electric dipole allowed transition in the monomer, divided by the inter molecular distance cubed. Thus, the stronger the absoption band, the greater will be the exciton band splitting. One observes also that the r-dependence makes this a comparatively long range interaction.

For a dimer with arbitrary mutual orientations of molecular axes with respect to an x, y, z co-ordinate frame (Fig.1) the energy of interaction is given by

$$\mathcal{E} = - \frac{M_u^2}{r_{uv}^3} (2 \cos\theta_u^z \cos\theta_v^z - \cos\theta_u^x \cos\theta_v^x - \cos\theta_u^y \cos\theta_v^y) \quad (19)$$

Where again M_u represents the transition moment in a free molecule, and $\cos\theta_u^x$,$\cos\theta_u^y$, $\cos\theta_u^z$ represent the cosines of the angles which the transition moment M_u for molecule u makes with the x, y, z axes.

Selection Rules :

Although in the molecular dimer two exciton states

theoretically result from the exciton splitting, both of these may not necessarily be observed as allowed spectral transitions. In fact, which exciton stationary states may be reached by electric dipole transitions from the ground state is a strictly geometry-determined problem.

Let us examine the spectral selection rules by evluating the martix elements of the electric dipole operator between the ground state and the stationary exciton states of the dimer. Thus, the transition moment vector of the dimer is given by

$$\mathbf{M}^{I} = \int\int \Psi_G \, (\mathcal{M}_u + \mathcal{M}_v) \, \Psi_I \, d\tau_u \, d\tau_v$$

$$\mathbf{M}^{II} = \int\int \Psi_G \, (\mathcal{M}_u + \mathcal{M}_v) \, \Psi_{II} \, d\tau_u \, d\tau_v \qquad (20)$$

Where $\mathcal{M}_u, \mathcal{M}_v$ are the electric dipole operators corresponding to the molecular electronic co-ordinates of molecules u and v. Evaluating these, and because of orthogonality and normalization properties of the intramolecular state wave functions following values of trasition moments are obtained

$$\mathbf{M}^{I} = 1/\sqrt{2} \, (\mathbf{M}_v + \mathbf{M}_u)$$

and (21)

$$\mathbf{M}^{II} = 1/\sqrt{2} \, (\mathbf{M}_v - \mathbf{M}_u)$$

For the card-pack dimer we had defined as required phase

relations for the wave functions Ψ_I and Ψ_{II}, $M_u = -M_v$. Therefore, for the parallel or card-pack dimer of Fig. 1, the transition moments corresponding to the stationary exciton states of Fig.2 are:

$$M^{I} = 1/\sqrt{2}\,(M_u - M_u) = 0$$

and (22)

$$M^{II} = 1/\sqrt{2}\,(M_v + M_v) = 2M_v/\sqrt{2}$$

Thus, the transition moments for the dimer are given as super positions of the transition moments for the individual molecules. According to the above equation the oscillator strength (f) for electric dipole transitions between singlet states of the dimer Ψ_G and Ψ_I is zero. For the transiton to singlet state Ψ_{II} since

$$f \propto (M^{II})^2 = 2M_v^2 \quad \text{or} \quad f_{II,dimer} = 2\, f_{monomer}$$

an allowed transition with no change of intensity per monomer is predicted.

3.1.3. SPECTRAL PROPERTIES OF DIMERS IN TERMS OF EXCITON THEORY :

Three characteristics of Vander Waals dye molecule parallel

dimers have been recognized in the literature. These are (a) The absoption spectrum characteristically blue shifts by 2000-4000 cm^{-1} in these dimers, (b) the prominent fluorescence of the monomer is invariably quenched, and (c) the relatively inefficient phosphorescence of the monomer becomes the predominant luminescence in the dimer. Simpson et al.(60) and McRae and Kasha (29) have interpreted these properties in dye molecule dimers and polymers on the basis of the molecular exciton splitting and selection rules in the dimer. In the monomer, absorption to the lowest singlet excited state is strongly allowed, and the very rapid fluorescence emission competes with excitation of the lowest molecular triplet state. In the dimer, the allowed exciton state is at significantly higher energy than the singlet excited state of the monomer: a blue shift is thus accounted for in case of the card-pack, or parallel dimer. However, collisions rapidly deactivate the excited dimer to its lower singlet exciton stationary state. But this state is a metastable singlet state with an improbable fluorescence capacity. Further deactivation of the dimer to the triplet state becomes the most probable path for the excitation. Thus the fluorescence is quenced, and a very strong triplet state to ground singlet state emission is observed. Reference 29, contains a general bibliography of the various experimental observations on spectral consequences of dye dimerization. The parallel or card-pack structure probably fits quite well to

vander waals dimers consisting of large planar dye molecules. However, numerous other dimer structures are possible, and the exciton model permits a qualitative and semi-quantitative discussion of such dimers as well. These have been described in references (59,61-63). In particular, for head-to-tail orientation of transition moments in the dimer, a strong red shift is predicted, with the upper exciton component forbidden in the dimer; whereas, in the oblique dimer, with mutual angle between molecular transition moments between 0 and π, both exciton components are observed with a spectral splitting as the characteristics result. These general dimer results may be gleaned from the linear polymer exciton model treated by McRae and Kasha (29). Rohatgi and Mukhopadhyay (64) studied the dimer spectra of fluorescein and some of its halogen derivatives in aqueous solution. From the splitting observed in the spectra, the inclination of the component molecules in a dimer has been obtained on application of the theory of exciton interaction. The distance R between the two component molecules in the dimer was also calculated for various geometries. In a more recent series of publication Arbeloa (51,65) studied molecular structures of the dimeric and trimeric states of fluorescein dianion. The absoption spectra of the dimer and trimer of the dye molecule in aqueous solution were evaluated. The geometric structures of both aggregates were determined using the exciton theory. The nature of the association forces was also studied. Evidence was

presented for the formation of eosin Y dimer as the highest aggregates of complexes between eosin Y and poly-L-lysin, poly (1-xylyl viologen) or cetyl-pyridium (66). The absorption spetra of these complexes have been obtained free from contamination by eosin Y monomer spectrum and was fitted with Gaussian band model, using a non linear least square fitting computer program. Using such models, exciton theory had been employed to calculate parameters such as orientation and molecular separation of the components of the eosin Y dimer. Where appropriate, these parameters have been compared with the dimensions of the repeating unit and the possible conformations of the polymer (66). Basu et al.(67) studied concentration effects on the absorption and emission properties of Ni(II) and Zn(II) tetra(p-venyl phenyl) porphyrins in benzene solutions. Where as exciton splitting of the soret band was observed for the Ni(II) complexe, only a hypochromic effect is observed for the Zn(II) complex. The exciton parameters were calculated for Ni complexes. Recently, Arbeloa et al. also studied the excitonic interaction and the nature of bonding in the aggregation of pheno-safranine from concentration dependent spectral changes (52).

By applying simple exciton theory in zero order an attempt has also been made to study the geometric structure of the trimer, as has been accomplished for xanthene aggregates (51-52). Molecular model showed that the angle θ between the chromophore

groups of the monomers is due to the steric effect between the phenyl groups. Neuman et al. in a recent publication put forward evidences of the formation of mixed dimers of basic dyes, which shows spectroscopic properties in accordance with exciton theory (53). The bands of these dimers can be found at wave lenghs shorter and longer than those of the forming dyes, with higher and lower excited states, respectively. These bands correspond to the transitions of both the in-phase (high energy) and out-of-phase (low energy) transition moment geometries, none of which are prohibited.

3.1.4. VIBRONIC EXCITON MODEL :

In the previous section, the molecular exciton model describes the resonance interaction of excited states of molecular aggregate systems with weak intermolecular binding. It should be stated at the outset that vibrational structure in spectra, and vibronic interactions have been neglected throughout the treatment. As such, the discussion apply perforce to aggregates of molecules which have intense or strongly allowed singlet-singlet transitions, with strong 0-0 vibronic bands.

The shapes of the monomer and the dimer spectra of dyes, howerer, often suggest that the degenerate exciton interaction in the dimer may correspond to the vibronic coupling case. Fulton

and Gouterman (68) described a model for more generally applicable vibronic coupling phenomenon. The theory refers to exciton coupling of degenerate levels and, accordingly, changes in total integrated intensities due to non-degenerate interactions were not considered. The changes in the shapes of the electronic absorption spectra of dimeric species related to those of the corresponding monomers thus have been attributed to exciton interactions between vibronic levels. Theories of exciton interaction in dimers, based on the adiabatic approximation (69) and developed from general discussions (70), through perturbational (71,72) and variational (73,74) calculations, culminated in the symmetry operator formulation of Fulton and Goutermann (68,75). Exciton interactions between a pair of identical chromophores were first considered (76) and formulated (77) in connection with studies of the concentration dependent properties of aqueous dye solutions. Exciton coupling in a dimer produces splitting of the excited states and if the strengh of this coupling is of the order of molecular vibrational quanta readily observable effects on steady state absorption spectra will ensue. Moreover, since exciton coupling occurs between transition moments of the interacting chromophores, it should be possible, in priciple, to infer the spatial conformation of the dimeric species from a knowledge of the relative intensities of the two transitions of the split exciton states (77).

Therefore, molecular spectra in the visible-UV region are

result of vibronic transitons and, accordingly, exciton interactions will produce the splitting of the monomeric bands into two series of vibronic exciton band (78) so that the overall intensities of minus and plus series (I^-,I^+) must correspond to the total intensities of all the bands in the two exciton transition series. The two major dimer bands normally observed, does not belong to two separate exciton series and there is much "intensity borrowing" as a result of the exciton perturbation between bands belonging to the same exciton series that produces very significant redistribution of the relative band intensities, particularly in the "plus" series, which may lead to very significant changes in the shapes of dimer spectra compared with the monomeric analogue . It follows that one may employ physical models of vibronic exciton interactions in order to be able to ascertain the relative contributions of the two exciton series to the intensity of the observed dimer spectra. Such model have been proposed (75,79) and applied to analyse the dimer spectra of dyes viz, Rhodamin B (80) and some pyronines (81). However, at first sight it might be concluded that vibronic theories of exciton coupling face prohibitive difficulties owing to the fact that molecules of many atoms possess a mumber of vibrational modes and their electronic transition may be accompanied by simultaneous changes in the vibrational quanta of the various fundamentals. Fortunately, it has been observed that vibronic transitions of molecules containing two or more condensed benzene ring at low

resolution in solution may be described in terms of single progressions in a dominant totally symmetric mode (82,83). For this reason vibronic exciton models involving just a single molecular vibrational mode may be applied to a great many experimental dimer spectra.

The effect of molecular vibration on exciton spectra is thus most appreciated in the non-stationary picture (84). Exciton coupling is equivalent to the delocalization of excitation energy, but the change in nuclear conformation on excitation produces a potential energy well which tends to localize the molecular excitation. Thus vibronic exciton coupling corresponds to competition between delocalization of the excitation through exciton interactions and the localizing tendency of the nuclear displacement. Numerical solution to this exciton problem for dimers has been presented (73), applied to absorption and fluorescence spectra (75) and circular dichroism (85) and extended to include, in addition to nuclear displacement the effect of nuclear momenta (89) on exciton transfer .

Kurucsev and coworkers (81,86-89) applied the similar as well as a modified model of Fulton and Gouterman (68,75) to the dimer species of a number of dyes. The procedure followed in fitting the derived spectrum by a theoretical dimer spectrum involved three major steps. First, the monomer spectrum has been analysed in terms of its vibronic bands. Next, by the use of some of the monomer parameters derived from this analysis shape of the

dimer spectrum has been fitted. Finally, the position of the calculated curves was shifted to bring it into coincidence with the spectrum. Some detail of this procedure relevent to the system studied in the present work are as follows :

The spectrum of the monomer has been analysed in terms of its vibronic bands by adopting the following assumptions : (i) only one fundamental vibrational mode need to be considered (ii) the difference in the force constants of the ground state and excited state oscillators may be disregarded (iii) the harmonic approximation applies (iv) the vibronic transition may be described satisfactorily by a Gaussion band shape. The assumptions lead to simple formulae for analysing the absorption spectrum of the monomer. The simplest physical model as described, to apply in dealing a vibronic progression is that of a displaced harmonic oscillator with Gaussion bands of constant band width requiring just five adjustable parameters in accordance with the formulae,

$$\bar{I}(\bar{\nu}) = I_{oo} \sum_{m} \frac{X^m}{m!} \left(1 + \frac{mV}{\bar{\nu}_{oo}} \right) \exp \left\{ - \frac{4\ln 2}{b_g^2} \left(\bar{\nu} - \bar{\nu}_{oo} - mV \right)^2 \right\} \qquad (23)$$

where I_{oo} is the intensity, $\bar{\nu}_{oo}$ is the position of the (0,0) band, b_g is the Gaussian band width, X the ratio of (1,0) to (0,0) band intensities and V the separation between the bands.

In general, intensity distribution within an electronic band

is represented well by Gaussian model. It is described accordingly, each vibronic band, (m,0) by formula

$$I_m(\bar{\nu}) = A_{m1} \exp \{- A_{m3} (\bar{\nu} - A_{m2})^2\} \qquad (24)$$

where $I_m(\bar{\nu})$ is the band intensity at wave number $\bar{\nu}$, A_{m1} is the peak height, A_{m2} is the position of the band centre, and

$$A_{m3} = \ln 2 / b_g^2$$

with $2b_g$ as the width of the band at half maximal intensity. The band width may be taken to be constant within a progression, so that one writes $A_{m3} = A_3$

It is also assumed that the ground and excited states are adequately described as "displaced" harmonic oscillators with the same force constant which has the following consequences :

(i) The band centres are separated by a constant distance V, so that $A_{m2} = A_{02} + mV$

(ii) The intensities of the bands obey a modified poisson distribution.

In particular, in the case of Gaussian bands the integrated intensities are proportional to the peak height A_{m1}, and these are related to one another through a parameter X which, in turn, is a measure of the displacement of the normal coordinate of vibration (s)

$$A_{m1} = \frac{X^m}{m!} A_{o1} \frac{A_{m2}}{A_{o2}} \qquad (25)$$

The complete progression may thus be defined in terms of five molecular parameters X, υ, A_{01}, A_{02} and A_3 as follows :

$$I(\bar{\nu}) = \sum_m \frac{X^m}{m!} A_{o1} \left(1 + \frac{mV}{A_{o2}} \right) \exp \left\{ - A_3^2 \left[\bar{\nu} - A_{o2} - mV \right]^2 \right\} \qquad (26)$$

Replacing the symbols of the above parameters by more common symbols and after minor rearrangement the equation takes the form of equation 23 as already described.

The monomer spectrum be then fitted to the above equation by the help of weighted least square program. A series of dimer spectra are calculated and compared with the shape of the derived spectrum.

The application of the theory involves diagonalising tridigonal Hermitian matrices which incorporate five parameters 9viz., the exciton coupling strengh (ε), the angle between the interacting transition moments (θ), the energy of the dimer transition in the hypothetical state $\varepsilon = 0$ (ν_{oo}^{D}), the vibronic spacing (V) and the nuclear displacement parameter (X).

3.2. EXPERIMENTAL :

Five progressively alkylated thiazine dyes viz. Thionine, Azure C(monomethyl thionine), Azure A(dimethyl thionine), Azure B(trimethyl thionine) and Methylene Blue(tetramethyl thionine) have been chosen for the present study. The dyes were supplied by Aldrich chemical company, U.K. All other chemicals were of analytical grade from Aldrich or B.D.H. and used as received. The structure of the dyes are represented below :

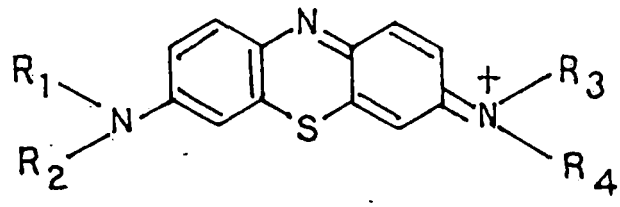

Thionine : $R_1 = R_2 = R_3 = R_4 = H$

Azure C : $R_1 = R_2 = R_3 = H$, $R_4 = CH_3$

Azure A : $R_1 = R_2 = H$, $R_3 = R_4 = CH_3$

Azure B : $R_1 = H$, $R_2 = R_3 = R_4 = CH_3$

Methylene Blue: $R_1 = R_2 = R_3 = R_4 = CH_3$

Purification of the dyes :

All the five dyes were found to contain coloured impurities. They were purified over a chromatographic column of silica gel using chloroform-methanol mixture as eluent. AzC was extracted efficiently with 8:2 chloroform-methanol mixture whereas, AzA was extracted with 7:3 solvent mixture. All other dyes were eluted by less polar solvent mixtures than that used for AzA. Finally they were recrystallised and dried at 50^{o}C under vacuum. Purity of the dye samples were checked by TLC using 8:2 water-acetic acid mixture as the mobile phase and purity of all dyes except AzC were found to be excellent. The commercial sample of AzC contained high percentage of insoluble materials in addition to other coloured impurities. Even after repeated chromatographic treatment it gave faint additional spot on the TLC plate indicating the presence of a small amount of impurity. However, although the purification of this dye was not upto the level of other four dyes, various analyses (spectral and analytical) showed that final purity of the dye was satisfactory.

Preparation of the stock solution of the dyes :

Stock solutions were prepared by accurately weighing vacuum dried samples of the dyes and dissolving them in double distilled water upto a definite volume. The concentration of these

solutions, stored in polypropylene bottle, was of the order of 10^{-3}M. Final concentration was estimated by reductimetric titration with Fe(II) inons as follows: (90)

5 ml. of the dye solution ($5x10^{-4}$M) was treated with sodium acetate (10 ml,1M), hydrochloric acid(8 ml,1M), sodium oxalate(15 ml,0.2M) and total volume diluted to 50 ml ($_pH \sim 3.95$) in a 150 ml beaker fitted with a three-holed stopper. The reaction mixture was then titrated by iron(II) solution ($2.5x10^{-3}$M) in nitrogen atmosphere (to prevent the aerial oxidation of the leuco-dye). The colour change was sharp and reversible for all the dyes.

Spectroscopic Measurements :

The absorption spectra of the dye solutions in aqueous and aqueous-ethanolic (5%, 10%, 15%, and 20%) media in the presence of 0.01M KCl solution were recorded by using Shimadzu (Japan) double beam UV-VIS Spectrophotometer (model UV-240) coupled with thermostatic arrangement (model TB-85). The spectra were taken at dye concentrations ranging from $5x10^{-6}$M to $8x10^{-4}$M in the temperature range from 20^0 to 50^0C, at 10^0C intervals. The spectra of the concentrated solutions (conc.> $8x10^{-5}$M) are recorded with a cell having 1mm. optical path length and for dilute solutions a cell of 1cm. path length is used. From the

variation of optical density produced by known changes of optical path, the absorptivity in the visible region of the spectrum are determined (51).

3.3 RESULTS AND DISCUSSION :

3.3.1. Studies on monomer-dimer equilibria of the dyes :

The nature of some representative visible absorption spectra of the dyes at different temperatures, concentrations and solvents are shown in figs. 3-23. As expected the spectra show considerable changes with the variation of concentrations in various solvents due to the formation of aggregates (64,91-93).

It is assumed that the absorption spectra of the dyes at concentration 5×10^{-6}M is the monomer spectrum (Figs. 24-28) because of the negligible presence of dimers and higher aggregates. The absorption spectrum of these dilute dye solutions does not change with temperature. The variation produced in the spectrum of concentrated solutions by an increase in temperature are due to dissociation of aggregates (51).

For monomer-dimer equilibrium :

$$M + M \rightleftharpoons D$$

the equilibrium constant for dimerization K_d, at any temperature

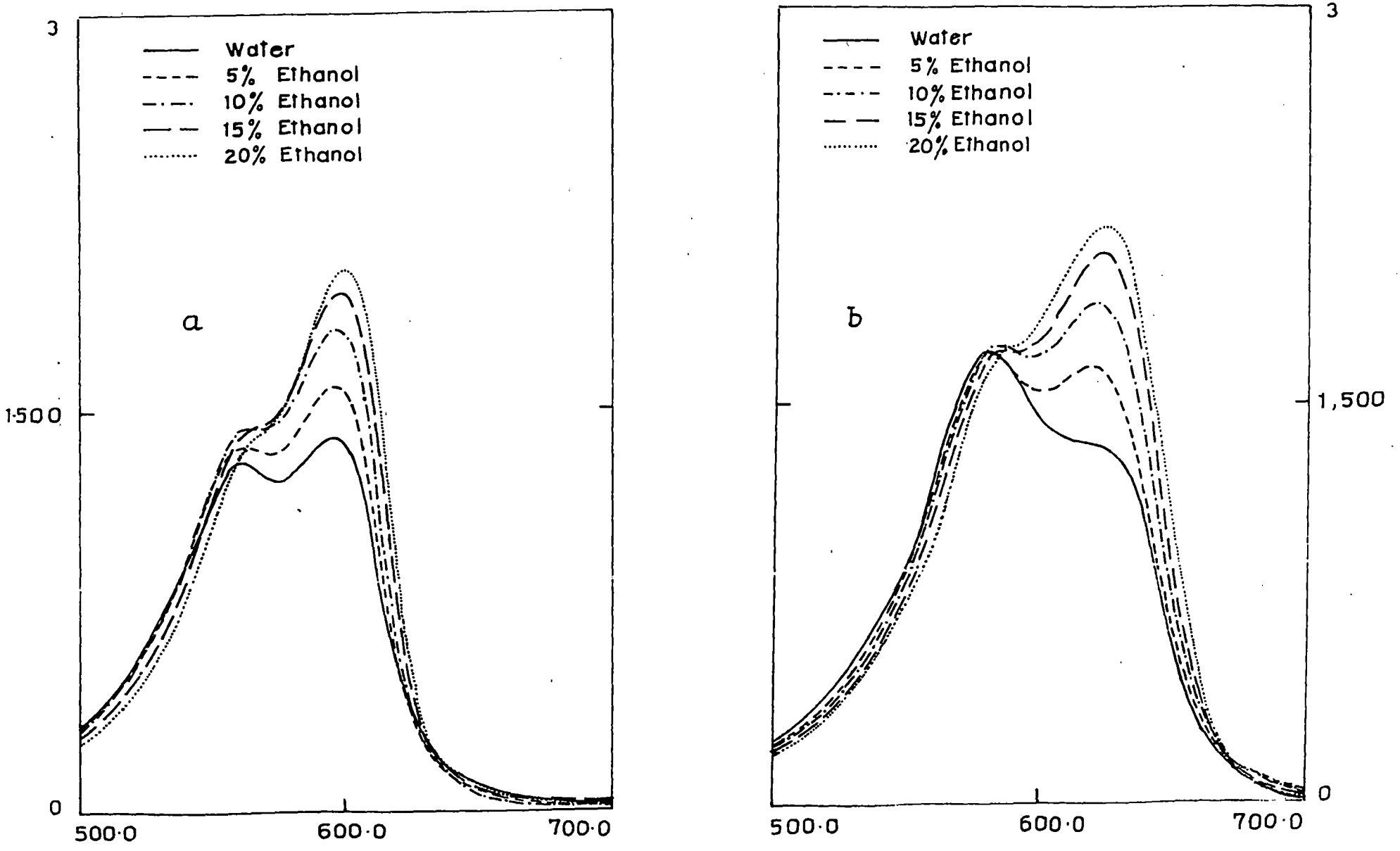

Fig.- 3 Visible Absorption spectra of (a) Thionine (4×10^{-4}M) at 30°C and (b) Azure C (5×10^{-4}M) at 40°C in water and Ethanol-water mixtures in presence of 0·01M KCl.

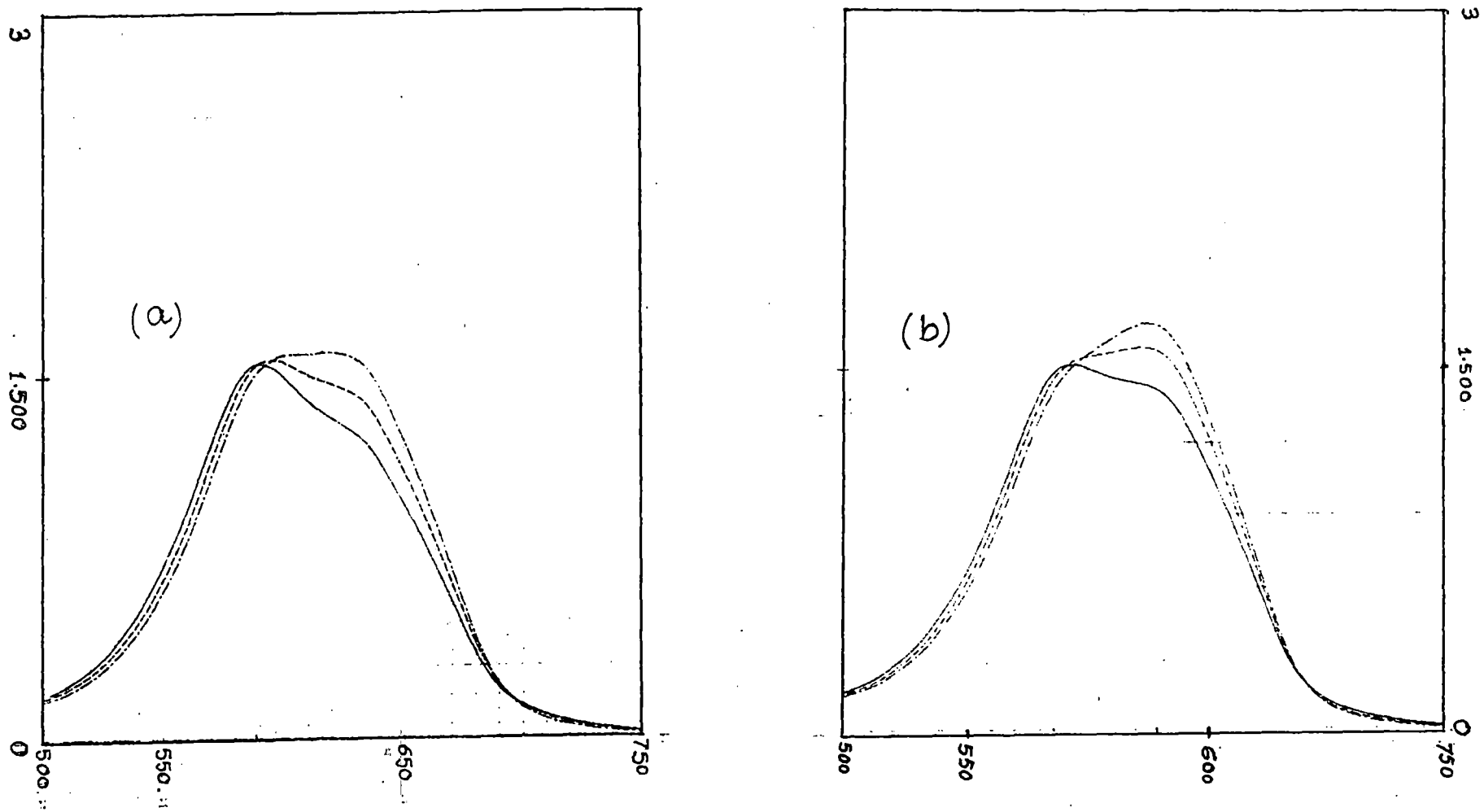

Fig. 4: Visible Absorption Spectra of Azure A ($4X10^{-4}M$) in (a) 5% Ethanol and (b) 10% Ethanol at different temperatures in the presence of 0.01 M KCl.

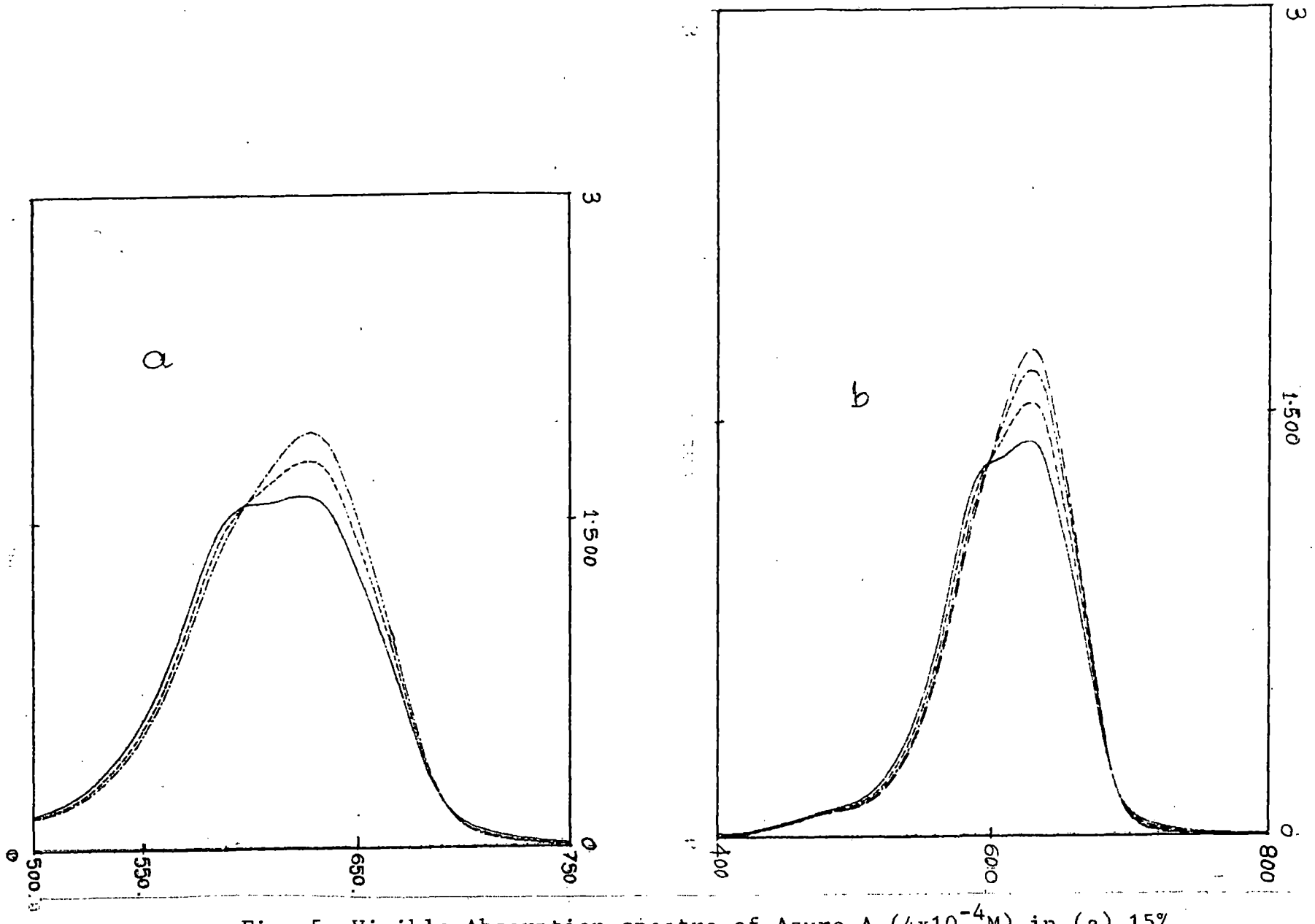

Fig. 5: Visible Absorption spectra of Azure A ($4x10^{-4}$M) in (a) 15% Ethanol and (b) 20% Ethanol at different temperatures in the presence of 0.01 M KCl

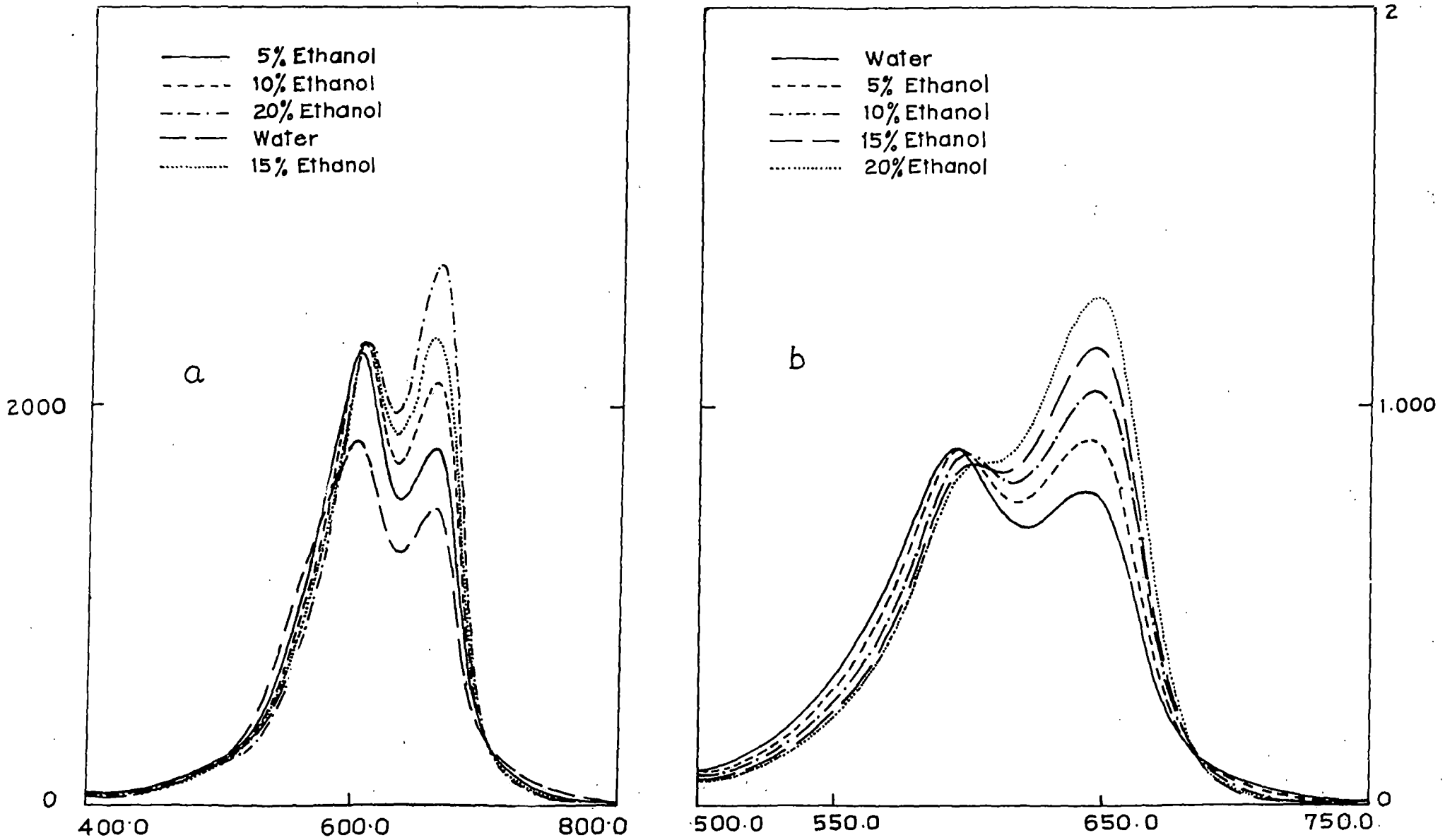

Fig.- 6 Visible Absorption spectra of (a) Methylene Blue (4×10^{-4} M) at 20°C and (b) Azure B (2×10^{-4} M) at 30°C in water and Ethanol-water mixtures in presence of 0.01 M KCl.

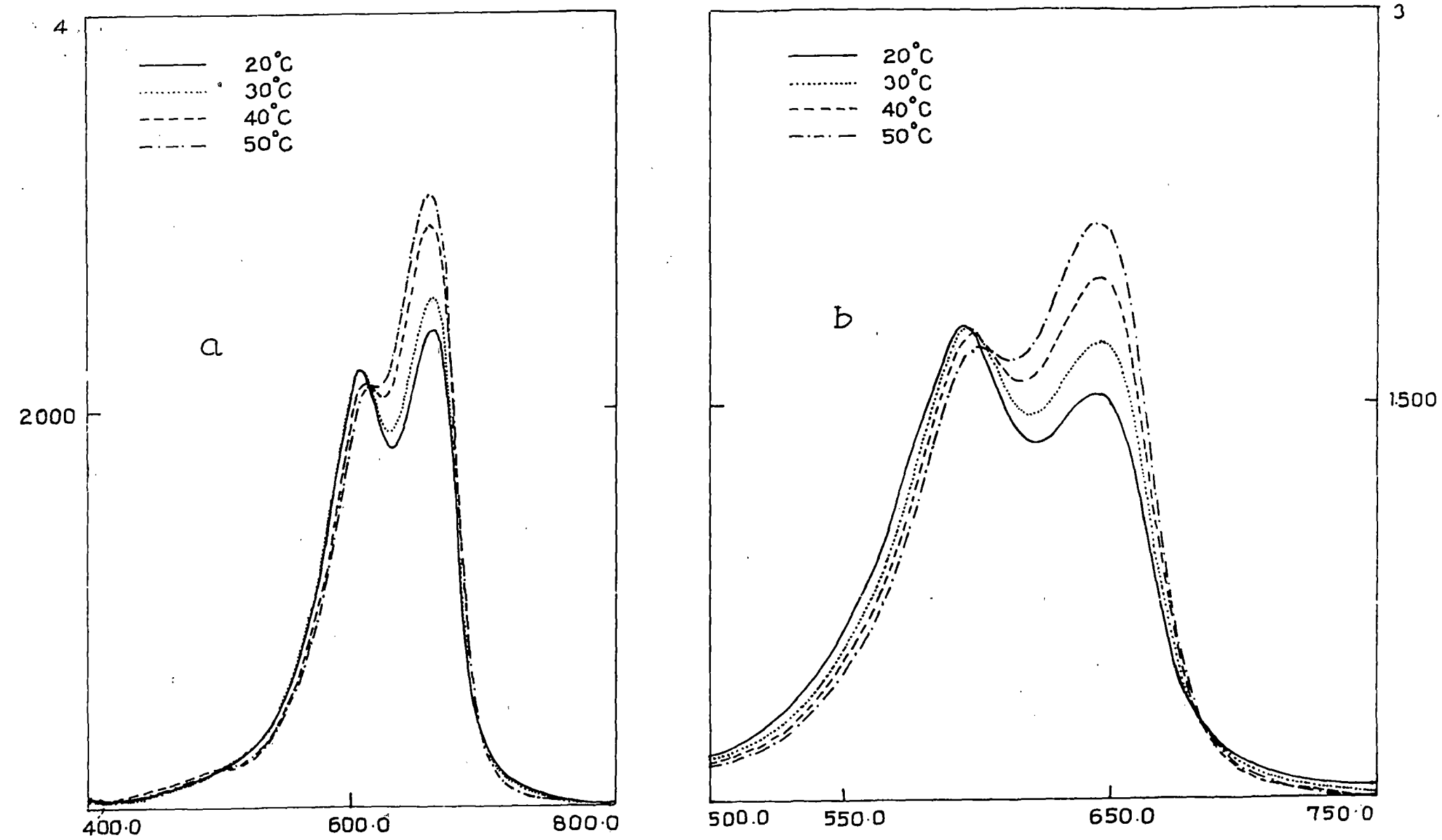

Fig. - 7 Visible Absorption spectra of (a) Methylene Blue (5×10^{-4} M) in 20% Ethanol- water mixture and (b) Azure B (4×10^{-4} M) in 10% Ethanol- water mixture at different temperatures in presence of 0·01M KCl .

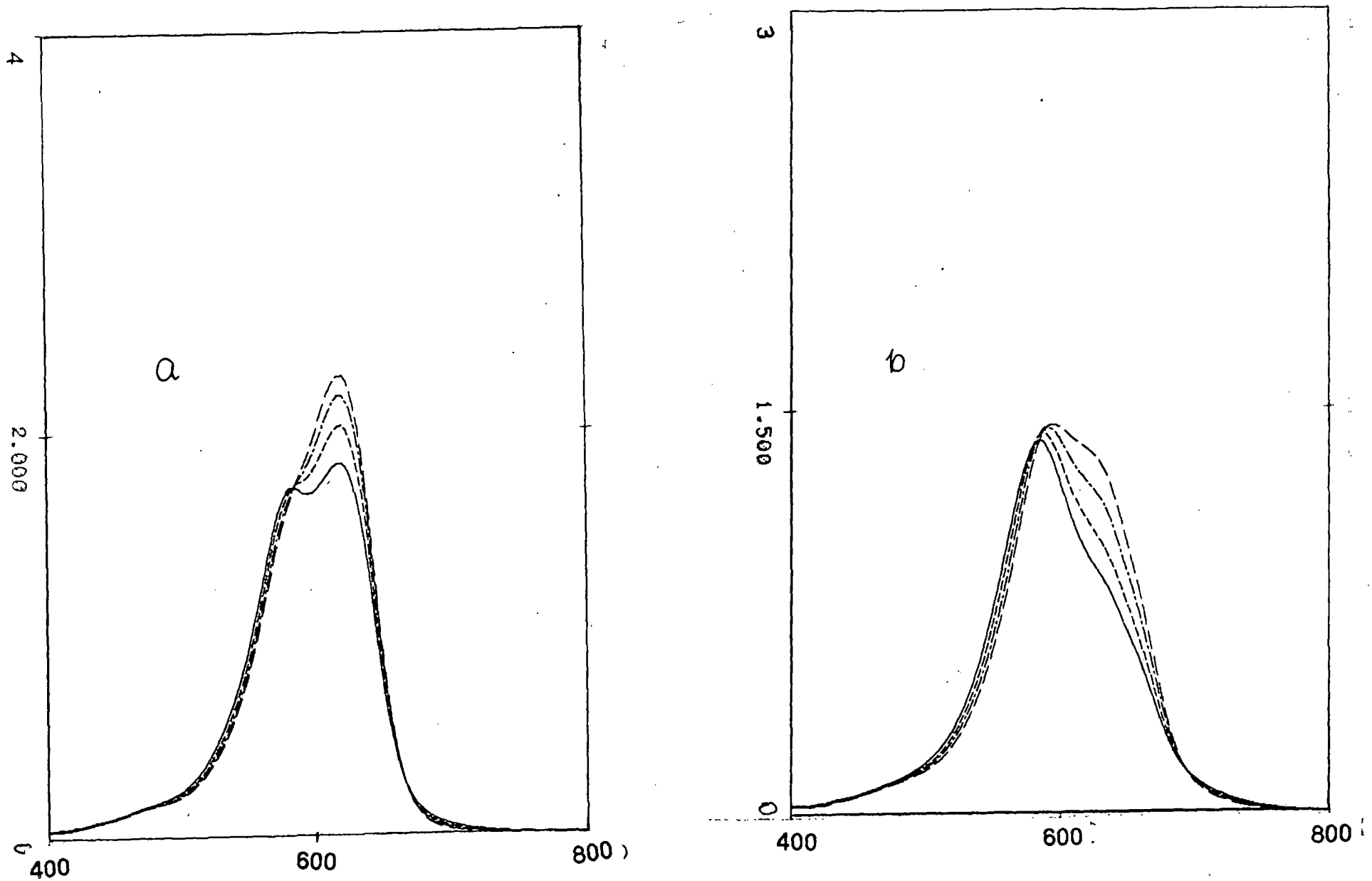

Fig. 8 Visible absorption spectra of (a) Azure C ($6x10^{-4}M$) in 20% Ethanol and (b) Azure A($4x10^{-4}M$) in water at different temperatures in the presence of 0.01 M KCl

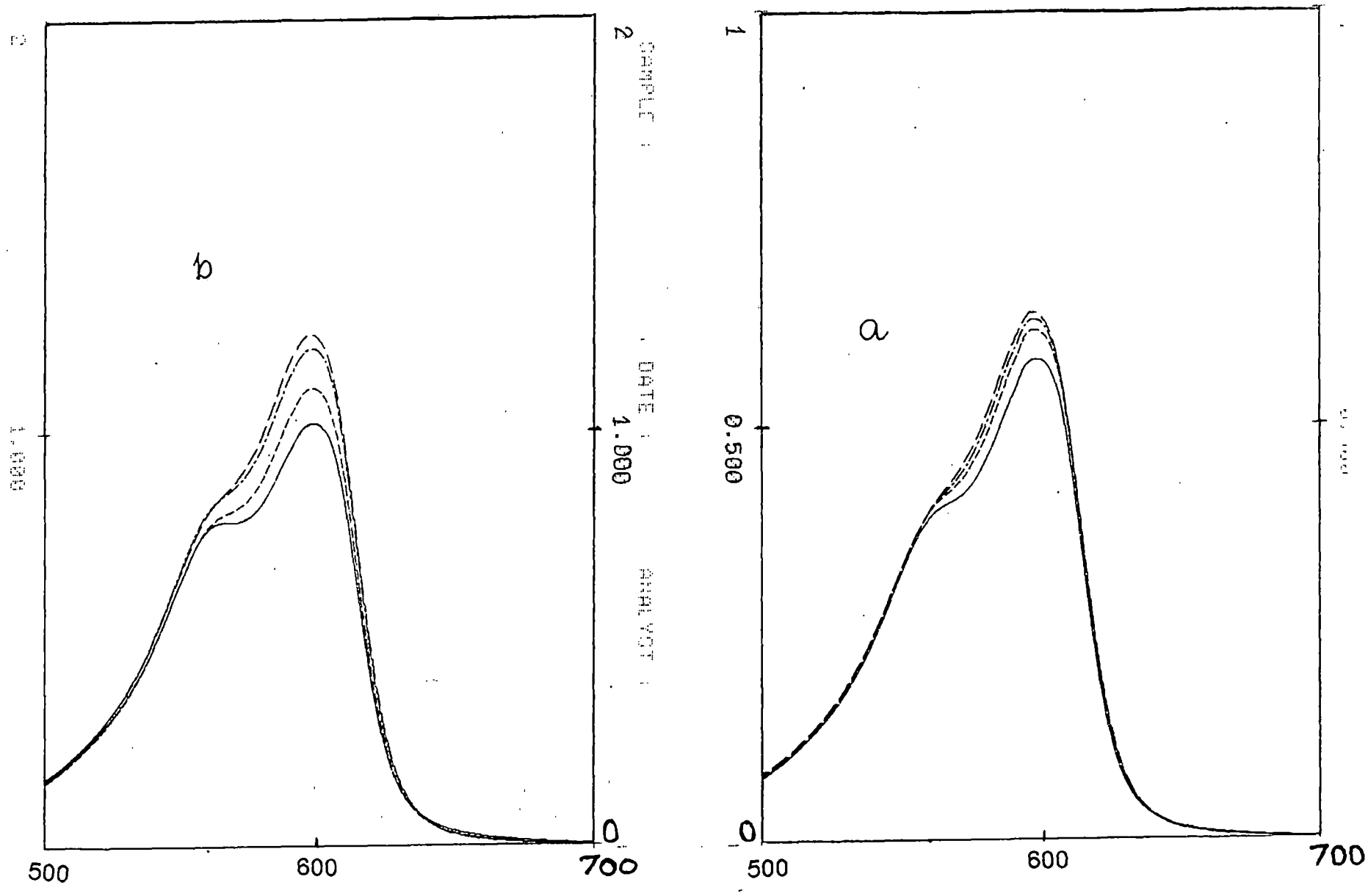

Fig. 9 Visible absorption spectra of Thionine (a) $2x10^{-4}$M and (b) $1x10^{-4}$M in 10% Ethanol at different temperatures in the presence of 0.01M KCl

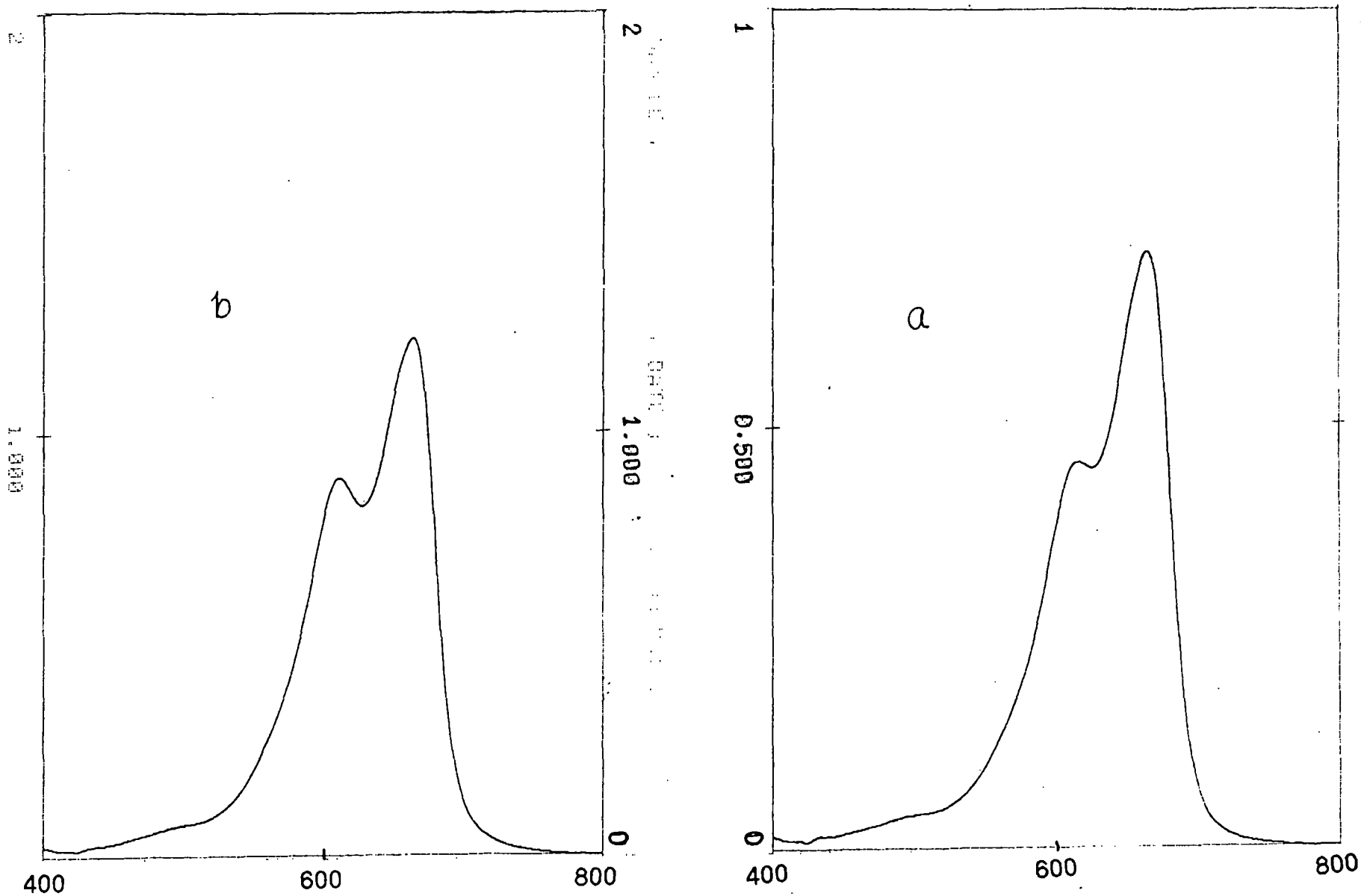

Fig. 10 Visible absorption spectra of Methylene Blue (a) $1x10^{-4}M$ and (b) $2x10^{-4}M$ in 20% Ethanol at $20^{0}C$ in the presence of 0.01M KCl

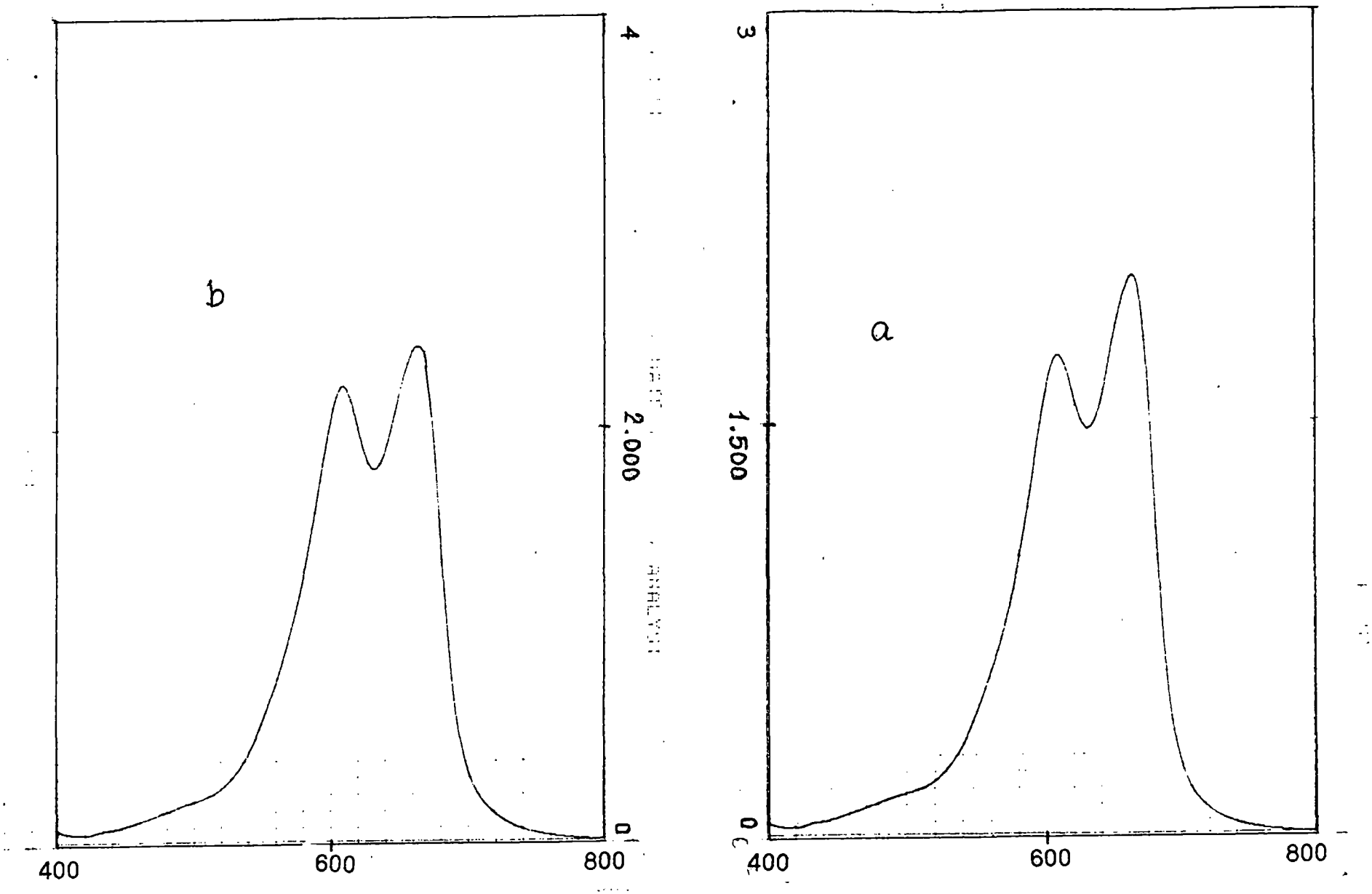

Fig. 11 Visible absorption spectra of Methylene Blue (a) $4x10^{-4}M$ and (b) $5x10^{-4}M$ in 20% Ethanol at $20^{0}C$ in the persence of 0.01M KCl.

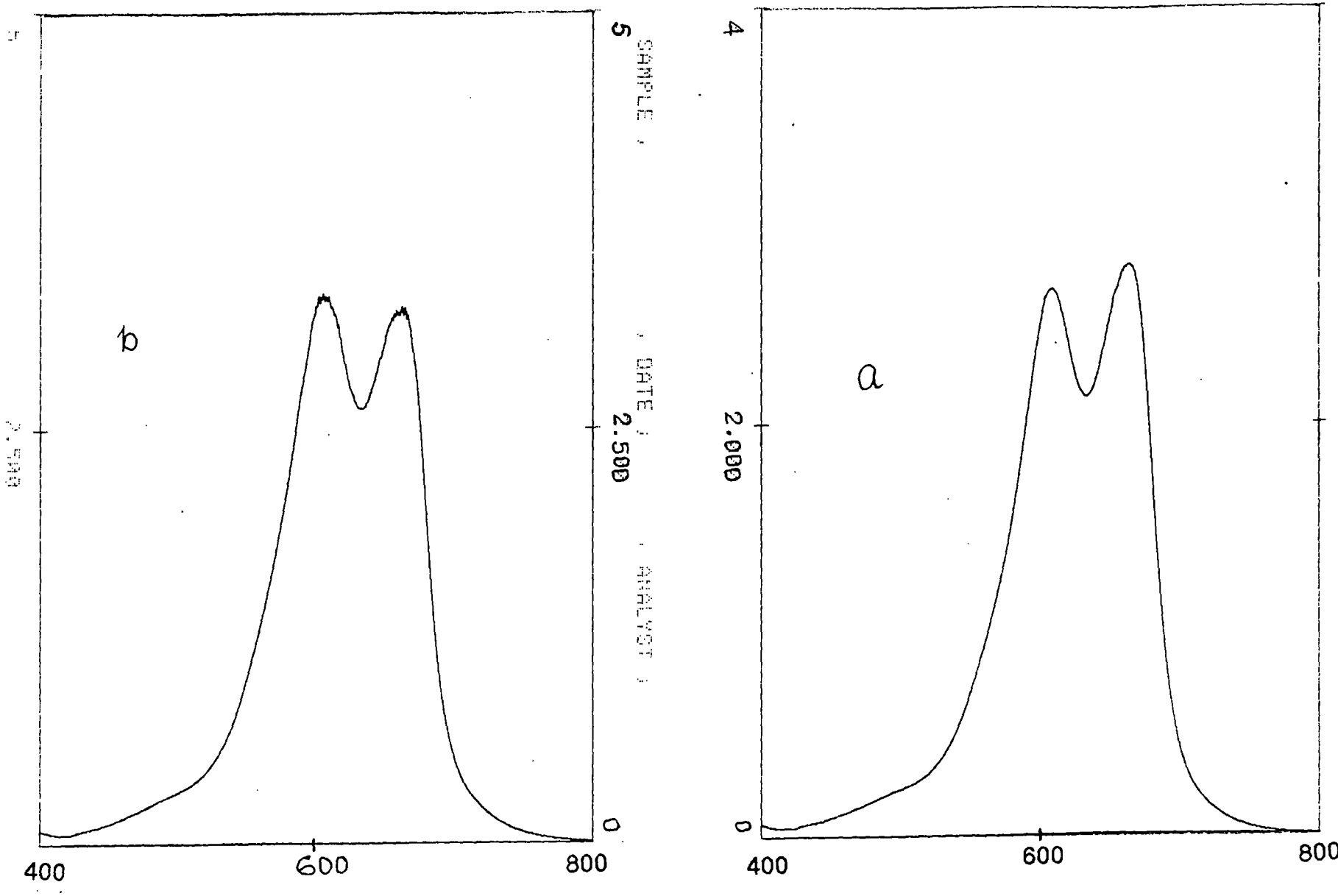

Fig. 12 Visible absorption spectra of Methylene Blue (a) 6×10^{-4}M and (b) 8×10^{-4}M in 20% Ethanol at 20^{0}C in the presence of 0.01M KCl.

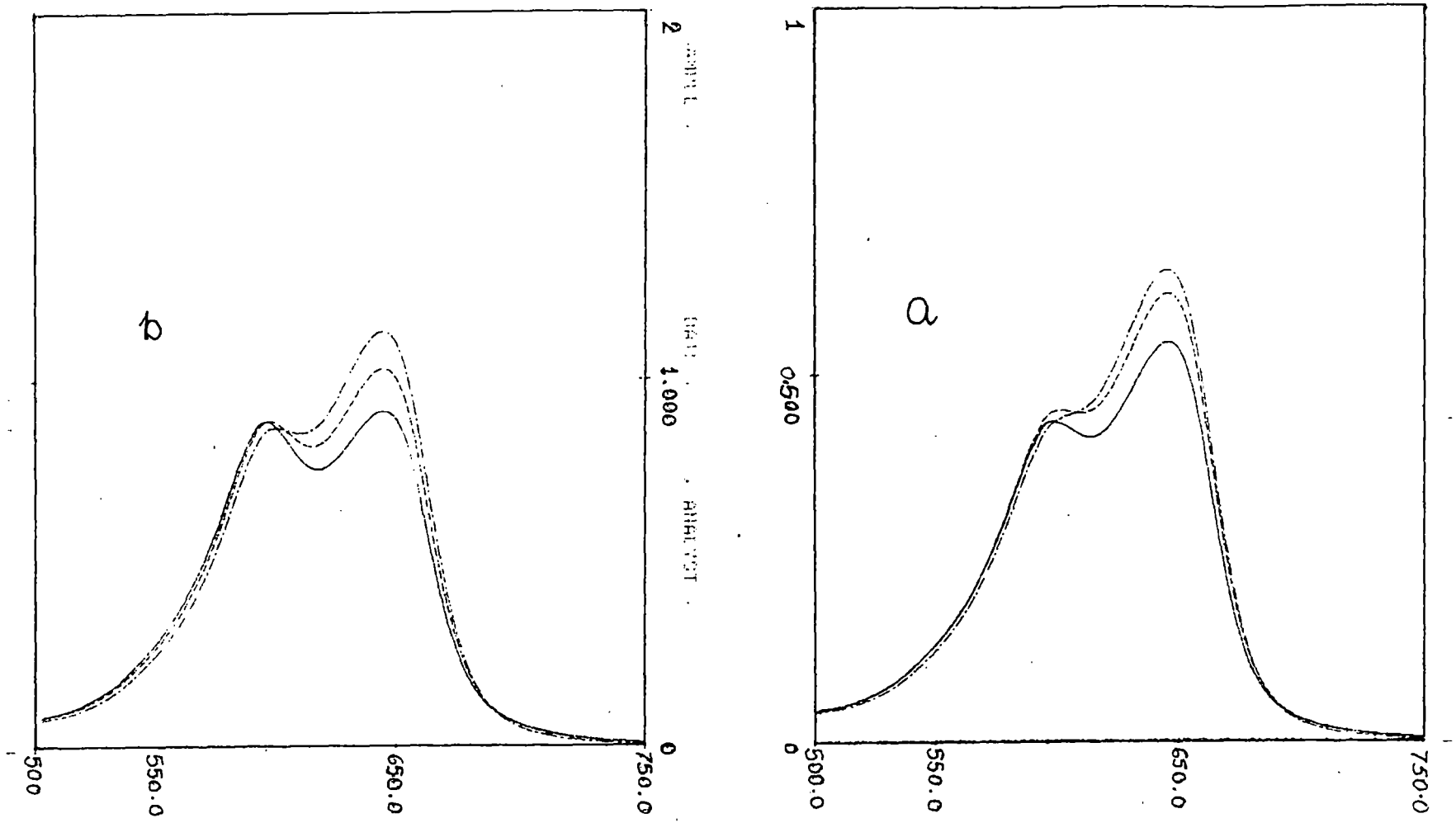

Fig. 13 Visible absorption spectra of Azure B (a) $1x10^{-4}$M and (b) $2x10^{-4}$M in 5% Ethanol at 30^0, 40^0 and 50^0C in the presence of 0.01M KCl.

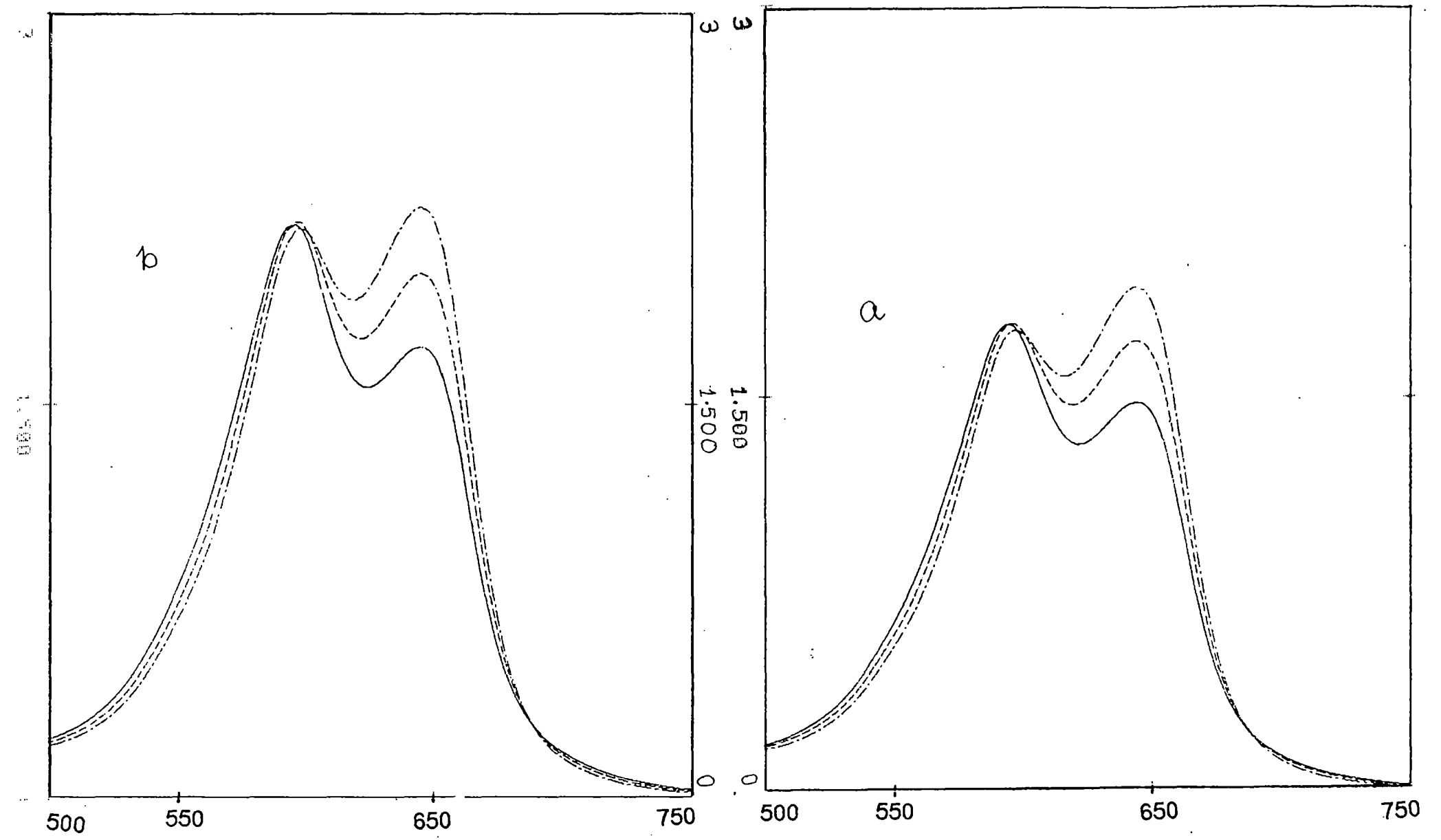

Fig. 14 Visible absorption spectra of Azure B (a) $4x10^{-4}M$ and (b) $5x10^{-4}M$ in 5% Ethanol at 30^0,40^0 and 50^0C in the presence of 0.01 KCl.

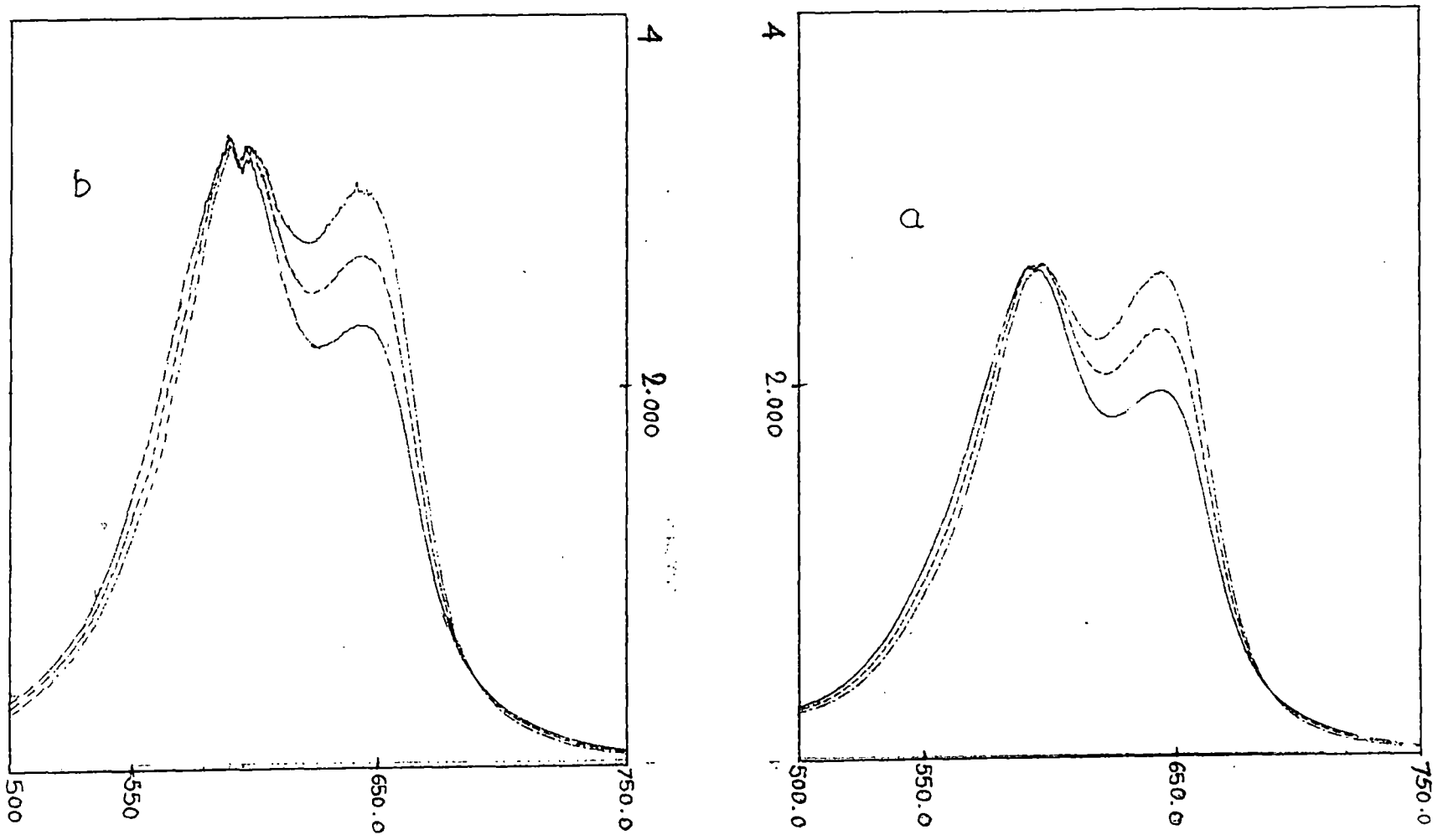

Fig. 15 Visible absorption spectra of Azure B (a) $6x10^{-4}M$ and (b) $8x10^{-4}M$ in 5% Ethanol at 30^0, 40^0 and 50^0C in the presence of 0.01M KCl.

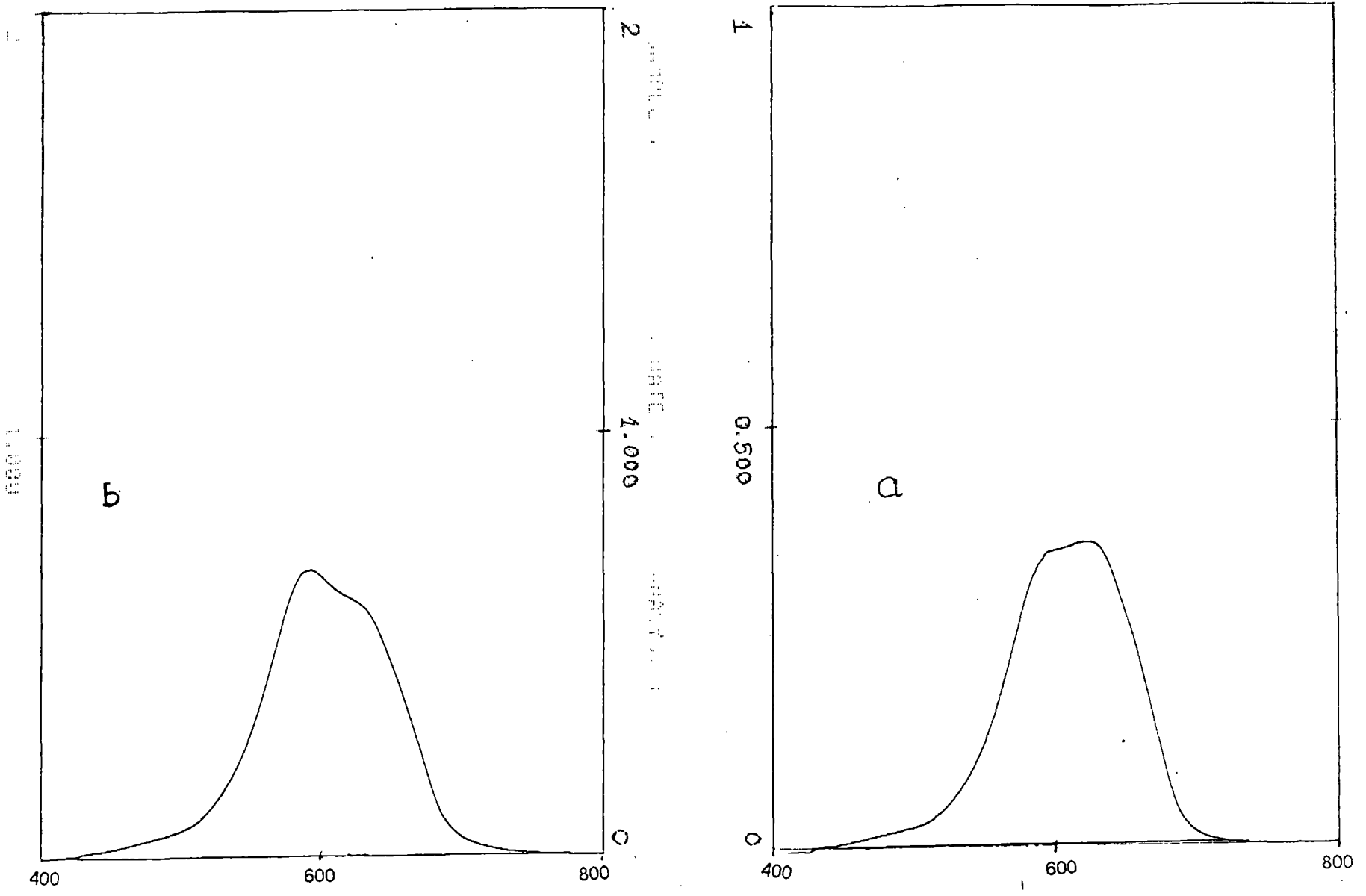

Fig. 16 Visible absorption spectra of Azure A (a) $1x10^{-4}M$ and (b) $2x10^{-4}M$ in 5% Ethanol at 20^0C in the presence of 0.01M KCl.

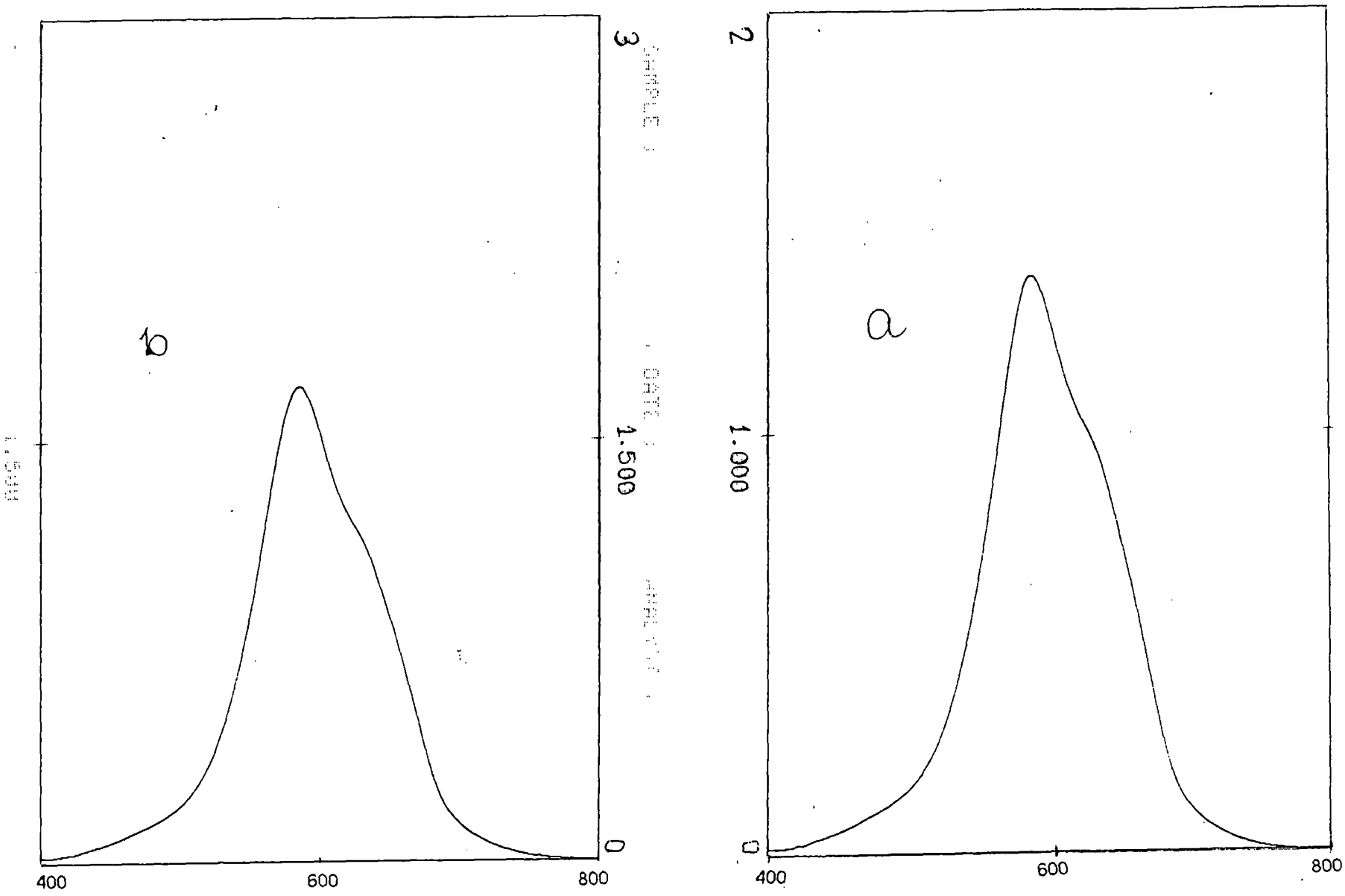

Fig. 17 Visible absorption spectra of Azure A (a) 4×10^{-4}M and (b) 5×10^{-4}M in 5% Ethanol at 20^{0}C in the presence of 0.01M KCl.

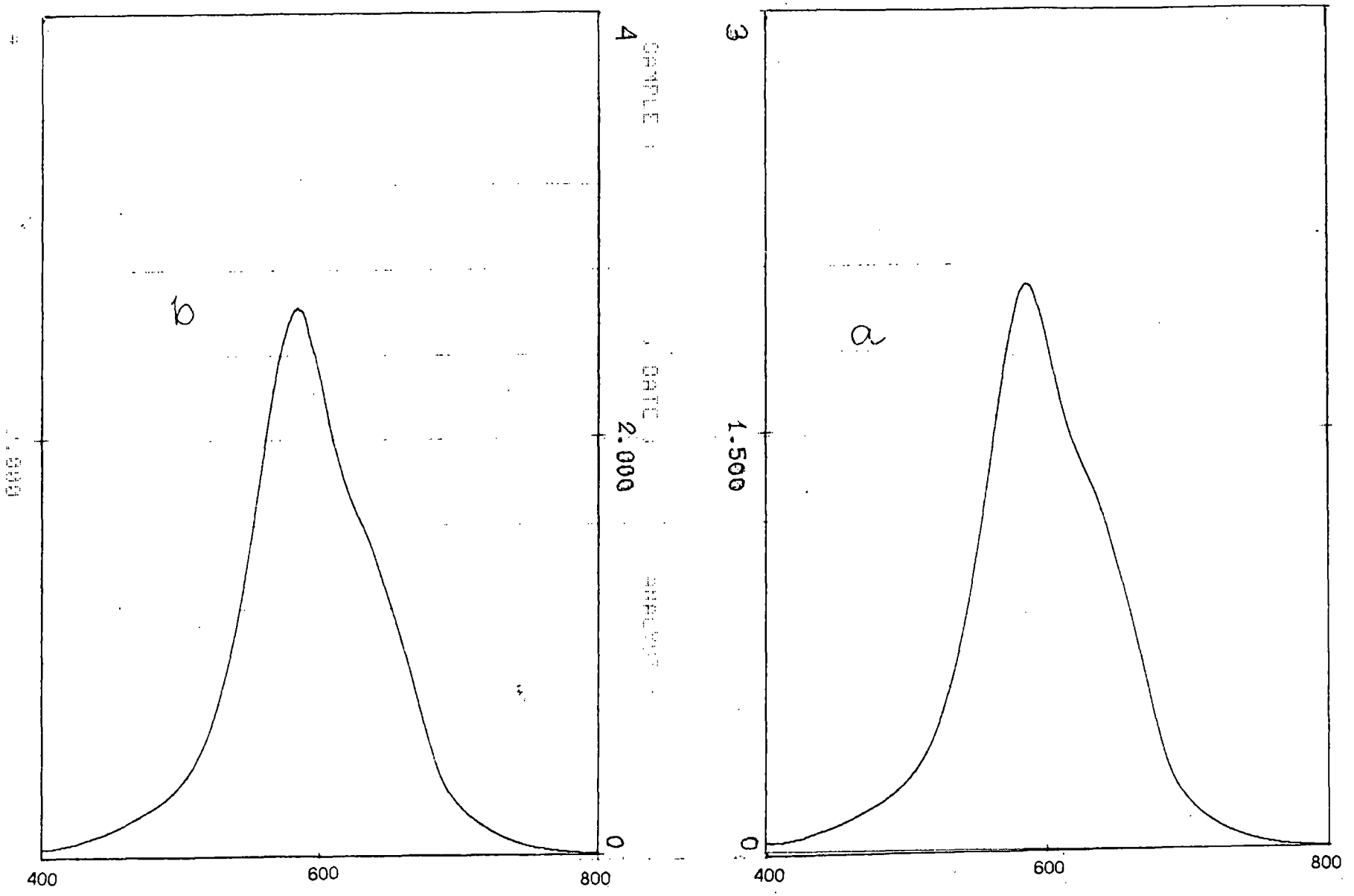

Fig. 18 Visible absorption spectra of Azure A (a) 6×10^{-4}M and (b) 8×10^{-4}M in 5% Ethanol at 20^{0}C in the presence of 0.01M KCl.

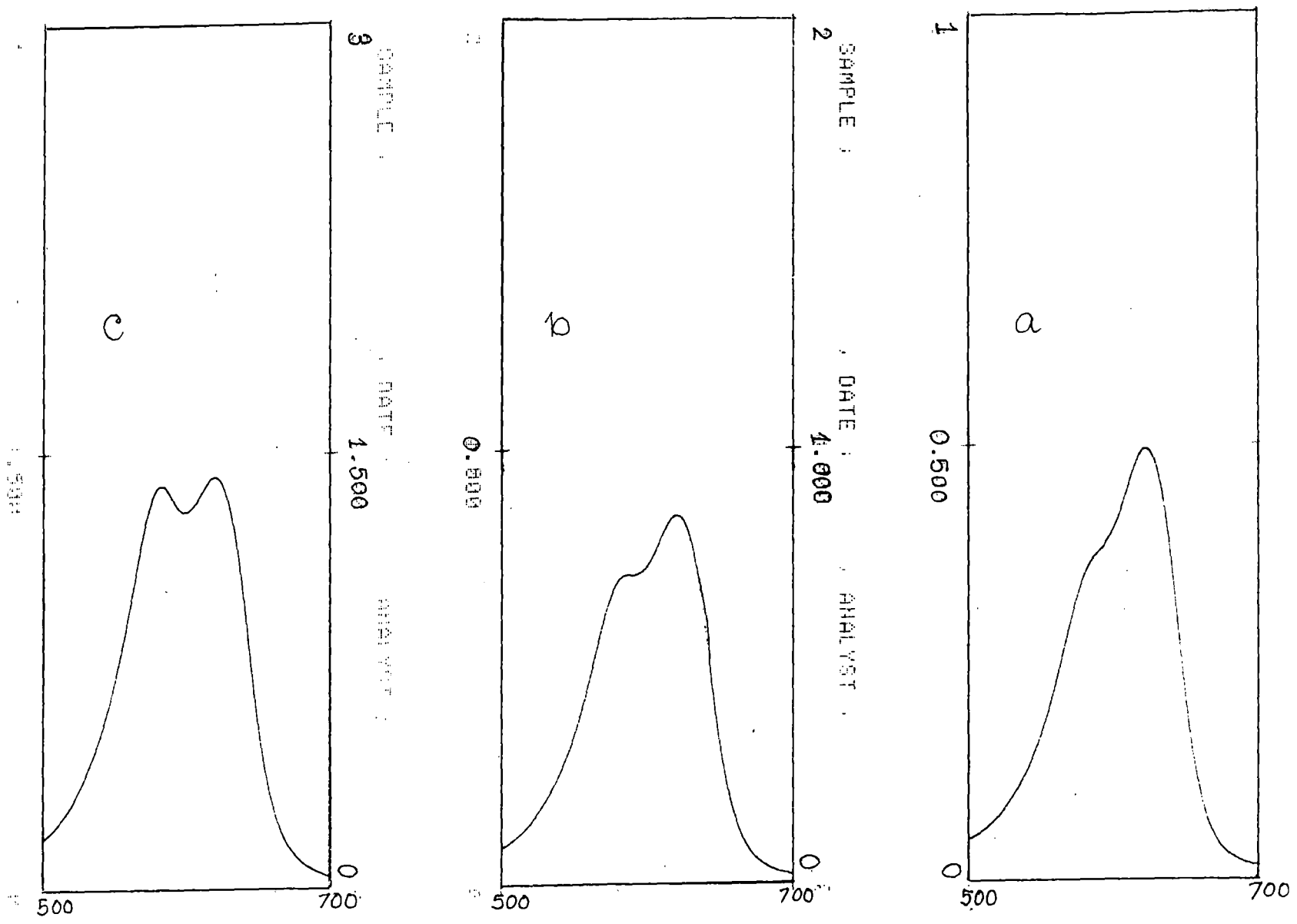

Fig. 19 Visible absorption spectra of Azure C (a) $1x10^{-4}M$, (b) $2x10^{-4}M$ and (c) $4x10^{-4}M$ in 10% Ethanol at 30^0C in the presence of 0.01M KCl.

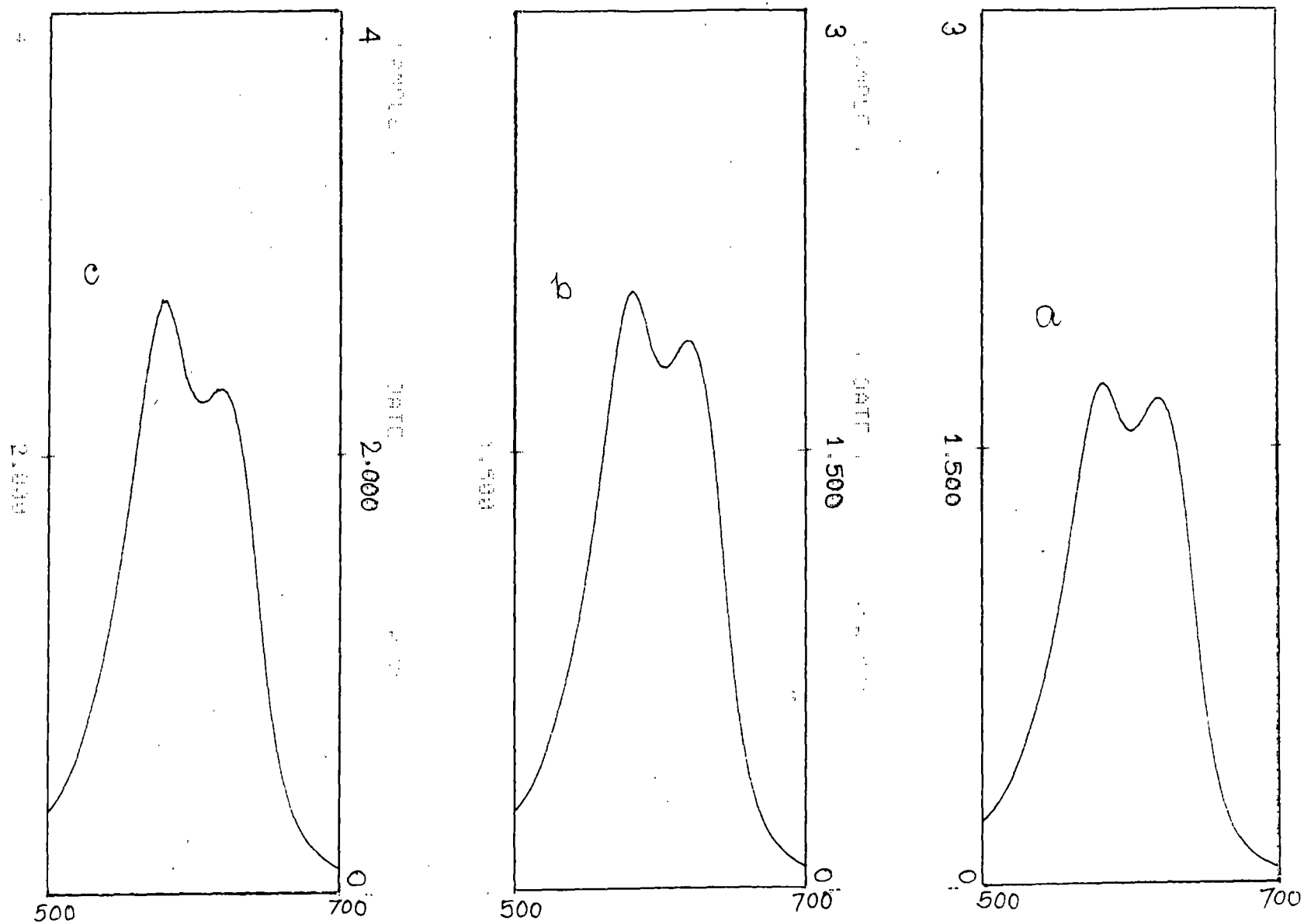

Fig. 20 Visible absorption spectra of Azure C (a) 5×10^{-4}M, (b) 6×10^{-4}M and (c) 8×10^{-4}M in 10% Ethanol at 30^{0}C in the presence of 0.01M KCl.

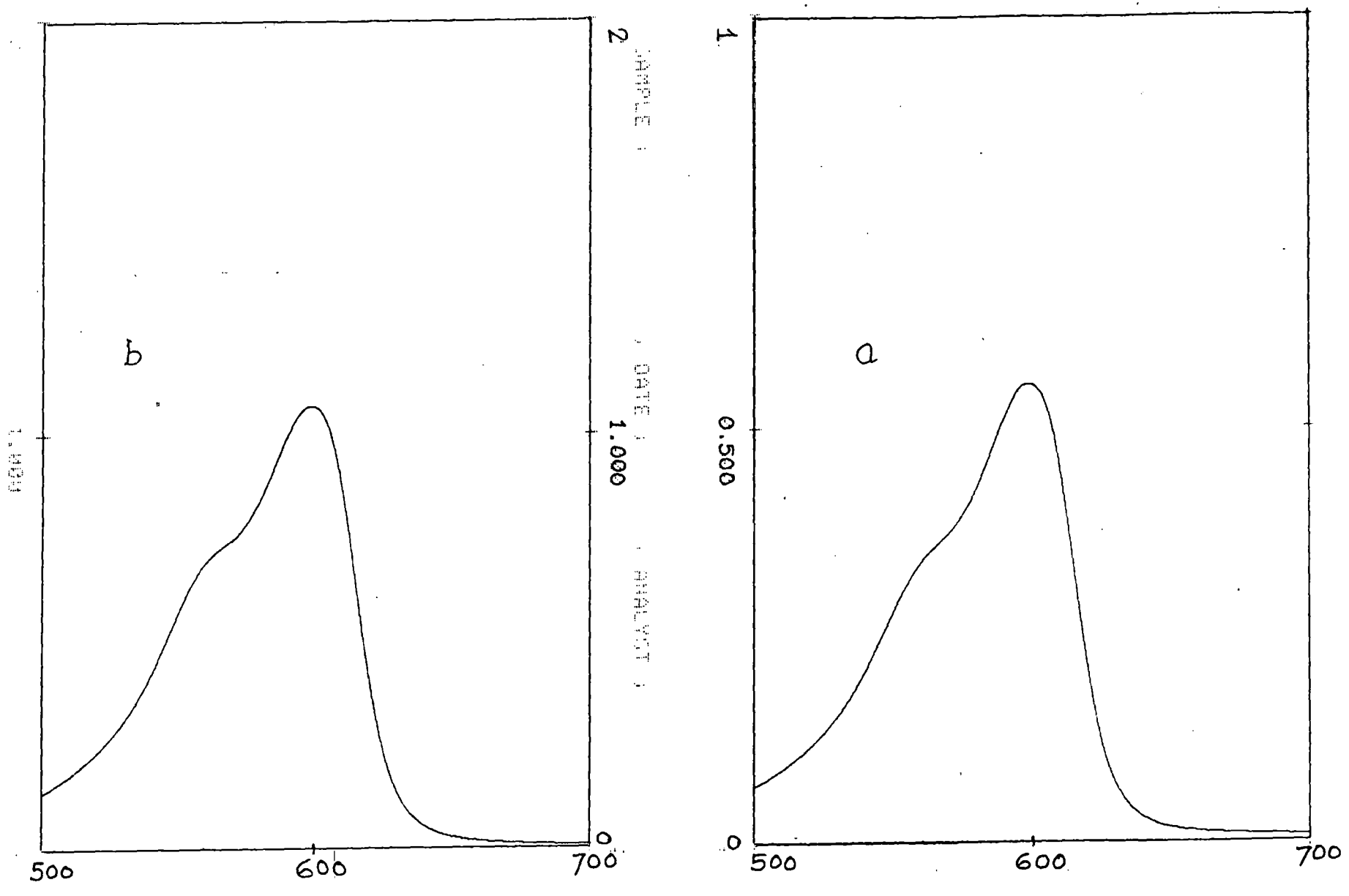

Fig.21: Visible Absorption spectra of Thionine (a) 1×10^{-4}M and (b) 2×10^{-4}M in 15% Ethanol at 30°C in the presence of 0.01 M KCl.

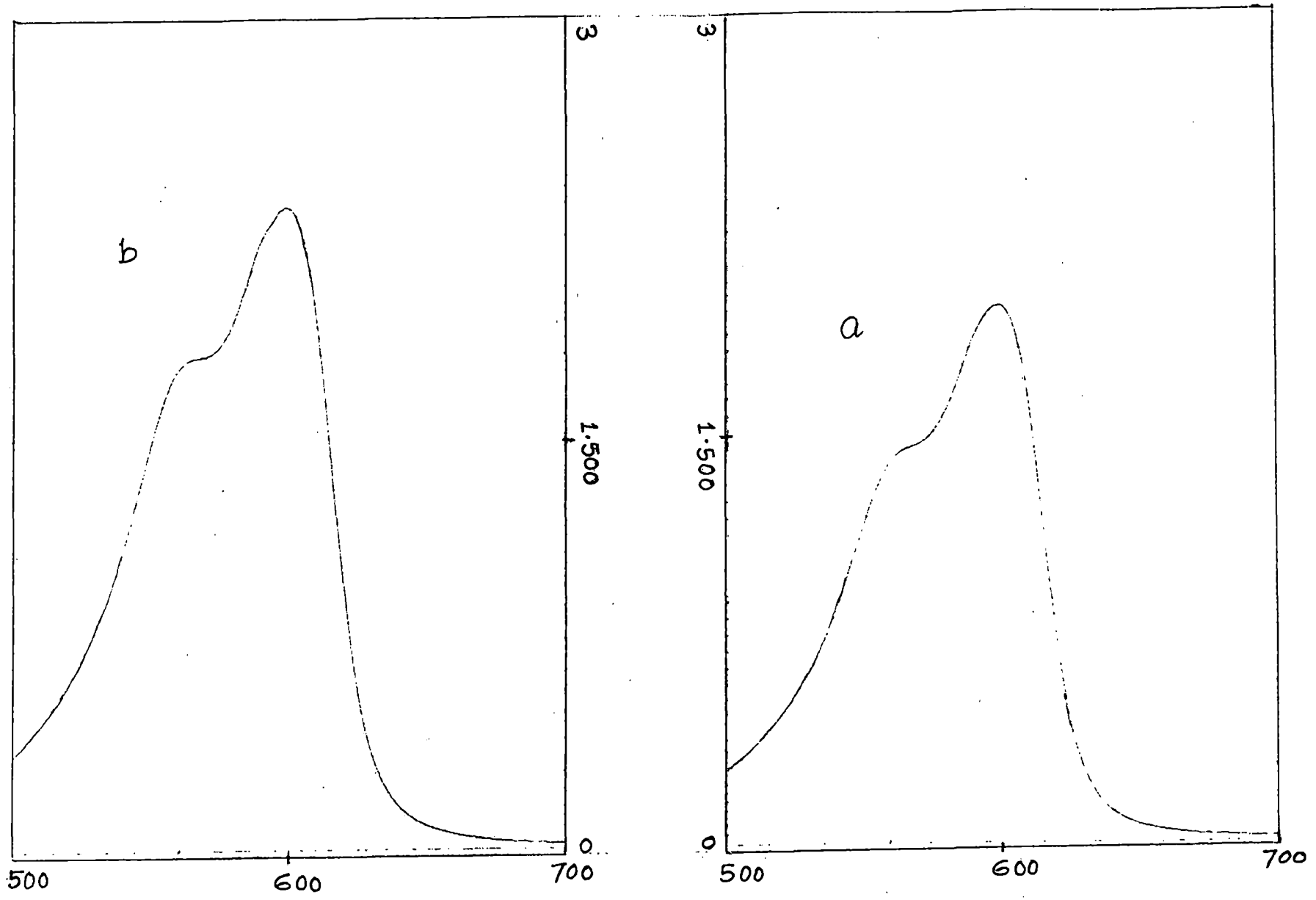

Fig.22: Visible Absorption spectra of Thionine (a) $4x10^{-4}$M and (b) $5x10^{-4}$M in 15% Ethanol at 30°C in the presence of 0.01 M KCl.

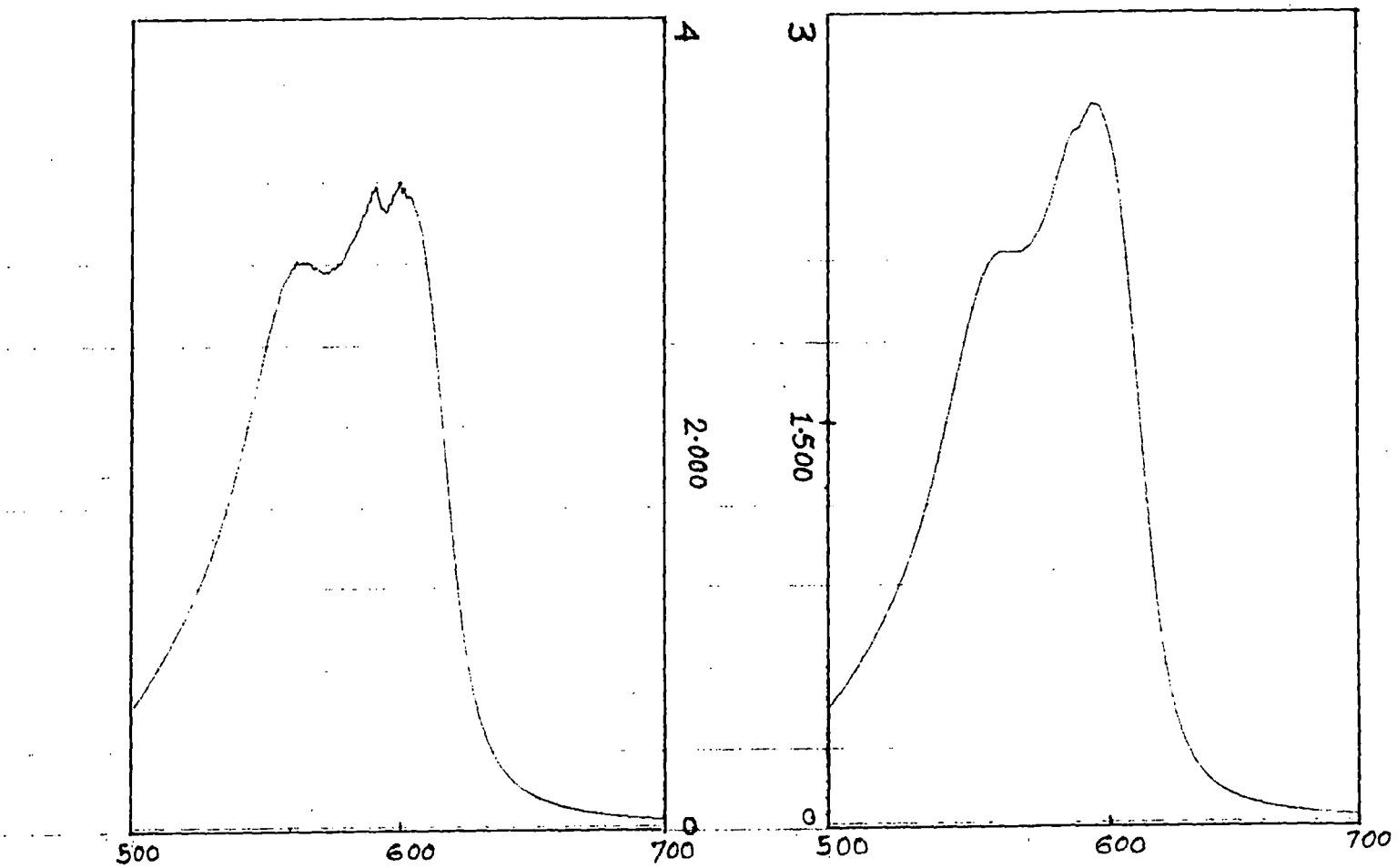

Fig.23: Visible Absorption spectra of Thionine (a) $6x10^{-4}M$ and (b) $8x10^{-4}M$ in 15% Ethanol at 30°C in the presence of 0.01 M KCl.

is expressed as

$$K_d = \frac{1-x}{2Cx^2} \qquad (27)$$

where the monomer and dimer concentrations are [M] = Cx and [D] = C(1−x)/2; x is the monomer molar fraction at a concentration C . The absorptivity of this concentration at frequancy ν is

$$\bar{\epsilon}_\nu = \epsilon^m_\nu .x + \epsilon^d_\nu (1-x) \qquad (28)$$

where ϵ^d_ν is the absorptivity of the monomer in the dimer. When x ≅ 1, for dilute solution, the spectrum is purely monomer spectrum, $\bar{\epsilon}_\nu = \epsilon^m_\nu$. The above equation can be resolved into the following forms :

$$\bar{\epsilon}_{\nu_m} = \epsilon^m_{\nu_m} .x + \epsilon^d_{\nu_m} (1-x)$$

$$\bar{\epsilon}_{\nu_d} = \epsilon^m_{\nu_d} .x + \epsilon^d_{\nu_d} (1-x) \qquad (29)$$

where ν_m and ν_d are the frequencies corresponding to maximum absorption in pure monomer and dimer spectra respectively and,

$\bar{\epsilon}_{\nu_m}$, the average absorptivity at ν_m.

$\bar{\epsilon}_{\nu_d}$, the average absorptivity at ν_d.

$\epsilon^m_{\nu_m}$, the absorptivity at ν_m in pure monomer spectrum.

$\epsilon^{d}_{\nu_m}$, the absorptivity at ν_m in pure dimer spectrum.
$\epsilon^{m}_{\nu_d}$, the absorptivity at ν_d in pure monomer spectrum.
$\epsilon^{d}_{\nu_d}$, the absorptivity at ν_d in pure dimer spectrum.

To know the monomer fraction (x), by which dimer spectrum ϵ^{d}_{ν} can be calculated from equation 28, the following method (51) is employed. The knowledge of absorptivity in the visible region, at high dye concentrations allows the use of the following iterative method. The parameter (R) is defined by the relation,

$$R \cong \frac{A_{\nu_d}}{A_{\nu_m}} = \frac{\epsilon^{m}_{\nu_d} .x + \epsilon^{d}_{\nu_d} (1-x)}{\epsilon^{m}_{\nu_m} .x + \epsilon^{d}_{\nu_m} (1-x)} \qquad (30)$$

For dilute solution $x \cong 1$, the equation 30 becomes

$$R_o = \frac{\epsilon^{m}_{\nu_d}}{\epsilon^{m}_{\nu_m}} \qquad (31)$$

The spectral differences between concentrated and dilute solutions show that $\epsilon^{d}_{\nu_m} < \epsilon^{d}_{\nu_d}$. We assume as a first approximation that $\epsilon^{d}_{\nu_m} << \epsilon^{m}_{\nu_m}$ and $\epsilon^{d}_{\nu_d} \cong \epsilon^{m}_{\nu_d}$ and therefore,

$$x^{(1)} = R_o / R \text{ (first iterative value)}.$$

Then at every concentration, values of $K_d^{(1)}$, $\epsilon^{d(1)}_{\nu_d}$ and $\epsilon^{d(1)}_{\nu_m}$,

using equations 27 - 29, are found out.

From these average values of the absorptivities and using equation 30, a second value of the monomer fraction $x^{(2)}$ is determined. This value is again introduced in the iteration process [calculations are made on a PC-AT (486 DX2) computer by means of a program written in BASIC language]. It is observed that three iterations are enough to make the difference between two consecutive monomer fraction values less than 0.001. Using the computed x value K_d is determined.

Values of λ_{max} and ϵ in the spectra of very dilute aqueous solution ($5x10^{-6}M$) as well as various aqueous-ethanolic solutions are shown in table 1. From the table it is seen that the absorbances near λ_{max} in these monomer spectra increase slightly as the percentage of ethanol increases.

The dimer absorption spectra, calculated by means of the equation 28, of all the five dyes are shown in Figs. 24-28. All the dimer spectra are composed of two bands of monomer with their maxima at greater and smaller energy than the monomer maximum respectively (51). Some of the characteristics of dimer spectra are listed in table 2. The dimerization constants (K_d) and the corresponding monomer fraction (x) of all the dyes at different temperatures and solvents are given in table 3-7. The dimerization constant decreases with the increase in temperature and percentage of ethanol in the medium. This clearly indicates that the dissociation of aggregates is favoured with the rise of

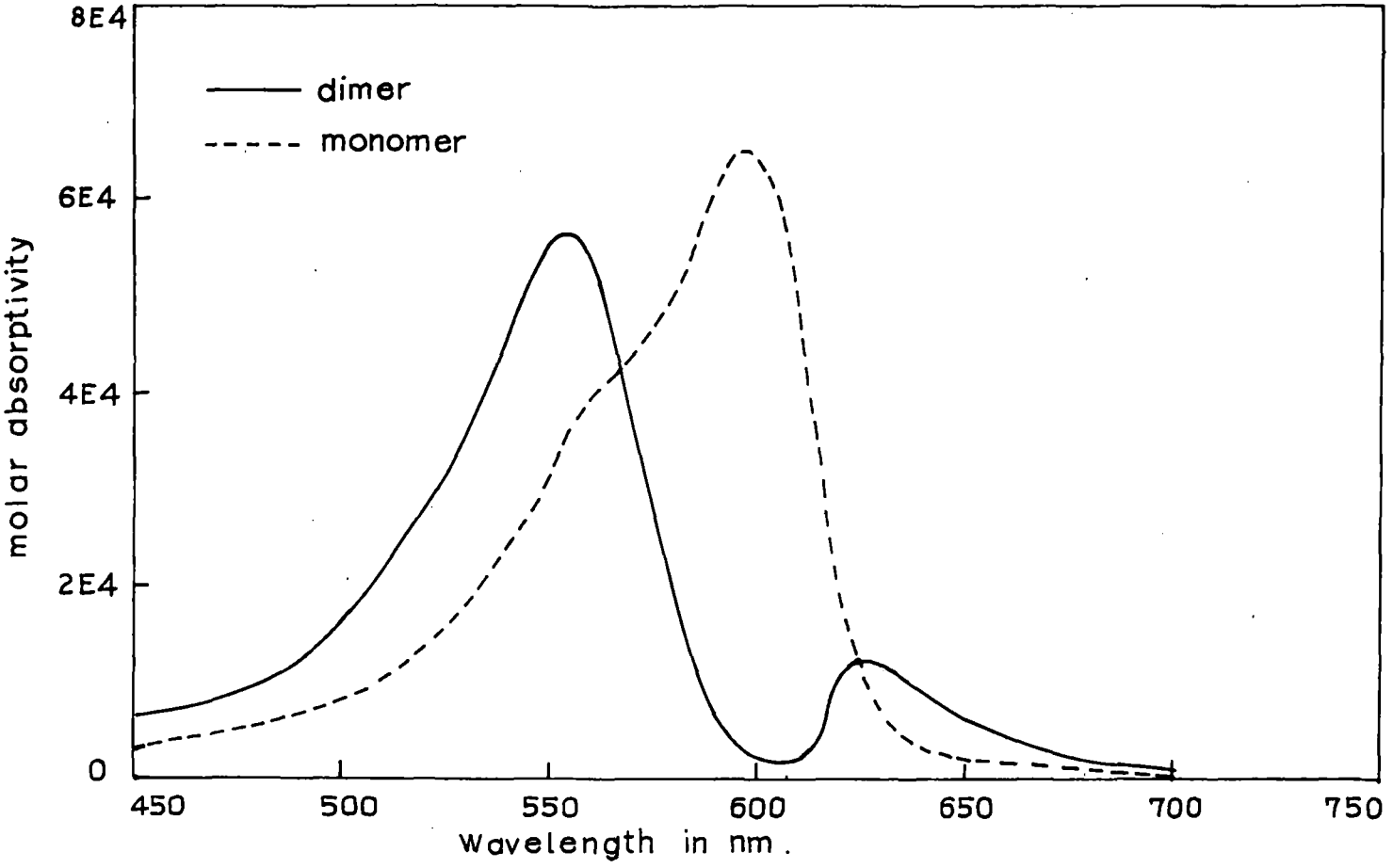

Fig. 2.4 Absorption spectra of Thionine .

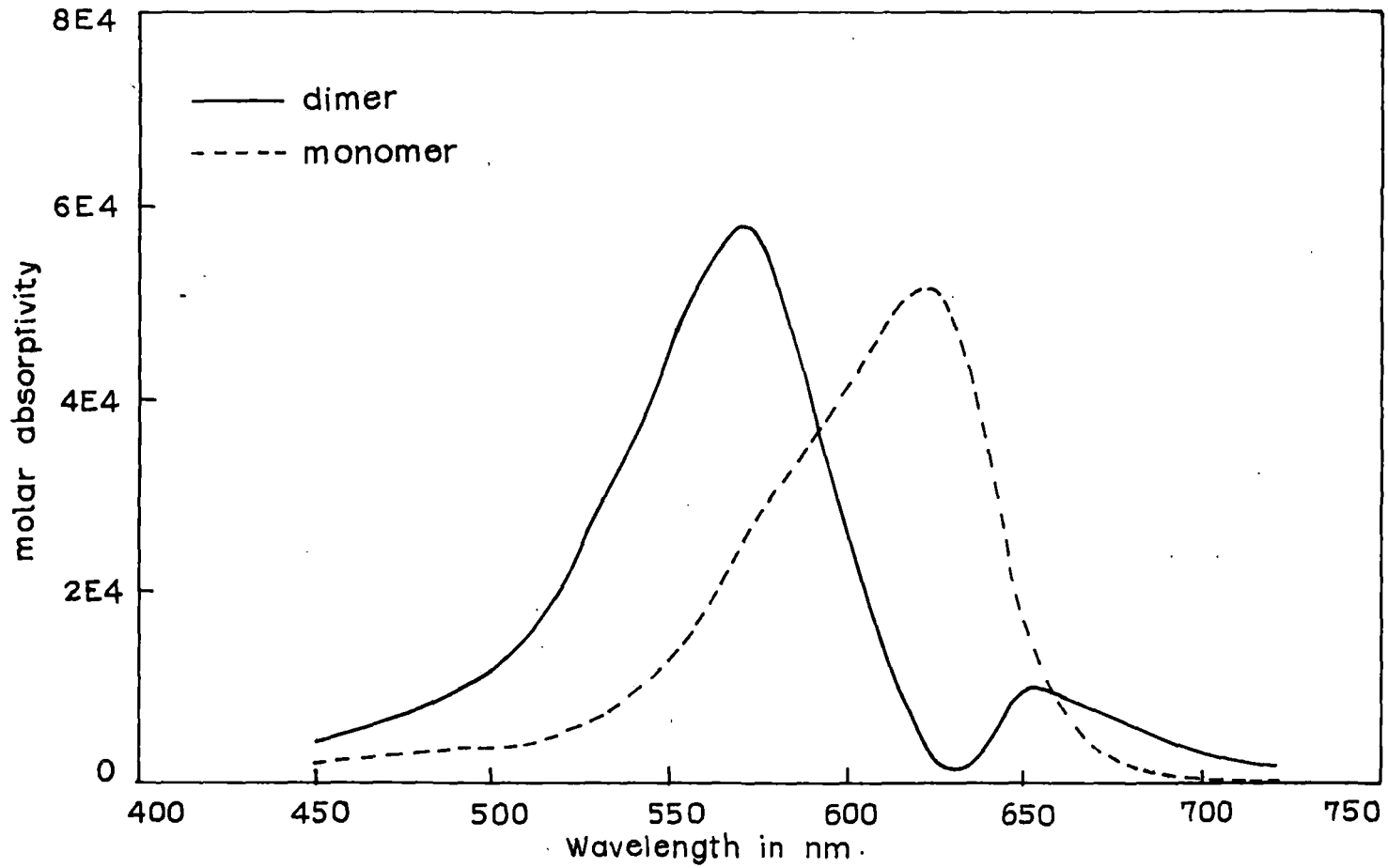

Fig. 25 Absorption spectra of Azure C.

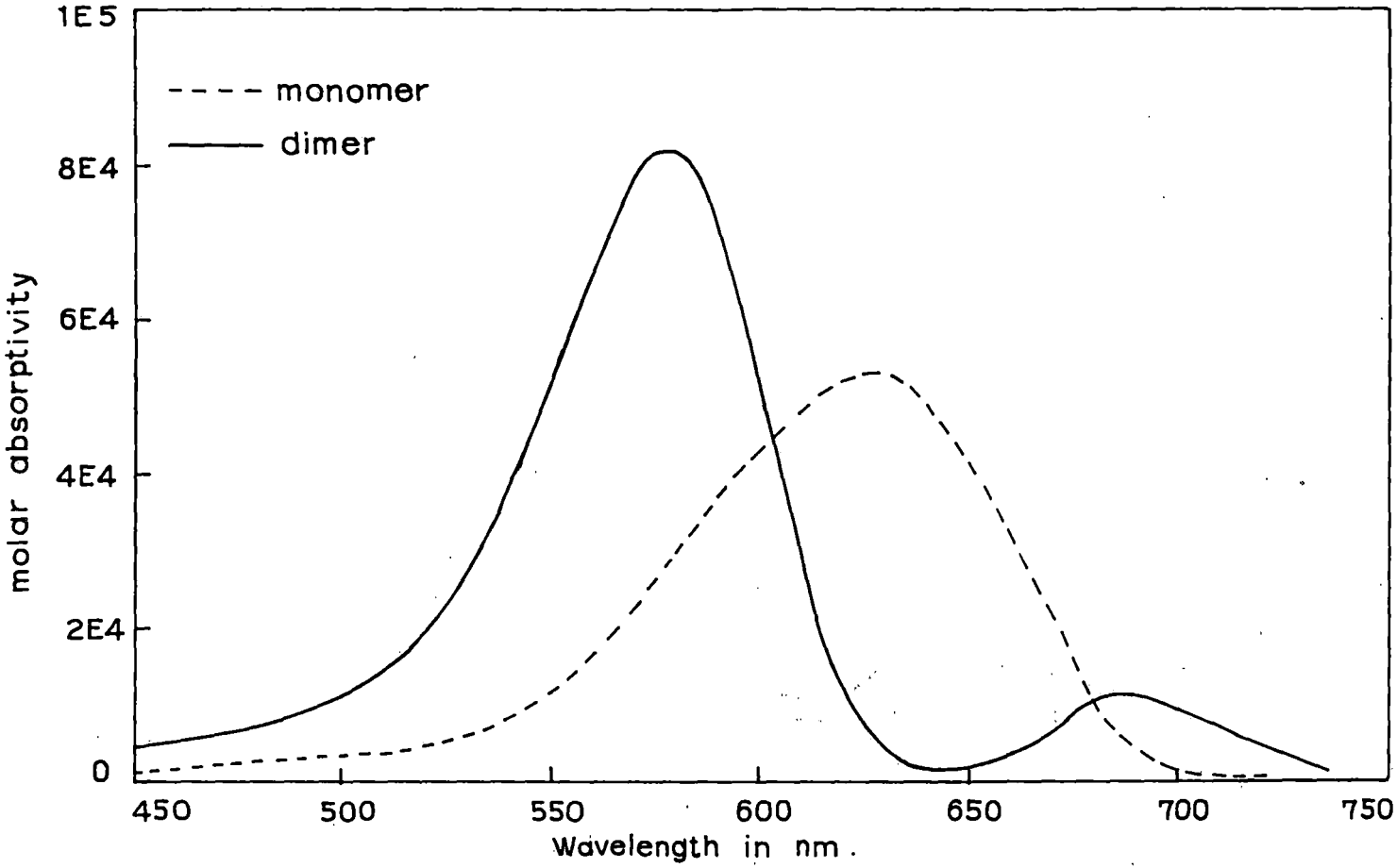

Fig.26 Absorption spectra of Azure A

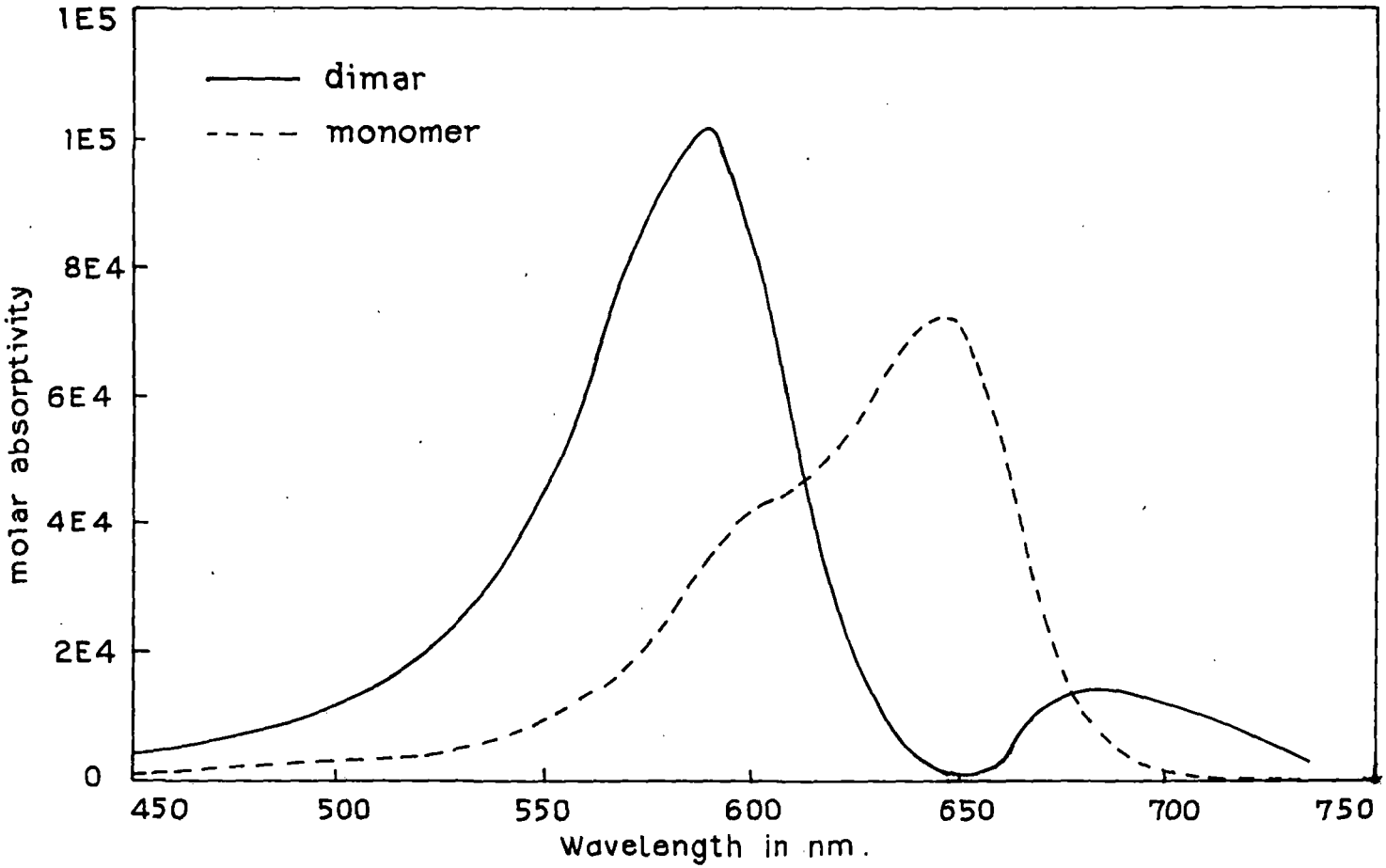

Fig.27 Absorption spectra of Azure B

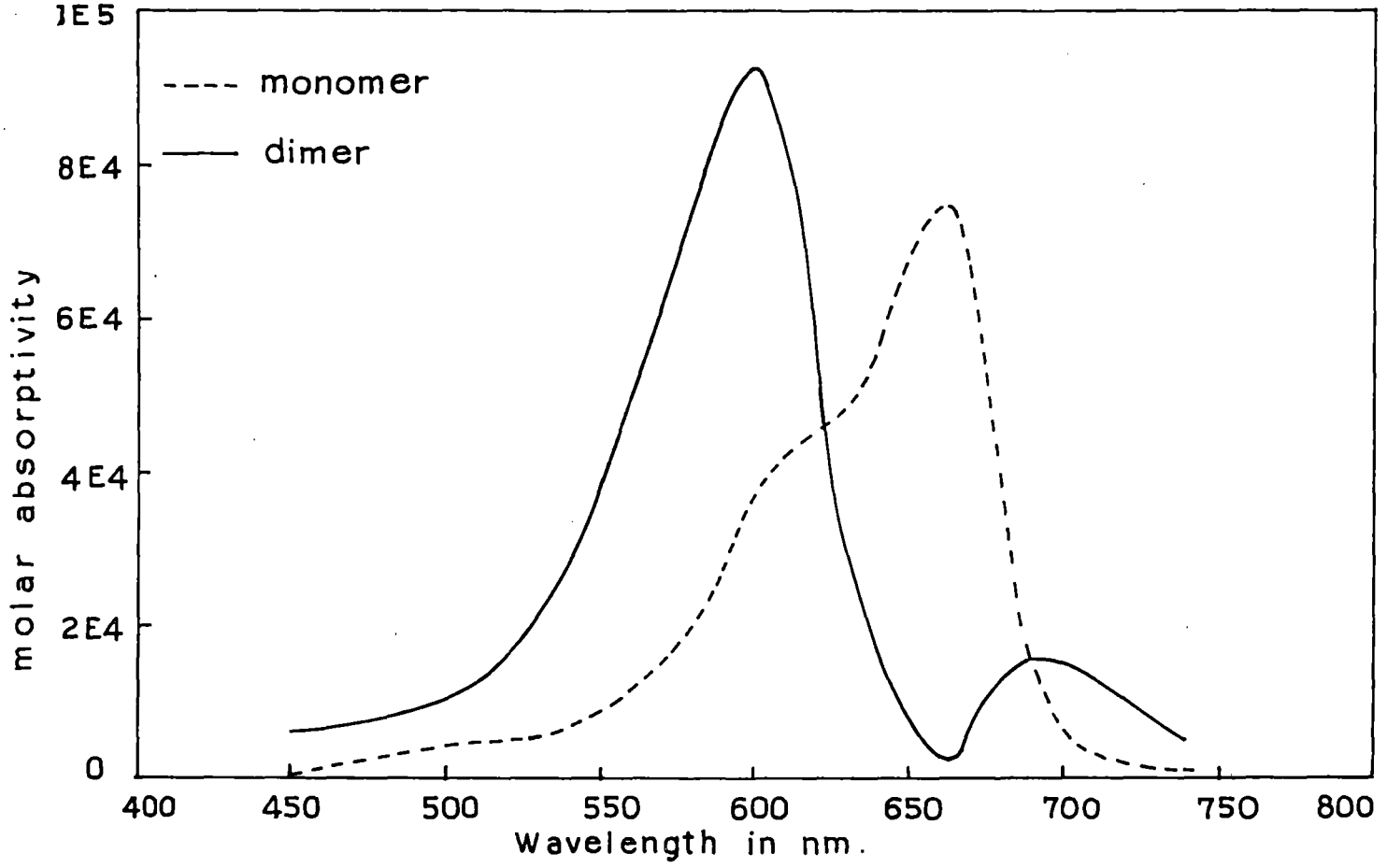

Fig.28 Absorption spectra of Methylene Blue .

Table-1

Some of the characteristics of monomer spectra of the dyes in aqueous and aqueous-ethanolic solvents

	Th	AzC	AzA	AzB	MB
Water					
λ_{max} (nm)	596	620	630	645	661
$\epsilon \times 10^{-4}$	6.16	4.96	5.18	6.90	7.20
5% EtOH					
λ_{max} (nm)	596	620	630	645	664
$\epsilon \times 10^{-4}$	6.48	4.88	5.46	7.04	7.34
10% EtOH					
λ_{max} (nm)	597	622	631	647	666
$\epsilon \times 10^{-4}$	6.52	4.98	5.58	7.22	7.40
15% EtOH					
λ_{max} (nm)	600	624	633	648	668
$\epsilon \times 10^{-4}$	6.60	5.28	5.74	7.62	7.50
20% EtOH					
λ_{max} (nm)	602	624	634	649	668
$\epsilon \times 10^{-4}$	6.76	5.22	5.76	7.66	7.64

Table-2

Some of the characteristics of dimer spectra of the dyes in aqueous medium

Dye	λ_1 (nm)	λ_2 (nm)	$\epsilon_1 \times 10^{-4}$	$\epsilon_2 \times 10^{-4}$
Th	555	630	5.62	1.11
AzC	571	651	5.75	0.96
AzA	575	687	8.17	1.16
AzB	588	682	10.11	1.50
MB	600	691	9.27	1.03

Table 3

Values of Dimerization Constant (K_d) and Monomer Fraction (X) of Thionine in Water at different temperatures and concentrations

Cons.$\times 10^{4}$M	X	Temp.	$K_d \times 10^{-3}$ (lit/mol)	Average $K_d \times 10^{-3}$ (lit/mol)
1.0	.7011		3.040	
2.0	.6121		2.587	
4.0	.5100	20°C	2.353	2.439
5.0	.4845		2.194	
6.0	.4511		2.247	
8.0	.4085		2.215	
1.0	.7794		1.815	
2.0	.6518		2.048	
4.0	.5739	30°C	1.617	1.761
5.0	.5212		1.761	
6.0	.4995		1.671	
8.0	.4540		1.655	
1.0	.7970		1.597	
2.0	.6912		1.615	
4.0	.6123	40°C	1.292	1.380
5.0	.5715		1.311	
6.0	.5457		1.271	
8.0	.5072		1.197	
1.0	.8464		1.072	
2.0	.7401		1.186	
4.0	.6597	50°C	0.977	1.053
5.0	.6232		0.970	
6.0	.5730		1.083	
8.0	.5318		1.034	contd.

Table-3

Values of Dimerization Constant (K_d) and Monomer Fraction (X) of Thionine in 5% Ethanol at different temperatures and concentrations

Cons.x10^4M	X	Temp.	K_d x10^{-3} (lit/mol)	Average K_d x10^{-3} (lit/mol)
1.0	.7272		2.578	
2.0	.6480		2.095	
4.0	.5522	20°C	1.834	1.893
5.0	.5289		1.683	
6.0	.5027		1.639	
8.0	.4664		1.532	
1.0	.7618		2.051	
2.0	.6923		1.604	
4.0	.6079	30°C	1.325	1.447
5.0	.5774		1.267	
6.0	.5497		1.241	
8.0	.5076		1.194	
1.0	.7838		1.759	
2.0	.7274		1.287	
4.0	.6517	40°C	1.024	1.135
5.0	.6425		0.865	
6.0	.5925		0.966	
8.0	.5540		0.908	
1.0	.7889		1.695	
2.0	.7562		1.065	
4.0	.6820	50°C	0.854	1.029
5.0	.6558		0.800	
6.0	.6114		0.865	
8.0	.5557		0.898	contd.

Table-3

Values of Dimerization Constant (K_d) and Monomer Fraction (X) of Thionine in 10% Ethanol at different temperatures and concentrations

Conc.x10^4M	X	Temp.	K_d x10^{-3} (lit/mol)	Average K_d x10^{-3} (lit/mol)
1.0	.7709		1.927	
2.0	.6734		1.800	
4.0	.5772	20°C	1.585	1.631
5.0	.5328		1.645	
6.0	.5232		1.451	
8.0	.4837		1.378	
1.0	.7934		1.640	
2.0	.7260		1.299	
4.0	.6323	30°C	1.149	1.220
5.0	.6097		1.049	
6.0	.5733		1.081	
8.0	.5215		1.099	
1.0	.8107		1.439	
2.0	.7570		1.059	
4.0	.6796	40°C	0.867	1.003
5.0	.6513		0.821	
6.0	.6202		0.822	
8.0	.5358		1.010	
1.0	.8196		1.341	
2.0	.7828		0.885	
4.0	.7258	50°C	0.650	0.817
5.0	.6957		0.628	
6.0	.6647		0.632	
8.0	.5828		0.767	contd.

Table-3

Values of Dimerization Constant (K_d) and Monomer Fraction (X) of Thionine in 15% Ethanol at different temperatures and concentrations

Cons.x10^4M	X	Temp.	K_d x10^{-3} (lit/mol)	Average K_d x10^{-3} (lit/mol)
1.0	.7780		1.832	
2.0	.6959		1.569	
4.0	.5747	20°C	1.686	1.805
5.0	.5223		1.750	
6.0	.4792		1.889	
8.0	.4163		2.104	
1.0	.8153		1.388	
2.0	.7845		0.874	
4.0	.7004	30°C	0.763	0.895
5.0	.6652		0.756	
6.0	.6395		0.734	
8.0	.5638		0.857	
1.0	.8404		1.129	
2.0	.8175		0.682	
4.0	.7498	40°C	0.556	0.696
5.0	.7343		0.492	
6.0	.6729		0.601	
8.0	.5951		0.714	
1.0	.8391		1.141	
2.0	.8319		0.607	
4.0	.7747	50°C	0.469	0.625
5.0	.7655		0.400	
6.0	.7103		0.478	
8.0	.6090		0.658	

contd.

Table-3

Values of Dimerization Constant (K_d) and Monomer Fraction (X) of Thionine in 20% Ethanol at different temperatures and concentrations

Cons.x10^4M	X	Temp.	K_d x10^{-3} (lit/mol)	Average K_d x10^{-3} (lit/mol)
1.0	.8672		0.882	
2.0	.7689		0.977	
4.0	.6811	20°C	0.859	0.825
5.0	.6660		0.753	
6.0	.6366		0.747	
8.0	.5904		0.734	
1.0	.8867		0.720	
2.0	.8161		0.690	
4.0	.7422	30°C	0.585	0.630
5.0	.7054		0.592	
6.0	.6945		0.527	
8.0	.6077		0.663	
1.0	.8760		0.807	
2.0	.8620		0.464	
4.0	.8117	40°C	0.357	0.507
5.0	.7759		0.372	
6.0	.7221		0.443	
8.0	.6241		0.603	
1.0	.9217		0.460	
2.0	.8721		0.420	
4.0	.8290	50°C	0.310	0.413
5.0	.8011		0.309	
6.0	.7344		0.410	
8.0	.6337		0.569	

Table-4

Values of Dimerization Constant (K_d) and Monomer Fraction (X) of Azure C in Water at different temperatures and concentrations

Conc.x10^4M	X	Temp.	K_d x10^{-3} (lit/mol)	Average K_d x10^{-3} (lit/mol)
1.0	.6634		3.821	
2.0	.5757		3.200	
4.0	.4748	20°C	2.911	2.953
5.0	.4493		2.726	
6.0	.4240		2.669	
8.0	.3971		2.389	
1.0	.7071		2.928	
2.0	.6239		2.415	
4.0	.5126	30°C	2.318	2.350
5.0	.4810		2.242	
6.0	.4557		2.183	
8.0	.4231		2.012	
1.0	.7175		2.743	
2.0	.6853		1.674	
4.0	.5788	40°C	1.570	1.746
5.0	.5458		1.524	
6.0	.5163		1.512	
8.0	.4749		1.454	
1.0	.7442		2.309	
2.0	.7352		1.224	
4.0	.6447	50°C	1.068	1.290
5.0	.6093		1.052	
6.0	.5767		1.060	
8.0	.5323		1.031	

contd.

Table-4

Values of Dimerization Constant (K_d) and Monomer Fraction (X) of Azure C in 5% Ethanol at different temperatures and concentrations

Cons.x10^{4}M	X	Temp.	K_d x10^{-3} (lit/mol)	Average K_d x10^{-3} (lit/mol)
1.0	.7219		2.667	
2.0	.5934		2.886	
4.0	.4904	20°C	2.647	2.615
5.0	.4661		2.456	
6.0	.4317		2.539	
8.0	.3907		2.493	
1.0	.7799		1.808	
2.0	.6538		1.976	
4.0	.5477	30°C	1.884	1.860
5.0	.5110		1.872	
6.0	.4859		1.814	
8.0	.4402		1.804	
1.0	.7880		1.706	
2.0	.7122		1.418	
4.0	.5983	40°C	1.402	1.479
5.0	.5626		1.381	
6.0	.5215		1.465	
8.0	.4698		1.501	
1.0	.7994		1.569	
2.0	.7486		1.121	
4.0	.6747	50°C	0.892	1.045
5.0	.6462		0.847	
6.0	.6014		0.917	
8.0	.5509		0.924	contd.

Table-4

Values of Dimerization Constant (K_d) and Monomer Fraction (X) of Azure C in 10% Ethanol at different temperatures and concentrations

Cons.x10^4M	X	Temp.	K_d x10^{-3} (lit/mol)	Average K_d x10^{-3} (lit/mol)
1.0	.7208		2.686	
2.0	.6133		2.569	
4.0	.5045	20°C	2.433	2.176
5.0	.5223		1.750	
6.0	.4792		1.889	
8.0	.4470		1.729	
1.0	.7803		1.803	
2.0	.7092		1.444	
4.0	.5895	30°C	1.476	1.560
5.0	.5522		1.468	
6.0	.5144		1.528	
8.0	.4553		1.641	
1.0	.8283		1.251	
2.0	.7670		0.989	
4.0	.6658	40°C	0.942	1.012
5.0	.6330		0.915	
6.0	.5891		0.986	
8.0	.5391		0.990	
1.0	.8398		1.135	
2.0	.7880		0.853	
4.0	.7233	50°C	0.660	0.757
5.0	.7008		0.608	
6.0	.6636		0.636	
8.0	.6113		0.649	

contd.

Table-4

Values of Dimerization Constant (K_d) and Monomer Fraction (X) of Azure C in 15% Ethanol at different temperatures and concentrations

Conc.x10^4M	X	Temp.	K_d x10^{-3} (lit/mol)	Average K_d x10^{-3} (lit/mol)
1.0	.7654		2.002	
2.0	.7070		1.465	
4.0	.6079	20°C	1.326	1.286
5.0	.6141		1.023	
6.0	.5825		1.025	
8.0	.5603		0.875	
1.0	.8591		0.953	
2.0	.7763		0.927	
4.0	.6779	30°C	0.876	0.924
5.0	.6352		0.903	
6.0	.5988		0.931	
8.0	.5459		0.952	
1.0	.8748		0.817	
2.0	.8247		0.643	
4.0	.7399	40°C	0.593	0.666
5.0	.6965		0.625	
6.0	.6666		0.624	
8.0	.6006		0.691	
1.0	.8786		0.786	
2.0	.8461		0.537	
4.0	.7833	50°C	0.441	0.525
5.0	.7529		0.435	
6.0	.7157		0.462	
8.0	.6595		0.489	

contd.

Table-4

Values of Dimerization Constant (K_d) and Monomer Fraction (X) of Azure C in 20% Ethanol at different temperatures and concentrations

Conc.x10^4M	X	Temp.	K_d x10^{-3} (lit/mol)	Average K_d x10^{-3} (lit/mol)
1.0	.8047		1.507	
2.0	.7631		1.016	
4.0	.6939	20°C	0.794	0.926
5.0	.6624		0.769	
6.0	.6450		0.711	
8.0	.5846		0.759	
1.0	.8401		1.131	
2.0	.8069		0.741	
4.0	.7479	30°C	0.563	0.667
5.0	.7193		0.542	
6.0	.7004		0.508	
8.0	.6505		0.515	
1.0	.8437		1.097	
2.0	.8319		0.607	
4.0	.7813	40°C	0.447	0.552
5.0	.7631		0.406	
6.0	.7500		0.370	
8.0	.6990		0.384	
1.0	.8802		0.773	
2.0	.8428		0.553	
4.0	.8146	50°C	0.349	0.489
5.0	.8015		0.309	
6.0	.7728		0.317	
8.0	.7269		0.323	

Table–5

Values of Dimerization Constant (K_d) and Monomer Fraction (X) of Azure A in Water at different temperatures and concentrations

Cons.x10^4M	X	Temp.	K_d x10^{-3} (lit/mol)	Average K_d x10^{-3} (lit/mol)
1.0	.5962		5.680	
2.0	.5123		4.645	
4.0	.4195	20°C	4.123	4.495
5.0	.3759		4.416	
6.0	.3541		4.291	
8.0	.3310		3.816	
1.0	.6493		4.158	
2.0	.5655		3.395	
4.0	.4506	30°C	3.381	3.381
5.0	.4167		3.359	
6.0	.3926		3.283	
8.0	.3783		2.713	
1.0	.6956		3.145	
2.0	.6262		2.382	
4.0	.5064	40°C	2.405	2.433
5.0	.4793		2.265	
6.0	.4432		2.361	
8.0	.4211		2.040	
1.0	.7433		2.322	
2.0	.6811		1.718	
4.0	.5747	50°C	1.609	1.728
5.0	.5379		1.597	
6.0	.4911		1.758	
8.0	.4854		1.364	contd.

Table-5

Values of Dimerization Constant (K_d) and Monomer Fraction (X) of Azure A in 5% Ethanol at different temperatures and concentrations

Cons.x10^4M	X	Temp.	K_d x10^{-3} (lit/mol)	Average K_d x10^{-3} (lit/mol)
1.0	.6690		3.696	
2.0	.5668		3.370	
4.0	.4705	20°C	2.988	2.834
5.0	.4499		2.887	
6.0	.4404		2.264	
8.0	.4402		1.802	
1.0	.7620		2.048	
2.0	.6371		2.234	
4.0	.5179	30°C	2.246	2.135
5.0	.4900		2.124	
6.0	.4581		2.150	
8.0	.4235		2.008	
1.0	.8366		1.166	
2.0	.7148		1.395	
4.0	.5957	40°C	1.423	1.401
5.0	.5292		1.680	
6.0	.5264		1.423	
8.0	.4907		1.321	
1.0	.9022		0.600	
2.0	.7895		0.844	
4.0	.6714	50°C	0.911	0.859
5.0	.6200		0.988	
6.0	.5965		0.944	
8.0	.5618		0.867	contd.

Table-5

Values of Dimerization Constant (K_d) and Monomer Fraction (X) of Azure A in 10% Ethanol at different temperatures and concentrations

Cons.$\times 10^{4}$M	X	Temp.	$K_d \times 10^{-3}$ (lit/mol)	Average $K_d \times 10^{-3}$ (lit/mol)
1.0	.7594		2.085	
2.0	.6053		2.692	
4.0	.5289	20°C	2.104	2.121
5.0	.5041		1.951	
6.0	.4655		2.054	
8.0	.4369		1.843	
1.0	.8198		1.340	
2.0	.7180		1.367	
4.0	.6026	30°C	1.367	1.359
5.0	.5585		1.415	
6.0	.5223		1.459	
8.0	.5059		1.206	
1.0	.8736		0.827	
2.0	.7862		0.864	
4.0	.6770	40°C	0.880	0.892
5.0	.6332		0.914	
6.0	.5927		0.965	
8.0	.5554		0.900	
1.0	.9160		0.500	
2.0	.8511		0.513	
4.0	.7473	50°C	0.565	0.567
5.0	.6875		0.660	
6.0	.6823		0.568	
8.0	.6267		0.593	contd.

Table-5

Values of Dimerization Constant (K_d) and Monomer Fraction (X) of Azure A in 15% Ethanol at different temperatures and concentrations

Cons. $\times 10^{4}$ M	X	Temp.	$K_d \times 10^{-3}$ (lit/mol)	Average $K_d \times 10^{-3}$ (lit/mol)
1.0	.7482		2.248	
2.0	.6855		1.673	
4.0	.6596	20°C	0.978	1.356
5.0	.6004		1.108	
6.0	.5477		1.256	
8.0	.5607		0.873	
1.0	.8849		0.734	
2.0	.8000		0.780	
4.0	.6682	30°C	0.928	0.873
5.0	.6246		0.962	
6.0	.5931		0.963	
8.0	.5609		0.872	
1.0	.9564		0.237	
2.0	.8565		0.488	
4.0	.7373	40°C	0.603	0.553
5.0	.7016		0.605	
6.0	.6434		0.717	
8.0	.6073		0.665	
1.0	.9660		0.181	
2.0	.8890		0.350	
4.0	.8144	50°C	0.349	0.350
5.0	.7860		0.346	
6.0	.7435		0.386	
8.0	.6608		0.485	contd.

Table-5

Values of Dimerization Constant (K_d) and Monomer Fraction (X) of Azure A in 20% Ethanol at different temperatures and concentrations

Cons.$\times 10^{4}$M	X	Temp.	$K_d \times 10^{-3}$ (lit/mol)	Average $K_d \times 10^{-3}$ (lit/mol)
1.0	.8364		1.168	
2.0	.7844		0.875	
4.0	.6604	20°C	0.973	0.990
5.0	.6188		0.995	
6.0	.5826		1.024	
8.0	.5540		0.908	
1.0	.8786		0.786	
2.0	.8441		0.546	
4.0	.7317	30°C	0.626	0.630
5.0	.6913		0.645	
6.0	.6602		0.649	
8.0	.6469		0.527	
1.0	.9118		0.530	
2.0	.8941		0.330	
4.0	.7969	40°C	0.399	0.420
5.0	.7570		0.423	
6.0	.7308		0.420	
8.0	.6859		0.417	
1.0	.9229		0.452	
2.0	.9238		0.222	
4.0	.8429	50°C	0.276	0.309
5.0	.8054		0.299	
6.0	.7880		0.284	
8.0	.7279		0.320	

Table-6

Values of Dimerization Constant (K_d) and Monomer Fraction (X) of Azure B in water at different temperatures and concentrations

Cons.x10^{4}M	X	Temp.	K_d x10^{-3} (lit/mol)	Average K_d x10^{-3} (lit/mol)
1.0	.4996		10.021	
2.0	.3950		9.690	
4.0	.3091	20°C	9.033	8.981
5.0	.2847		8.824	
6.0	.2635		8.838	
8.0	.2503		7.477	
1.0	.5709		6.579	
2.0	.4534		6.646	
4.0	.3690	30°C	5.792	6.258
5.0	.3203		6.622	
6.0	.2984		6.561	
8.0	.2883		5.351	
1.0	.6437		4.299	
2.0	.5171		4.513	
4.0	.4011	40°C	4.652	4.471
5.0	.3681		4.662	
6.0	.3425		4.669	
8.0	.3238		4.029	
1.0	.6879		3.297	
2.0	.5915		2.918	
4.0	.4660	50°C	3.072	3.033
5.0	.4283		3.115	
6.0	.3952		3.226	
8.0	.3862		2.571	contd.

Table-6

Values of Dimerization Constant (K_d) and Monomer Fraction (X) of Azure B in 5% Ethanol at different temperatures and concentrations

Cons.$\times 10^{4}$M	X	Temp.	$K_d \times 10^{-3}$ (lit/mol)	Average $K_d \times 10^{-3}$ (lit/mol)
1.0	.5790		6.275	
2.0	.4585		6.435	
4.0	.3575	20°C	6.282	6.322
5.0	.3193		6.674	
6.0	.3033		6.308	
8.0	.2756		5.959	
1.0	.6475		4.203	
2.0	.5261		4.279	
4.0	.3997	30°C	4.694	4.579
5.0	.3674		4.683	
6.0	.3420		4.687	
8.0	.2982		4.930	
1.0	.7112		2.854	
2.0	.5891		2.958	
4.0	.4612	40°C	3.164	3.147
5.0	.4247		3.189	
6.0	.3939		3.254	
8.0	.3439		3.465	
1.0	.7689		1.954	
2.0	..6615		1.933	
4.0	.5338	50°C	2.044	2.084
5.0	.4984		2.018	
6.0	.4634		2.082	
8.0	.3920		2.472	contd.

Table-6

Values of Dimerization Constant (K_d) and Monomer Fraction (X) of Azure B in 10% Ethanol at different temperatures and concentrations

Cons.$\times 10^{4}$M	X	Temp.	$K_d \times 10^{-3}$ (lit/mol)	Average $K_d \times 10^{-3}$ (lit/mol)
1.0	.6331		4.574	
2.0	.5201		4.433	
4.0	.3866	20°C	5.128	4.778
5.0	.3599		4.941	
6.0	.3396		4.771	
8.0	.3010		4.818	
1.0	.7181		2.733	
2.0	.5808		3.106	
4.0	.4498	30°C	3.397	3.263
5.0	.4035		3.663	
6.0	.3764		3.667	
8.0	.3634		3.011	
1.0	.7763		1.855	
2.0	.6735		1.799	
4.0	.5317	40°C	2.070	2.096
5.0	.4730		2.355	
6.0	.4431		2.362	
8.0	.4142		2.133	
1.0	.8194		1.343	
2.0	.7271		1.290	
4.0	.6165	50°C	1.261	1.403
5.0	.5645		1.366	
6.0	.5128		1.543	
8.0	.4576		1.618	contd.

Table-6

Values of Dimerization Constant (K_d) and Monomer Fraction (X) of Azure B in 15% Ethanol at different temperatures and concentrations

Cons.x10^4M	X	Temp.	K_d x10^{-3} (lit/mol)	Average K_d x10^{-3} (lit/mol)
1.0	.6752		3.561	
2.0	.5930		2.892	
4.0	.4397	20°C	3.621	2.985
5.0	.4612		2.532	
6.0	.4080		2.962	
8.0	.4001		2.342	
1.0	.7809		1.801	
2.0	.6635		1.909	
4.0	.5340	30°C	2.042	1.965
5.0	.4902		2.121	
6.0	.4536		2.212	
8.0	.4491		1.706	
1.0	.8332		1.201	
2.0	.7431		1.163	
4.0	.6246	40°C	1.202	1.231
5.0	.5796		1.251	
6.0	.5337		1.363	
8.0	.5055		1.208	
1.0	.8578		0.965	
2.0	.8086		0.731	
4.0	.7019	50°C	0.756	0.832
5.0	.6539		0.809	
6.0	.6029		0.910	
8.0	.5713		0.820	contd.

Table-6

Values of Dimerization Constant (K_d) and Monomer Fraction (X) of Azure B in 20% Ethanol at different temperatures and concentrations

Cons.$\times 10^{4}$M	X	Temp.	$K_d \times 10^{-3}$ (lit/mol)	Average $K_d \times 10^{-3}$ (lit/mol)
1.0	.7780		1.832	
2.0	.6959		1.569	
4.0	.5666	20°C	1.686	1.805
5.0	.5223		1.750	
6.0	.4792		1.889	
8.0	.4163		2.104	
1.0	.8312		1.221	
2.0	.7403		1.184	
4.0	.6133	30°C	1.284	1.341
5.0	.5674		1.342	
6.0	.5174		1.501	
8.0	.4683		1.515	
1.0	.8640		0.910	
2.0	.7887		0.848	
4.0	.6956	40°C	0.786	0.982
5.0	.6391		0.883	
6.0	.5786		1.048	
8.0	.4789		1.419	
1.0	.8851		0.732	
2.0	.8206		0.666	
4.0	.7439	50°C	0.578	0.803
5.0	.6888		0.655	
6.0	.6099		0.873	
8.0	.4916		1.314	

Table-7

Values of Dimerization Constant (K_d) and Monomer Fraction (X) of Methylene Blue in Water at different temperatures and concentrations

Conc.$\times 10^{4}$M	X	Temp.	$K_d \times 10^{-3}$ (lit/mol)	Average $K_d \times 10^{-3}$ (lit/mol0
1.0	.5799		6.244	
2.0	.4757		5.789	
4.0	.3936	20°C	4.889	5.013
5.0	.3653		4.753	
6.0	.3464		4.536	
8.0	.3291		3.868	
1.0	.6447		4.272	
2.0	.5342		4.079	
4.0	.4322	30°C	3.798	3.685
5.0	.4002		3.743	
6.0	.3817		3.536	
8.0	.3801		2.680	
1.0	.7083		2.906	
2.0	.6016		2.750	
4.0	.4933	40°C	2.601	2.563
5.0	.4563		2.610	
6.0	.4346		2.494	
8.0	.4230		2.015	
1.0	.7771		1.884	
2.0	.6712		1.824	
4.0	.5532	50°C	1.824	1.793
5.0	.5176		1.800	
6.0	.4833		1.843	
8.0	.4571		1.623	contd.

Table-7

Values of Dimerization Constant (K_d) and Monomer Fraction (X) of Methylene Blue in 5% Ethanol at different temperatures and concentrations

Cons.x10^4M	X	Temp.	K_d x10^{-3} (lit/mol)	Average K_d x10^{-3} (lit/mol)
1.0	.6606		3.887	
2.0	.5378		3.992	
4.0	.4377	20°C	3.667	3.543
5.0	.4097		3.514	
6.0	.3903		3.333	
8.0	.3705		2.865	
1.0	.7216		2.671	
2.0	.6065		2.673	
4.0	.5008	30°C	2.488	2.461
5.0	.4628		2.506	
6.0	.4461		2.318	
8.0	.4159		2.109	
1.0	.7841		1.755	
2.0	.6638		1.906	
4.0	.5545	40°C	1.810	1.831
5.0	.5086		1.899	
6.0	.4791		1.890	
8.0	.4475		1.723	
1.0	.8502		1.035	
2.0	.7580		1.052	
4.0	.6344	50°C	1.134	1.124
5.0	.5919		1.164	
6.0	.5560		1.196	
8.0	.5123		1.160	contd.

Table-7

Values of Dimerization Constant (K_d) and Monomer Fraction (X) of Methylene Blue in 10% Ethanol at different temperatures and concentrations

Cons.$\times 10^{4}$M	X	Temp.	$K_d \times 10^{-3}$ (lit/mol)	Average $K_d \times 10^{-3}$ (lit/mol)
1.0	.7135		2.813	
2.0	.6035		2.720	
4.0	.4997	20°C	2.504	2.531
5.0	.4580		2.583	
6.0	.4356		2.477	
8.0	.4173		2.090	
1.0	.7842		1.754	
2.0	.6748		1.785	
4.0	.5484	30°C	1.876	1.844
5.0	.5076		1.910	
6.0	.4711		1.985	
8.0	.4448		1.752	
1.0	.8471		1.065	
2.0	.7497		1.113	
4.0	.6180	40°C	1.250	1.203
5.0	.5756		1.280	
6.0	.5398		1.315	
8.0	.5068		1.199	
1.0	.8837		0.743	
2.0	.8006		0.777	
4.0	.7017	50°C	0.756	0.801
5.0	.6535		0.811	
6.0	.6014		0.918	
8.0	.5759		0.799	contd.

Table-7

Values of Dimerization Constant (K_d) and Monomer Fraction (X) of Methylene Blue in 15% Ethanol at different temperatures and concentrations

Conc.$\times 10^{4}$ M	X	Temp.	$K_d \times 10^{-3}$ (lit/mol)	Average $K_d \times 10^{-3}$ (lit/mol)
1.0	.7817		1.786	
2.0	.7226		1.328	
4.0	.5399	20°C	1.972	1.628
5.0	.5150		1.823	
6.0	.4839		1.831	
8.0	.4789		1.420	
1.0	.8848		0.735	
2.0	.7717		0.957	
4.0	.6233	30°C	1.211	1.153
5.0	.5773		1.267	
6.0	.5274		1.415	
8.0	.4893		1.332	
1.0	.9178		0.487	
2.0	.8420		0.556	
4.0	.7227	40°C	0.663	0.779
5.0	.5862		1.233	
6.0	.6278		0.787	
8.0	.5466		0.948	
1.0	.9231		0.450	
2.0	.9048		0.290	
4.0	.8436	50°C	0.274	0.417
5.0	.7887		0.339	
6.0	.7108		0.476	
8.0	.6050		0.674	contd.

Table-7

Values of Dimerization Constant (K_d) and Monomer Fraction (X) of Methylene Blue in 20% Ethanol at different temperatures and concentrations

Conc.$\times 10^{4}$M	X	Temp.	$K_d \times 10^{-3}$ (lit/mol)	Average $K_d \times 10^{-3}$ (lit/mol)
1.0	.8457		1.078	
2.0	.7551		1.073	
4.0	.6349	20°C	1.132	1.055
5.0	.5842		1.218	
6.0	.5617		1.157	
8.0	.6079		0.663	
1.0	.8624		0.924	
2.0	.7861		0.864	
4.0	.6759	30°C	0.886	0.890
5.0	.6288		0.938	
6.0	.5952		0.951	
8.0	.5891		0.774	
1.0	.9119		0.529	
2.0	.8752		0.407	
4.0	.7926	40°C	0.412	0.536
5.0	.7299		0.506	
6.0	.6803		0.575	
8.0	.5781		0.788	
1.0	.9714		0.151	
2.0	.9211		0.232	
4.0	.8044	50°C	0.377	0.408
5.0	.7520		0.438	
6.0	.6957		0.523	
8.0	.5923		0.726	

temperature and percentage of ethanol. At a particular temperature and in aqueous medium the dimerization constant increases with increase in methyl substitution upto azure B which is a trimethyl derivative of thionine but the value of the constant (K_d) decreases in case of methylene blue. At 20^0C in aqueous medium, the K_d values are 2.44×10^3, 2.95×10^3, 4.50×10^3, 8.98×10^3 and 5.01×10^3 lit/mol for Th, AzC, AzA, AzB and MB respectively. This indicates that the increased hydrophobicity in dye molecule upon methylation increases dimerization tendency due to increased hydrophobic interaction, which in turn minimize the contact area of the dyes with water. However, in case of methylene blue, steric hindrance is probably very high and the dimerization constant is decreased to some extent. It is evident that the strength of aggregation largely depends on the structure of the dye molecules, nature of the solvent and the temperature.

In order to know the nature of bonding between the monomers in the dimer some important thermodynamic functions of dimerization have been determined. Using Van't Hoff equation the enthalpy of dimerization ΔH^o is calculated (Figs. 33-37). The changes in the standard free energy and entropy due to dimerization are also evaluated from the following equations,

$\Delta G^o = - RT \ln K_d$ and $\Delta S^o = (\Delta H^o - \Delta G^o) /T$ respectively.

The calculated values of the functions at 30^oC are given in table 8. In the calculations it is assumed that ΔG values are linear between 20^oC and 50^oC temperature range. ΔG and ΔH values for the

Table-8

Values of thermodynamic functions of the dyes at $30^{\circ}C$ in aqueous and aqueous-ethanolic media.

Solvent	$-\Delta H$ (KJ/mol)	$-\Delta G$ (KJ/mol)	$-\Delta S$ (J/mol/K)
	Thionine		
Water	21.61	18.82	9.20
5% EtOH	19.78	18.33	4.78
10% EtOH	18.54	17.91	2.07
15% EtOH	18.29	17.02	4.19
20% EtOH	17.46	16.02	4.75
	Azure C		
Water	22.86	19.55	10.92
5% EtOH	23.69	18.96	15.62
10% EtOH	26.60	18.52	26.68
15% EtOH	23.69	17.20	21.43
20% EtOH	19.95	16.38	11.79
	Azure A		
Water	26.68	20.48	20.46
5% EtOH	34.58	19.32	50.36
10% EtOH	33.25	18.16	49.80
15% EtOH	32.92	17.05	32.86
20% EtOH	32.59	16.24	53.96

Table-8

Values of thermodynamic functions of the dyes at 30^{0}C in aqueous and aqueous-ethanolic media

Solvent	$-\Delta H$ (KJ/mol)	$-\Delta G$ (KJ/mol)	$-\Delta S$ (J/mol/K)
	Azure B		
Water	28.26	22.01	20.62
5% EtOH	29.09	21.23	25.97
10% EtOH	31.75	20.37	37.55
15% EtOH	33.25	19.09	46.73
20% EtOH	23.27	18.13	16.96
	Methylene Blue		
Water	26.85	20.68	20.36
5% EtOH	29.76	19.46	33.39
10% EtOH	32.84	18.91	45.97
15% EtOH	28.43	17.76	35.21
20% EtOH	24.94	17.10	25.87

five thiazine dyes are negative and do not differ very much upon progressive methyl substitution, there is, however, a general trend of increasing effect of methylation in aqueous medium. On the other hand, ΔS values, which are also negative, increases to much larger extent due to methyl substitution. The latter observation supports the view that the aggregated dyes are more ordered than free monomer dyes and such order is more pronounced

as more and more bulky methyl groups are substituted in the dye molecule. In general, the high values of ΔH and ΔS can be attributed to the role of hydrogen bonding in aggregate formation apart from hydrophobic and $\pi-\pi$ interactions.

3.3.2 Analysis of dimer spectra in terms of Molecular Exciton Model

The dimer spectra can be interpreted by using Exciton theory which predicts a splitting of the electronic transitions in the dimer. The decomposition of the dimer spectrum into two bands shows that the monomer visible spectrum corresponds to an electronic transition with two vibronic bands and not two electronic transitions (Figs. 24-28). The point dipole-point dipole approximation of the point multipole expression of the theory of molecular exciton coupling has been extended and applied to all thiazine dimers in concentrated solutions. Briefly, using the values of the oscillators strength of the low (f_1) and high (f_2) frequency electronic components (the J-band and H-band respectively) of the dimer spectra, the angle θ, between the main oscillators of the two molecules can be determined by the expression,

$$f_1/f_2 = \tan^2 \theta/2 \qquad (32)$$

The distance (R') between the centres of the two molecules can be calculated from the resonance ineteraction energy, U (a term which is equal to half the separation between the electronic band maxima of the splitted dimer spectrum and equivalent to ϵ_0 of page 37) (66).

The relationship between the interaction energy, strength of transition dipole and the geometry of the dimer is given by the general equation :

$$U = \frac{|M|^2}{R'^3} (\cos\theta + 3 \cos^2\phi) \qquad (33)$$

where $|M|^2$ is the square of the transition moment of the monomer, θ is the angle between polarization axes for the monomer and ϕ is the angle between the polarization direction and the line joining the centres of the two component molecules (51). The following equation can be used directly to determine oscillator strength of a derivative spectrum :

$$f = 4.32\times10^{-9} \int \epsilon(\nu) d\nu \qquad (34)$$

However, it is more convenient to modify the equation to make it easier to analyse spectra measured as a function of wavelength instead of frequency. If the dispersion relationship $C=\lambda\nu$ is used to substitute for ν in the above equation, the alternative

reletionship

$$f = (0.0432/\lambda_o^2) \int \epsilon(\lambda) d\lambda \qquad (35)$$

may be derived. In this expression $\epsilon(\lambda)$ has units of lit./mol-cm. and λ is in nm. λ_o is the wavelength at the peak of a smoothed envalope containing the spectrum (94).

The oscillator strength (f) of the dimer is calculated from the relationship

$$f = (0.0432/\lambda_o^2) L \int \epsilon(\lambda) d\lambda \qquad (36)$$

where, $L = \dfrac{9n_o^2}{(n_o+2)^2}$ = Loerntz factor ;

n_o is the refractive index of the solvent (42). L is introduced to correct for the solvent effect and the value for water is taken as 0.848.

Twist angle (θ) calculated for the dimers are presented in table 9 (For the calculation of f_1 and f_2 values for each dimer spectrum, measurement of the area under the J and H bands of the spectra was done by counting small divisions of graph paper.). The transition moment M is calculated using the relationship,

$$f = 4.704 \times 10^{29} \bar{\nu} M^2 \qquad (37)$$

where, $\bar{\nu}$ is in cm^{-1} of the dimer at maximum ϵ in the dimer spectrum. The values of the oscillator strength and the transition moment of the dyes are shown in table 10.

The distance (R') between monomers in a dimer is model dependent, i.e, it depends on the geometric disposition. To explain dimer band splitting, two models allowing the two transitions are possible (51,93). In model I, the monomers are in parallel planes with a twist angle θ while in model II, they are in the same plane forming an angle θ. The interaction energy in these models are as follows :

Model I ($\theta=\theta$ and $\phi = 90^{o}$; Sandwitch dimer with a twist angle θ)

$$U = - \frac{|M|^2 \cos\theta}{R_I'^3} \qquad (38)$$

Model II ($\theta=\theta$ and $\phi=\theta$; Coplanar inclined angle dimer)

$$U = - \frac{|M|^2}{R_{II}'^3} (\cos\theta + 3\cos^2\phi) = - \frac{|M|^2}{R_{II}'^3} (\cos\theta + 3\sin^2\theta/2) \qquad (39)$$

where R_I' and R_{II}' are the distances between the monomers in the dimers in model I and II respectively.

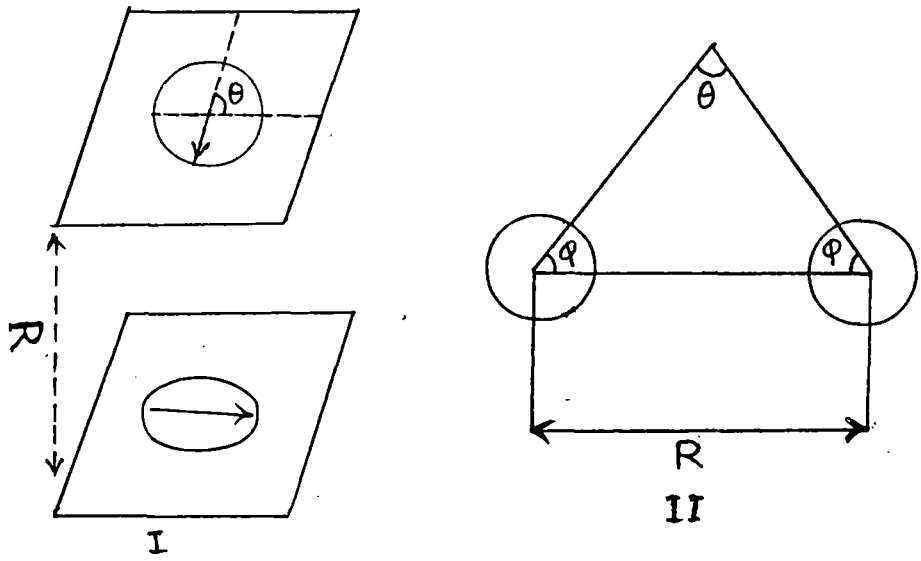

Model I refers to the case of non-planar transition dipoles where the molecules are arranged in a sandwitch dimer (card pack) orientation with angle θ, the angle of skew between the polarization direction of the absorption oscillators of each dye molecule. Rohatgi and Mokhopadyay (64) and Arbeloa (51) considered this to be the likely arrangement for self associated fluorescein dimer in concentrated solution. Model II refers to the "coplanar inclined angle dimer" of the 'oblique' arrangement where θ is the angle between the planes of the xanthene ring. Twist angles θ's and distances R''s between monomer units in dimer have been calculated for all the alkylated thiazine dyes in aqueous solution adopting above models of dimers. The dimeric structures of thionine and its derivatives are shown in fig. 43. Substituting the values of $|M|^2$, U and θ the distance R_I and R_{II} for all the dyes are calculated (Table 9 and 10).

Table-9

Excitonic parameters of the dimers of thiazine dyes

Dye	Twist angle (θ, deg.)	ν (cm^{-1})	Intermolecular distance (A) R'_I	R'_{II}
Thionine	34.8	1072.5	6.01	6.61
Azure C	28.4	1076.5	6.38	6.80
Azure A	28.5	1417.5	5.95	6.75
Azure B	30.2	1172.0	6.06	6.65
Methylene Blue	31.7	1097.5	6.76	7.30

Table-10

Values of transition moments and oscillator strength of dimers of thiazine dyes :

Dye	Square of the transition moments $\|M\|^2 \times 10^{36}$ esu	Oscillator strength "f"
Thionine	56.23	0.4766
Azure C	63.20	0.5207
Azure A	67.23	0.5500
Azure B	59.96	0.4797
Methylene Blue	78.81	0.6179

The twist angle for the thionine is found to be the largest among all the dyes (34.8^{o}) and AzC shows the smallest twist angle of 28.4^{o}. While the twist angles displayed by all the five dyes are close to each other, no systematic variation is observed on progressive alkylation of the dye molecule. It seems apparent that apart from the steric effect due to the additon of successive methyl groups in the dye molecule, hydrophobic as well as electron donating nature of methyl groups are also involved. Apparently the increased hydrophobic interaction due to methyl substitution as well as for their electron donating nature, a stronger field is created such that the dipoles tend towards parallel alingment resulting in the decrease in θ upon introduction of two methyl groups successively in the thionine molecule. In other words, a better $\pi-\pi$ interaction between two monomer molecules as a result of successive additon of two methyl groups may cause the observed alignment. Further substitution of methyl groups probably increase steric hindrance resulting in the increase of the angle θ between the dipoles.

It should be mentioned in this context that the angle between the transition moments of two monomers of methylene blue as reported by Bergmann and O'Konski (42) was only 13^{o}. The twist angle calculated for the present study are much higher than that reported by above authors. However, the present observation is consistent with the more recent study for a number of dye systems (28).

On the other hand, intermolecular distance between two monomer molecules in a dimer as calculated according to model I varies from 5.59 to 6.76Å ; while the same varies from 6.61 to 7.30Å when calculated according to model II.

As mentioned earlier, previous researches (51-52,64) on monomer- dimer studies of some fluorescein and others dyes reveal that model I is the more reasonable one as the distance between the monomers according to model I is close to that in the crystalline state. The distances between the transition dipoles in the dimers as revealed in the present systems are somewhat higher than observed previously for fluorescein or rhodamine dyes. But the values calculated according to model I are somewhat less. In view of this and the observation of the previous workers on a number of dyes it may be argued that model I may be appropriate for the present systems also. However, these models represent only the ideal cases and the real structure may only approximate to one of them. It is noteworthy that although the exciton theory as applied in the present systems is over simplification for the problem of dye aggregation, the interdipole distances R' computed therefrom appears to be reasonable if proper geometry of the aggregate is taken into consideration.

3.3.3 Analysis of dimer spectra in terms of Vibronic Exciton Model

In view of some successes achieved by molecular vibronic exciton model in interpreting spectra of dye aggregates, the monomer and dimer spectra of the five thiazine dyes are further analysed by vibronic exciton band model as described in section 3.1.4. Although some authors claim that the resonance interactions of excited state of molecular aggregates with weak intermolecular binding as just described for molecular exciton model is comparatively simple technique and presents reasonable interpretation of molecular aggregates, a short account of analysis by vibronic exciton model is presented as follows, which includes more recent developments in exciton theory. The additional advantage of the model is that it allows one to analyse the dimer in further detail with respect to the strength of exciton coupling, the frequency and intensity of band origin, band width etc.

Figs.28-32 reproduce the experimental monomer spectra and the fitted monomer spectra of the dyes. The monomer vibronic spectra were fitted assuming that the spectra are due largely to a single harmonic vibronic progression in accordance with Gal and coworkers (88). The spectra were fitted to a 5-parameter Gaussion equation 23 which has already been described (section 3.1.4.).

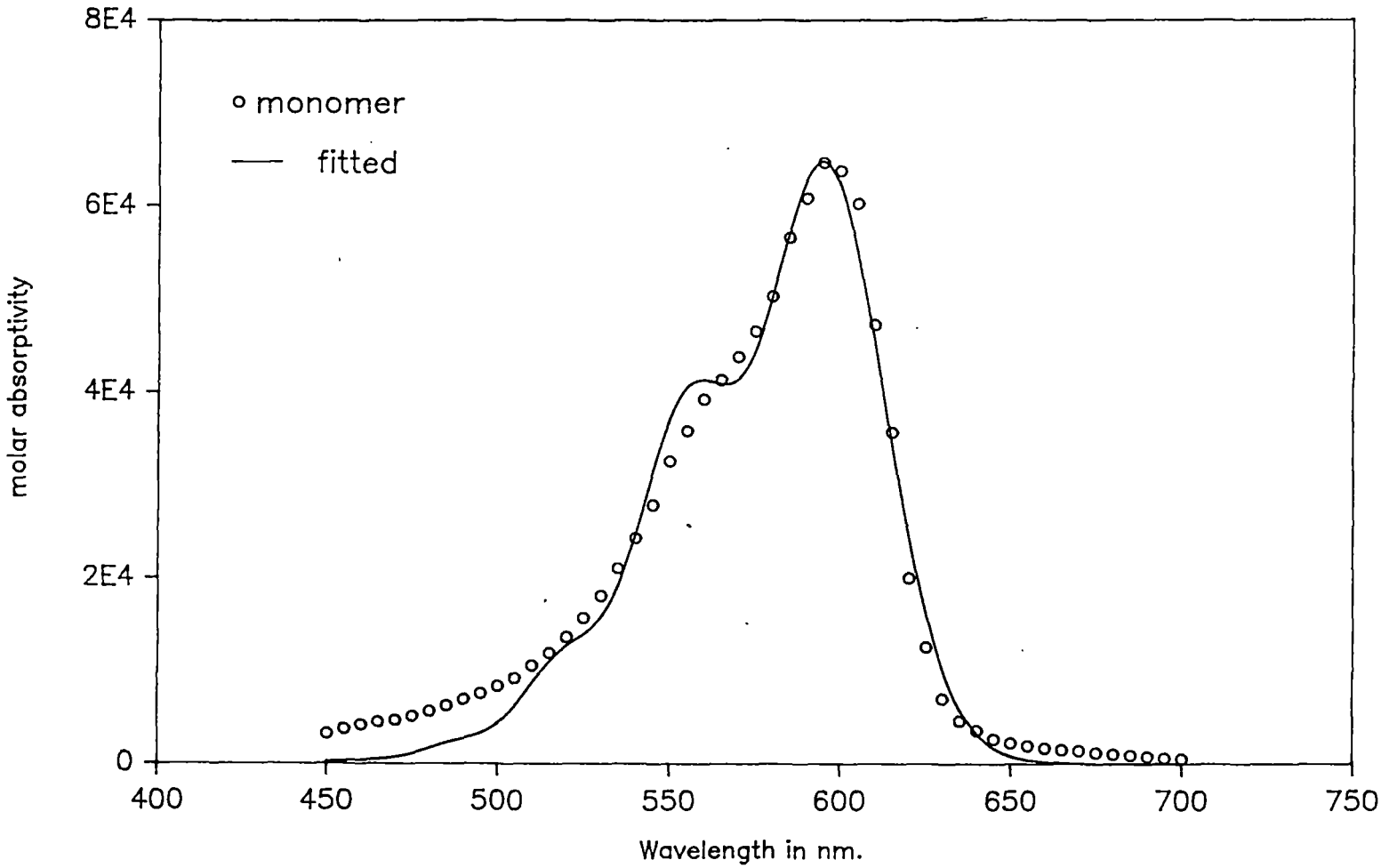

Fig.28 Absorption spectra of Thionine (5×10^{-6}M) in the presence of 0.01M KCl at 30^{0}C using 1 cm. cell.

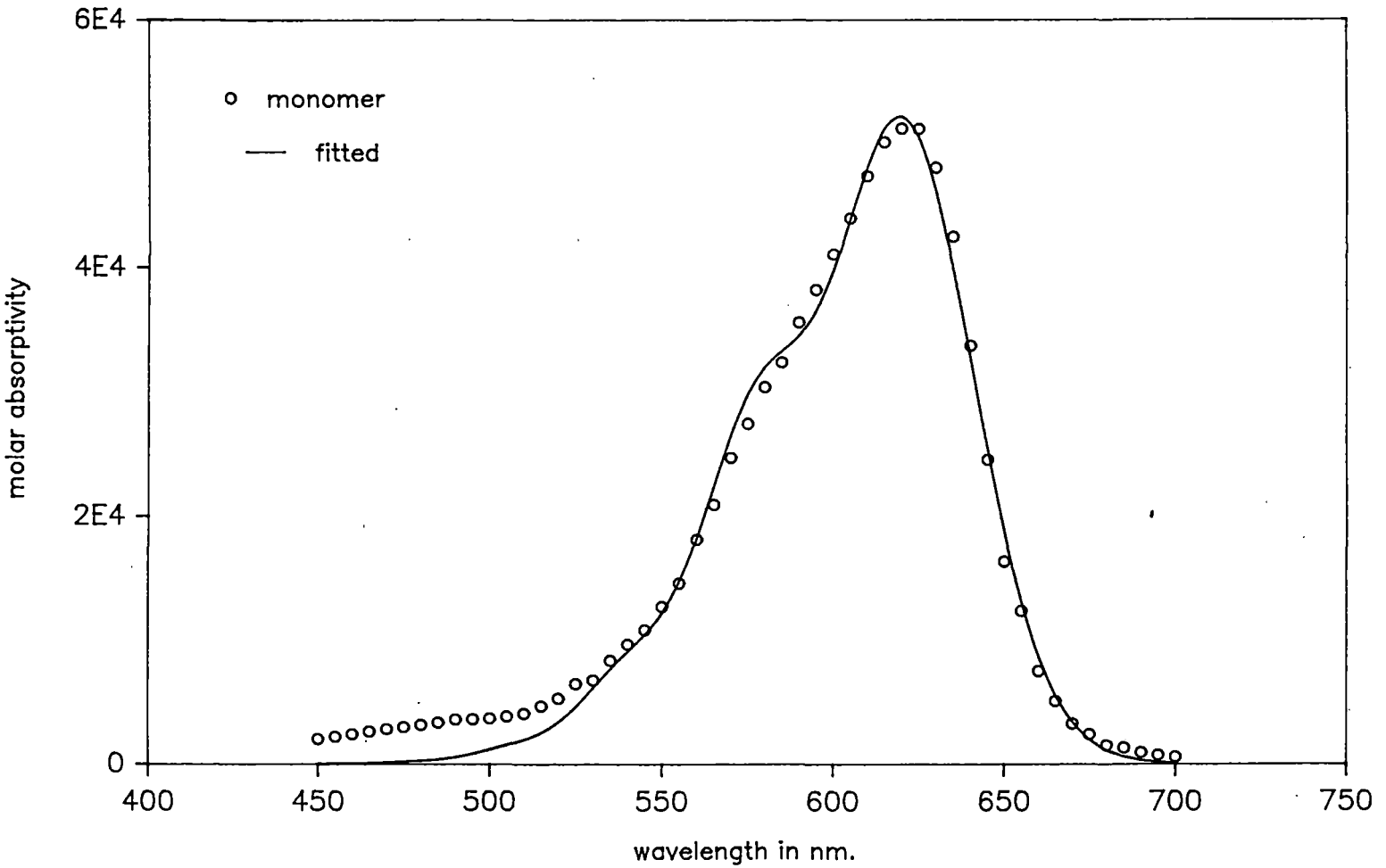

Fig.29 Absorption spectra of Azure C ($5x10^{-6}$M) in the presence of 0.0.1 M KCl at 30^{0}C using 1cm. cell.

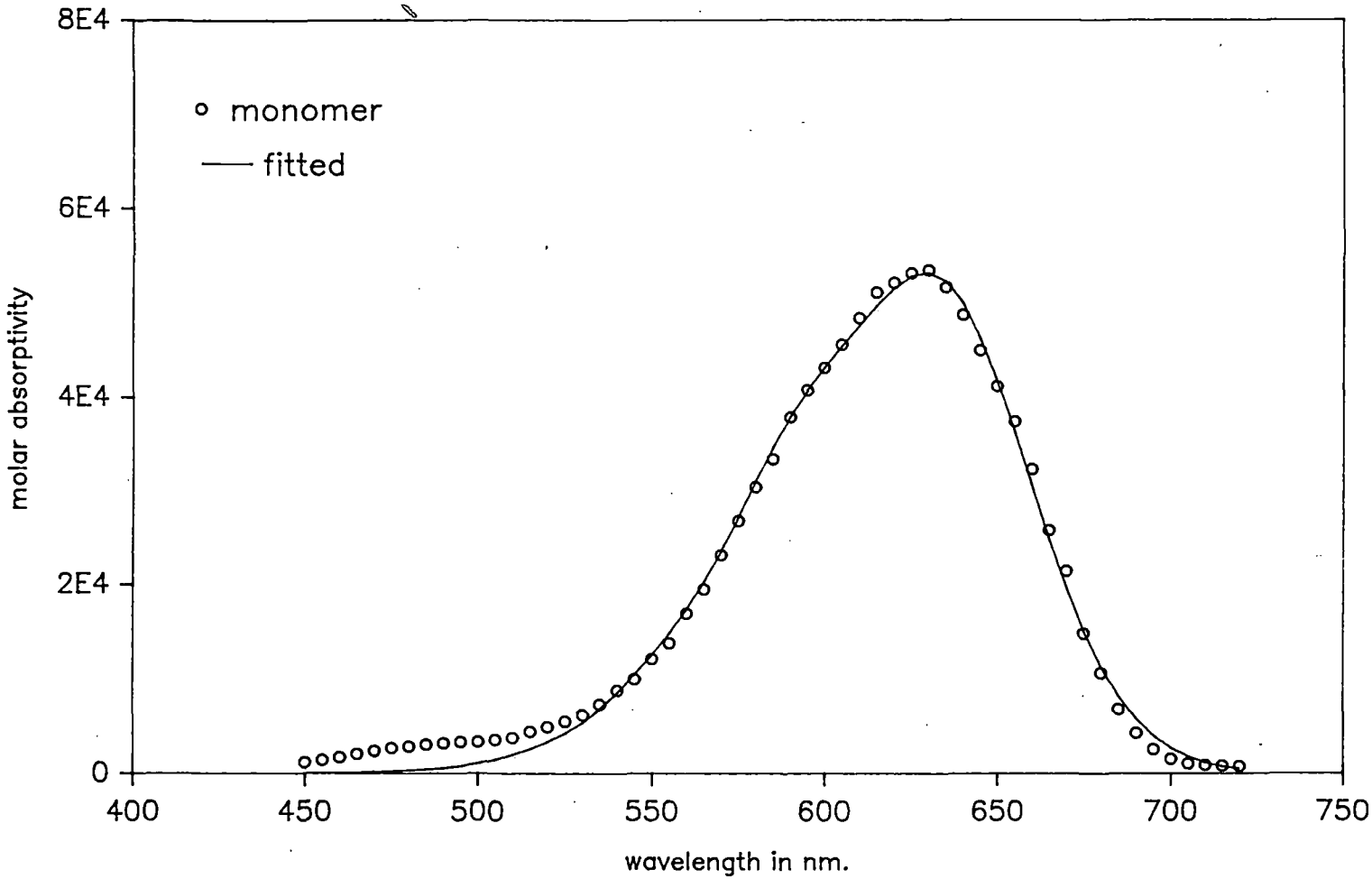

Fig.30. Absorption spectra of Azure A (5×10^{-6}M) in the presence of 0.01M KCl at 30^{0}C using 1cm. cell.

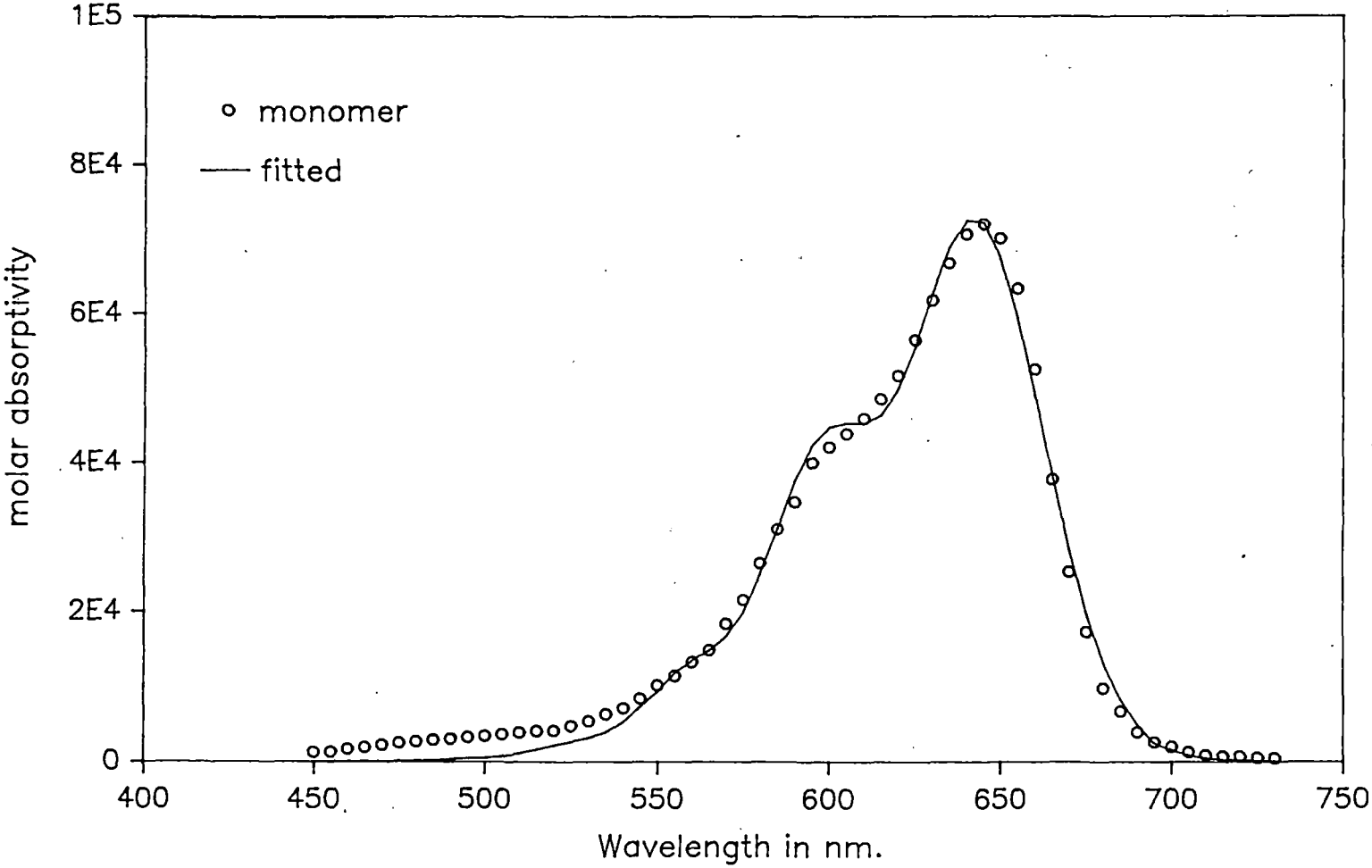

Fig.31. Absorption spectra of Azure B (5×10^{-6}M) in the presence of 0.0.1M KCl at 30^{0}C using 1cm. cell.

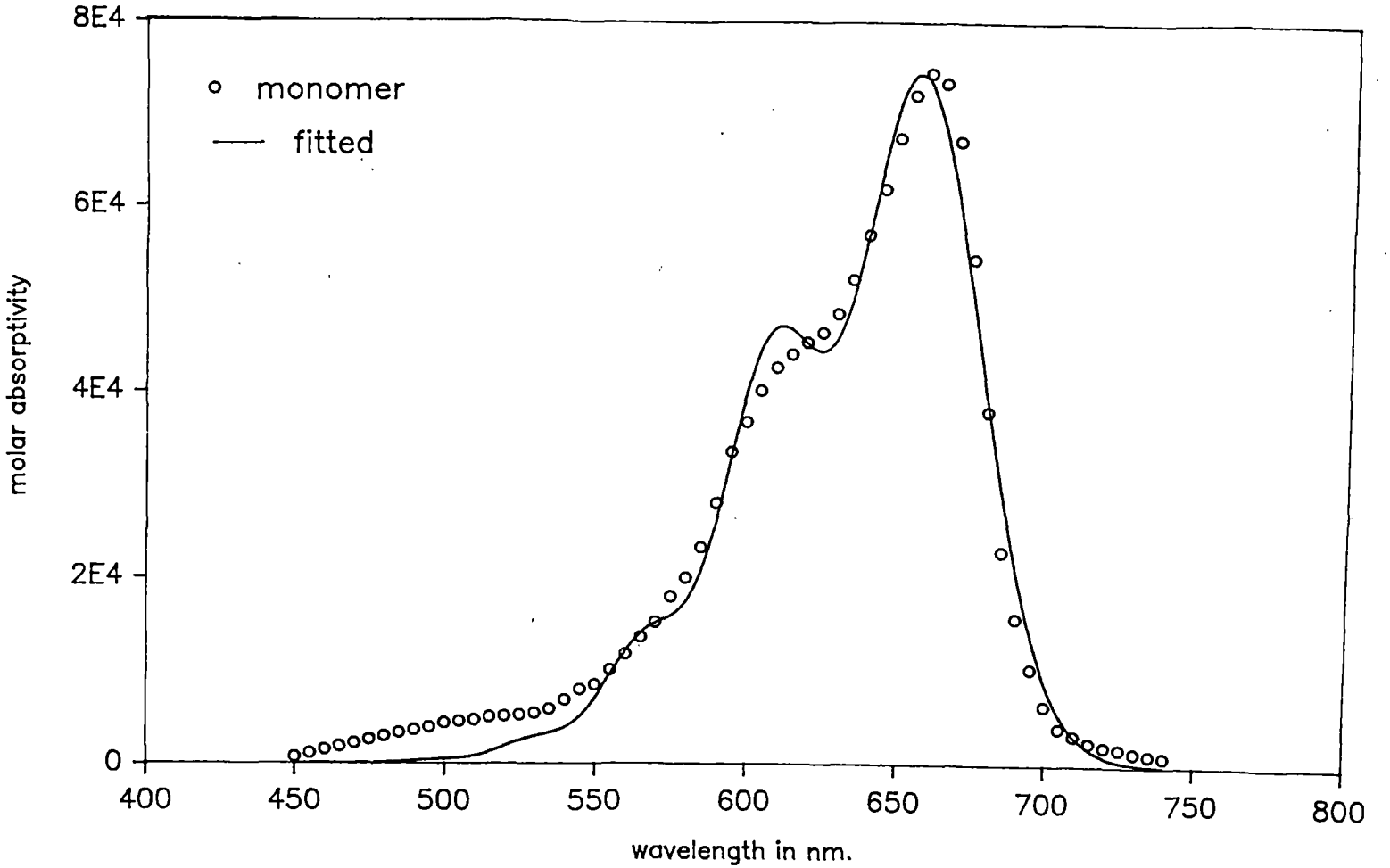

Fig.32.Absorption spectra of Methylene Blue (5×10^{-6}M) in the presence of 0.0.1M KCl at 30^{0}C using 1cm. cell

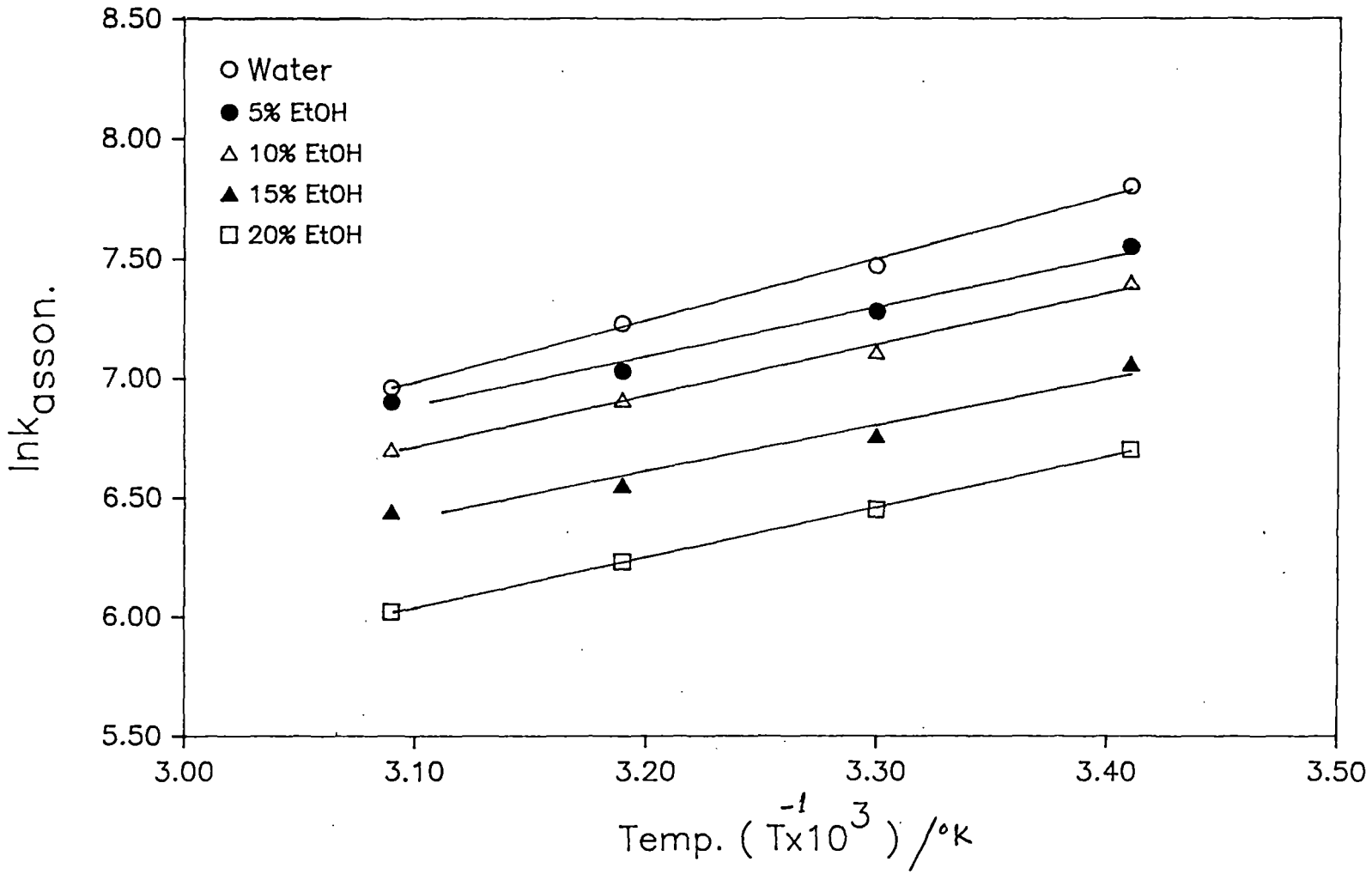

Fig.33 Plot of lnk vs 1/T for Thionine in different solvents

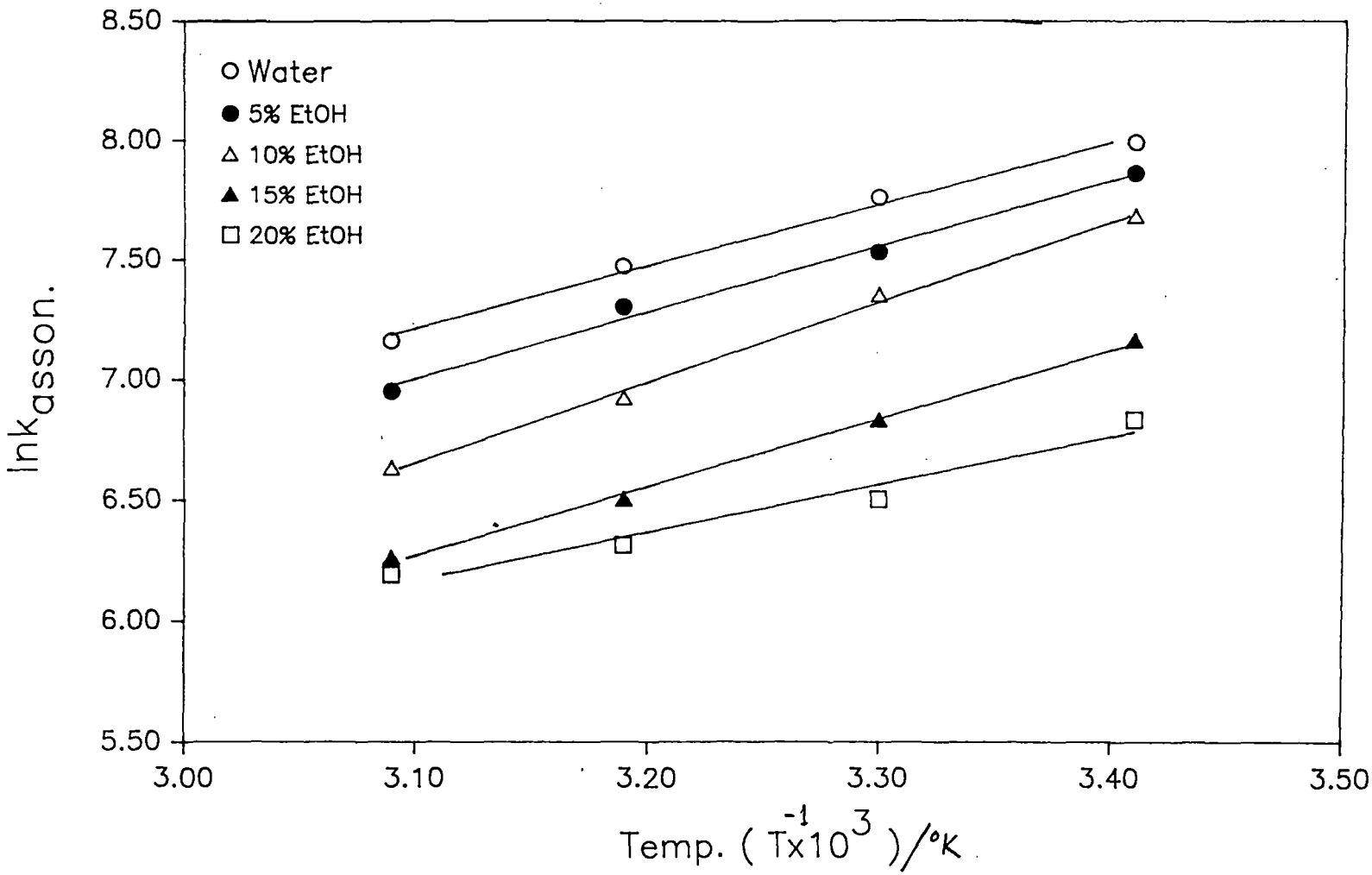

Fig.34 Plot of lnk vs 1/T for Azure C in different solvents

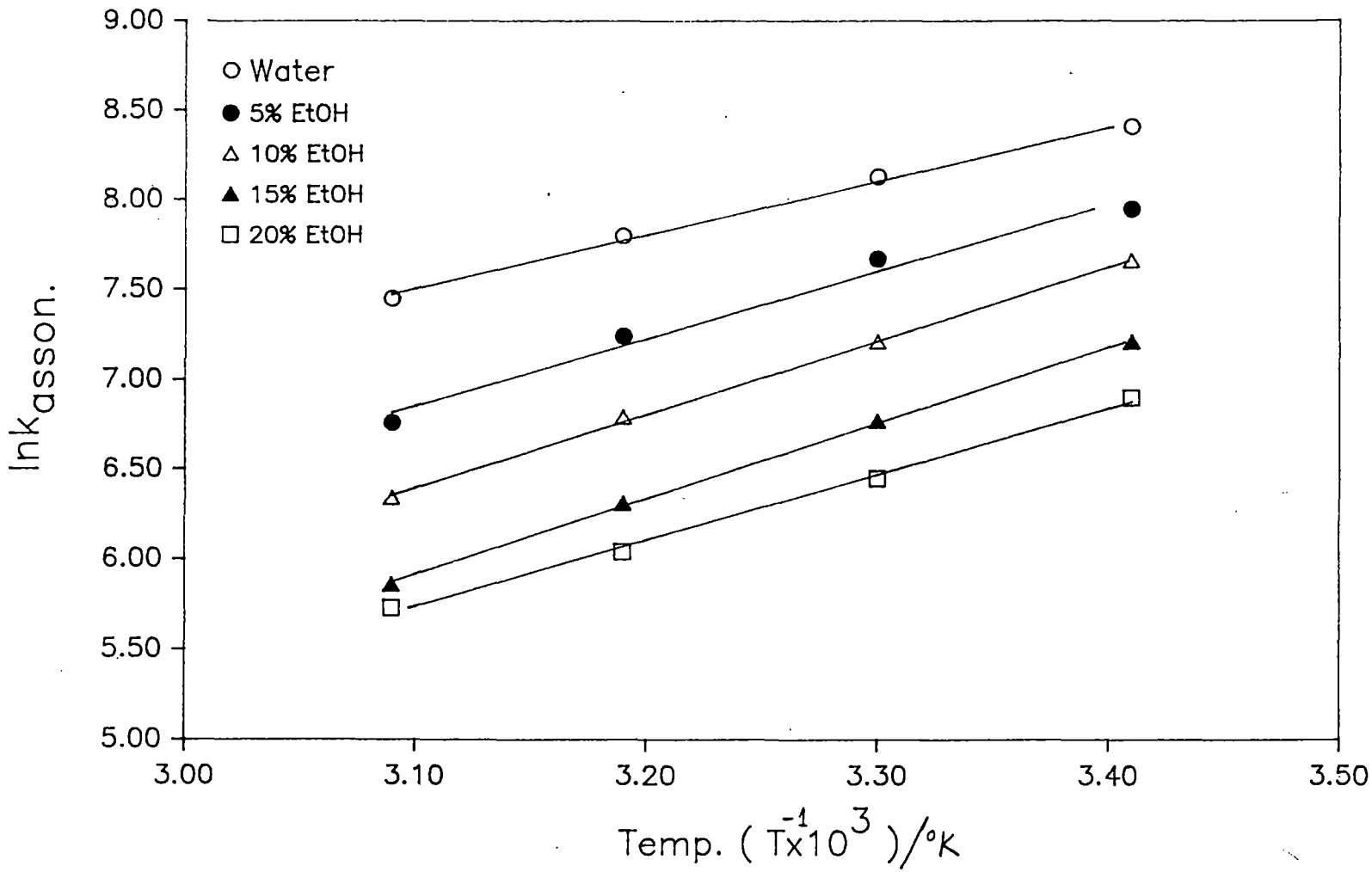

Fig.35 Plot of lnk vs 1/T for Azure A in different solvents

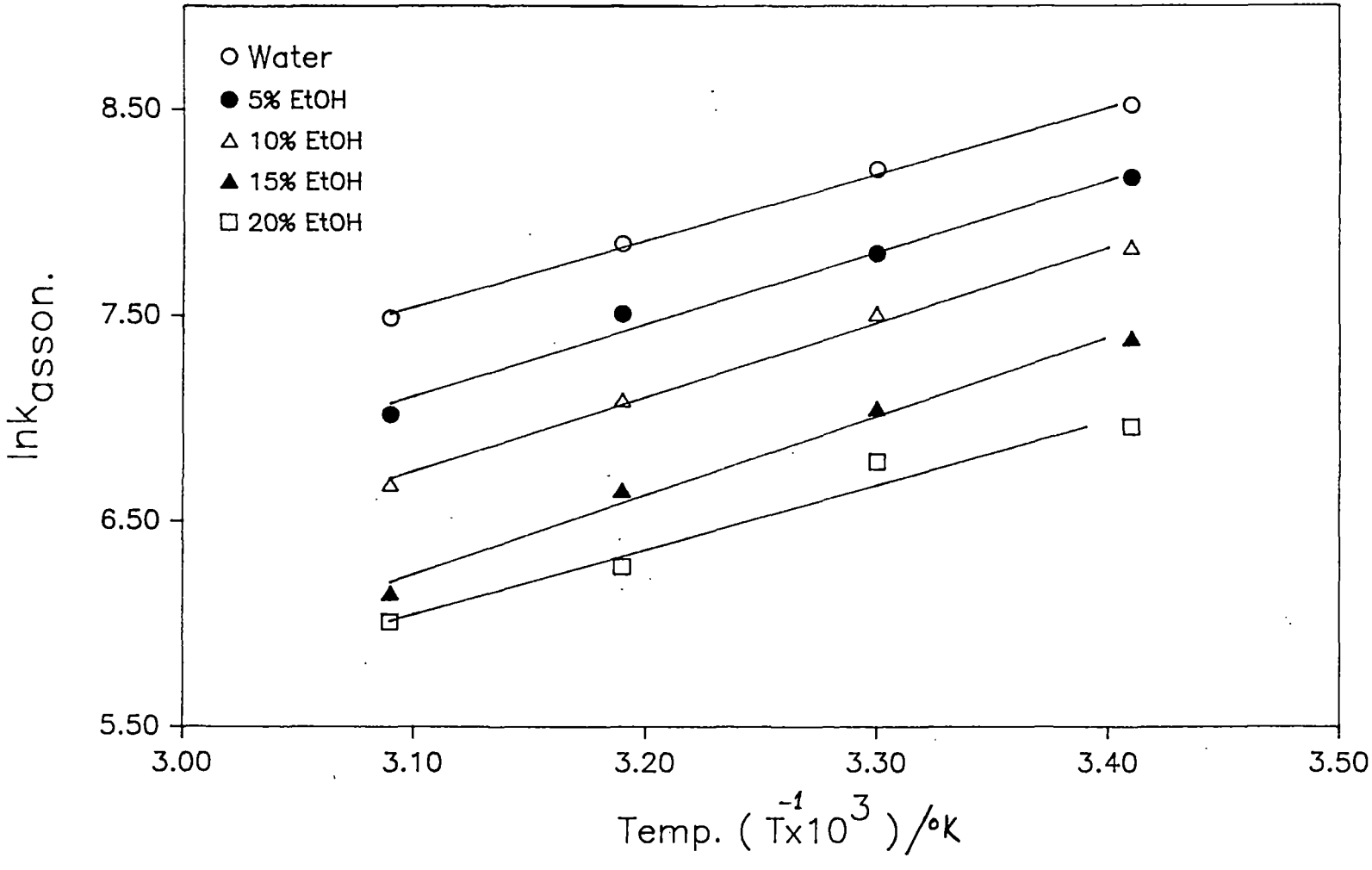

Fig.36 Plot of Ink vs 1/T for Methylene Blue in different solvents

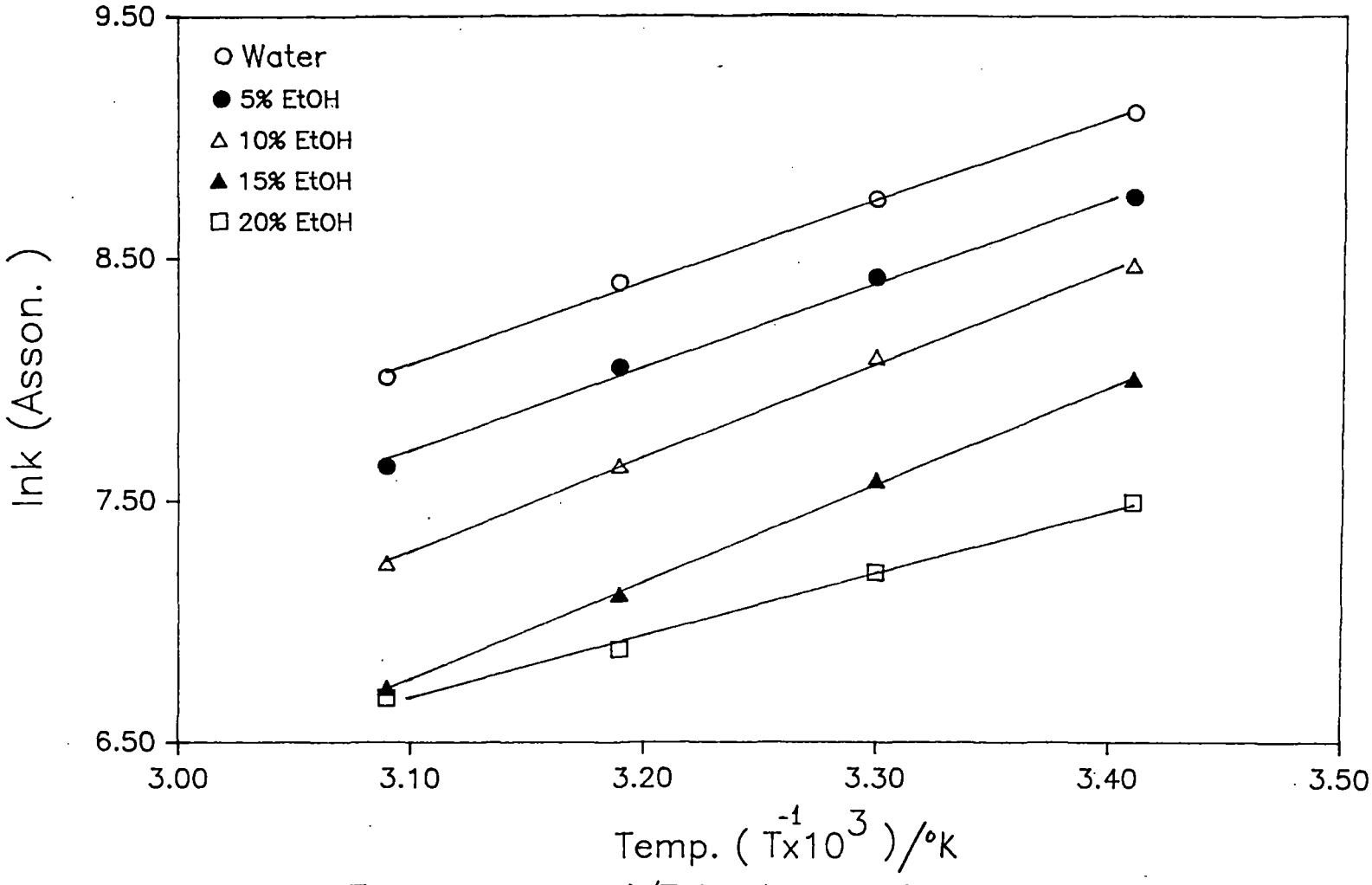

Fig.37 Plot of lnk vs 1/T for Azure B in different solvents

[monomer spectral data are fitted to the five parameter Gaussion equation 23 on a PC-AT (486 DX2) computer by means of a general non linear weighted least square program (95) properly adopted in the present circumstances]. Satisfactory results were obtained by trancating the summation after six bands. This fitting is done because some of the monomer fitting parameters are needed to fit subsequently the dimer spectra.

Among the five parameters ν_{oo} and I_{oo} are the position and the intensity respectively of the (0,0) band origin; the band origions are assumed to be separated by the constant wave number V. The Gaussian band half intensity width of each band is given by b_g. Finally, X is the ratio of the (1,0) to (0,0) band intensities : it is related to the equilibrium nuclear conformation in the two electronic states. Values of all the five parameters for each of five dyes are listed in table 11. Fairly well fittings of the monomer spectra of most of the dyes indicate that the persent physical model describing a vibronic progression of a displaced harmonic oscillator with Gaussian bands of constant band width requiring five adjustable parameter (equatoin 23) may be adopted to the present dye systems. However, although the fitting of the monomer spectra of AzC, AzA and AzB with the 5 parameter Gaussian equation is fairly well, considerable deviation is observed near the shoulders of monomer spectra of Th and MB. The parameter X is related to the displacement of the normal coordinate of vibration, R'', through the formula,

$$X = (2\pi^2 c V \mu)\ R''^2$$

where μ is the reduced mass of the oscillator, c is the velocity of light and other symbols have their usual meaning (fig. 44). It is possible to give R'' a relatively simple interpretation in terms of changes in the bond lengths between the atoms of the aromatic ring system (Fig 44). It may also be of interest that there appears to be some evidence and justification in favour of an assertion that the parameters I_{oo} and X are corelated (96)

Figs. 38-42 show the experimentally derived as well as calculated dimer spectra of thiazine dyes, viz.,Th, AzC, AzA, AzB and MB. In calculating theoretical spectra, values for some parameters (V and X) are taken from the corresponding monomer spectra. The dimer spectra were fitted to the adiabatic model described by Gianneschi et al.(81,89). As mentioned in section 3.1.4. of the present chapter, the theory involves diagonalising tridiagonal Hermitian matrices which incorporate five parameters: the exciton coupling strength (ε), the angle between the interacting transition moments, the energy of the dimer transition ($\bar{\nu}_{oo}$), the vibronic spacing (V) and the nuclear displacement parameter (X). The numerical results consist of the energies and relative intensities of the exciton bands from which the dimer spectrum is generated by associating a Gaussian band of width b_g with each calculated vibronic line and summing over all the Gaussian bands. Again to a good approximation, b_g, is taken

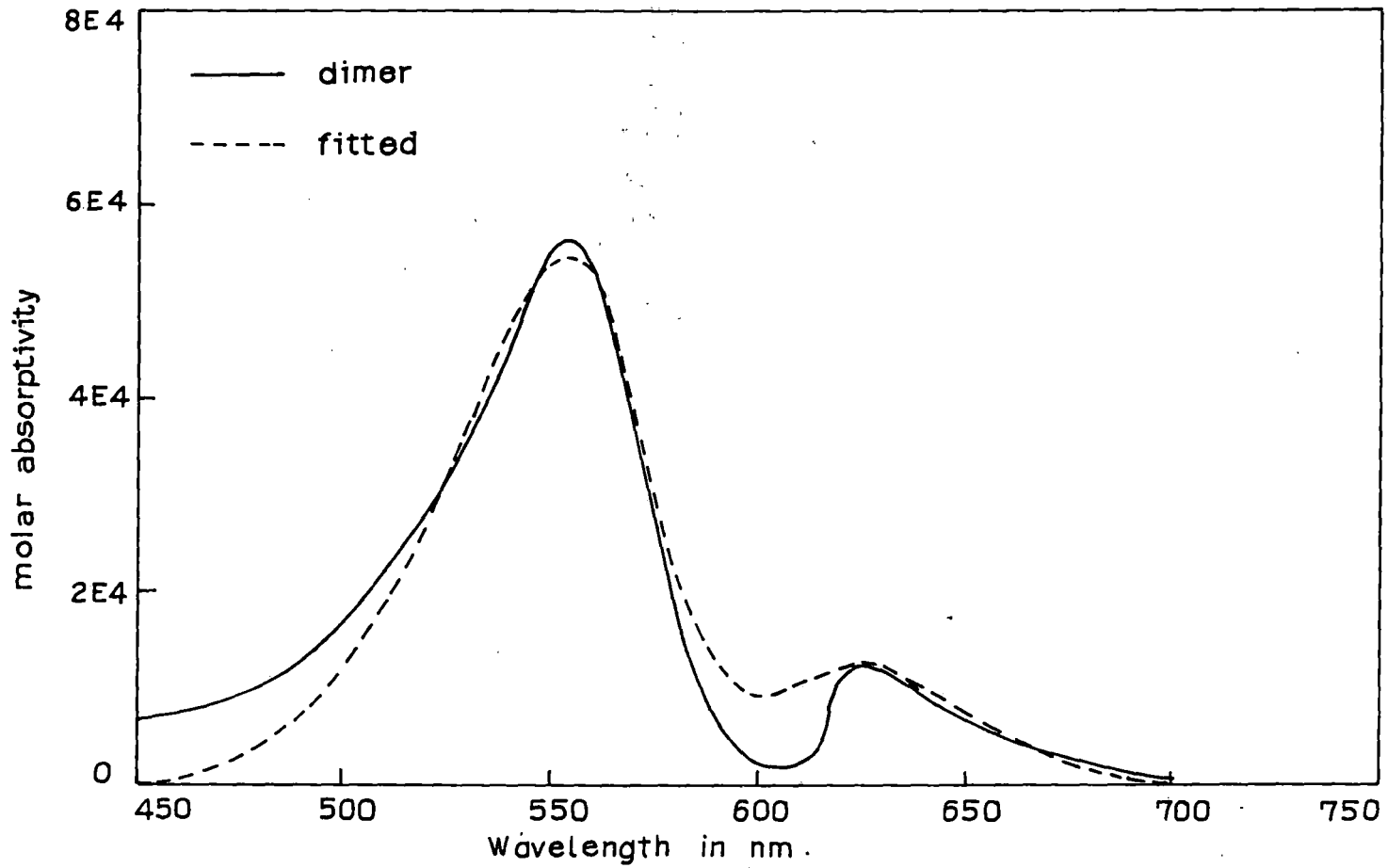

Fig. 38 Absorption spectra of Thionine dimer.

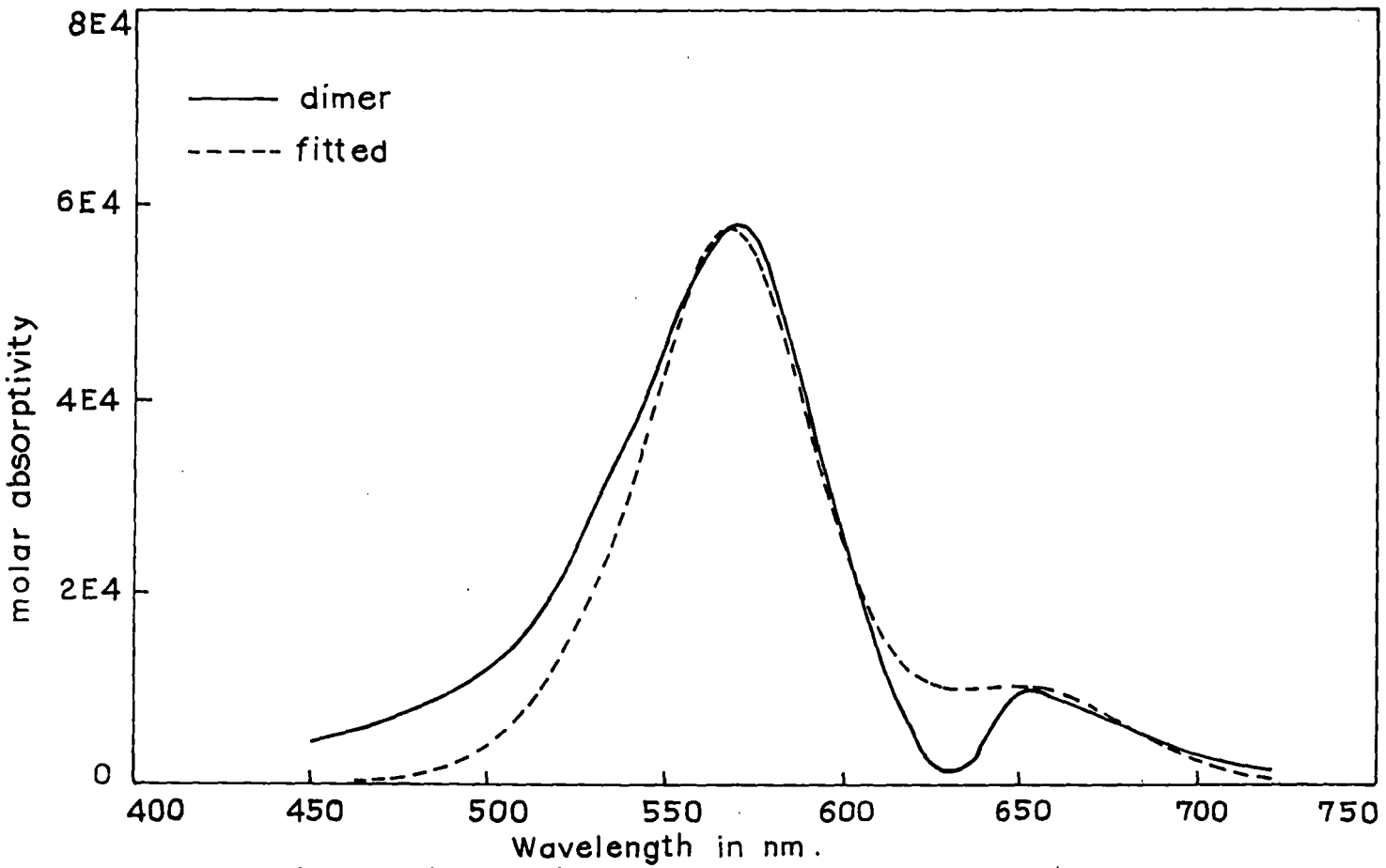

Fig.39 Absorption spectra of Azure C dimer.

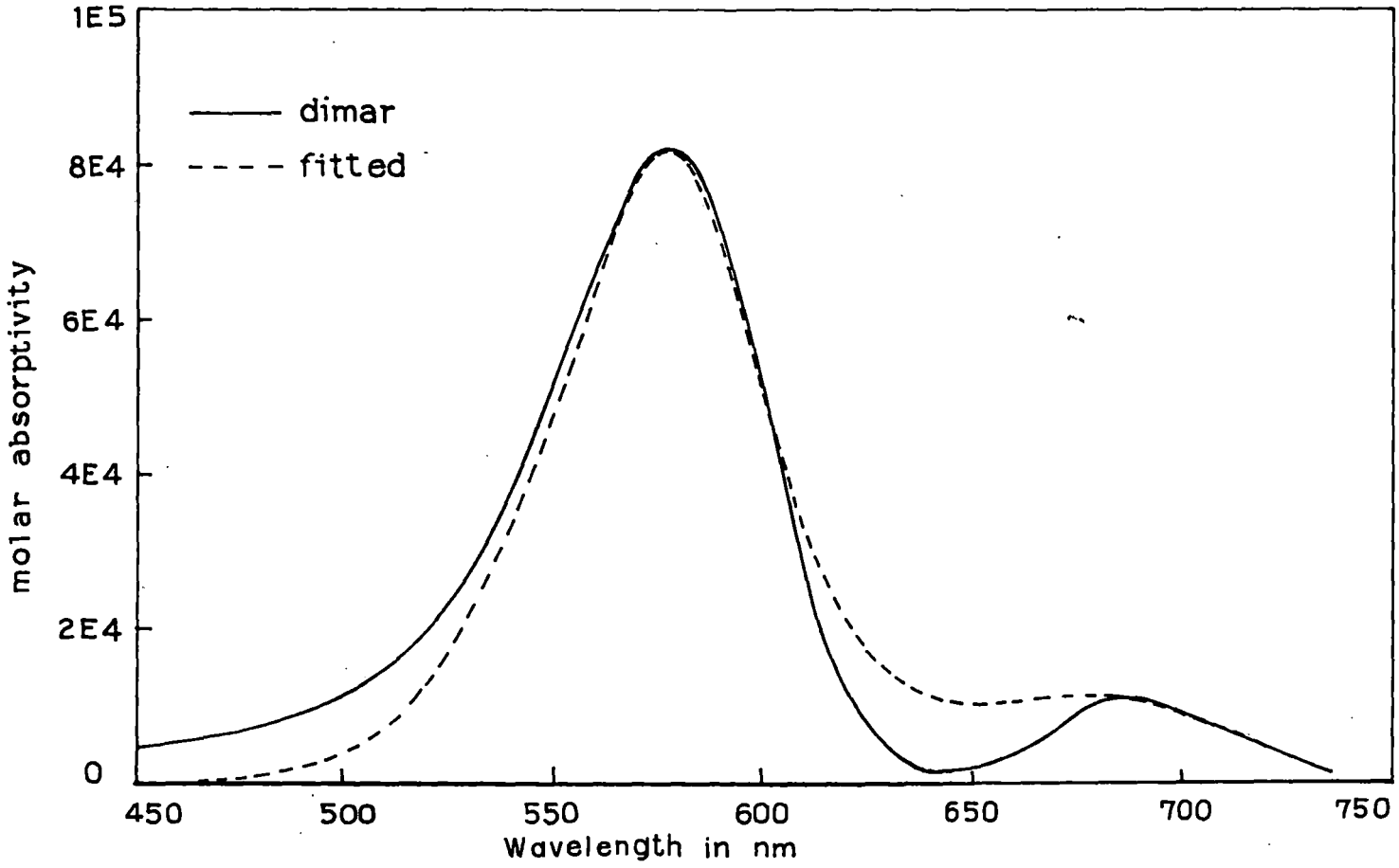

Fig. 40 Absorption spectra of Azure A dimer

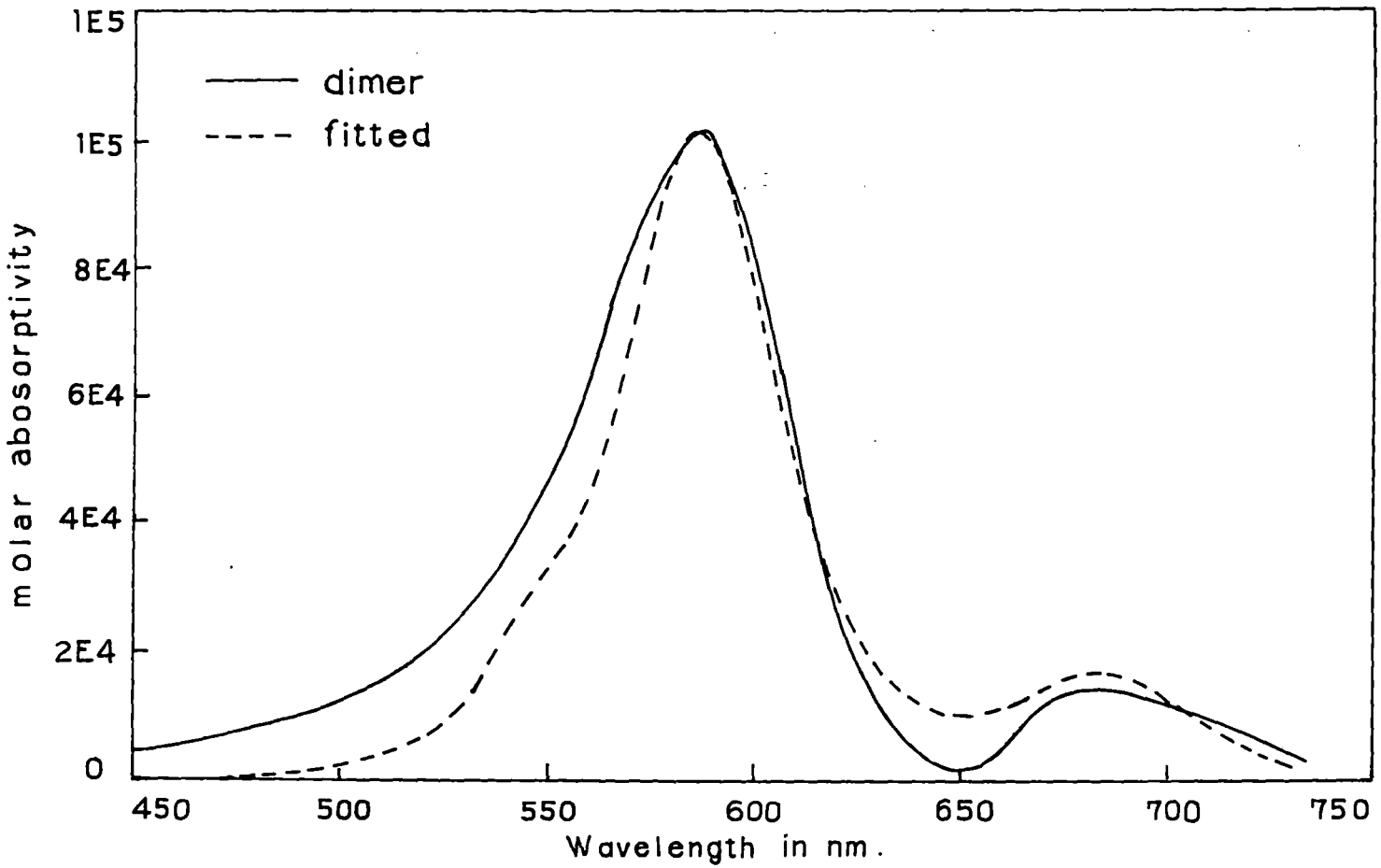

Fig.41 Absorption spectra of Azure B

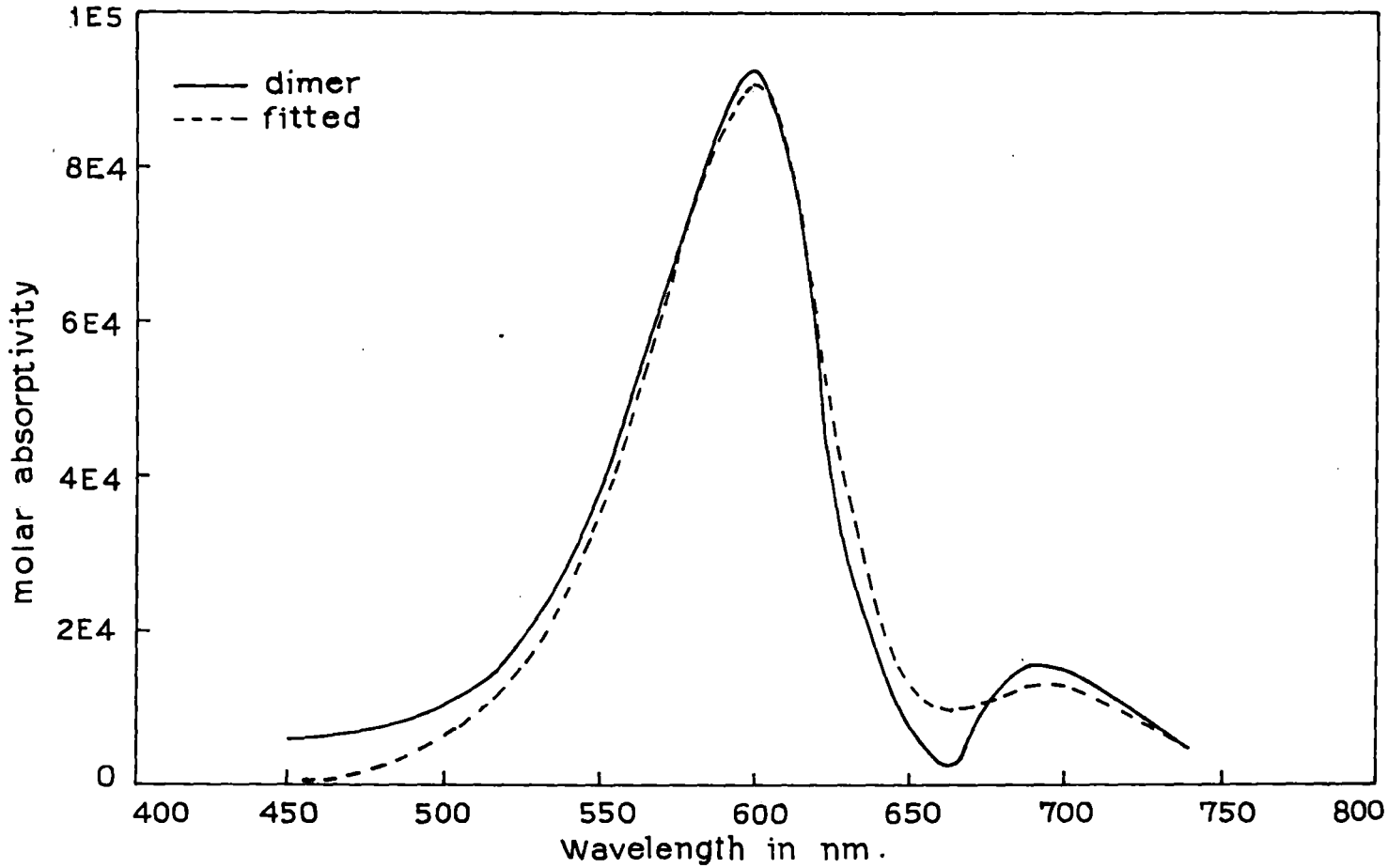

Fig. 42 Absorption spectra of Methylene Blue dimer.

to equal the corresponding monomeric value. [calculations and fittings of dimer spectra were done partly in this department on a PC-AT (486 DX2) computer and partly in the department of Chemistry, University of South Australia, by means of a weighted least square program (81,89)]. All the calculated dimer spectra in Figs. 38-42, refer to zero angle between the transition moments i.e., the minimum series is zero in each case. However, fittings are not always very well, specially at the lower and higher energy regions of the dimer spectra. The fitting may be somewhat improved by replacing the fitted monomer constants V and X by corresponding parameters fit in analysing the dimer spectra. But, such a procedure has been avoided because in that case the significance of V and X would become obscure. The dimer fitting parameters for all the five thiazine dyes are shown in table 12. We note that $\bar{\nu}_{oo}$, which is the position of the (0,0) band of each of the two monomers in the dimer, undergoes a hypsochromic shift relative to that of the free monomer (table 11,12); such a hypsochromic shift is attributed to the differences in Vander Waals (solvent-solute and solute-solute) interactions between the two systems. Theoretically the minus series affects predominantly the low energy region of the spectrum whereas the plus series affects the high energy region (81). But no amount of discrepency from the minus series can explain the discrepancy between the model proposed by Fulton (75) and the experimental spectra for the dye system. However, minus series is included in

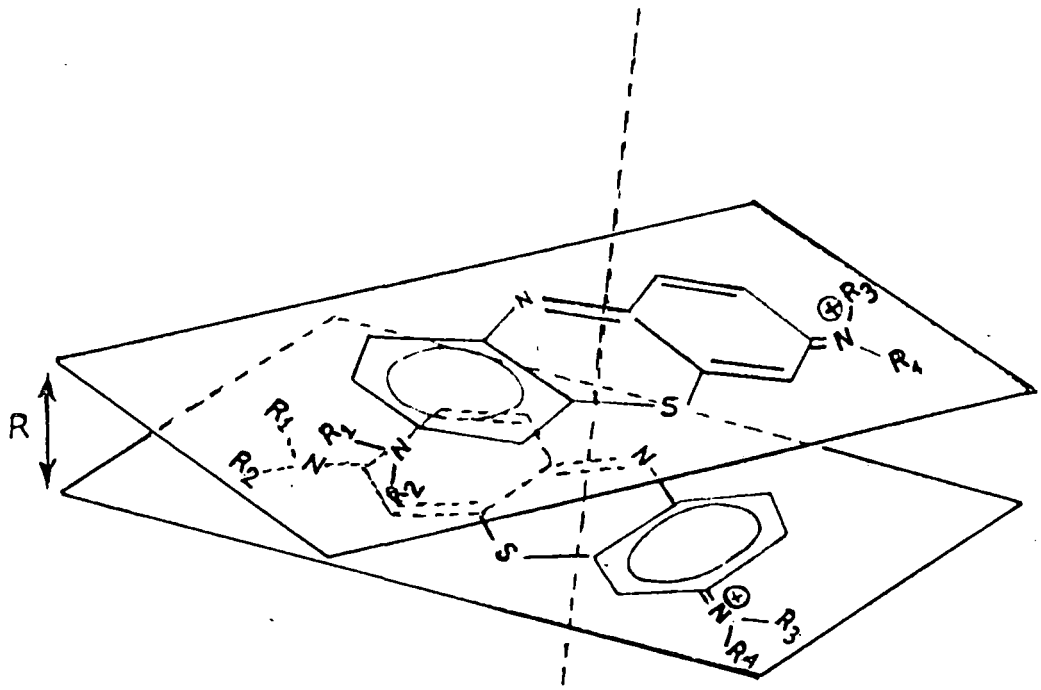

Fig.43: Geometric structure of dimer of Thionine and its derivatives

Thionine : $R_1 = R_2 = R_3 = R_4 = H$

Azure C : $R_1 = R_2 = R_3 = H$, $R_4 = CH_3$

Azure A : $R_1 = R_2 = H$, $R_3 = R_4 = CH_3$

Azure B : $R_1 = H$, $R_2 = R_3 = R_4 = CH_3$

Methylene Blue : $R_1 = R_2 = R_3 = R_4 = CH_3$

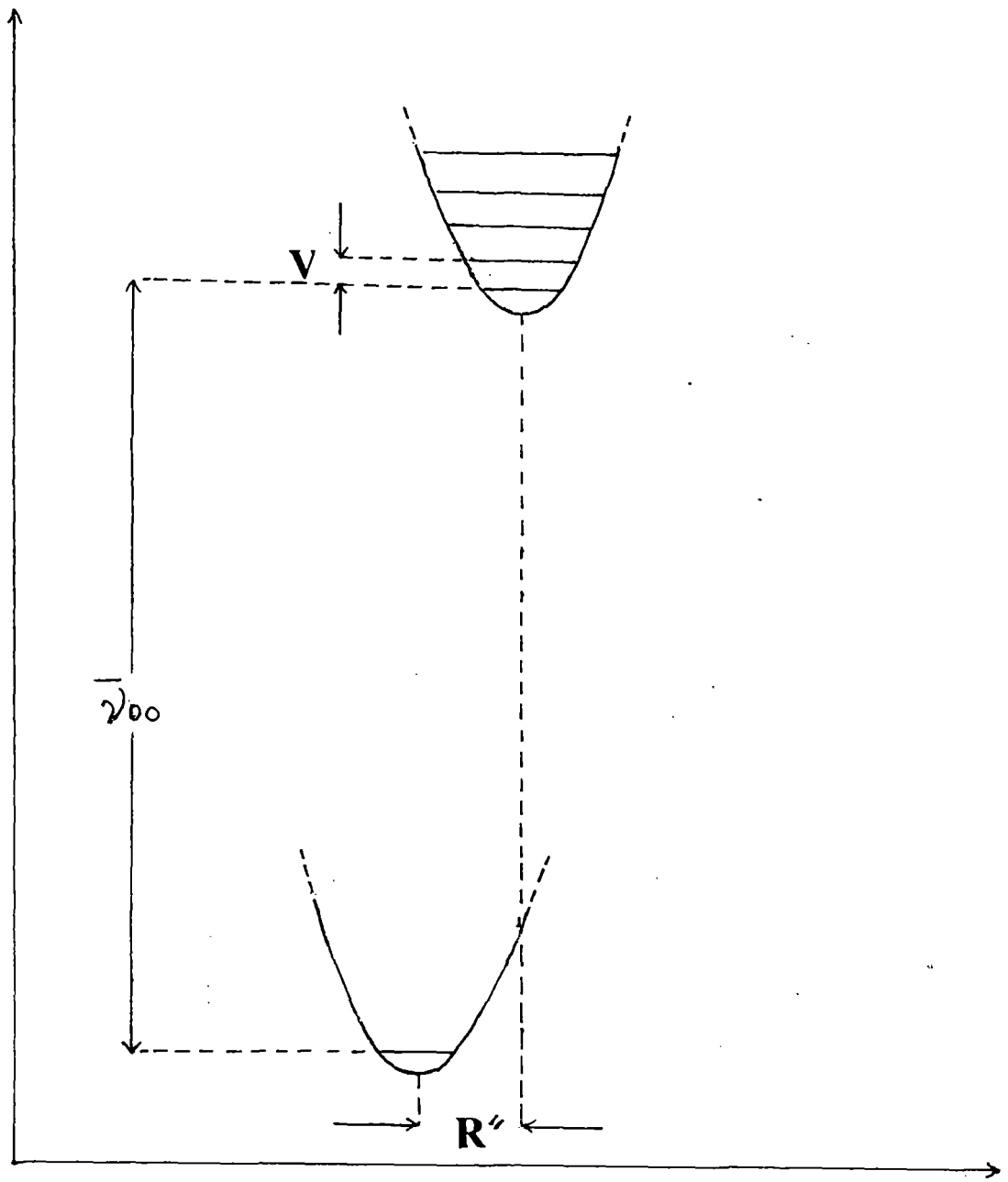

Fig.44: Schematic potential energy diagram in absorption.

Table 11

Monomer Parameters for the five Thiazine dyes Spectra with standard deviations:

	Th	AzC	AzA	AzB	MB
I_{oo}	63380±1575	50300±992	46700±1520	71180±1091	73260±1470
$\bar{\nu}_{oo}(cm^{-1})$	16778±450	16103±441	15723±643	15552±290	15197±300
V (cm^{-1})	1217±76	1182±79	1131±131	1155±48	1204±55
X	0.56±0.036	0.52±0	0.61±0.067	0.54±0.023	0.56±0.027
$b_g(cm^{-1})$	1116±33	1185±30	1402±47	1070±20	1052±24

Table 12

Dimer Parameters for the five Thiazine dyes:

	Th	AzC	AzA	AzB	MB
ε	0.90	1.00	1.15	1.05	1.10
$\bar{\nu}_{oo}(cm^{-1})$	16393	15873	15385	15267	14925
V (cm^{-1})	1220	1182	1130	1155	1204
X	0.56	0.52	0.61	0.54	0.56
$b_g(cm^{-1})$	1100	1400	1400	1200	1200

many dye systems previously to produce the longer low energy "shoulder" which is not observed in the spectra of the present thionine and alkyl substituted dyes (81). Table 12 shows that the value of exciton interaction parameter (ε) varies from 0.90 to 1.15 for five thiazine dyes with the lowest value for Th and the hightest for AzA. These relatively small values of interaction parameters provide some support for the model. However, further study in this area is in progress in our laboratory.

CHAPTER 4

ELECTROCHEMICAL STUDIES OF THE DYES ON CLEAN AND MODIFIED ELECTRODES

4.1. INTRODUCTION AND REVIEW OF THE PREVIOUS WORKS :

Cyclic voltammetry is perhaps the most powerful electroanalytical technique for the study of electroactive species. Various electrochemical aspects of photogalvanic solution during the photochemical reactoin have been studied successfully by many workers with the aid of this technique. The ease of the measurement has also resulted in extensive use of the technique.

Electrochemical properties of rhodamine B by cyclic voltammetry at fixed and rotating disk electrode were studied by Austin et al.(97). During electrode modification, the surface coating was deposited by voltage cycling and formed only when the anodic potential exceeded 1.24 V, at which stage rhodamine B was deethylated and converted to rhodamine 110. This was then reversibly oxidized to form the surface modifying species. The prominent oxidation and reduction peaks were observed at 1.18 and 1.10 V respectively in the cyclic voltammogram of rhodamine B at an unmodified SnO_2 glass electrode, which were suppressed by the surface modification. Rotating disk measurement gives a value of $3.2\pm0.2\times10^{-6} cm^2 sec^{-1}$ for the diffusion co-efficient of 9.6×10^{-4}M rhodamine B in aqueous 0.05M H_2SO_4. Cyclic voltammetric measurement gives a value of $1\times10^{-2} cm\ sec^{-1}$ for the rate constant

of quasi-reversible oxidation of rhodamine B which occurs around 1.18V at an SnO_2 glass electrode. Bauldrey and Archer (98) have reviewed the literature on the electrochemical and non electrochemical modificaton of the electrode surfaces and have proposed a mechanism for the electrochemical deposition of layers of thionine and related dyes using the information gained from cyclic voltammetric studies of these systems. Quickenden and bassett (99) have studied the anodic deposition of the dye from aqueous rhodamine B solution to gold electrodes and found that substantial deethylation occured during the deposition process and that the electrodes thus coated possessed enhanced photosensitivity. Bowen (100) has examined rhodamine B solution by cyclic voltammetry using Pt electrode and also determined the electron transfer rate constant for the Fe^{3+}/Fe^{2+} couple at rhodamine B coated Pt electrode by rotating disk method. However, the author did not determine the electrodic rate constants for electron transfer to and from rhodamine B at such electrodes.

The cyclic voltammetric behaviour of chloropromazine (CPZ) at a carbon paste electrode in aqueous 0.1M HCl showed two anodic waves with peak potentials of +0.66 and +0.99V Vs. SCE, corresponding to the oxidation of CPZ to its cation radical (CPZ^+) and subseqently to its dication (CPZ^{2+}) (101,102). Upon the scan reversal only the cation radical is found to be sufficiently stable to yield a cathodic wave. The dication reacts very rapidly in this medium, so that the reduction of dication is

not observable even at scan rates upto 50 V/s.

In genaral, chemical or electrochemical oxidation of N-substituted phenothiazine in aqueous solution has been shown to yield the corresponding sulphoxides through the formation of mono-cations which are prone to facile hydrolysis in neutral and less acidic medium as compared to that in more acidic media (103). On the other hand, a linear dependence of voltammetric peak current on the square root of the scan rates suggests that the cyclic voltammetric behaviour of thionine, which is attributed to two electron reduction of thionine to leucothionine, is of the diffusion type (104). Quickenden and Harrison (105) studied electrochemical properties of thionine by cyclic voltammetry at uncoated and thionine coated photoelectrodes. Examining the cyclic voltammograms obtained during the deposition of thionine on Au and SnO_2 electrodes, they observed that the height of the characteristic thionine oxidation and reduction peaks increased with the number of cycles to asymptotic limits after about 70 cycles in the case of a Au electrode and after 500 cycles in the case of SnO_2. The areas within the voltammograms similarly reach plateu values. Because the areas, ($\int Idt$), I being the current and t the time, are also independent of cycle speed, it can be concluded that complete oxidation and reduction of the electroactive species occur during each cycle, thus validating the use of areas under peaks for determining layer thickness.

During the cyclic deposition process on Au, the thionine reduction and leucothionine oxidation peaks which are originally at 0.43 and 0.49V respectively, shift in turn to 0.49 and 0.54V, and a small shoulder appears at about 0.43V. However, during the deposition on SnO_2, the thionine reduction peak at 0.435V does not shift. But the oxidation peak moves from 0.535 to 0.550V, and the shoulder on the reduction peak appears only temporarily during the middle stage of the deposition. Albery et al.(106) observed that the reduction of thionine on clean Pt-electrode was reversible whereas on the coated electrode it was nearly reversible. From the measurement of the kinetic parameters for different electrodes, they concluded that the electrochemical rate constant was decreased for electrodes coated at higher voltages and for longer times. In particular, there was a significant reduction in rate constant for electrodes coated at 1.4V or above for periods longer than one hour.

The reduction of methylene blue was studied by Wopschall and Shain (107) to test the theory of cyclic voltammetry for the case in which the product of the electrode reaction was strongly adsorbed. A brief investigation of the mechanism of two electron electrode reduction, using both aqueous ethanol and aprotic solvent systems, indicated that the reduction probably proceeded through successive one electron charge transfer, with a rapid reversible protonation interposed between the charge transfers. The intermediate appeared to be more easily reduced than

methylene blue.

In a recent study on electrochemical aspects of reaction between leucodye and Fe^{+3} in dye based photogalvanic systems, Murthy et al. (108) examined the electrochemical reduction of thionine and methylene blue in the presence of Fe^{+3} in terms of catalytic regeneration mechanism. The catalytic current due to the homogeneous chemical reaction between leucothionine and leucomethylene blue dyes and Fe^{+3} have been used to estimate rate constants.

Chemical modification of electrodes is a major area of current interest in electroanalytical chemistry and photoelectrochemistry. Techniques such as covalent attachment or casting of polymer films on electrodes are widely employed as a means of modification. In electrochemical and photoelectrochemical studies of dye incorporated clay modified electrode, Kamat (25) observed that clay modified electrode exhibits a quasi-reversible oxidation wave (E_{pa} = 0.280V, E_{pc} = 0.190V vs SCE) which is comparable to the reversible wave of thionine in aqueous solution (E_{pa} = 0.265V, E_{pc} = 0.205V vs. SCE). This shows that the electrochemical identity of the dye has been retained in the clay film. Such an electrochemical behaviour was similar to one observed with Albery's (106) thionine coated electrode. Presence of polyvinyl alcohol and colloidal Pt in the clay film was found to be critical in attaining better electrochemical activity of the clay modified electrode. In

agreement with the work reported earlier (109) only a fraction of the incorporated dye was found to be electroactive in the clay film.

The dependence of the peak current on the square root of the scan rates was linear, thereby suggesting the observed cyclic voltammogram of SnO_2/clay-thionine as diffusion type. Normally, one would have expected a surface wave for these modified electrodes. The diffusion type cyclic voltammetric behaviour observed in the present case suggests that the charge transport within the film is limited either by the diffusion of the electroactive dye to the electrode surface or by an electron hopping process within the clay film (25).

In a review on clay modified electrode, Fitch (110) mentioned that one of the attractive features of clays for use in electrode modification is the high reactivity of the clay surface with organics. This feature can be exploited to localize an organic substrate in close proximity to the electrode to enhance an electrochemical process. Inoue and Yoneyma (111) capitalized on this feature in the study of electropolymerization of aniline in the clay support. Following the same rationale, Rusling et al. (112) attempted to combine the adsorption of organics with the CEC of clays to enhance the electroreduction of the aryl halogen, dibromobenzene. The clay modified electrode has been used to support RuO_2 near the electrode surface (113) . In this application, catalytic current for the reduction of

$Ru(bpy)_2[bpy(CO_2)_2]$ was observed in which $Ru(bpy)_2[bpy(CO)_2]$ shuttled charge to a substrate, thought to be RuO_2. The authors suggested that RuO_2 was involved in the oxidation of H_2O. Further utilization of clays lies in its potential to impart chiral selectivity to the reaction. Yamagishi and Aramata (114) found that a clay modified electrode exposed to D-$Ru(phen)_3^{2+}$ showed no increase in currents on exposure to additional solutions of D-$Ru(phen)_3^{2+}$, but showed an increase in current on exposure to L-$Ru(phen)_3^{2+}$. Their conclusion was that the primed [D-$Ru(phen)_3^{2+}$] clay accommodated the L form of the complex via stereoselective packing. In a similar fashion, Fitch et al.(115) observed larger reduction currents from recemic vs. enantiomeric solution of $Cr(bpy)_3^{3+}$. They concluded that the recemic solution allowed for more efficient packing of the complex on the clay surface. Electrochemical behaviour of $Fe(CN)_6^{3-/4-}$ ions at H-,Na- and Ca-montmorillonite modified Pt-electrodes incorporating methylene blue and neutral red cationic dyes was investigated recently by cyclic voltammetry (116). The rate of the redox process was found to be mainly determined by the structure of the film of clay mineral particles.

In addition to the clay minerals another potential inorganic modifier is zeolite. Recent reviews on the material science aspects of the zeolites and the use of zeolites to coat electrodes (24,117) have included discussions on the use of and interest in zeolite layers on electrodes.

An understanding on the mechanism of the charge transport, control of the pore dimensions to enhance transport properties, and complete elucidation of the role of the electrolyte in ion exchange reaction and charge conduction are absolutely required.

As mentioned in chapter 1, the most successful PG cell for solar energy conversion is the ferrous/thionine cell yet, this too is far from having ideal coversion effeciency (118,119). In this PG cell the photoreduction of thionine (Th) by Fe(II) ions produces semithionine (S) and Fe(III) ions. Semithionine rapidly disproportionates to Th and leucothionine(L). Structures of thionine, leucothionine and semithionine are shown in chapter 1 (page 3). The adventage of the above system lies in achieving partial selectivity of charge carriers for appropriate electrodes. However, greatest efficiency would be obtained with a PG cell in which each electrode is perfectly selective for a different couple. Unfortunately, in homogeneous solution, thermal back reaction of electron transfer also takes place. This dissipation of free energy creates a considerable problem in the use of ferrous/thionine PG cell for any practical purposes (120). The following reaction scheme adequately summerizes the whole process, including the relevant recombination reactions ($_{P}H$ 3) (121)

$$Th + Fe(II) + H^{+} \xrightarrow{h\nu} S + Fe(III)$$

$$2S + H^{+} \rightleftharpoons Th + L$$

Back reaction :

$$S + Fe(III) \longrightarrow Th + Fe(II) + H^{+}$$

$$L + Fe(III) \longrightarrow S + Fe(II) + 2H^{+}$$

However, the homogeneous reaction scheme is very complicated and must be properly characterized. Solubility as well as aggregation characteristics of dyes are important criteria which control PG output. As already mentioned (chapter 1), alkyl substitution in dyes affect both these characteristics and , this promted to undertake the present series of progressively alkylated thiazine dyes for a detail study on homogeneous reactions with Fe(III) ions. Electrode reaction coupled with chemical reaction is an interesting subject of investigation for electrochemists (122). The electrochemical reaction of progressively alkylated thiazine dyes to corresponding leucodyes at the stationary electrode in the presence of Fe(III) ions may be described by what is called "catalytic regeneration mechanism", according to which an initial electroactive species is regenerated by the homogeneous chemical reaction . This mechanism can be described by the following scheme (122),

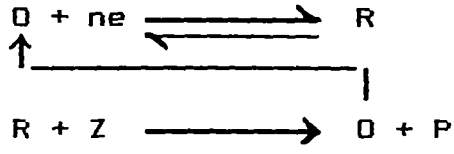

(40)

If applied judiciously, this technique may yield kinetic parameters of the chemical reaction from a simlpe electrochemical experiment. Although thermal back reactions have been studied by flash photolysis technique in considerable detail (121,123-125) the former technique has been applied only recently for the homogeneous reaction relevant to Ferrous/Thionine PG cell. Kinetic parameters were also determined using an indium doped SnO_2 electrode assuming a pseudo first order reaction condition to prevail even though the experimental result did not always conform with the theory (108). In view of the pivotal importance of the nature of the electrode surface in such a study and also to examine the role of the hydrophobic interaction, if any, on the reaction kinetics, an electrochemical study on the reaction between the alkyl derivatives of thiazine leucodyes with Fe(III) on a glassy carbon electrode (GCE) which has been found to be well behaved in the present set of system is also undertaken in the present investigation.

In the next part of the chapter electrochemical properties of progressively alkylated five thiazine dyes and the electrode phenomena involved therein have been studied by cyclic voltammetry in different media at stationary clean electrode as well as at modified electrode. Thionine and methylene blue are also reinvestigated in the same experimental conditions in order to compare the results and for the sake of systemetic study of the selected series of the dyes. The electrochemical processes at the electrodes involving dyes in the presence of Fe^{+3} as an

oxidant have also been examined in terms of catalytic regeneration mechanism.

4.2 EXPERIMENTAL :

Cyclic voltammetric experiments with the selected cationic dyes viz. Thionine, Azure C, Azure A, Azure B , and Methylene Blue are carried out in water, water-ethanol mixture and triton X-100, a nonionic amphiphile, at $25\pm1^{0}C$ to understand their electrochemical behaviour on glassy carbon electrode (GCE). In the present study these dyes are also incorporated in the clay and zeolite films cast on the GCE to study electrochemical behaviour of the dye molecules at the modified electrode.

Various characteristics of the dyes, their structure and method of purification, are persented in chapter 3. Preparation of pure Na-montmorillonite, used as clay in the study, and its CEC have been described in chapter 5. The zeolite, ZSM-5 (Si/Al≅ 30, surface area= 400 m^2/g), is used as received. All other chemicals used are of analytical grade.

Colloidal Pt is prepared by refluxing 0.168 g/lit. (H_2PtCl_6) in a water : ethanol (1:1) mixture containing 3% polyvinyl alcohol (126). Colloidal suspensions are prepared from Na-montmorillonite and ZSM-5 using the method employed by Kamat

(25), i.e. by dispersing 10 g of Na-montmorillonite and ZSM-5 separately in 100 ml of water and are centrifuged at 6000 rpm for 1 hour . The clay and zeolite content of the supernatant colloidal suspensions are found to be 8 and 7 g/lit. respectively.

The casting of the clay and zeolite films on the GCE (diameter 3.2 mm, BAS, USA Part No.MF 2012) is done in the following way (109). One part of the clay or zeolite suspension is mixed with two parts of colloidal Pt suspension and 0.1 ml of the mixed suspension is placed over the previously cleaned GCE. After drying for several hours in air the electrode is dipped into the concentrated ($\sim 1\times10^{-3}$M) dye solution for 15 minutes. The electrodes, referred to as modified, are then washed throughly with water.

Cyclic voltammetric experiments are carried out employing BAS cyclic voltammograph (USA, model CV-27) fitted with a three undivided electrode cell and a Houston X-Y recorder (Model-100). The experiments are performed taking 25 ml dye solution in the presence of 0.1M H_2SO_4 or 0.1M KCl as a supporting electrolyte with one working GCE (MF-2012), one Pt auxiliary electrode and a saturated calomel reference electrode at 25 ± 1^0C. All solutions are purged with pure nitrogen before the experiment.

Cyclic Voltammetry at Clean GCE :

Cyclic voltammograms of the dye solutions ($5x10^{-5}$M) are recorded in water, water-ethanol (1:1) mixture and triton X-100 (0.001M) at various scan rates up to 300 mvs^{-1} using 0.1M H_2SO_4 as the supporting electrolyte. Cyclic voltammograms of the concentrated ($\geq 1x10^{-4}$M) dye solutions are also recorded at different scan rates using 0.1M KCl as supporting electrolyte at various $_pH$.

Cyclic Voltammetry at Modified Electrode :

Washed GCE/clay-dye and GCE/zeolite-dye are used as the working electrode and cyclic voltammograms are recorded dipping the electrode just only in 0.1M H_2SO_4 at various scan rates upto 300 mvs^{-1}.

4.3. RESULTS AND DISCUSSION :

4.3.1. Electrochemical studies on Clean Electrode :

In solution the dyes form dimers and higher aggregates at high concentrations (above 10^{-5}M). The dimerization constant values of the dyes in water and water-ethanol mixtures (5%, 10%,

15% and 20%) at different temperatures are given in table 3-7 in chapter 3. In aqueous medium at $30^{0}C$ the values are $1.76x10^{3}$, $2.35x10^{3}$, $3.38x10^{3}$, $6.25x10^{3}$, and $3.68x10^{3}$ for Th, AzC, AzA, AzB and MB respectively. Aggregation property of the dyes is an important factor for the interpretation of the cyclic voltammetric data.

All the dyes are reduced to the colourless leuco-dyes on forward scan and oxidized back to the corresponding coloured dyes on the reverse scan (Figs. 45-54) (104). The system undergoes reversible electrode reaction on the GCE in 0.1M H_2SO_4, (supporting electrolyte), upto scan rate 100 mvs^{-1} in water, water-ethanol and triton X-100 media. Others criteria, namely separation of the peak potentials and the half peak potential values are also in conformity with reversibility of the system upto the above scan rate. The values are given in table 13-17. The values of anodic peak current (I_{pa}) and cathodic peak current (I_{pc}) should be identical for a simple reversible (fast) couple. That is,

$$I_{pa}/I_{pc} = 1$$

But this ratio (shown in table 13-17) deviates from unity even at the slow scan rates. However, the deviation becomes less if the calculation is done using the following equation,

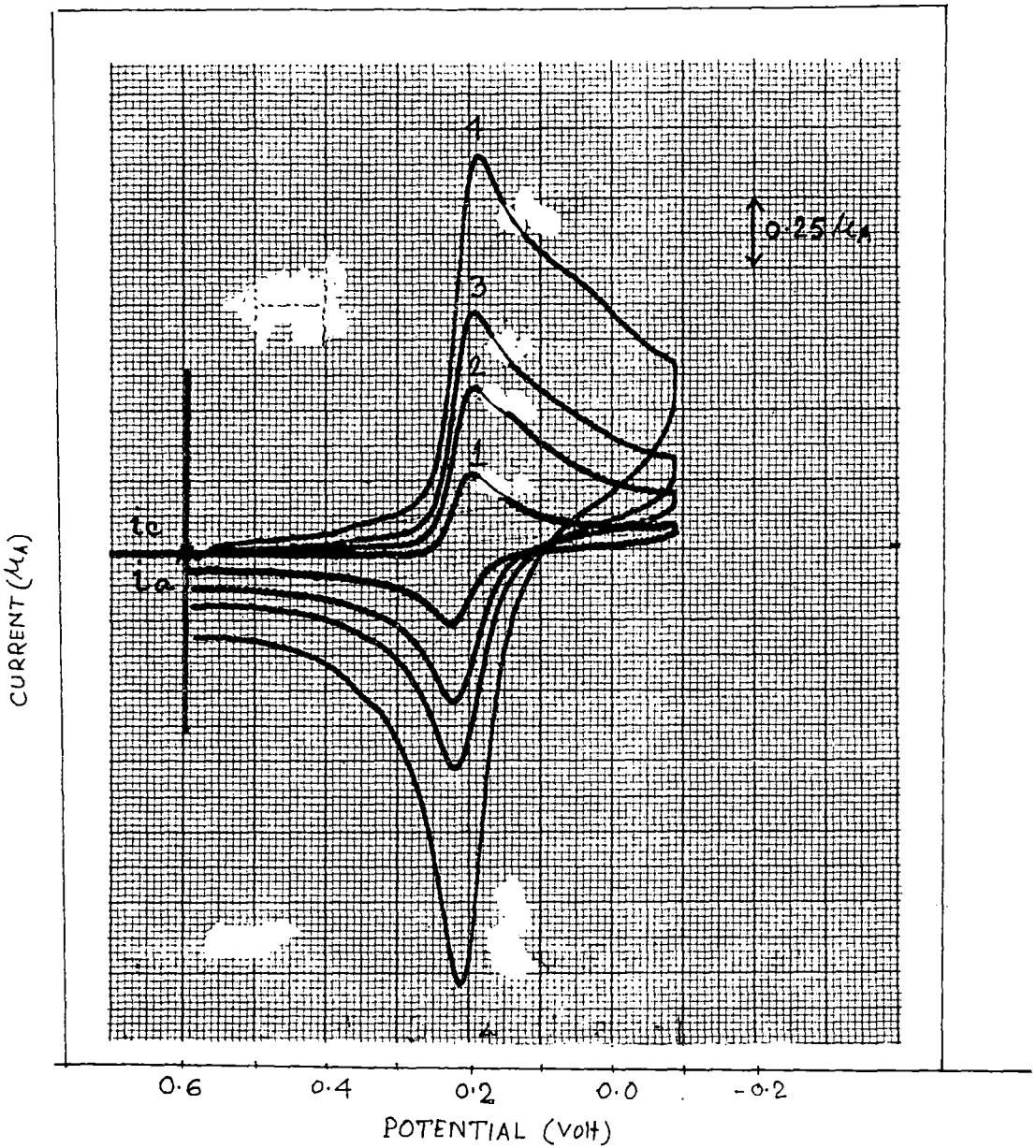

Fig.45: Cyclic Voltammograms of thionine ($5x10^{-5}$M) in water with scan rates [1-4], 5, 10, 20 and 40 mVs^{-1} in the presence of 0.1 M H_2SO_4.

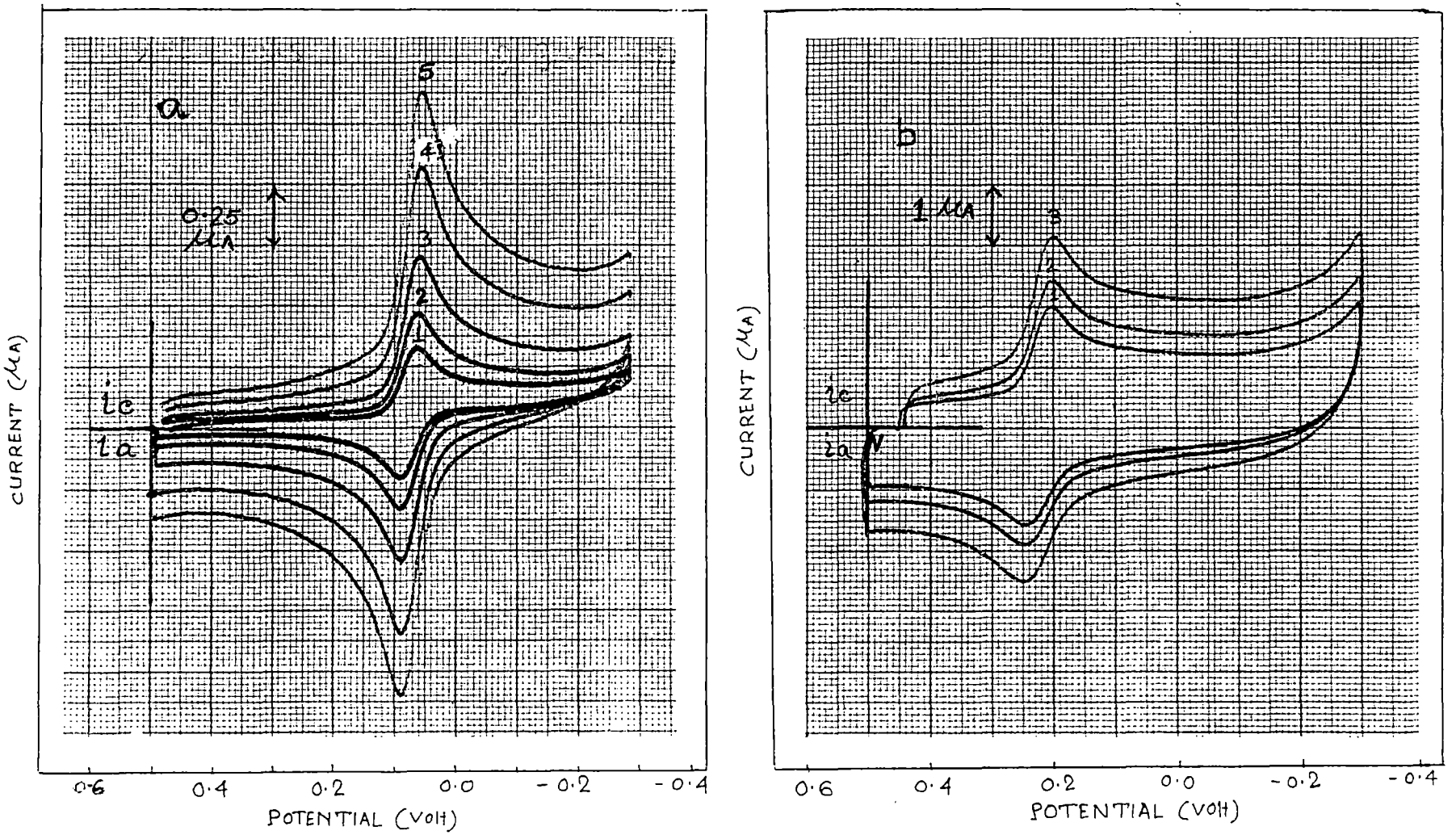

Fig.46: Cyclic Voltammograms of thionine ($5x10^{-5}$M) in (a) 50% Ethanol with scan rates [1-5] 5, 10, 20, 40, and 60 mVs^{-1} and (b) in 0.001 M triton X-100 with scan rates [1-3] 150, 200 and 300 mVs^{-1} in the presence of 0.1 M H_2SO_4.

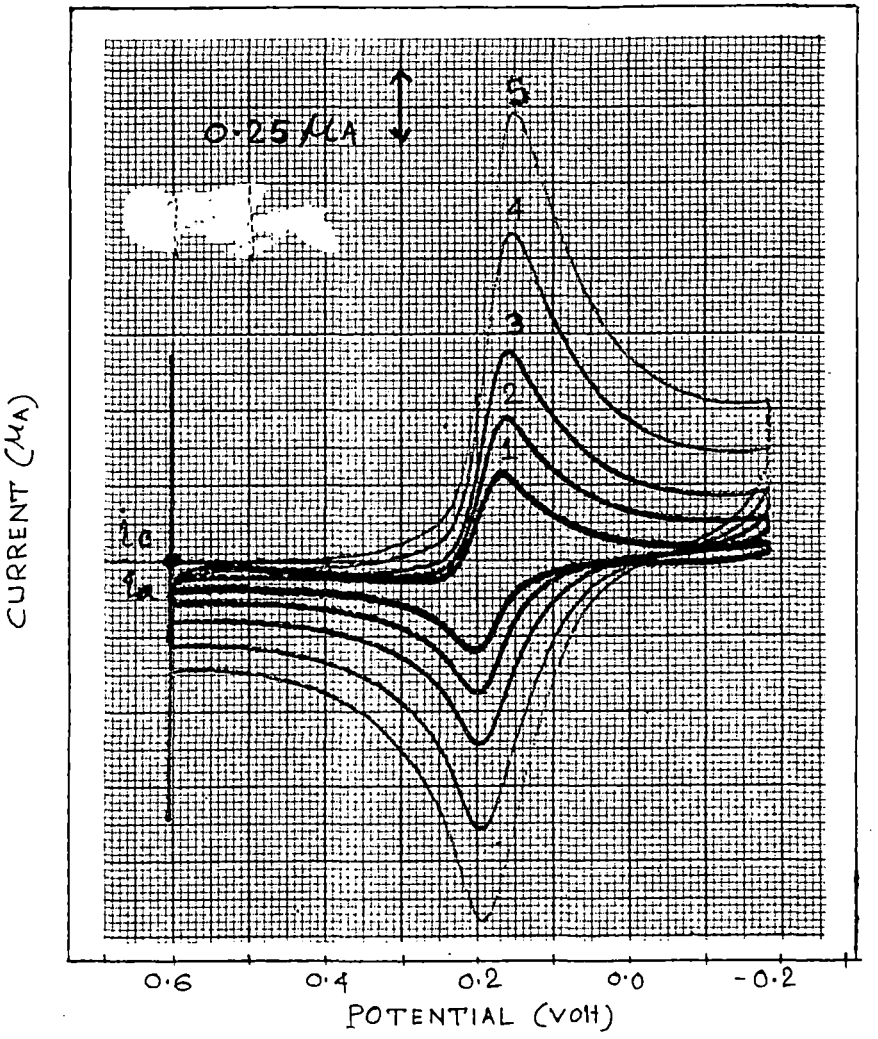

Fig. 47 : Cyclic Voltammograms of Azure C ($5x10^{-5}$M) in water with scan rates [1-5] 5, 10, 20, 40 and 60 mVs^{-1} in the presence of 0.1 M H_2SO_4.

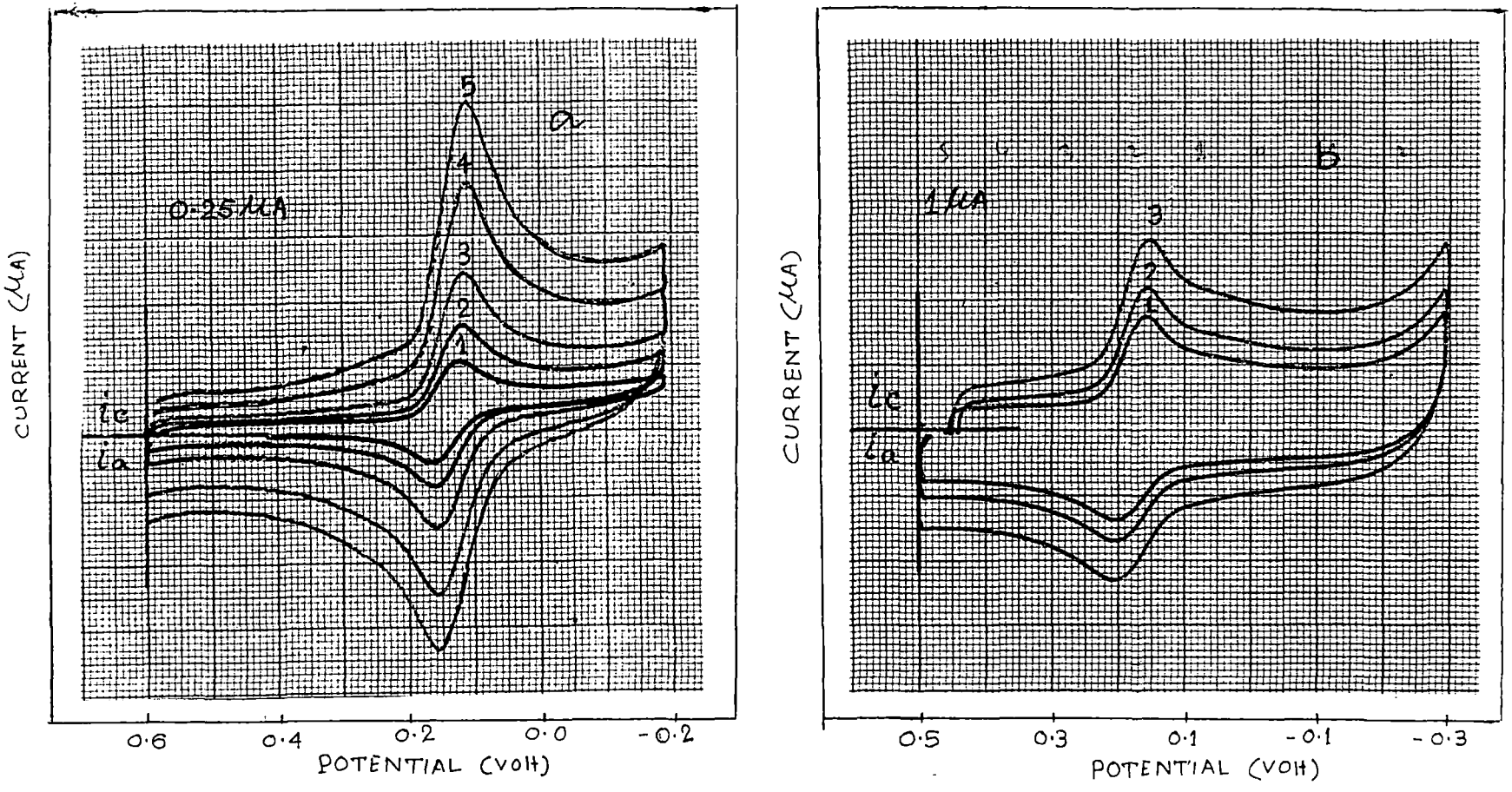

Fig.48: Cyclic voltammograms of Azure C ($5x10^{-5}$M) in (a) 50% Ethanol with scan rates [1-5] 5, 10, 20 40 and 60 mVs^{-1} and in (b) 0.001 M triton X-100 with scan rates [1-3] 150, 200 and 300 mVs^{-1} in the presence of 0.1 M H_2SO_4.

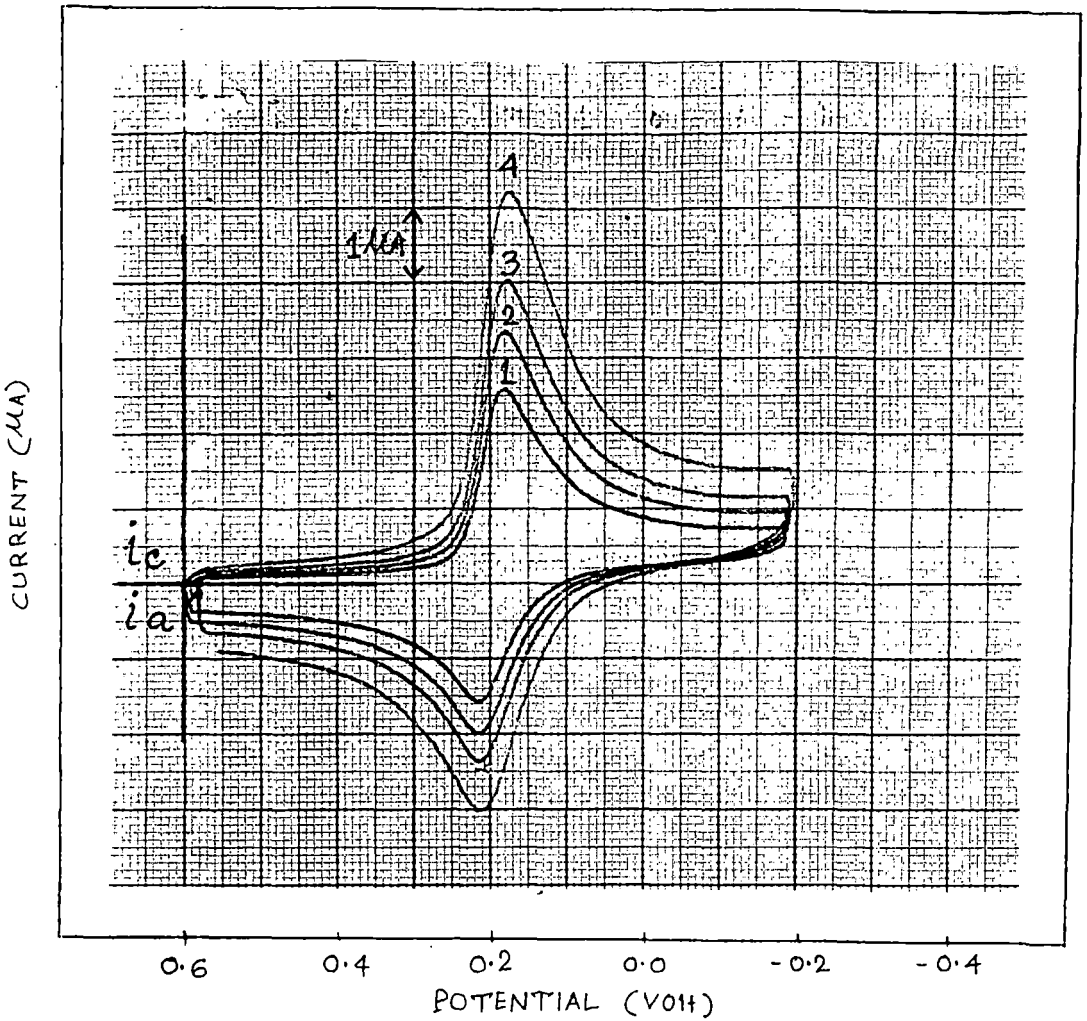

Fig.49: Cyolic Voltammograms of Azure A ($5\text{x}10^{-5}$M) in water with scan rates [1-4] 100, 150, 200 and 300 mVs^{-1} in the presence of 0.1 M H_2SO_4.

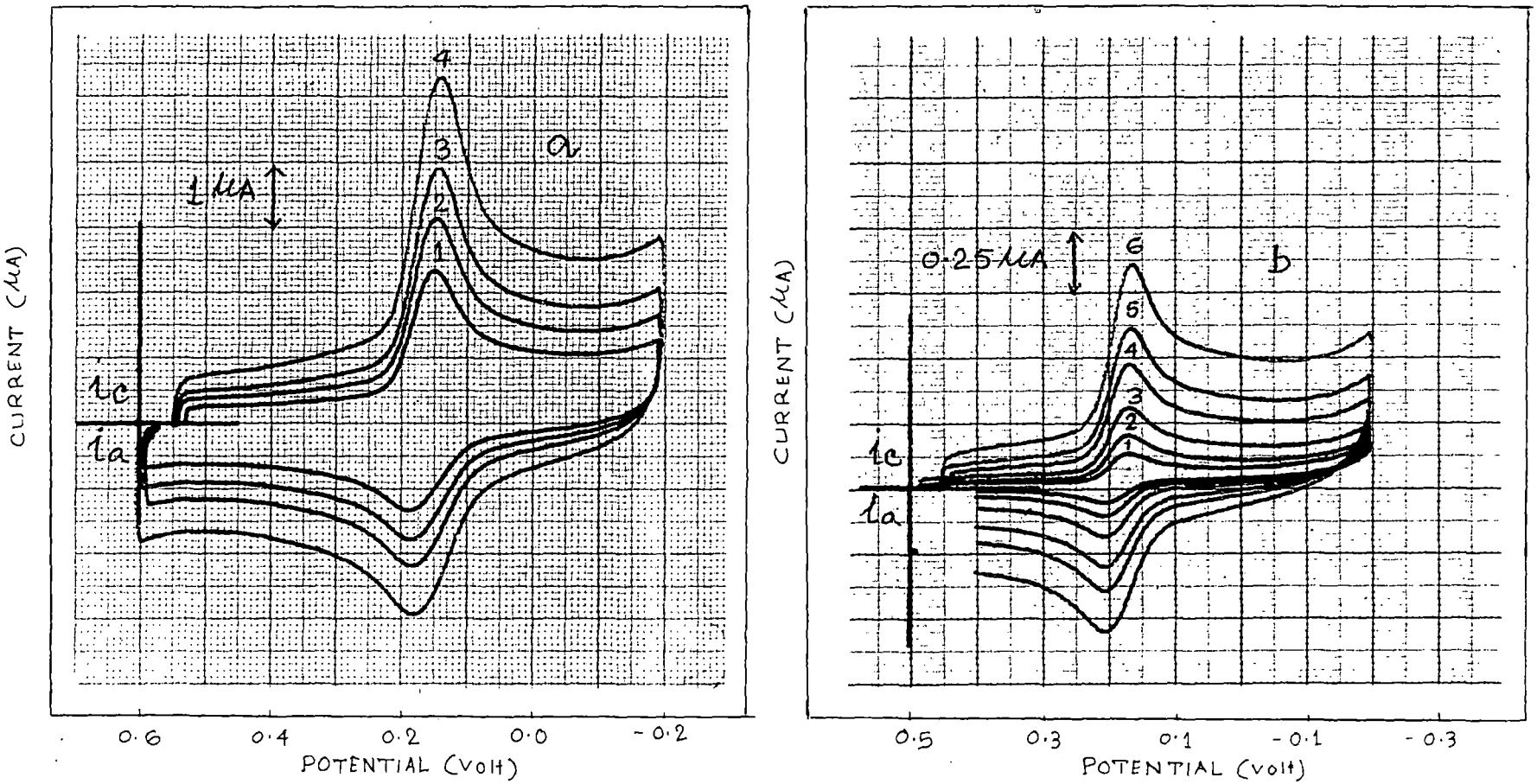

Fig.50: Cyclic Voltammograms of Azure A ($5x10^{-5}$M) in (a) 50% Ethanol with scan rates [1-4] 100, 150, 200 and 300 mVs^{-1} and in (b) 0.001 M triton x-100 with scan rates [1-6] 5, 10, 20, 40, 60 and 100 mVs^{-1} in the presence of 0.1 M H_2SO_4.

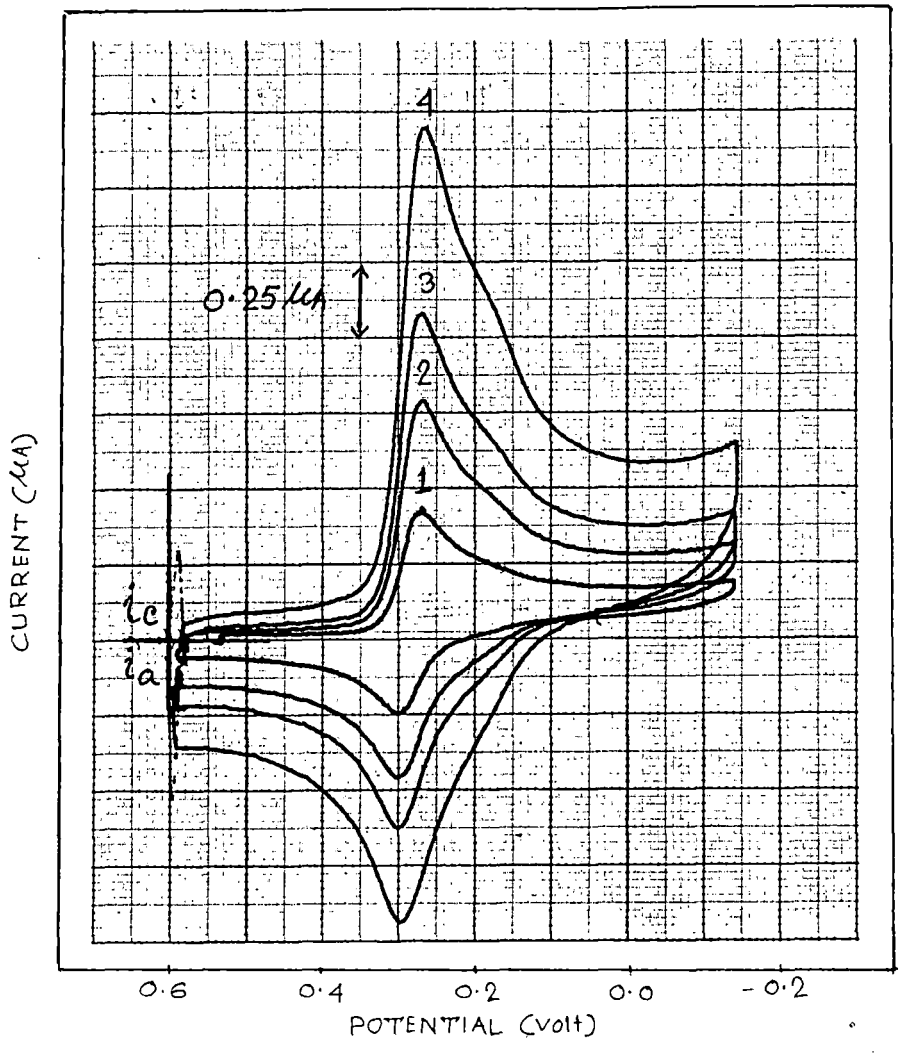

Fig. 51 : Cyclic Voltammograms of Azure B ($5x10^{-5}M$) in water with scan rates [1-4] 5, 10, 20 and 40 mVs^{-1} in the presence of 0.1 M H_2SO_4.

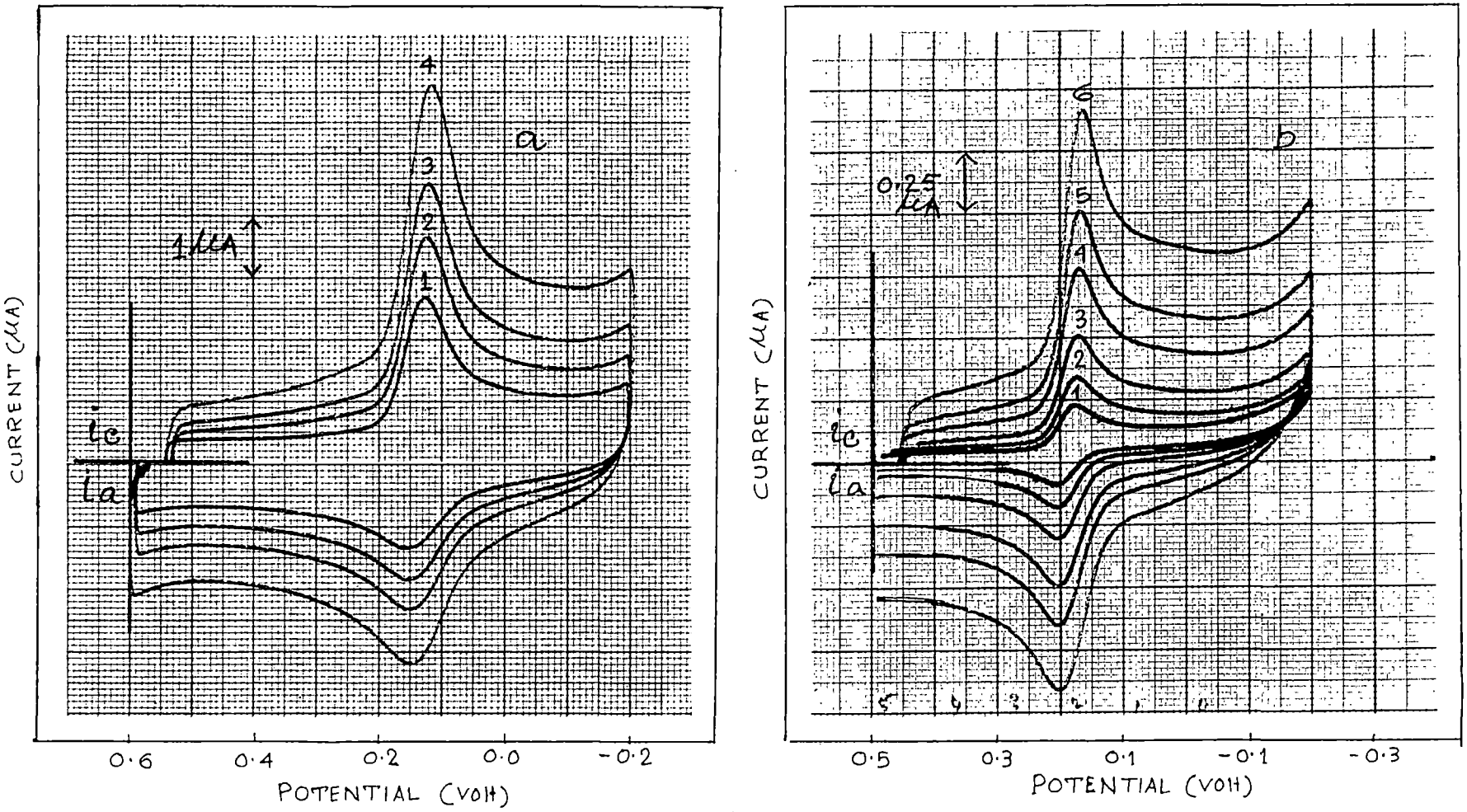

Fig. 52 : Cyclic Voltammograms of Azure B ($5x10^{-5}$M)in 50% Ethanol with scan rates [1-4] 100, 150, 200 and 300 mVs^{-1} and in (b) 0.001M triton x-100 with scan rates [1-6] 5, 10, 20, 40, 60 and 100 mVs^{-1} in the presence of 0.1 M H_2SO_4.

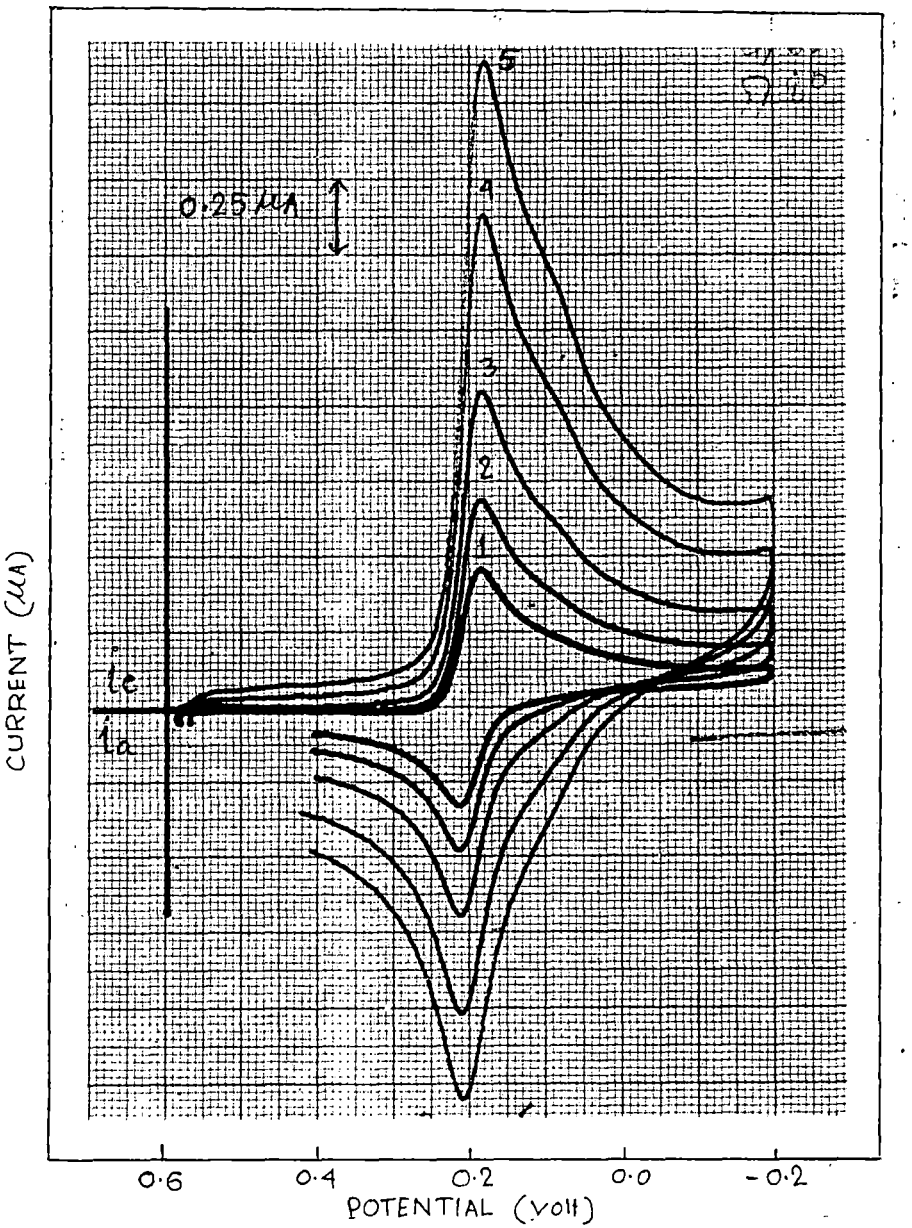

Fig. 53 : Cyclic Voltammograms of Methylene Blue ($5x10^{-5}$M) in water with scan rates [1-5] 5, 10, 20, 40 and 60 mVs^{-1} in the presence of 0.1 M H_2SO_4.

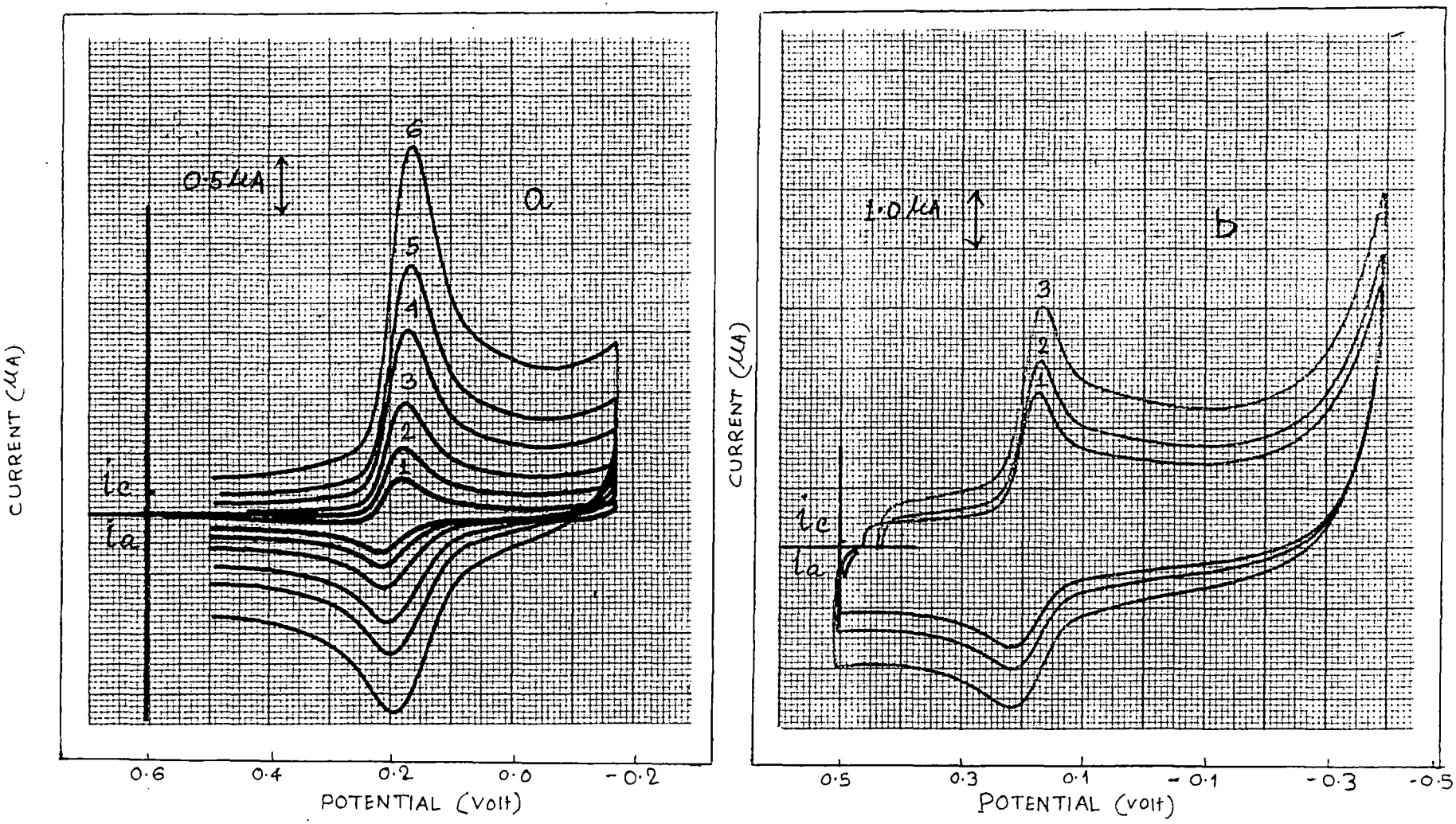

Fig. 54 : Cyclic Voltammograms of Methylene Blue ($5x10^{-5}$M) in (a) 50% Ethanol with scan rates [1-6] 5, 10, 20, 40, 60 and 100 mVs^{-1} and in (b) 0.001 M triton x-100 with scan rates [1-3] 150, 200 and 300 mVs^{-1} in the presence of 0.1 M H_2SO_4.

$$\frac{I_{pa}}{I_{pc}} = \frac{(I_{pa})_0}{(I_{pc})_0} + \frac{0.485\ (I_{\lambda})_0}{I_{pc}} + 0.086$$

as suggested by Nicholson (127) and Gary (128). The values for $I_{pa}/I_{pc} < 1$, which decrease futher with increasing scan rates suggest that the electrogenerated leucodyes are involved in reactions which prevent their reoxidation upon scan reversal.

Cyclic voltametric measurements of 5×10^{-5}M dye solution in the presence of 0.1M H_2SO_4 are consistent with two electron reversible redox couples of dye / leucodye pairs upto scan rate 100 mvs^{-1}. The formal potential values for the two electron dye/leucodye couples are found to be 0.205, 0.175, 0.207, 0.281 and 0.196V (average values for scan rate between 5-100 mvs^{-1}) for Th, AzC, AzA, AzB and MB respectively in aqueous medium. But the value of $0.058/\Delta E$ is rather low for all dyes. Wopschall and shain (107) also found a low value (1.66) of this parameter contrary to the coulometric value of 2 for methylene blue, and interpreted it as due to the result of two successive one electron reversible charge transfer, with fast protonation of the intermediate to form a species which is more easily reduced than methylene blue. Separation between the peak potentials (ΔE_p) increases slowly with the increase in scan rate in all the solvents because the dye/leucodye couple deviate more and more from the reversibility. Quasi-reversibility of the electrode processes in the present system is also apparent from the

Table-13

Electrochemical data for Cyclic Voltammetry of $5x10^{-5}$M Thionine in different media in the presence of 0.1M H_2SO_4

S.R.	E_{pa}	E_{pc}	ΔE_p	i_{pa}/i_{pc}	$E_{pc/2}-E_{pc}$	$i_{pc}v^{-1/2}$	$.058/\Delta E_p$
				Water			
5	.225	.195	.030	.87	.025	3.93	1.93
10	.223	.193	.030	.89	.026	5.50	1.93
20	.220	.190	.030	.90	.027	5.32	1.93
40	.220	.190	.030	.98	.030	6.25	1.93
60	.215	.185	.030	.93	.032	6.15	1.93
100	.215	.185	.030	.95	.032	6.65	1.93
150	.213	.183	.030	.90	.033	7.49	1.93
200	.213	.182	.031	.97	.033	7.72	1.93
300	.210	.180	.031	.98	.035	8.59	1.93
				EtOH-Water (50% v/v)			
5	.190	.160	.030	.87	.027	3.93	1.93
10	.190	.160	.030	.90	.027	3.88	1.93
20	.190	.158	.032	.91	.028	4.07	1.81
40	.192	.155	.037	.91	.032	4.32	1.57
60	.192	.155	.037	.81	.036	4.61	1.57
100	.193	.152	.041	.80	.038	4.75	1.41
150	.193	.150	.043	.79	.042	4.90	1.35
200	.194	.150	.044	.74	.042	5.15	1.32
300	.195	.148	.047	.72	.045	5.57	1.23
				.001M TX-100			
5	.235	.205	.030	.94	.030	3.02	1.93
10	.235	.204	.031	.80	.030	3.10	1.87
20	.236	.203	.033	.89	.032	3.19	1.75
40	.237	.202	.035	.85	.033	3.25	1.65
60	.238	.200	.038	.82	.035	3.38	1.53
100	.240	.198	.042	.75	.036	3.48	1.38
150	.242	.197	.045	.79	.040	3.61	1.29
200	.243	.197	.046	.78	.045	3.60	1.26
300	.245	.196	.049	.79	.048	3.47	1.18

Table-14

Electrochemical data for Cyclic Voltammetry of $5x10^{-5}M$ Azure C in different media in the presence of 0.1M H_2SO_4

S.R.	E_{pa}	E_{pc}	ΔE_p	i_{pa}/i_{pc}	$E_{pc/2}-E_{pc}$	$i_{pc}v^{-1/2}$	$.058/\Delta E_p$
				Water			
5	.198	165	.033	.80	.035	5.00	1.75
10	.198	.163	.035	.88	.035	5.25	1.65
20	.196	.160	.036	.80	.037	4.96	1.61
40	.195	.158	.037	.76	.038	5.50	1.56
60	.191	.150	.041	.84	.040	5.64	1.41
100	.185	.145	.040	.83	.042	6.33	1.45
150	.182	.140	.042	.79	.042	6.46	1.38
200	.182	.135	.047	.77	.043	6.04	1.23
300	.180	.130	.050	.77	.045	7.31	1.16
				EtOH-Water (50% v/v)			
5	.162	.118	.044	.89	.040	3.21	1.32
10	.158	.116	.042	.83	.041	3.25	1.38
20	.156	.113	.043	.87	.043	3.28	1.35
40	.153	.110	.043	.83	.044	3.50	1.35
60	.152	.108	.044	.72	.045	3.99	1.32
100	.151	.107	.044	.69	.045	4.11	1.32
150	.150	.105	.045	.65	.047	4.39	1.29
200	.150	.103	.047	.61	.049	4.70	1.23
300	.150	.100	.050	.57	.050	5.12	1.16
				.001M TX-100			
5	.195	.160	.035	.80	.035	2.85	1.66
10	.196	.158	.038	.80	.037	2.50	1.55
20	.197	.157	.040	.80	.038	2.84	1.45
40	.198	.156	.042	.72	.039	3.13	1.38
60	.199	.155	.044	.81	.040	3.28	1.32
100	.200	.154	.046	.74	.041	3.32	1.26
150	.202	.153	.049	.69	.041	3.36	1.18
200	.203	.152	.051	.69	.043	3.58	1.14
300	.204	.150	.054	.63	.045	3.47	1.07

Table-15

Electrochemical data for Cyclic Voltammetry of 5×10^{-5}M Azure A in different media in the presence of 0.1M H_2SO_4

S.R.	E_{pa}	E_{pc}	ΔE_p	i_{pa}/i_{pc}	$E_{pc/2}-E_{Pc}$	$i_{pc}v^{-1/2}$	$.058/\Delta E_p$
				Water			
5	.229	.198	.031	.89	.028	6.43	1.87
10	.226	.195	.031	.88	.028	6.25	1.87
20	.224	.192	.032	.83	.030	6.38	1.81
40	.222	.191	.031	.79	.032	6.75	1.87
60	.220	.188	.032	.73	.035	6.97	1.81
100	.218	.186	.032	.69	.038	8.22	1.87
150	.216	.182	.034	.65	.040	8.01	1.70
200	.214	.180	.034	.61	.043	8.05	1.70
300	.212	.178	.034	.59	.045	8.40	1.70
				EtOH-Water (50% v/v)			
5	.205	.175	.030	.90	.030	3.92	1.93
10	.206	.172	.034	.84	.030	4.15	1.70
20	.207	.170	.037	.77	.032	4.60	1.57
40	.208	.168	.040	.66	.035	5.12	1.45
60	.210	.167	.043	.62	.038	5.32	1.35
100	.212	.165	.047	.58	.038	6.01	1.23
150	.213	.160	.053	.51	.040	6.59	1.09
200	.214	.155	.059	.48	.042	6.93	0.98
300	.215	.150	.065	.44	.043	7.49	0.89
				.001M TX-100			
5	.200	.170	.030	.80	.032	3.57	1.93
10	.202	.168	.034	.86	.032	3.50	1.70
20	.204	.166	.038	.80	.034	3.54	1.53
40	.206	.164	.042	.71	.035	3.50	1.38
60	.208	.162	.046	.74	.037	3.89	1.26
100	.210	.160	.050	.62	.040	4.11	1.16
150	.212	.158	.054	.65	.043	4.39	1.07
200	.214	.156	.058	.63	.046	4.25	1.00
300	.215	.155	.060	.61	.050	4.20	0.96

Table-16

Electrochemical data for Cyclic Voltammetry of $5x10^{-5}$M Azure B in different media in the presence of 0.1M H_2SO_4

S.R.	E_{pa}	E_{pc}	ΔE_p	i_{pa}/i_{pc}	$E_{pc/2}-E_{pc}$	$i_{pc}v^{-1/2}$	$.058/\Delta E_p$
				Water			
5	.300	.270	.030	.87	.028	5.54	1.93
15	.300	.268	.032	.85	.029	6.00	1.81
25	.298	.265	.033	.84	.030	6.17	1.76
50	.297	.262	.035	.84	.035	6.93	1.66
100	.295	.260	.035	.77	.038	7.59	1.66
150	.294	.260	.034	.73	.040	8.01	1.70
200	.293	.258	.035	.66	.042	8.05	1.66
300	.293	.257	.036	.58	.045	8.04	1.61
				EtOH-Water (50% v/v)			
5	.165	.135	.030	.80	.030	3.57	1.93
10	.165	.132	.033	.82	.032	4.25	1.76
20	.165	.130	.035	.81	.034	4.78	1.66
40	.160	.127	.033	.78	.034	5.50	1.76
60	.160	.125	.035	.76	.038	6.04	1.66
100	.150	.120	.030	.61	.042	6.96	1.93
150	.148	.116	.032	.59	.043	7.24	1.81
200	.146	.112	.034	.53	.044	7.49	1.70
300	.145	.110	.035	.52	.045	7.31	1.66
				.001M TX-100			
5	.205	.175	.030	.85	.032	2.50	1.93
10	.203	.173	.030	.81	.032	2.75	1.93
20	.201	.170	.031	.80	.035	2.66	1.87
40	.200	.168	.032	.78	.036	2.88	1.81
60	.198	.163	.035	.68	.038	2.97	1.66
100	.196	.159	.037	.66	.042	3.08	1.57
150	.196	.159	.037	.65	.044	3.36	1.57
200	.194	.154	.040	.66	.047	3.36	1.45
300	.194	.152	.042	.61	.048	3.29	1.38

Table-17

Electrochemical data for Cyclic Voltammetry of 5×10^{-5}M Methylene Blue in different media in the presence of 0.1M H_2SO_4

S.R.	E_{pa}	E_{pc}	ΔE_p	i_{pa}/i_{pc}	$E_{pc/2}-E_{pc}$	$i_{pc}v^{-1/2}$	$.058/\Delta E_p$
				Water			
5	.215	.183	.032	.84	.028	6.78	1.81
10	.215	.182	.033	.81	.030	6.75	1.76
20	.214	.181	.033	.75	.032	7.27	1.76
40	.212	.180	.032	.61	.032	7.75	1.81
60	.210	.180	.030	.61	.035	8.20	1.93
100	.205	.175	.030	.63	.036	9.01	1.93
150	.200	.170	.030	.65	.037	9.56	1.93
200	.197	.165	.032	.66	.038	10.06	1.81
300	.195	.160	.035	.65	.040	10.97	1.66
				EtOH-Water (50% v/v)			
5	.215	.180	.035	.87	.027	5.71	1.66
10	.212	.178	.034	.72	.028	5.50	1.70
20	.210	.174	.036	.60	.030	5.85	1.61
40	.205	.170	.035	.53	.032	6.75	1.66
60	.200	.160	.040	.52	.032	6.55	1.45
100	.195	.155	.044	.52	.034	7.59	1.45
150	.180	.140	.040	.44	.035	8.27	1.45
200	.178	.135	.043	.43	.036	8.95	1.35
300	.175	.130	.045	.41	.038	9.32	1.29
				.001M TX-100			
5	.210	.180	.030	.75	.025	4.29	1.93
10	.212	.180	.032	.75	.028	4.00	1.81
20	.214	.178	.036	.73	.029	4.07	1.61
40	.215	.178	.037	.72	.030	4.13	1.57
60	.216	.176	.040	.71	.031	4.61	1.45
100	.216	.175	.041	.60	.033	4.90	1.41
150	.218	.174	.044	.55	.035	5.17	1.32
200	.218	.173	.045	.52	.038	5.15	1.29
300	.220	.172	.048	.51	.040	5.30	1.21

difference between the peak potentials (ΔE_p) and the half peak potential ($E_{pc}-E_{pc/2}$), where in an ideal reversible reaction these values should be 30 mv (129). However, appreciable deviation of ΔE_p from ideal reversible value is apparent only at very high scan rates, which suggests that electrodic processes involved are very fast.

The plots of i_{pc} as a function of $v^{1/2}$ (i_{pc} measured for forward scan of the first cycle) indicate that the variation of the current is linear with $v^{1/2}$ upon scan rate of $\sim$ 100 mvs^{-1} and the line drawn through the experimental points at slow scan rates passes through the origin (figs. 55-59). At higher scan rates, the points deviate from the straight line in all the solvents studied. The slope of the plots vary from solvent to solvent due to the variation of diffusion coefficients. The foregoing observation also indicates that the electrode process is diffusion controlled at slow scan rates.

The effective diffusion coefficient values of the dyes in water, water-ethanol (50% v/v) and triton X-100 are summerized in table 18. The values have been calculated, using the Randles Seveik equation (122), from the slope of the curves plotting I_{pc} vs. $v^{1/2}$ (Figs.55-59) upto the scan rate (v) 20 mVs^{-1}. The values for methylene blue and thionine are 5.70×10^{-6} cm^2s^{-1} and 3.05×10^{-6} cm^2s^{-1} respectively on GCE. A value of 7.6×10^{-6} cm^2s^{-1} for MB and 2.28×10^{-6} cm^2s^{-1} for thionine were reported by previous workers measured at Pt-wire type HMDE and indium doped SnO_2 electrode

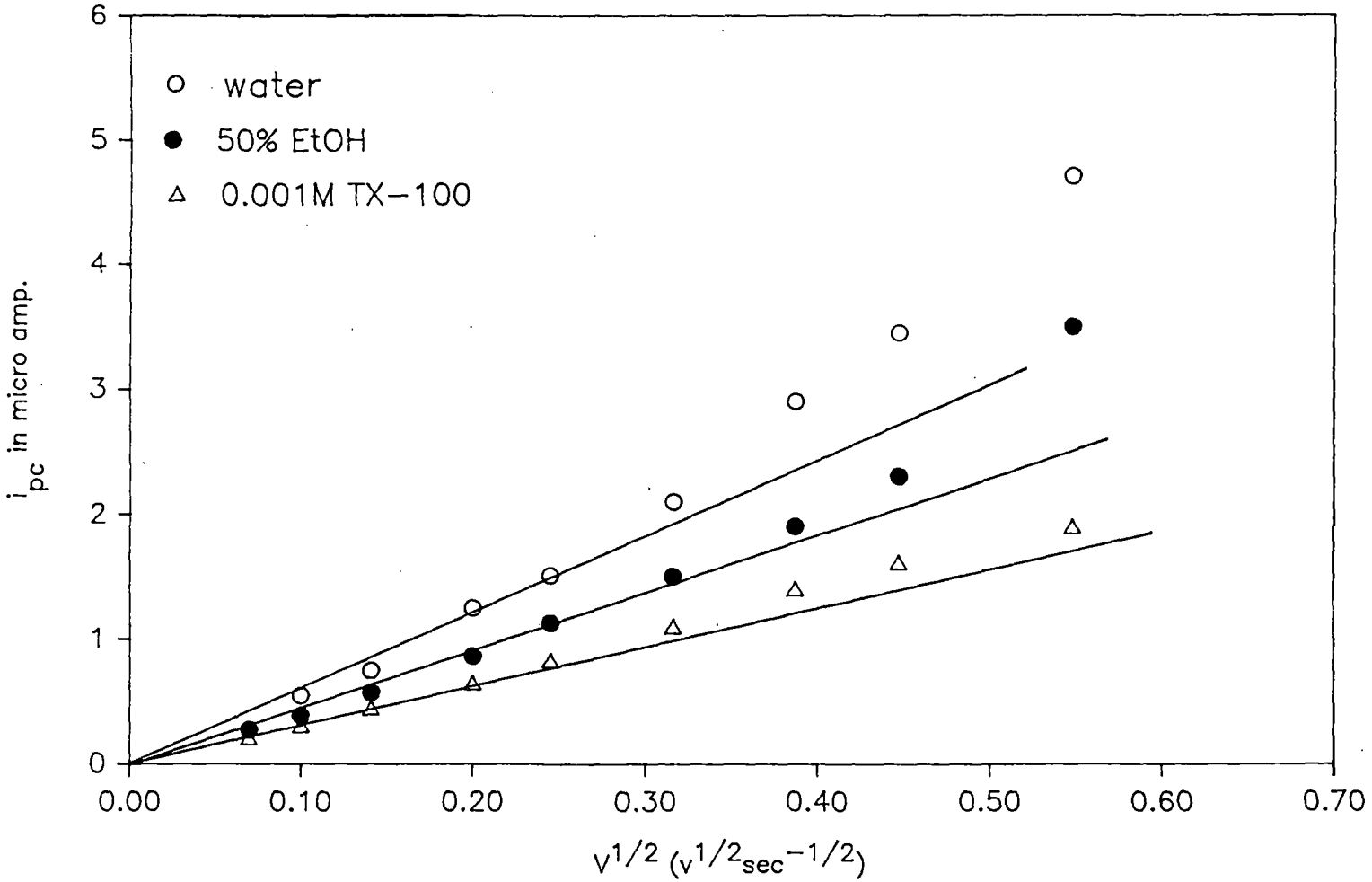

Fig.55 Plot of cathodic peak currents as a function of (scan rates)$^{1/2}$ for Thionine ($5x10^{-5}$M) in different solvents at GCE.

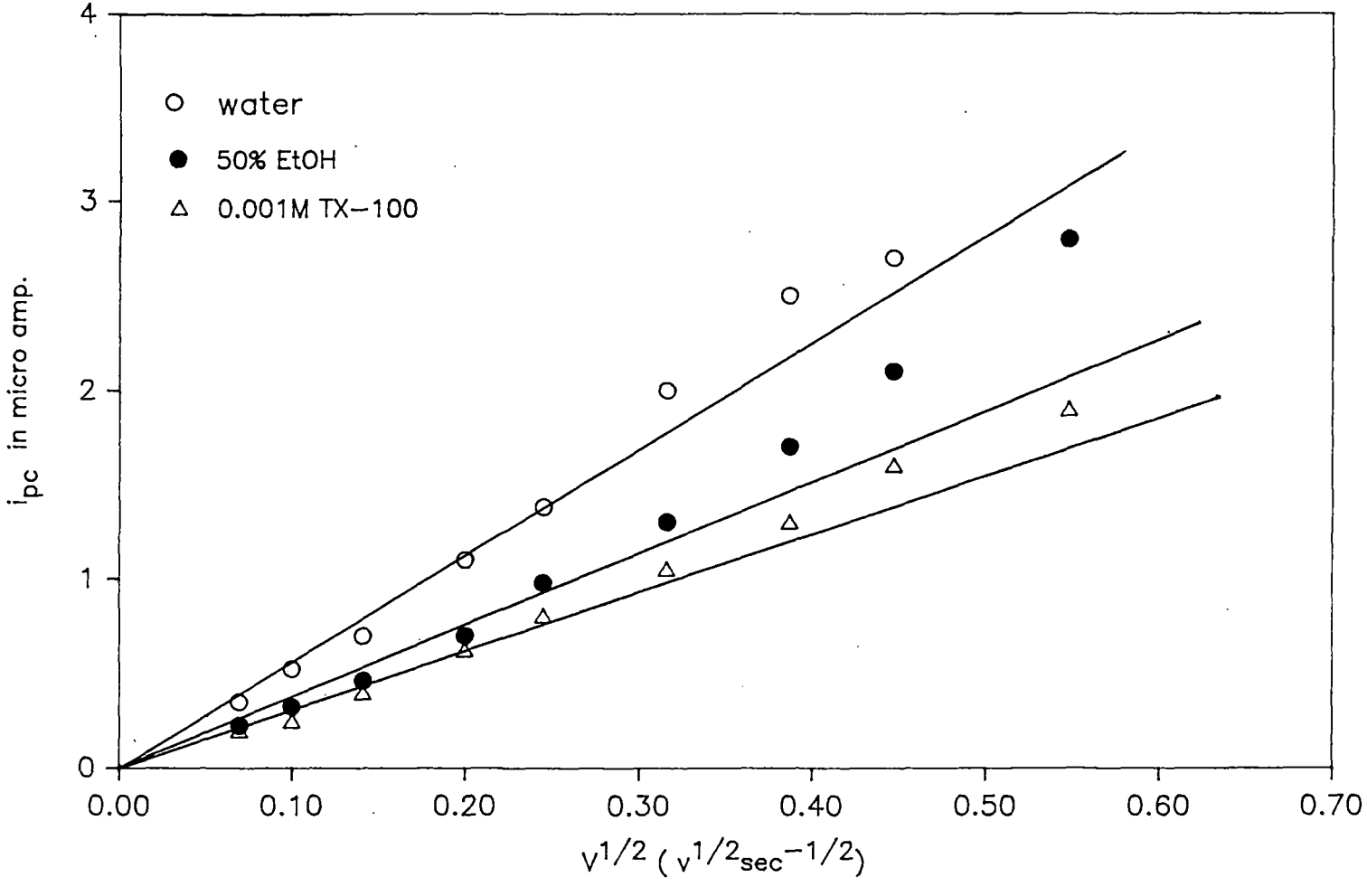

Fig.56 Plot of cathodic currents as a function of (scan rates)$^{1/2}$ for Azure C ($5x10^{-5}$M) in different solvents at GCE.

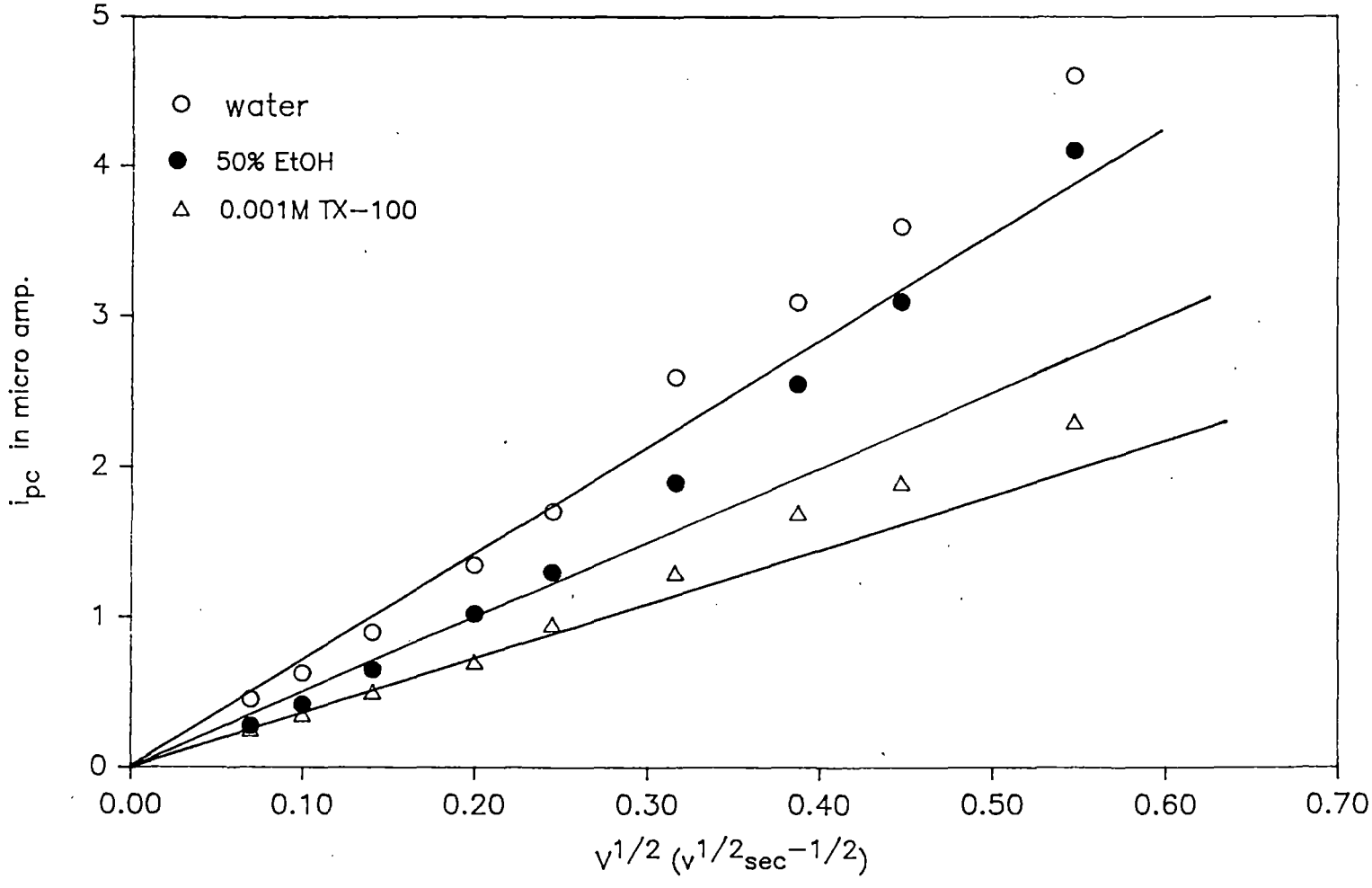

Fig.57 Plot of cathodic peak currents as a function of (scan rates)$^{1/2}$ for Azure A (5×10^{-5}M) in different solvents at GCE.

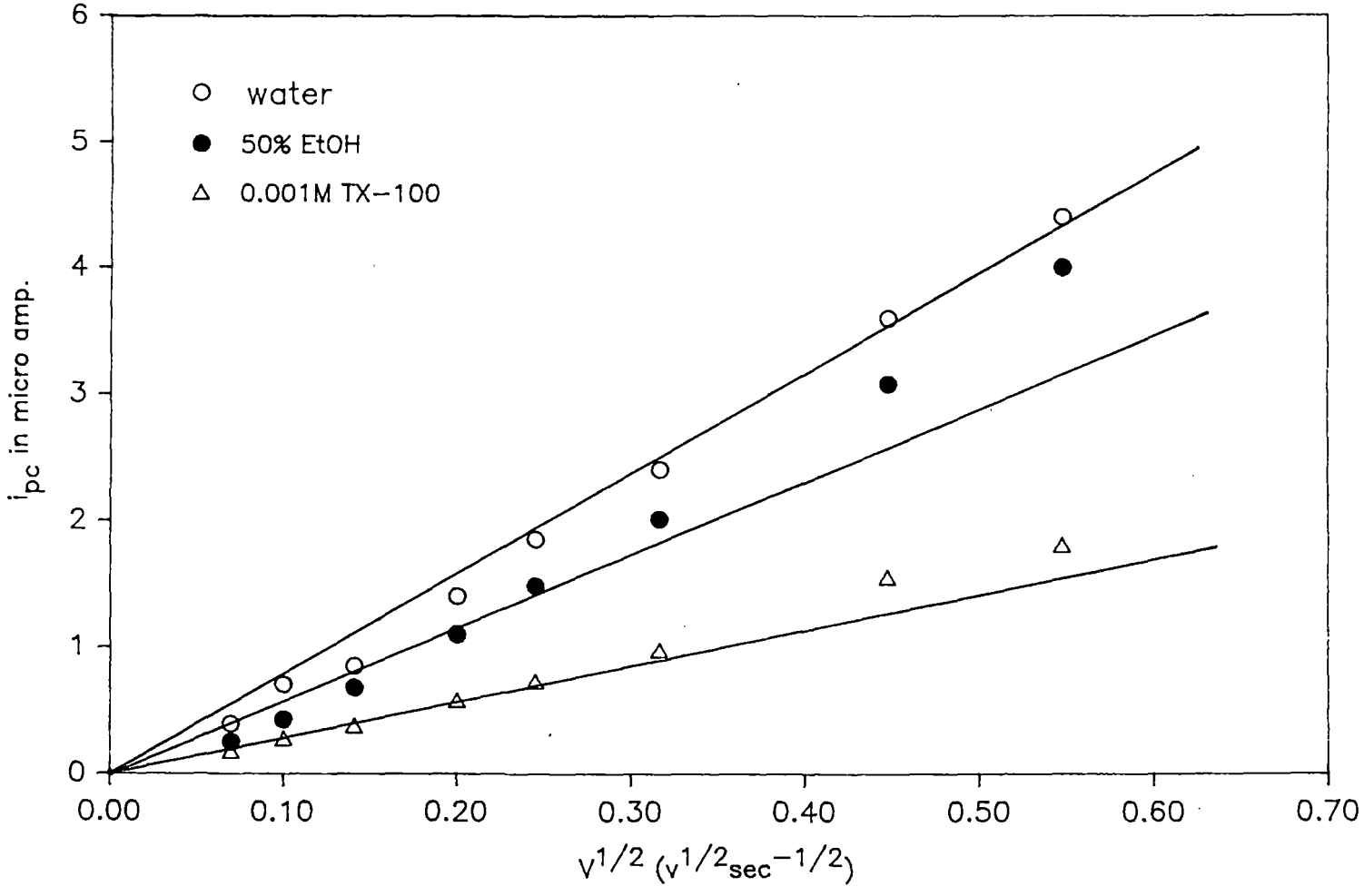

Fig.58 Plot of cathodic peak currents as a function of (scan rates)$^{1/2}$ for Azure B (5×10^{-5}M) in different solvents at GCE.

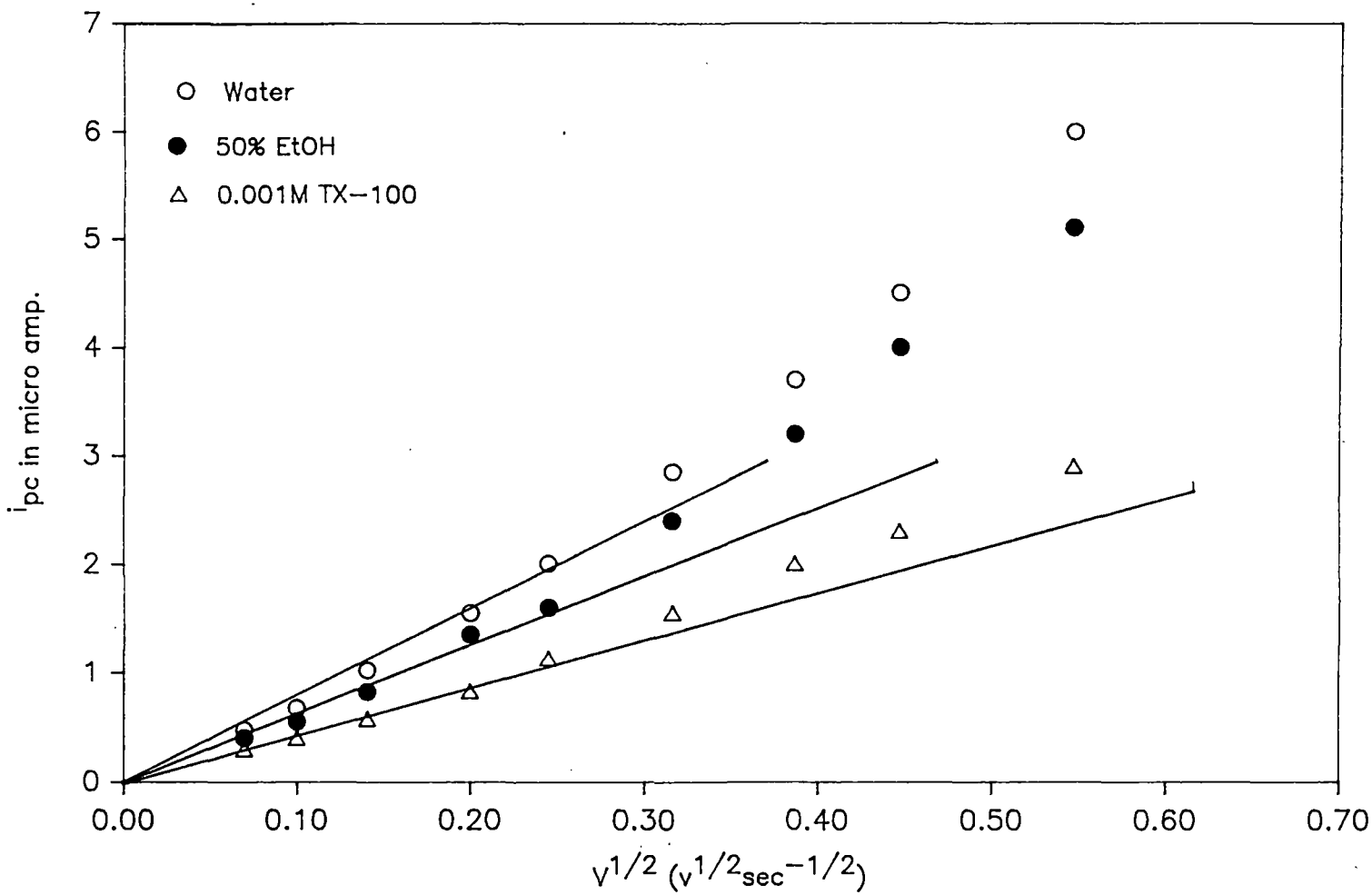

Fig.59 Plot of cathodic peak currents as a function of (scan rates)$^{1/2}$ for Methylene Blue ($5x10^{-5}$M) in different solvents at GCE

Table-18

Values of Diffusion Coefficient of the dyes in different medium

D.C.x 10^{6} ($cm^{2}s^{-1}$)

Dye	Water	EtOH	TX-100
Thionine	3.05	1.80	1.10
Azure C	2.66	1.16	0.87
Azure A	4.40	2.29	1.36
Azure B	4.13	2.47	0.76
Methylene Blue	5.70	3.70	1.80

(108,107). AzC has the lowest value ($2.66x10^{-6}$ $cm^{2}s^{-1}$ in water) in the present study. And there is no systemetic change in the diffusion coefficient values with the progressive alkylation. But the effect of solvent is very prominent. With the variation of polarity and viscosity of the medium, the values of the diffusion coefficient change significantly.

Previous workers deposited dye layers on metal electrode by maintaining the electrode at some emperically selected potential while it was immersed in a solution of the dye (99,130-133) Quickenden and Harrison (105) on the other hand, developed a method of deposition of dye layers by repetative cycling of the

potential scan. From the comparison of the CV's obtained when the thionine coated electrodes are immersed in background and thionine containing electrolyte that the thionine and leucothionine peaks observed with the coated electrodes originates almost entirely from the dye coating, rather than for any thionine in solution.

In figs. 60,61 results of repetative cycle of voltage scan on a GCE for the present dyes are shown. The behaviour of thionine and four other dyes at 6.5×10^{-5}M (in 0.1M H_2SO_4) on GCE, is substantially different from the previous study of thionine on Au-electrode (98,105). Instead of a progressive increase of anodic and cathodic currents on cycling, the peak currents in the present systems decrease. The peak current attains a constant value in each case after 10-20 cycles. This behaviour is to some extent similar to that of rhodamine B on SnO_2 glass electrode (97). Of course, in the latter case currents were found to decrease continuously on every repetative cycle and ultimately merged with the background currents. Present results suggest that under the experimental conditions, although previuosly assumed tendency of the thionine dye adsorption on a GCE surface is rather weak in the presence of 0.1M H_2SO_4, partial electrode poisoning towards the process of oxidation and reduction of the adsorbed dyes may be responsible for such observation. However, it is also reported by the previous workers that the cyclic voltammogram does not change with repeated cycling unless a certain potential is

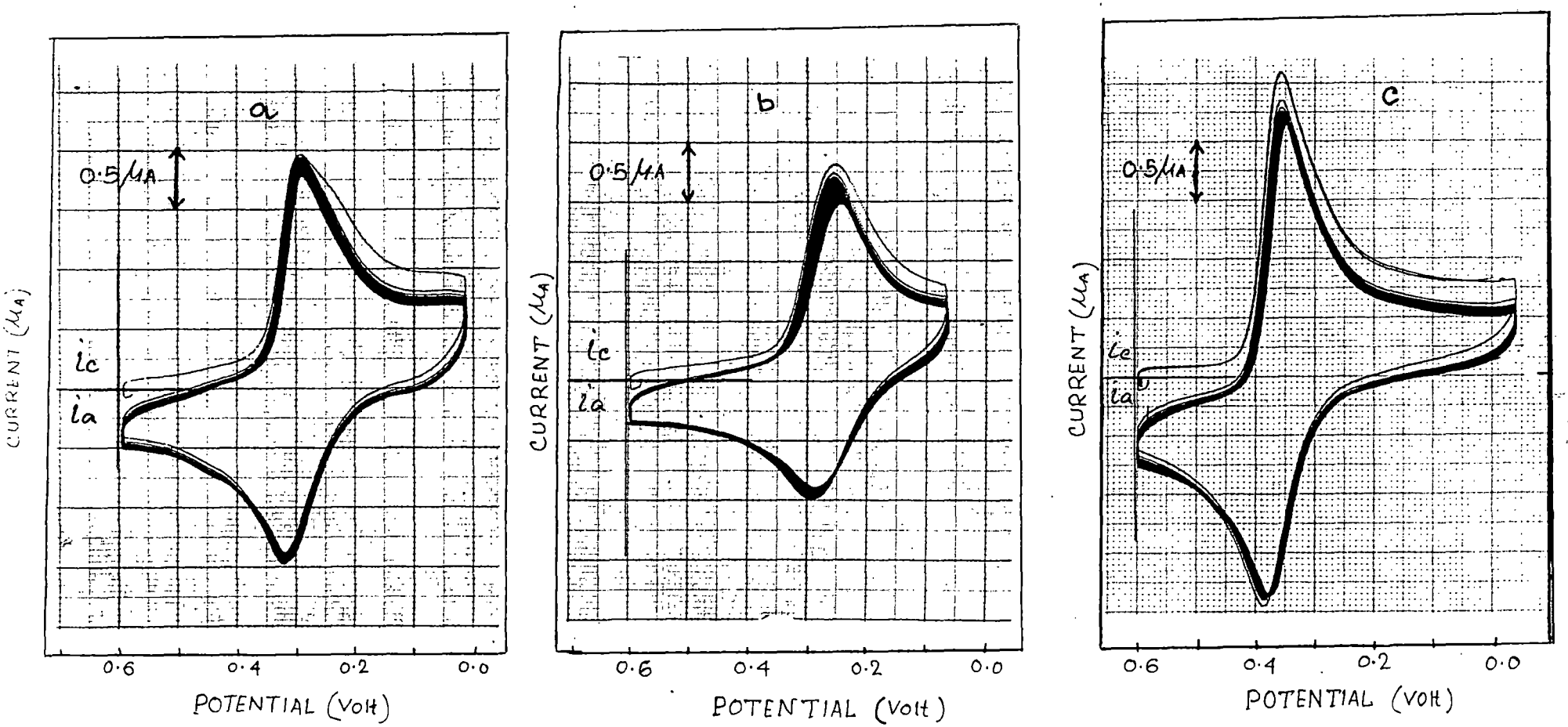

Fig. 60 : Cyclic Voltammograms of (a) Thionine (6.50×10^{-5}M), (b) Azure C (6.50×10^{-5}M) and (c) Azure A (6.50×10^{-5}M) with repeatitive cycling at scan rate 100 mVs^{-1} in the presence of 0.1 M H_2SO_4.

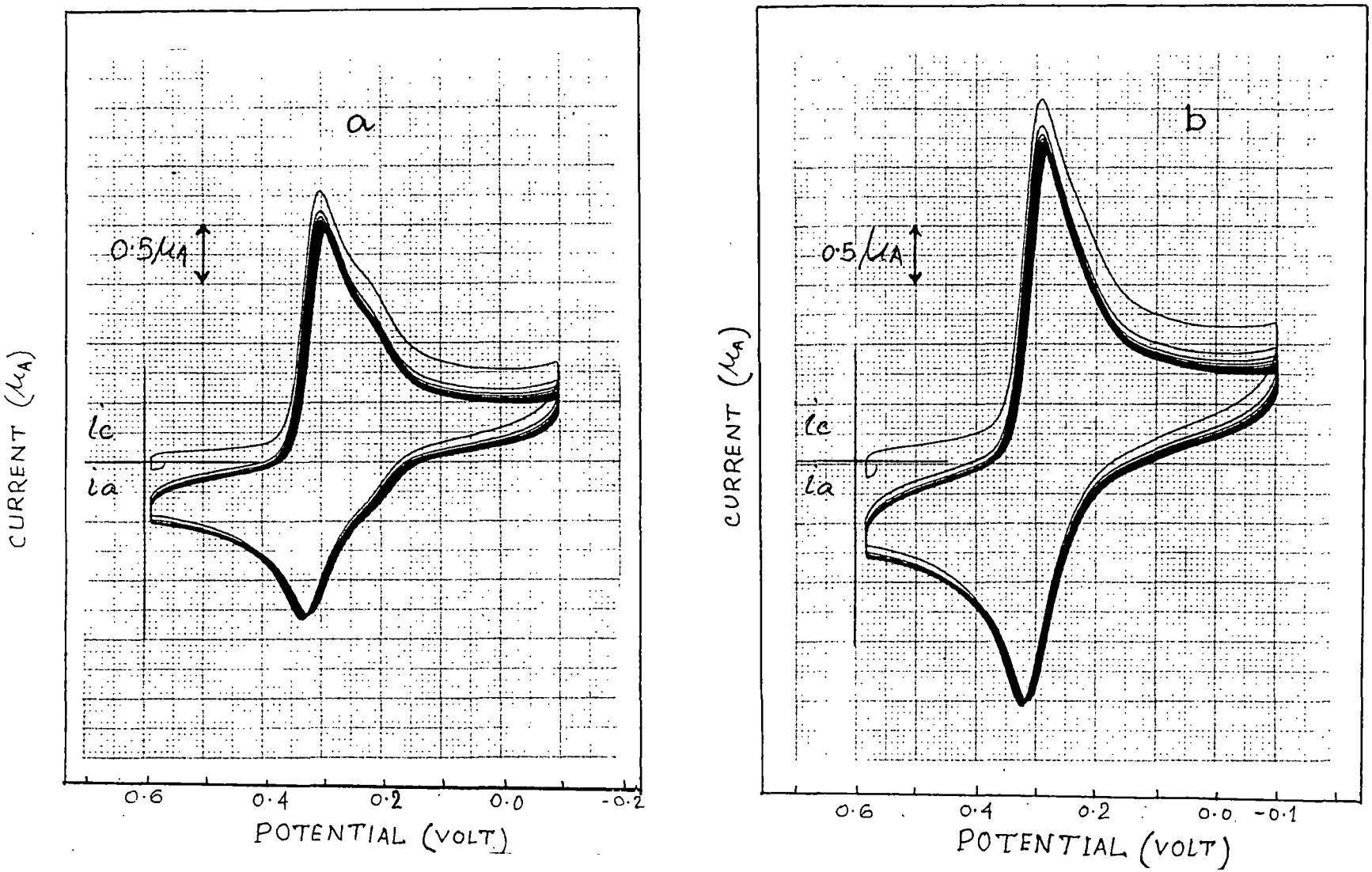

Fig. 61 : Cyclic Voltammograms of (a) Azure B (6.50×10^{-5}M) and (b) Methylene Blue (6.50×10^{-5}M) with repeatitive cycling at scan rate 100 mVs^{-1} in the presence of 0.1 M H_2SO_4.

exceeded during sweep (97). It has been shown that for concentration below about 0.2×10^{-3}M the methylene blue system fits the simple theory of cyclic voltammetry in which the adsorption of the reactant is ignored (107). It was argued that above 0.2×10^{-3}M concentrations, the adsorption of methylene blue must be considered. In Figs. 62-66 representative cyclic voltammograms of the dyes (1×10^{-4}- 2×10^{-4}M) in the presence of 0.1M KCl at various $_{p}$H's are shown. It is evident from the figures that the presence of 0.1M KCl and at comparatively higher $_{p}$H's, both anodic and cathodic peak potentials are shifted toward more negative potentials than those observed in the presence of 0.1M H_2SO_4. Moreover, the voltammograms display cathodic and anodic post/pre peaks which are the characteristics of strong adsorption of reactant and/or products. Observed nature of the voltammograms vis-a-vis the adsorption characteristics of various dyes are summerized in table 19. At a cocncentration of 1×10^{-4}M, thionine gives voltammograms with small cathodic prepeaks as well as anodic postpeaks at $_{p}$H 3.6-4.2 indicating that the products are strongly adsorbed. At $_{p}$H 5.3 and above, cathodic postpeaks and anodic prepeaks are observed which indicate strong adsorption of the reactant dye. Similarly AzC exhibits cathodic prepeak and anodic postpeak at $_{p}$H 4.1 indicating that the products are strongly adsorbed. At $_{p}$H 5.1 cathodic postpeak anodic prepeak appears which indicates that the reactant dye is also adsorbed strongly. However, at $_{p}$H 6.0 and above cyclic voltammograms are

Table-19

Effect of $_{P}H$ on the Cyclic Voltammograms of the dye solutions :

Dye	$_{P}H$	Changes/observations	Adsorption
Th	3.6	Pre cathodic and post	Product strongly adsorbed
($1x10^{-4}$M)		anodic peaks	
in 0.1M KCl	4.2	- Do -	- Do -
	5.3	Post cathodic and pre	Reactant strongly
		anodic peaks	adsorbed
	5.8	- Do -	- Do -
AzC	4.1	Pre cathodic and post	Product strongly adsorbed
($2x10^{-4}$M)		anodic peaks	
in 0.1M KCl	5.1	Post cathodic and pre	Reactant strongly adsorbed
		anodic peaks	
	6.0	Post anodic peak	Product strongly adsorbed
	7.0	Pre cathodic and pre	Product strongly adsorbed
		and post anodic peaks	
AzA	5.2	Pre cathodic and post	Product strongly adsorbed
($2x10^{-4}$M)		anodic peaks	
in 0.1M KCl	5.4	- Do -	- Do -
	5.7	- Do -	- Do -
	6.2	Anodic peak current is	Product weakly adsorbed
		greater than cathodic	

Table-19

Effect of $_{P}H$ on the Cyclic Voltammograms of the dye solutions :

Dye	$_{P}H$	Changes/observations	Adsorption
AzB	4.8	Post cathodic and pre	Reactant strongly adsorbed
($1x10^{-4}$M)		anodic peaks	
in 0.1M KCl	5.3	- Do -	- Do -
	5.7	Post anodic peak	Product strongly adsorbed
	6.2	Anodic peak currents high	Product weakly adsorbed
MB	4.6	Post cathodic and pre	Reactant strongly adsorbed
($1x10^{-4}$M)		anodic peaks	
in 0.1M KCl	4.8	- Do -	- Do -
	6.0	Anodic peak currents increase sharply	Product weakly adsorbed
	8.4	Slight cathodic post peak and anodic peak currents increase sharply	Both reactant and product adsorbed

suggestive of strong adsroption of products only. While voltammograms of AzA show evidence of strong product adsorption within the $_{P}H$ range of 5.2 and 6.2 , AzB exhibits evidence of

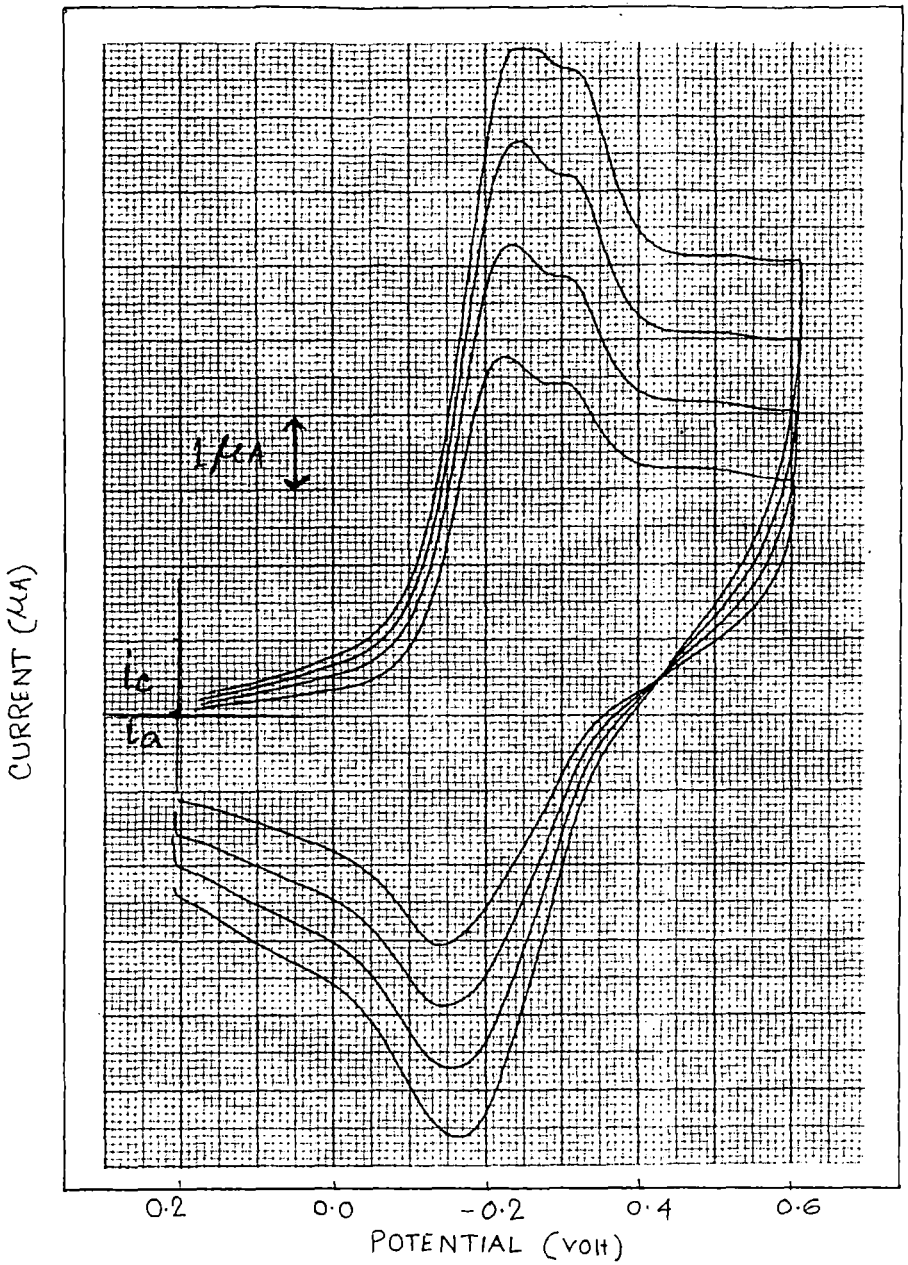

Fig. 62 : Cyclic Voltammograms of thionine ($1x10^{-4}$M) at $_{p}$H 5.8 in the presence of 0.1 M KCl at different scan rates.

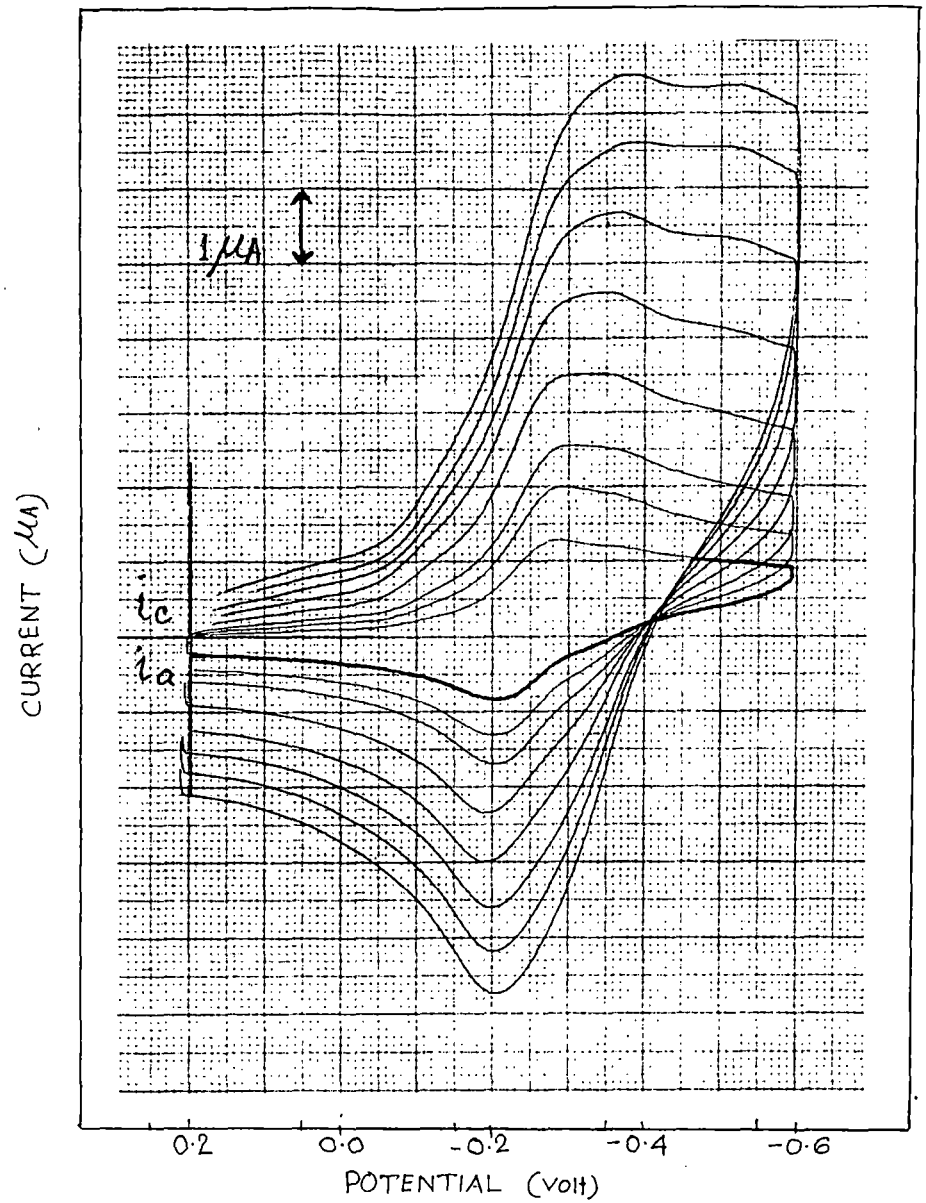

Fig. 63 : Cyclic Voltammograms of Azure C ($2x10^{-4}$M) at $_{p}$H 5.1 in the presence of 0.1 M KCl at different scan rates.

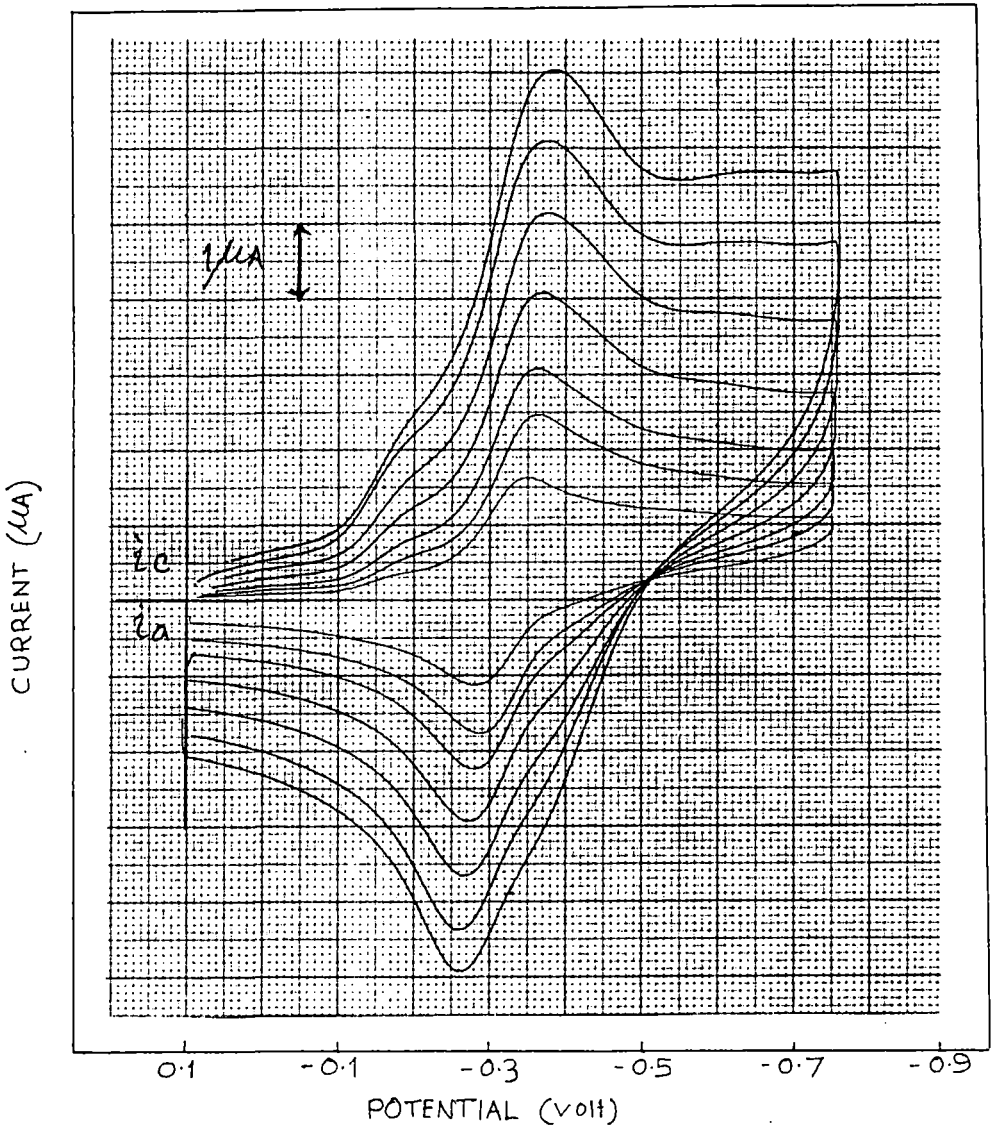

Fig. 64 : Cyclic Voltammograms of Azure A ($2x10^{-4}M$) at $_pH$ 5.2 in the presence of 0.1 M KCl at different scan rates.

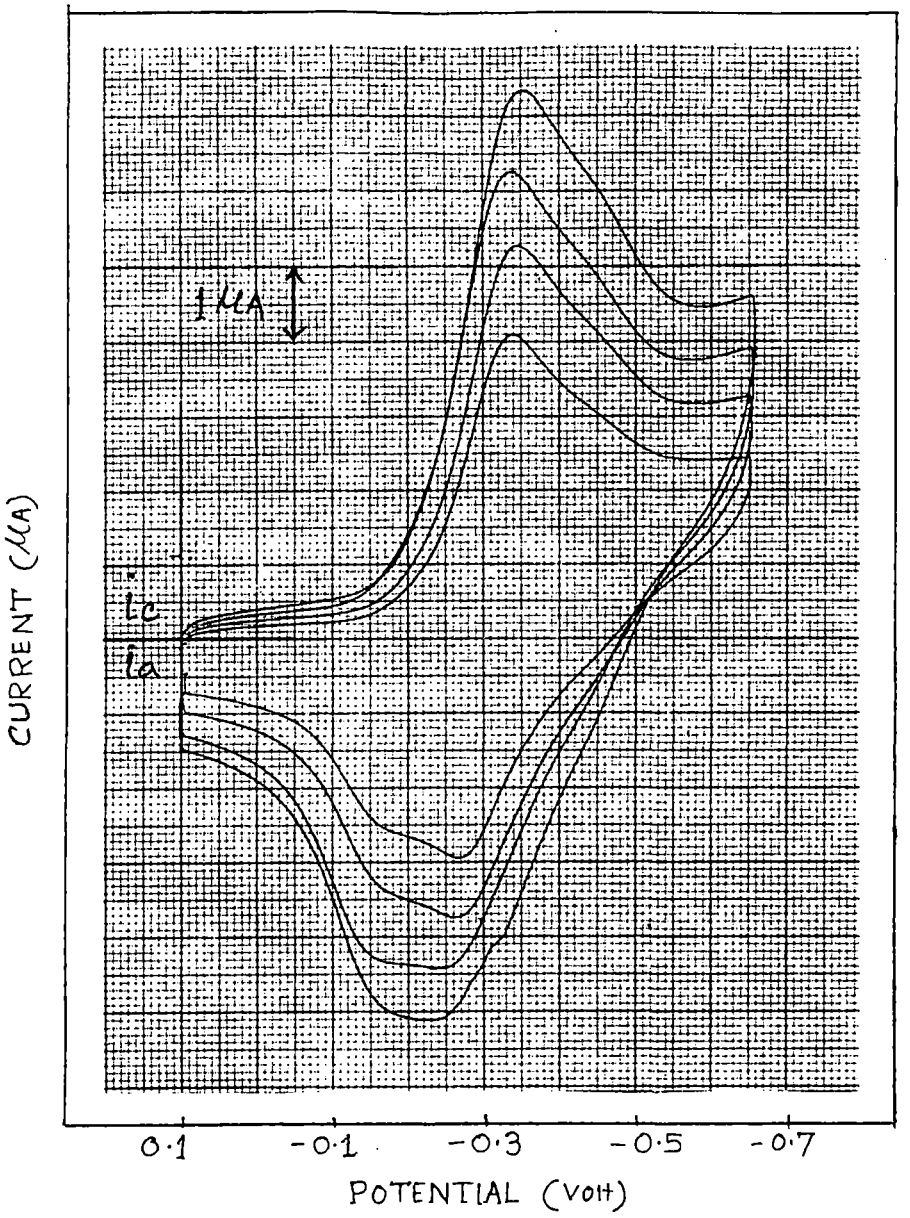

Fig. 65 : Cyclic Voltammograms of Azure B ($1x10^{-4}M$) at $_pH$ 5.7 in the presence of 0.1 M KCl at different scan rates.

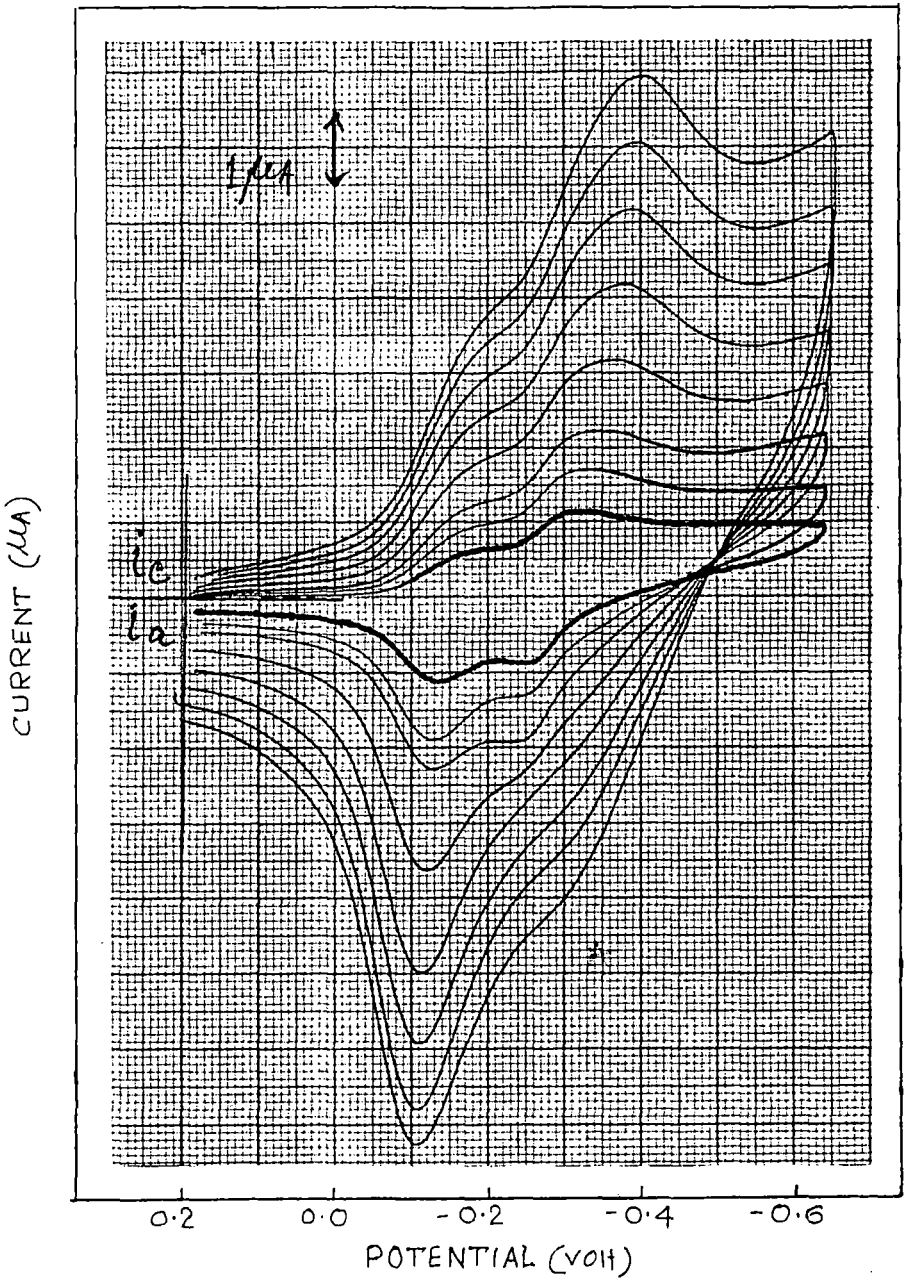

Fig. 66 : Cyclic Voltammograms of Methylene Blue ($1x10^{-4}$M) at $_{p}$H 4.6 in the presence of 0.1 M KCl at different scan rates.

reactant adsorption at low $_{p}H$ and product adsorption at high $_{p}H$ values. MB, on the other hand, gives cathodic postpeak and anodic prepeak upto $_{p}H$ of 4.8 indicating strong reactant adsorption, while at high $_{p}H$ both reactant and the product are adsorbed.

Sackett and coworkers (102) have also observed the $_{p}H$ dependence of the initial oxidation of promethazine whereas similar processes for chloropromazine were completely independent of $_{p}H$ above the value of zero. Apparently, the proximity of the highly charged ring system in the oxidized form lowers the $_{p}k_{a}$ of the side chain amine to cause the deprotonation. The $_{p}H$ dependence of the oxidation potential of promethazine has been noted even before and was attributed to electronic interaction between the ring system and the amine (134). Results indicated that oxidation of the ring lowers the $_{p}k_{a}$ of the side chain amine by at least 5 units, resulting in deprotonation of the amine in the oxidised form. Similarly in the case of thiazine dyes it can be argued that although amino nitrogen are very weakly basic, the same groups which could be protonated along the bridging nitrogen at low $_{p}H$ in leucodyes, are deprotonated at high $_{p}H$. While the effect of $_{p}H$ on the voltammograms of the present dyes are similar, enhanced irreversibility of the redox processes is also accompanied by certain changes in the shapes of the voltammogram at high $_{p}H$ values.

It has been shown that, for quasi-reversible electrode processes, the separation between the corresponding oxidation and reduction peaks in the cyclic voltammograms is a function of the corresponding electrodic rate constants. Nicolson (135) provided a table of the computed relationship between the peak separation and a kinetic factor ψ^{*}.The latter is related to the rate constant k for a quasi-reversible oxidation by

$$\psi = (D_{\emptyset}/D_{r})^{\alpha/2} k \{ D_{\emptyset}\pi v (nf/RT) \}^{-1/2} \qquad (41)$$

Where the subscripts $\emptyset$ and r designate oxidation and reduction processes respectively, and α is the electron transfer coefficient. It is assumed that the diffusion coefficient of the dyes and leucodyes are not very different, the quantity $(D_{\emptyset}/D_{r})^{\alpha/2}$ is very near to unity regardless of α and the rate constant for the electrodic oxidation of the dyes at a GCE can be obtained. Fig. 67 shows the working curve of the variation of peak potential separation with ψ, drawn for the relevant region of peak potential separation of the present study. Computed ψ values of this figure are taken from the table given by Nicolson (135). Table 20 gives the values of ψ at various scan rates for the electrodic processes of the present cationic dyes. Kinetic factors

---

This ψ is different from the wave function of chapter 3

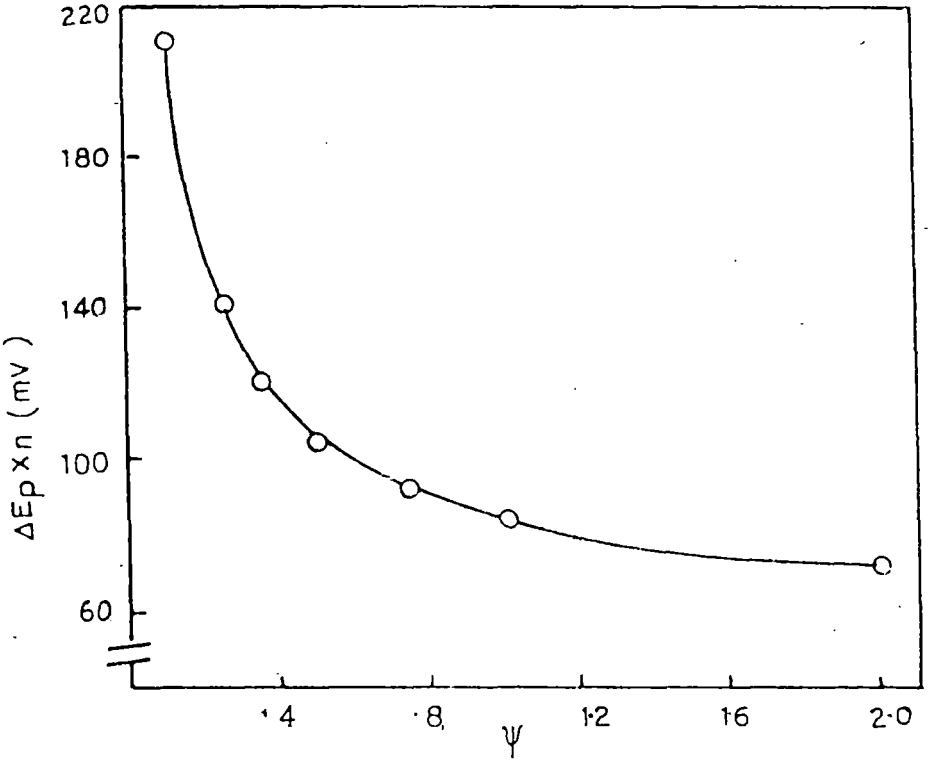

Fig : 6.7 Working curve showing variation of peak potential separation with ψ .

at the various scan rates are measured from the curve. When ψ's are sufficiently large, the results become identical to one where the electron transfer is assumed to be Nerstian. On the other hand, for the sufficiently small ψ, the back reaction for electron transfer is unimportant and the processes for oxidation and reduction can be treated separately as the totally irreversible case. At lower scan rates, all the thiazine dyes displayed reversible electrode reactions. Quasi-reversibilities are prominent above 300 mVs^{-1} scan rates. As such, kinetic measurement are made within the range 300-1000 mVs^{-1} scan rates. The heterogeneous rate constants of the electron transfer of the five dyes are given in table 20. The table shows that the order of the kinetic parameter is same for all the dyes. However, the values of the parameter increase slightly with alkylation in dye molecule from thionine to AzB, while MB gives a little lower value than AzB.

Table-20

Dye	Scan rate (Volt s^{-1})	$\Delta E_p x n$ (Volt)	ψ	$kx10^{-3}$ ($cm.s^{-1}$)
	1.0	0.140	0.24	6.55
	0.8	0.130	0.29	7.08
Th	0.6	0.120	0.35	7.61
	0.5	0.110	0.46	8.88
	0.4	0.100	0.58	10.02
	0.3	0.80	1.14	17.05

contd.

Table-20

Dye	Scan rate (Volt s^{-1})	$\Delta E_p x n$ (Volt)	ψ	$kx10^{-3}$ ($cm.s^{-1}$)
	1.0	0.130	0.29	7.39
	0.8	0.120	0.35	7.98
AzC	0.6	0.100	0.58	11.46
	0.5	0.900	0.78	14.07
	0.4	0.800	1.14	18.39
	0.3	0.700	---	---
	1.0	0.120	0.36	11.81
	0.8	0.110	0.46	13.49
AzA	0.6	0.100	0.58	14.74
	0.5	0.900	0.78	18.09
	0.4	0.800	1.14	23.65
	0.3	---	---	---
	1.0	0.130	0.29	10.04
	0.8	0.120	0.36	11.14
AzB	0.6	0.100	0.58	15.55
	0.5	0.900	0.78	19.09
	0.4	0.800	1.14	24.96
	0.3	---	---	---
	1.0	0.140	0.24	8.96
	0.8	0.120	0.36	12.02
MB	0.6	0.110	0.46	13.30
	0.5	0.100	0.58	15.31
	0.4	0.900	0.78	18.42
	0.3	---	---	---

4.3.2. Electrochemical studies on Modified Electrode :

Thiazine dye cations are among the substances most strongly adsorbed by clay minerals. The planar structure of these dyes exhibits a particularly strong interaction with expanded lattice clays such as montmorillonite and zeolite (ZSM-5) (detail in chapter 5). Dyes impregnated in either montmorillonite or zeolite layers are found to be electroactive under cyclic voltammetric experiments.

The cyclic voltammograms of GCE/clay-dye and GCE/zeolite-dye systems in 0.1M H_2SO_4 are shown in figs. 68-77. The electrochemical identity of the dye has been retained in both the clay and zeolite films. Current observed in the modified electrodes depends on both the porosity of the clay films and on the nature and number of sites responsible for the partitioning of the complex into the film. The porosity can be affected by the initial preparation of the film and the bathing solution. Ghosh and Bard (109) obtained swollen (porous) films by drying clay in the presence of polyvinyl alcohol (PVA). The presence of PVA was thought to force clay into a swollen configeration suitable for charge transport through the film. In the study of GCE/montmorillonite-dye and GCE/zeolite-dye electrodes, the presence of polyvinyl alcohol and Pt in the films was found to be critical in attaining better electrochemical activity of the modified electrodes. Electrode processes in the absence of any colloidal Pt in the films yield CV's having no well defined

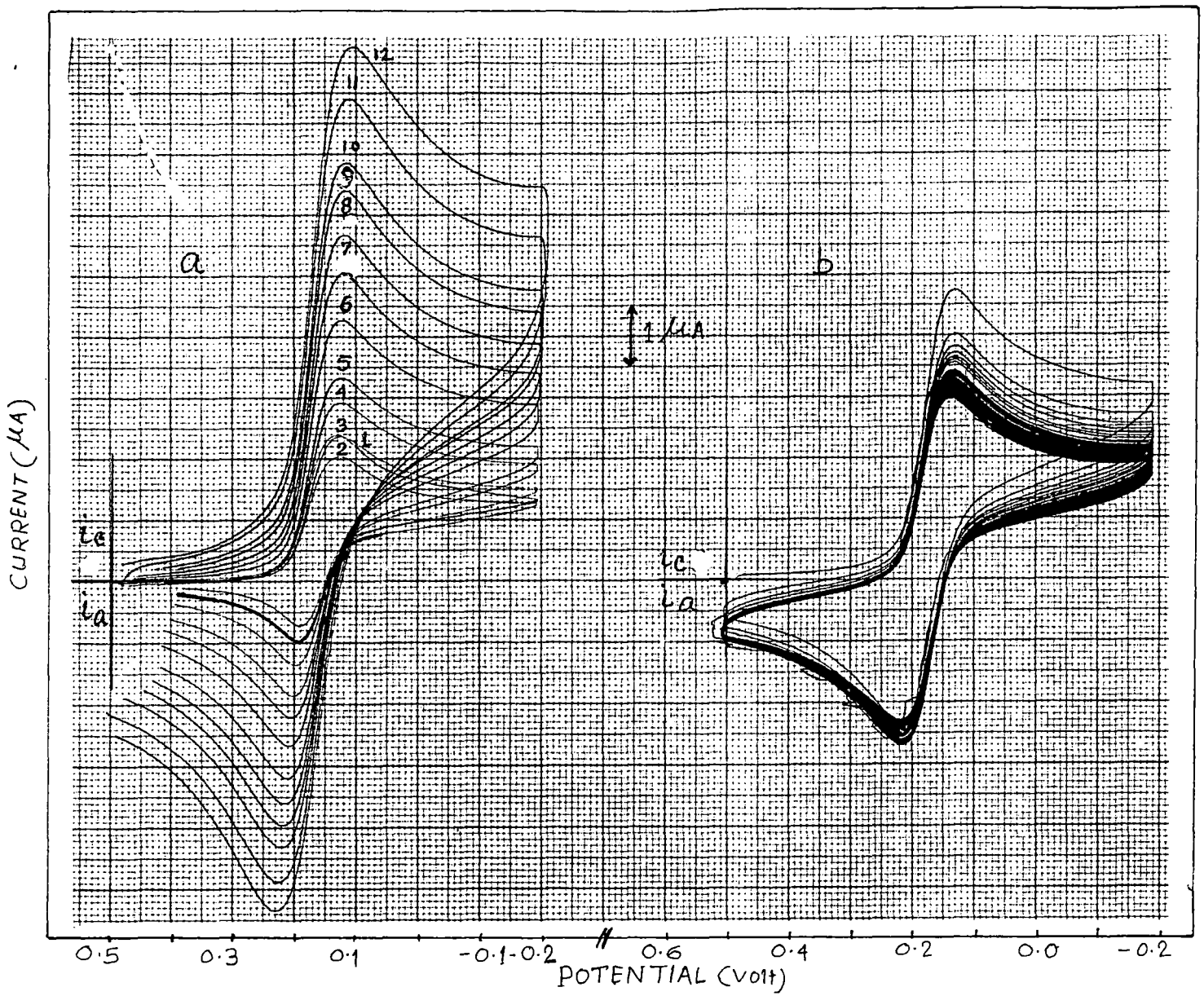

Fig. 68 : Cyclic Voltammograms of Thionine at montmorillonite modified electrode with scan rates (a) [1-12] 5, 10, 20, 40, 60, 100, 150, 200 250, 300, 400 and 500 mVs^{-1} and (b) repeatitive cycling with scan rate 100 mVs^{-1} in the presence of 0.1 M H_2SO_4.

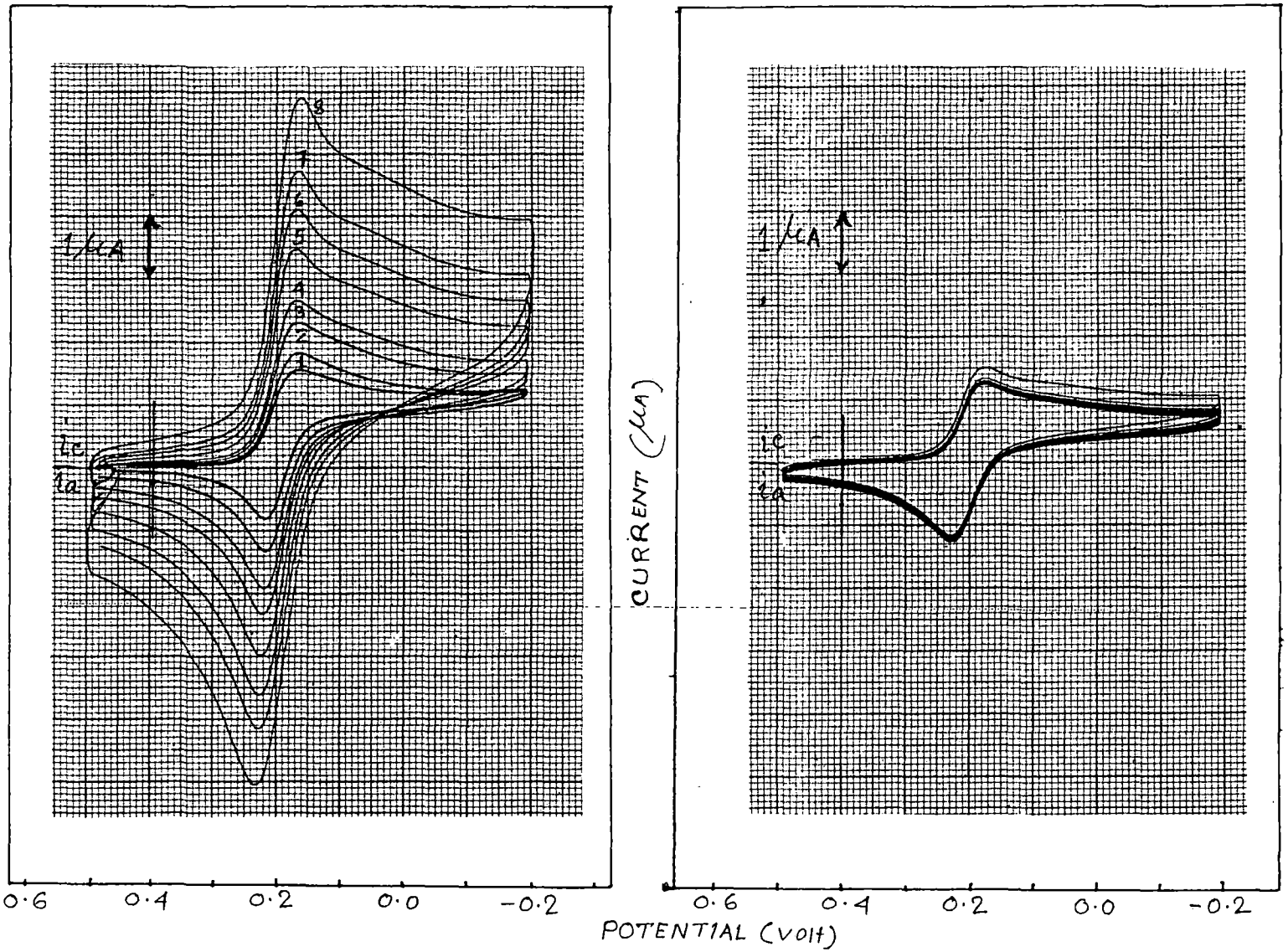

Fig. 69 : Cyclic Voltammograms of Thionine at ZSM-5 modified electrode with scan rates (a) [1-8] 10, 20, 40, 60, 100, 150, 200 and 300 mVs^{-1} and (b) repeatitive cycling with scan rate 100 mVs^{-1} in the presence of 0.1 M H_2SO_4.

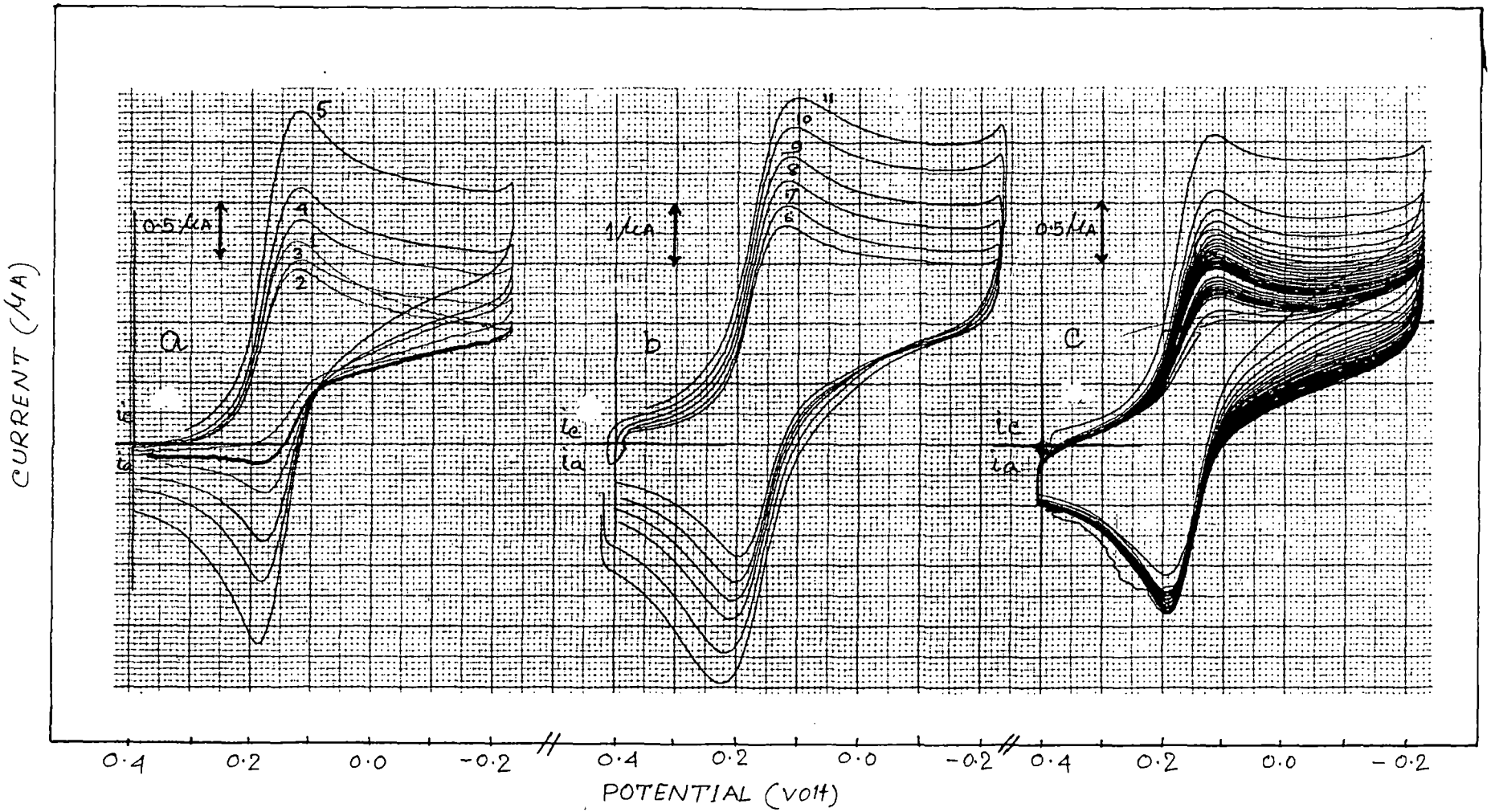

Fig. 70 : Cyclic Voltammograms of Azure C at montmorillonite modified electrode with scan rates (a) [1-5] 5, 10, 20, 40, 60, (b) [6-11] 100, 150, 200, 250, 300, 400 mVs^{-1} and (c) repeatitive cycling with scan rate 100 mVs^{-1} in the presence of 0.1 M H_2SO_4.

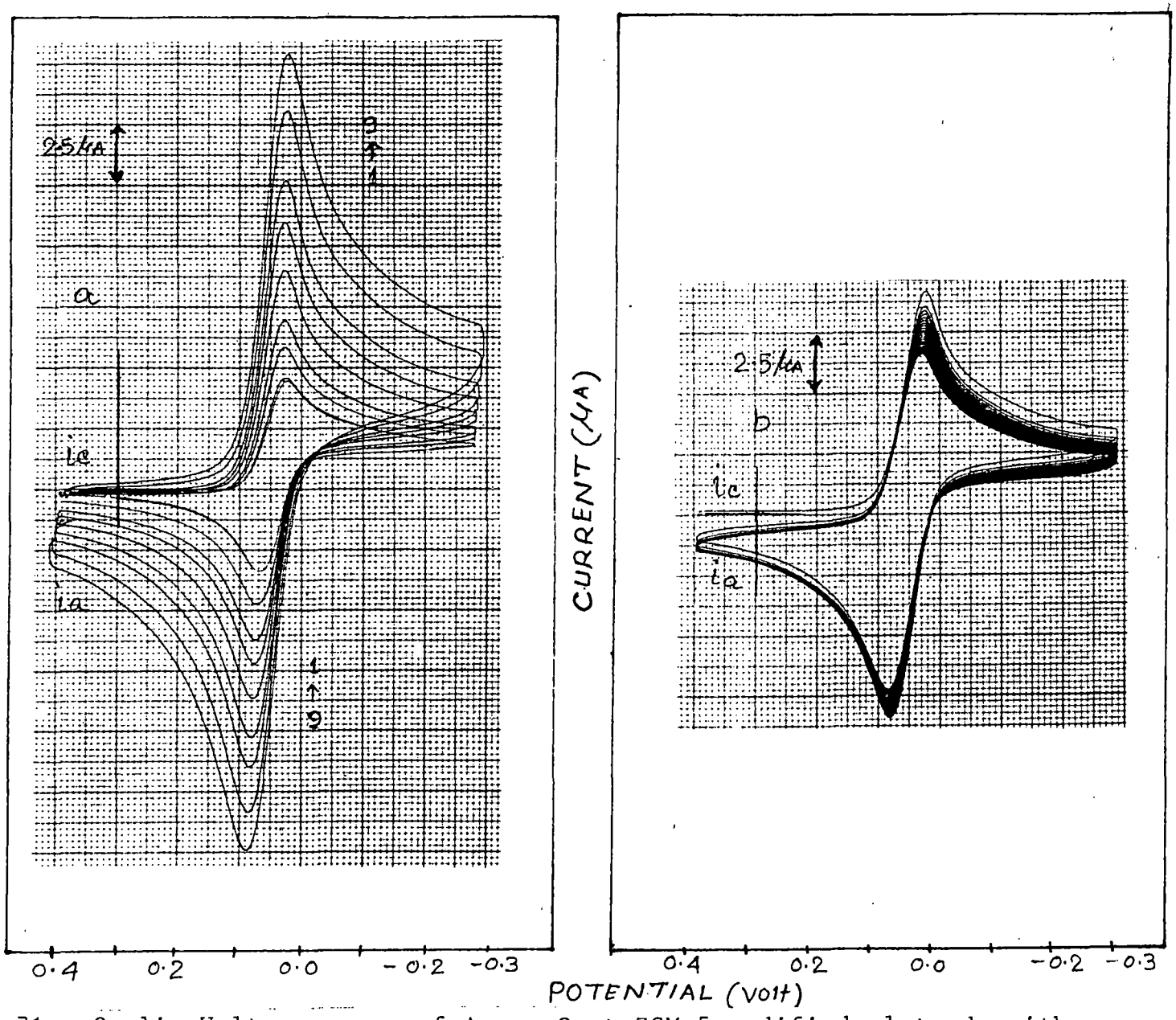

Fig. 71 : Cyclic Voltammograms of Azure C at ZSM-5 modified eletrode with scan rates (a) [1-9] 10,20,40,60, 100, 150, 200, 300 and 400 mVs^{-1} and (b) repeatitive cycling with scan rate 100 mVs^{-1} in the presence of 0.1M H_2SO_4.

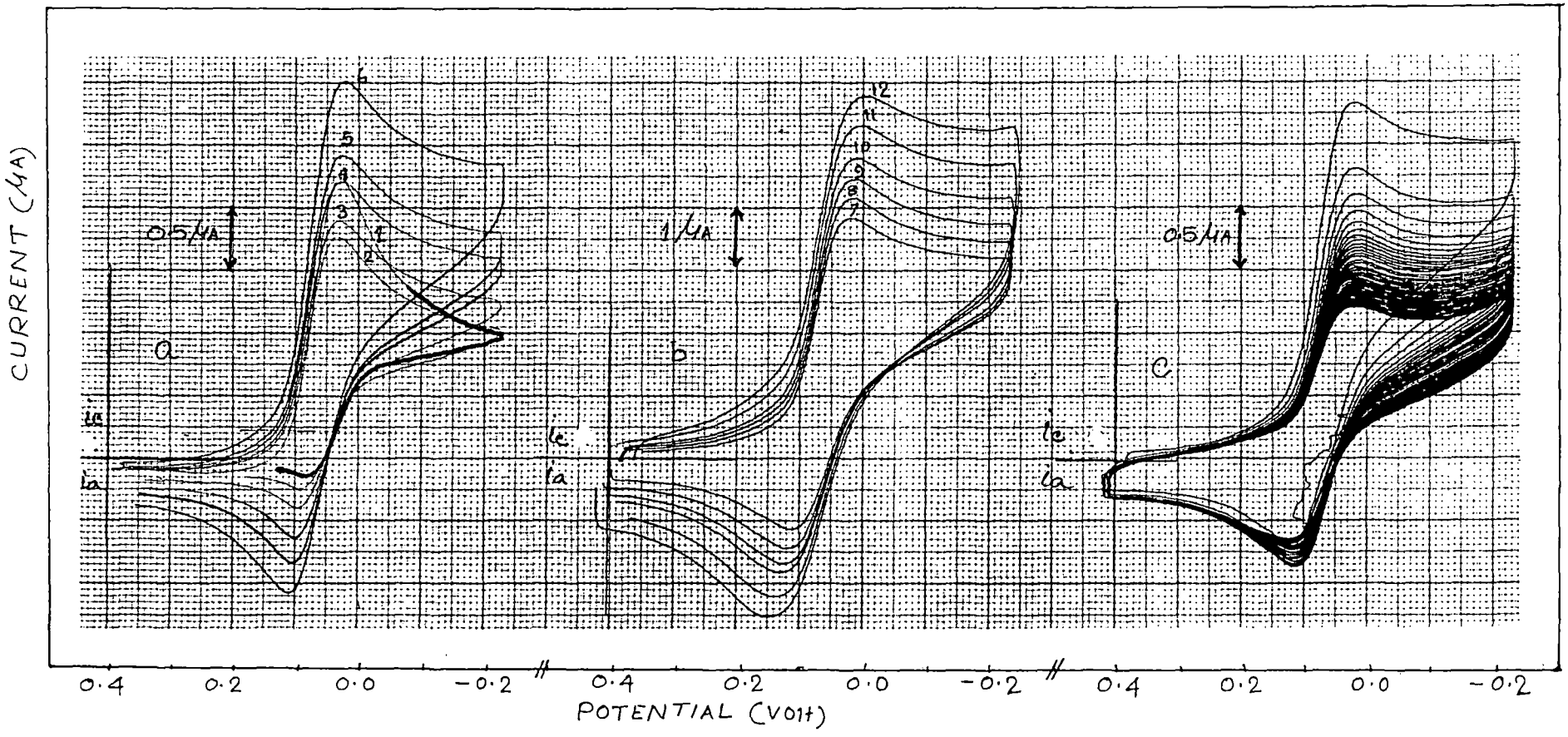

Fig. 72 : Cyclic Voltammograms of Azure A at montmorillonite modified electrode with scan rates (a) [1-6] 5, 10, 20, 40, 60, 100 (b) [7-12] 150, 200, 250, 300, 400, 500 mVs^{-1} and (c) repeatitive cycling with scan rate 100 mVs^{-1} in the presence of 0.1 M H_2SO_4.

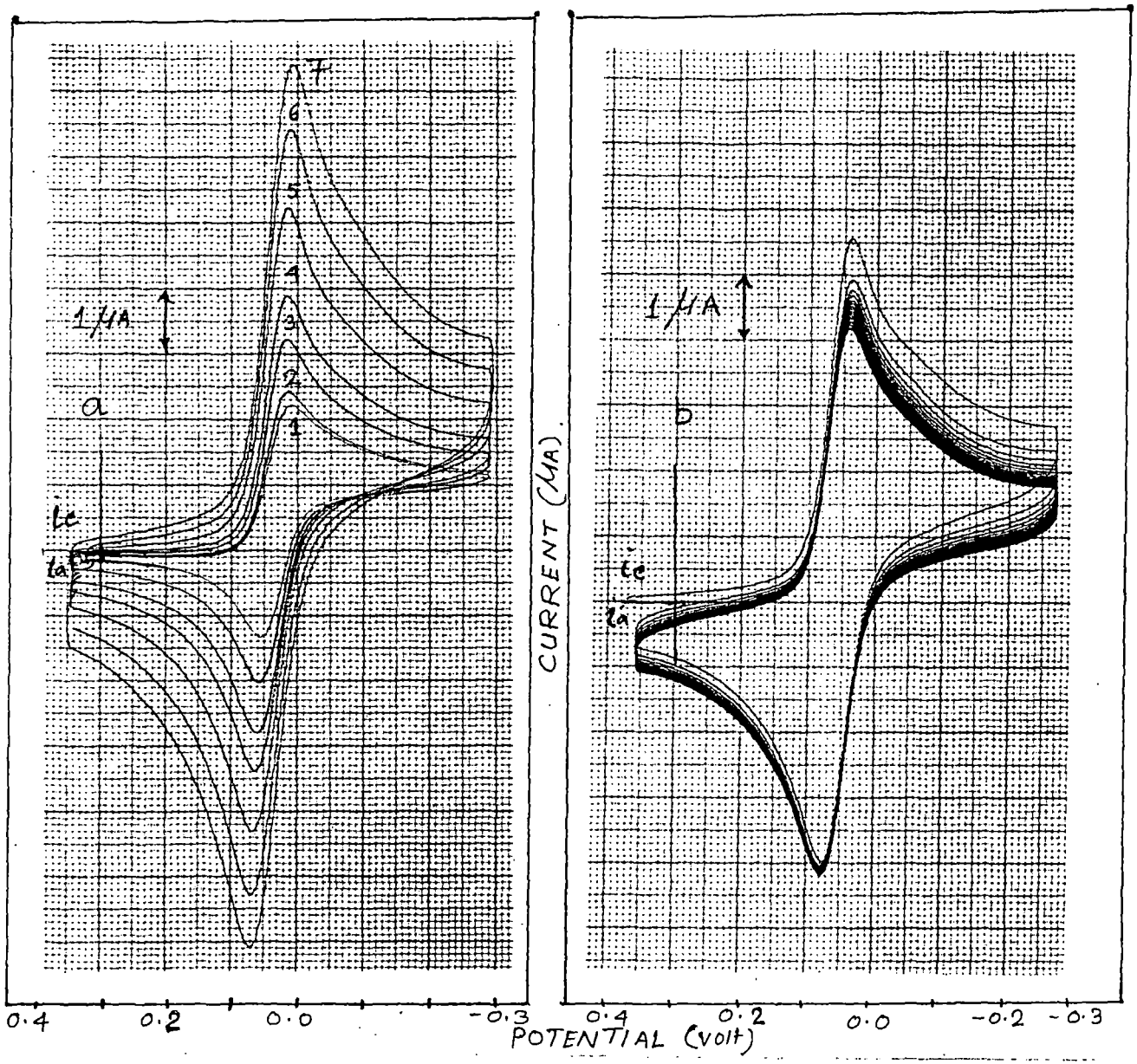

Fig. 73 : Cyclic Voltammograms of Azure A at ZSM-5 modified electrode with scan rates (a) [1-7] 10,20, 40, 60, 100, 150 and 200 mVs^{-1} and (b) repeatitive cycling with scan rate 100 mVs^{-1} in the presence of 0.1 M H_2SO_4.

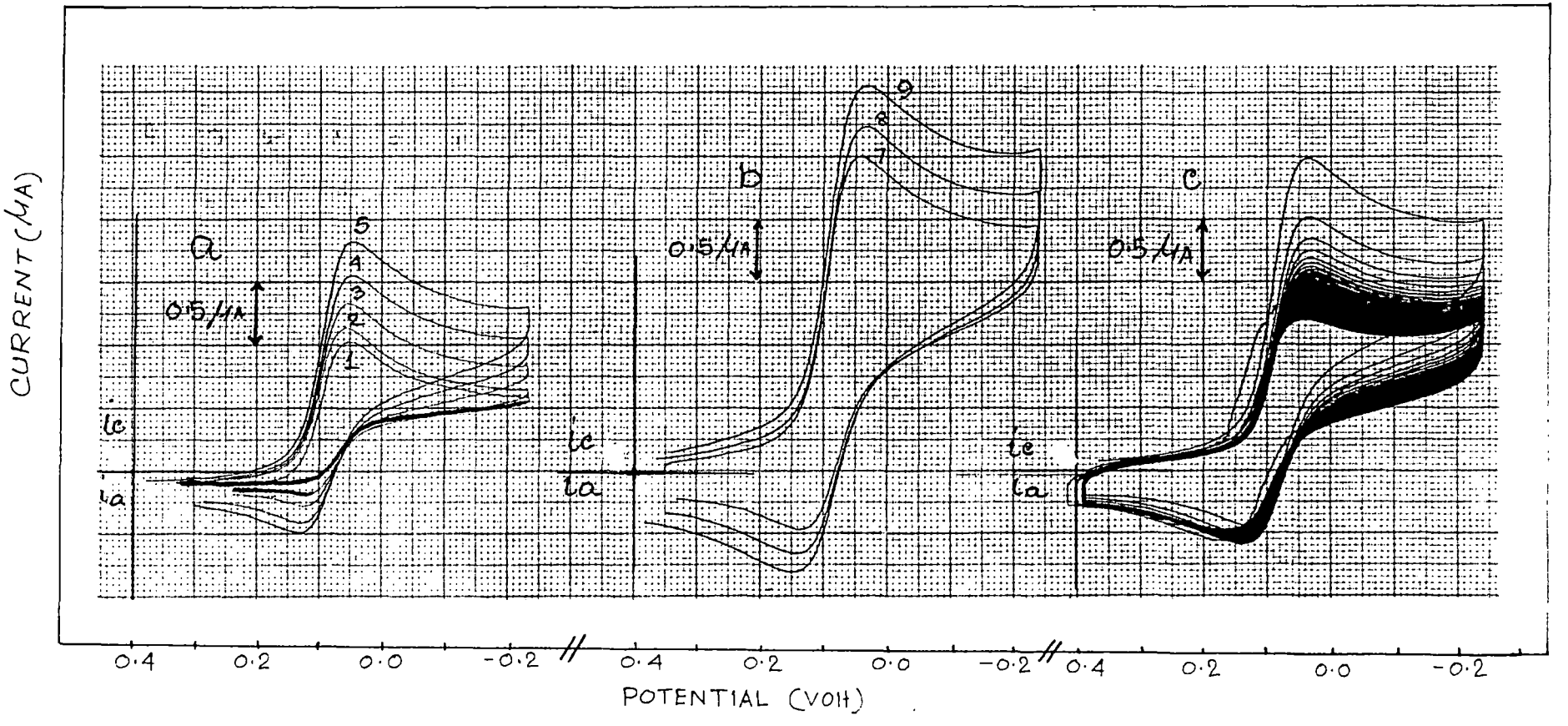

Fig. 74 : Cyclic Voltammograms of Azure B at montmorillonite modified electrode with scan rates (a) [1-5] 5, 10,20, 40, 60 (b) [7-9] 100, 150, 200 mVs^{-1} and (c) repeatitive cycling with scan rate 100 mVs^{-1} in the presence of 0.1 M H_2SO_4.

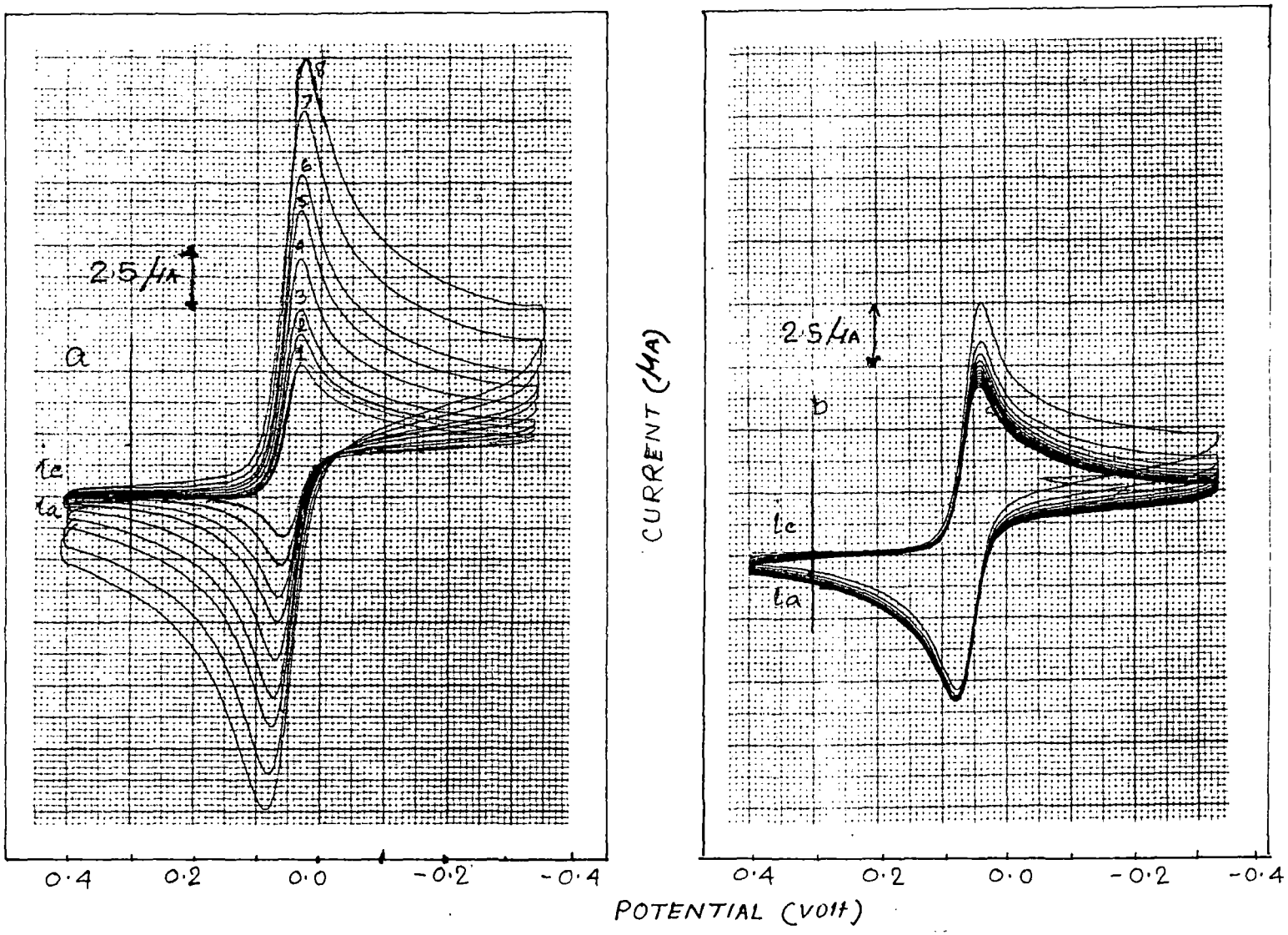

Fig. 75 : Cyclic Voltammograms of Azure B at ZSM-5 modified electrode with scan rates (a) [1-8] 10, 20, 40, 60, 100, 150, 200, 300 and 400 mVs^{-1} and (b) repeatitive cycling with scan rate 100 mVs^{-1} in the presence of 0.1M H_2SO_4.

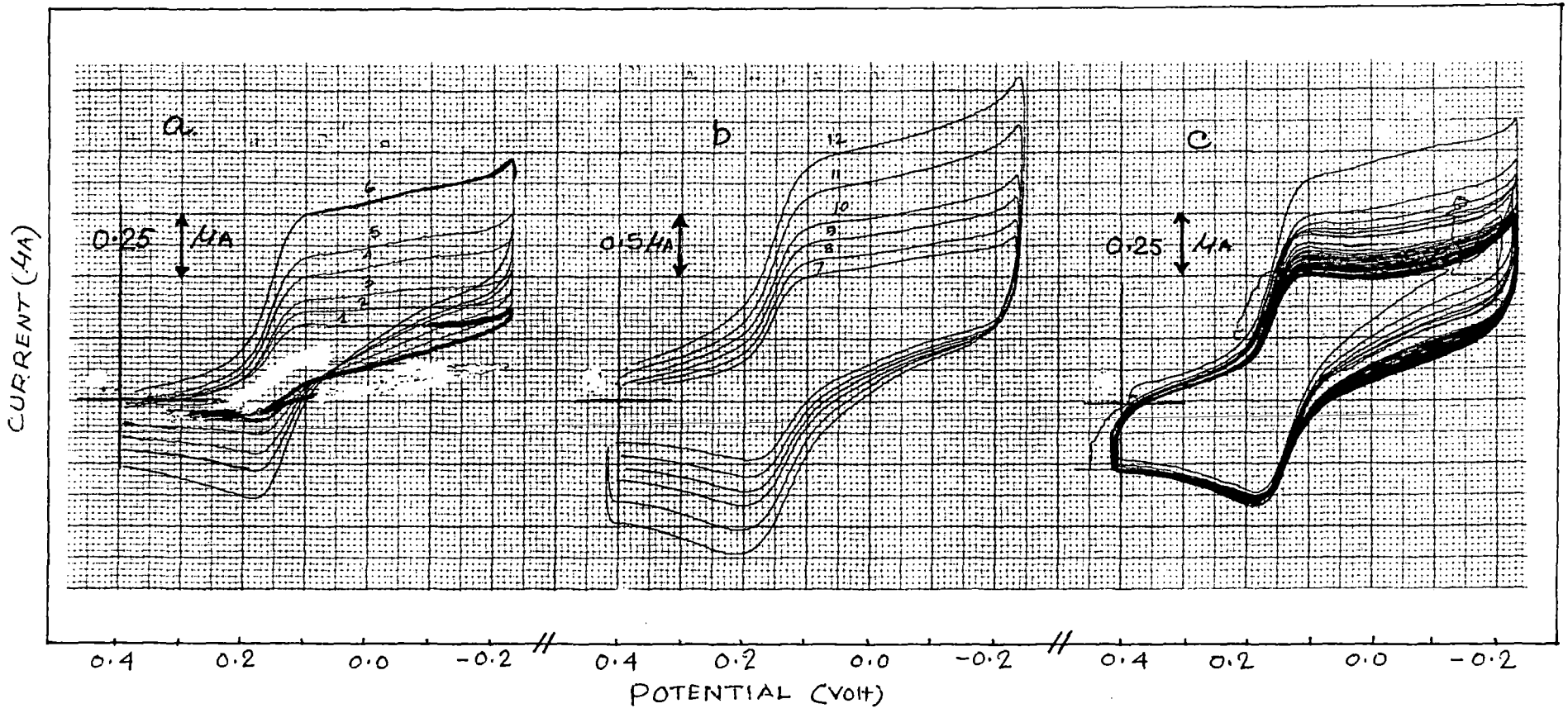

Fig. 76 : Cyclic Voltammograms of Methylene Blue at montmorillonite modified electrode with scan rates (a) [1-6] 5, 10, 20, 40, 60, 100 (b) [7-12] 150, 200, 250, 300, 400, 500 mVs^{-1} and (c) repeatitive cycling with scan rate 100 mVs^{-1} in the presence of 0.1 M H_2SO_4.

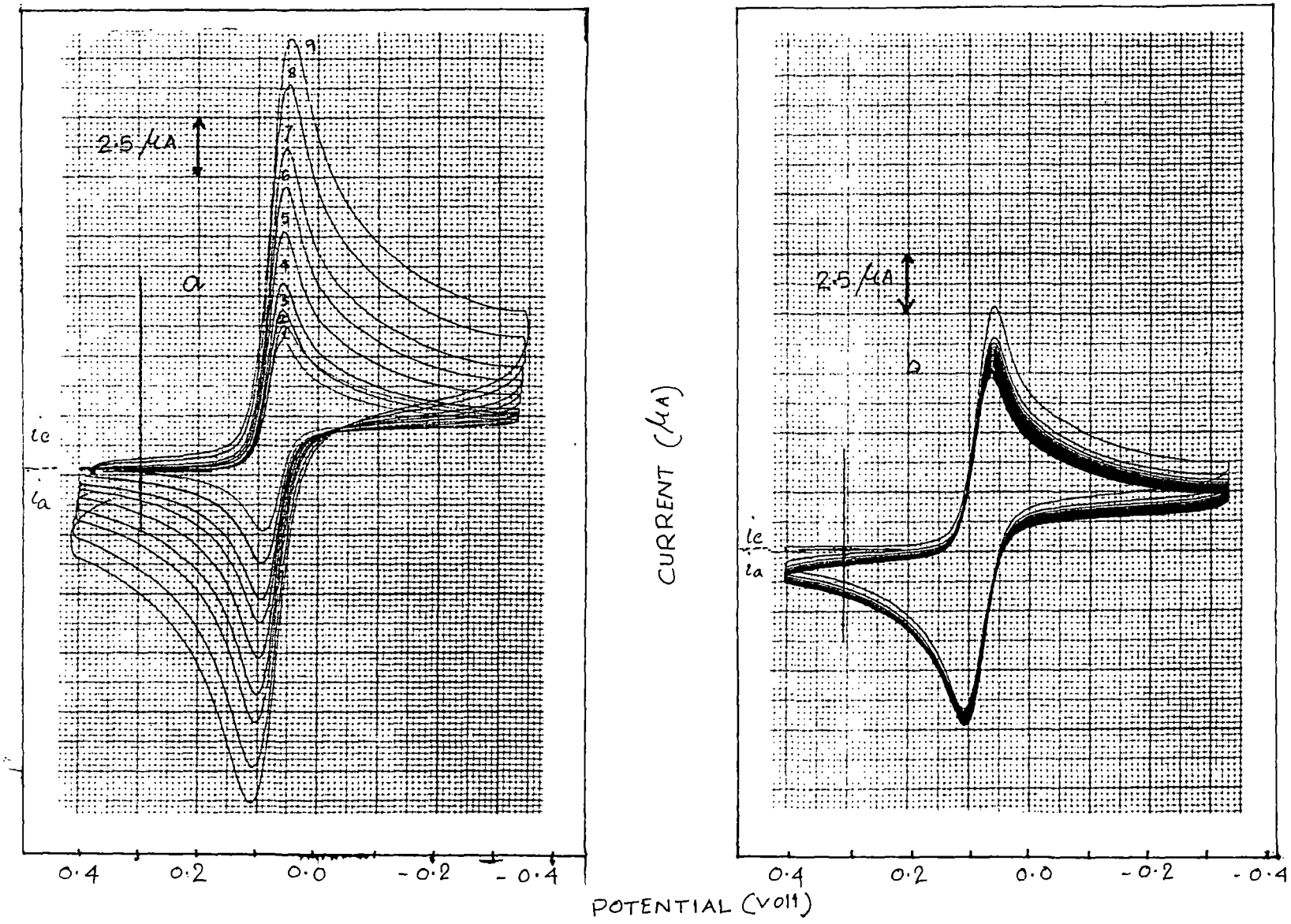

Fig. 77 : Cyclic Voltammograms of Methylene Blue at ZSM-5 modified electrode with scan rates (a) [1-9] 10,20, 40, 60, 100, 150, 200, 300 and 400 mVs^{-1} and (b) repeatitive cycling with scan rate 100 mVs^{-1} in the presence of 0.1 M H_2SO_4.

anodic or cathodic peaks, which restricts the analysis of the results. However, the montmorillonite modified and zeolite (ZSM-5) modified electrodes, when made conducting in the presence of colloidal Pt, exhibit quasi-reversible redox wave of the dyes (although the shapes of the CV's at the zeolite modified electrodes is more close to reversible wave), which are comparable to the reversible waves of dyes in aqueous solution at slow scan rates. Data pertaining to the position of peak potentials and current ratios (i_{pa}/i_{pc}), as a function of scan rate, are given in table 21-22. For scan rates above 100 mVs^{-1} i_{pc} is a linear function of $v^{1/2}$ (fig.78-82). At slower scan rates the points of i_{pc} vs. $v^{1/2}$ plots deviate significantly. Moreover, except thionine, the current output for all the dyes are substantially less in clay modified electrodes than that in zeolite modified electrode. This suggests that the observed cyclic voltammograms at the modified electrodes are of diffusion type only at high scan rates. Normally, one would have expected a surface wave for these modified electrodes. The diffusion type cyclic voltammetric behaviour observed in the present case shows that the charge transport within the film is limited either by the diffusion of the electroactive dye to the electrode surface or by an electron hopping process within the clay film.

Randles-Seveik equation (122) shows that the apparent diffusion coefficient, D_{app}, of thionine in clay modified electrode film (from current measurements in voltammograms) is of

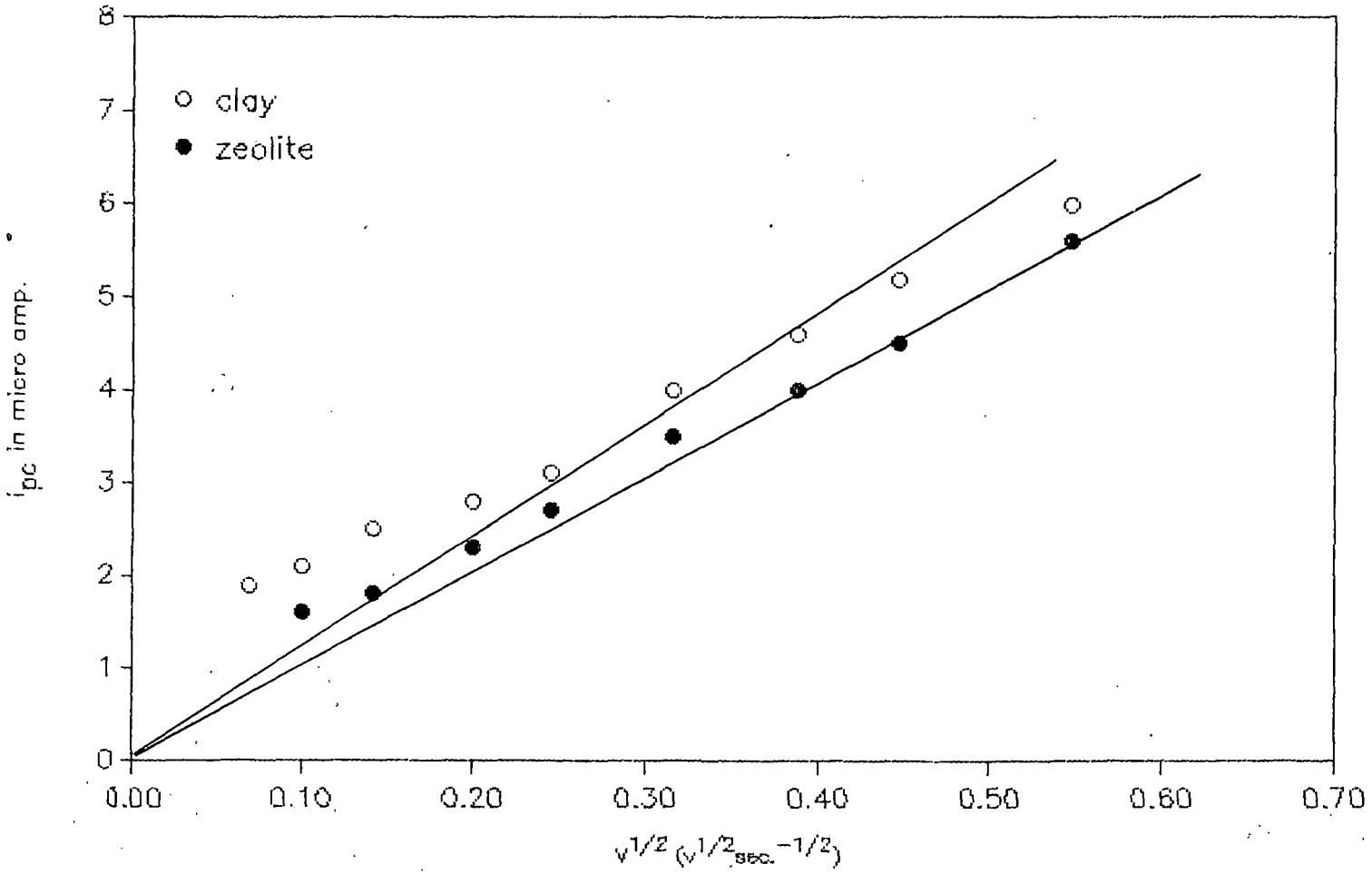

Fig.78 Plot of cathodic peak currents as a function of (scan rates)$^{1/2}$ for Thionine at modified GCE.

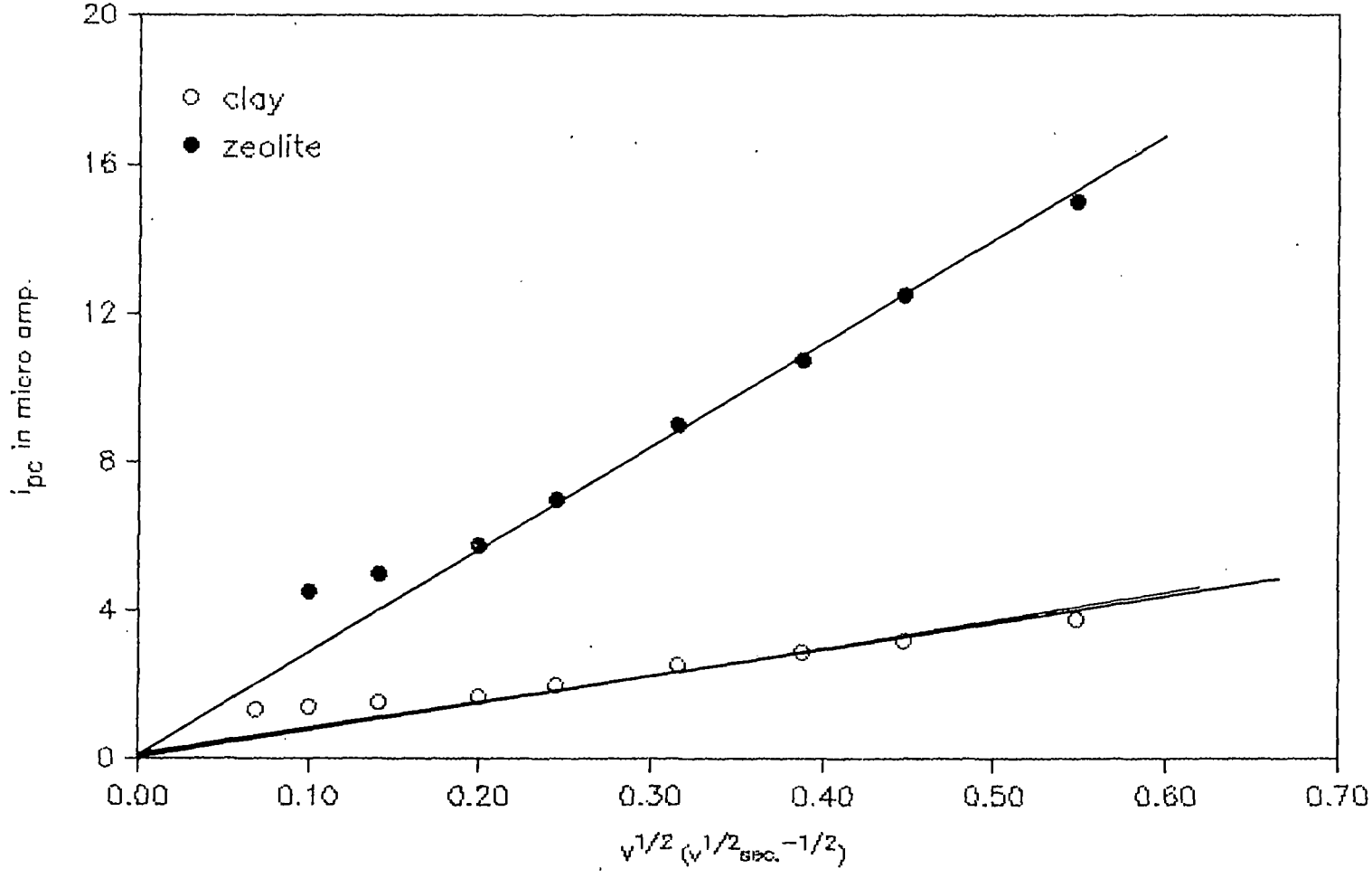

Fig.79 Plot of cathodic peak currents as a function of (scan rates)$^{1/2}$ for Azure C at modified GCE.

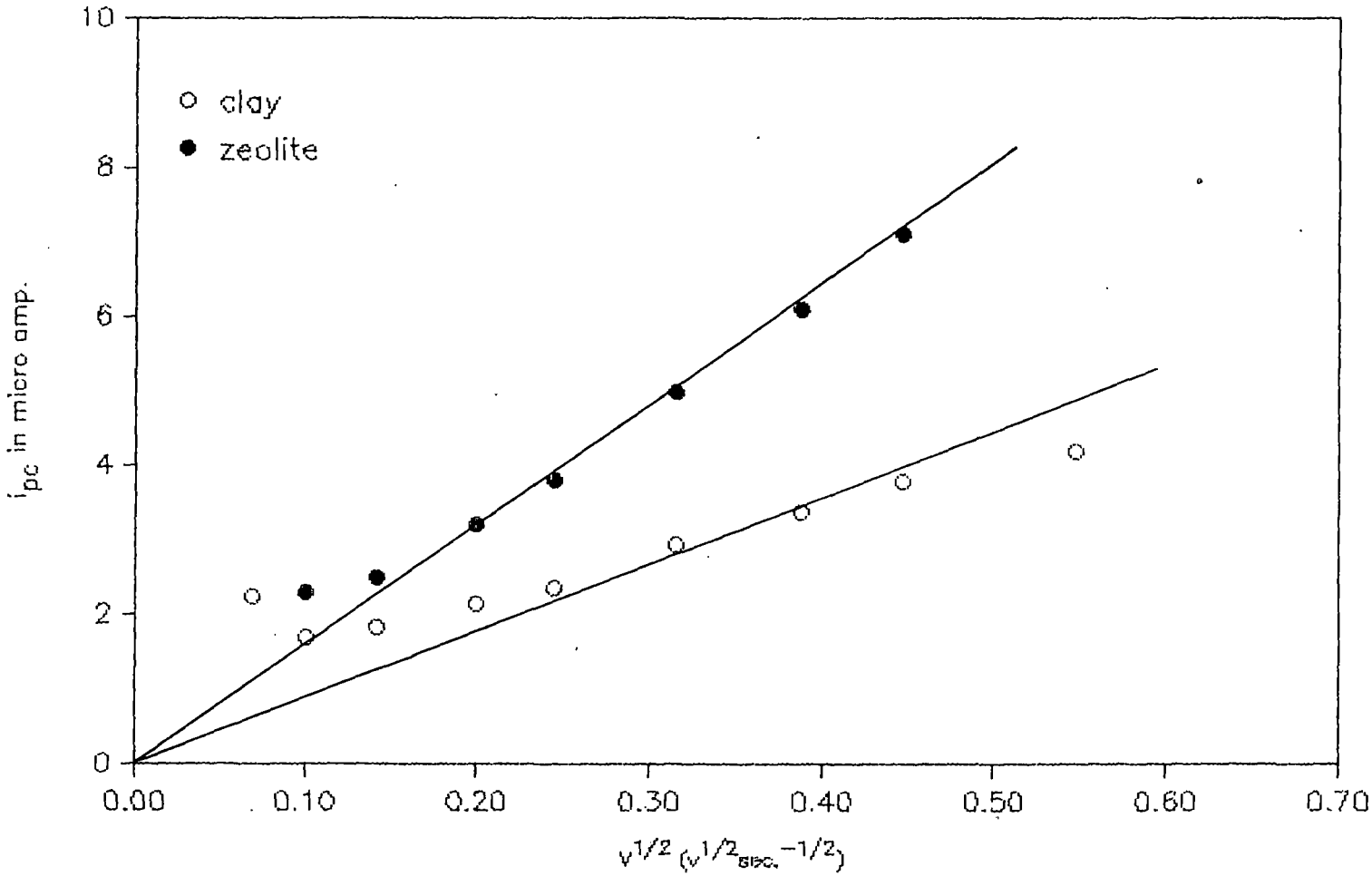

Fig.80 Plot of cathodic peak currents as a function of (scan rates)$^{1/2}$ for Azure A at modified GCE.

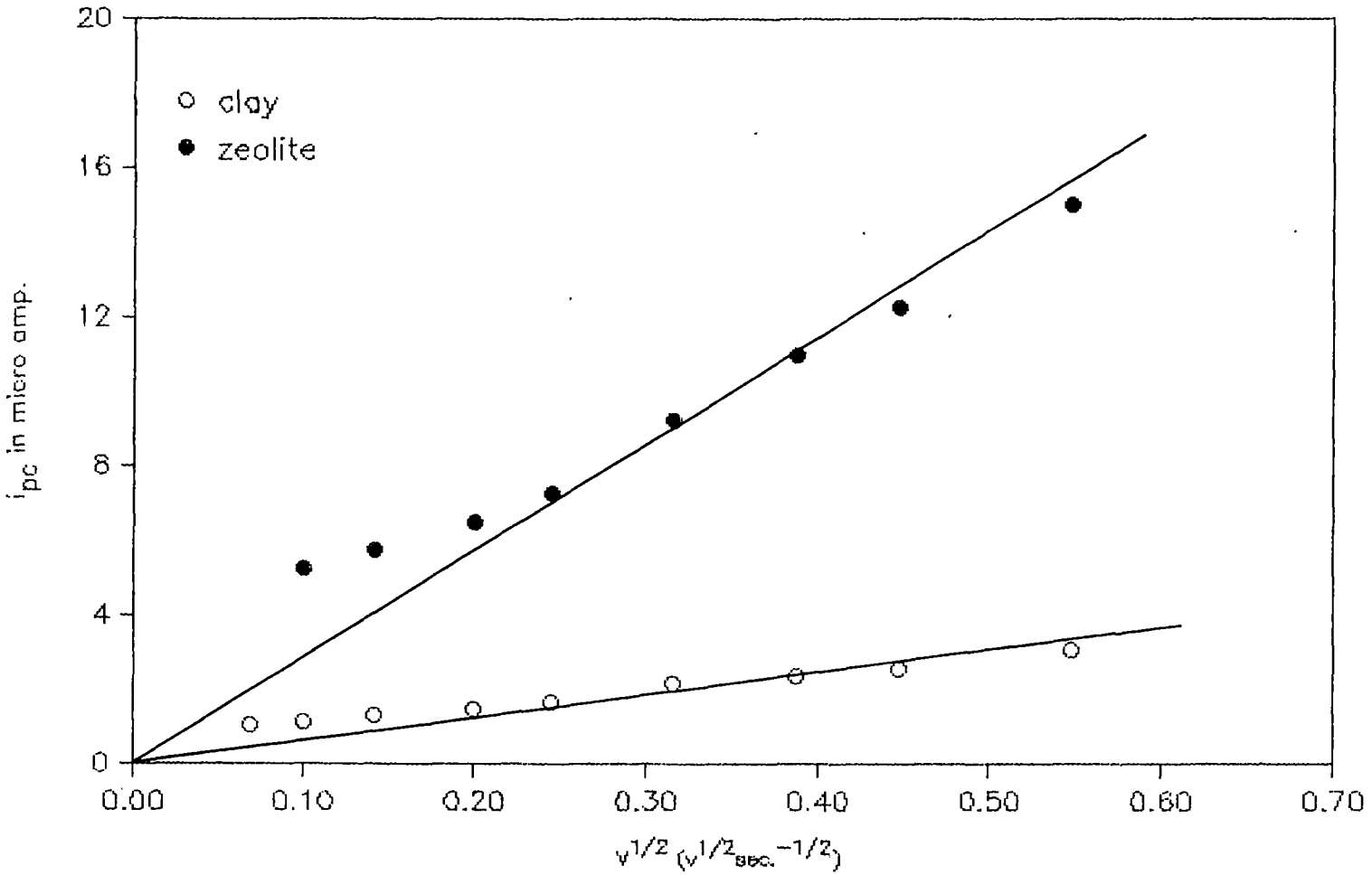

Fig.81 Plot of cathodic peak currents as a function of (scan rates)$^{1/2}$ for Azure B at modified GCE.

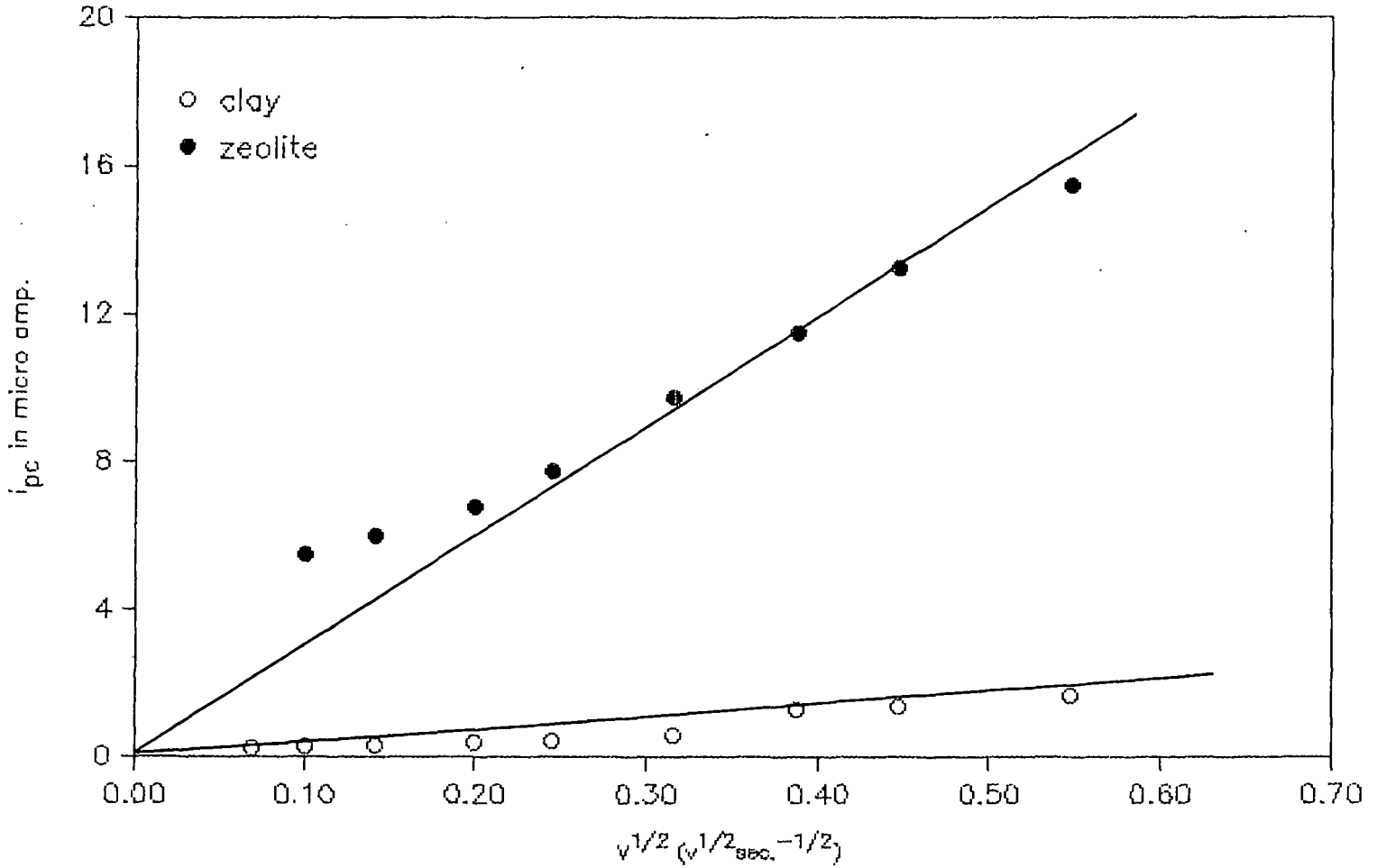

Fig.82. Plot of cathodic peak currents as a function of (scan rates)$^{1/2}$ for Methylene Blue at modified GCE.

Table-21

Electrochemical data for Cyclic Voltammetry of Dyes at modified (montmorillonite) GCE in the presence of 0.1M H_2SO_4

S.R. (mVs^{-1})	E_{pa}(V)	E_{pc}(V)	ΔE_p(V)	i_{pa}/i_{pc}	$i_{pc}v^{-1/2}$
		Thionine			
5	.190	.132	.058	.68	27.14
10	.195	.132	.063	.74	23.00
20	.198	.131	.067	.91	16.31
40	.201	.130	.071	.89	14.00
60	.206	.128	.078	.90	12.70
100	.210	.125	.085	.87	12.65
150	.215	.122	.093	.84	11.88
200	.220	.120	.100	.78	11.63
300	.228	.115	.113	.80	10.96
		Azure C			
5	.175	.125	.050	.40	19.28
10	.178	.123	.055	.41	14.28
20	.180	.122	.058	.74	10.99
40	.182	.122	.060	.79	8.50
60	.184	.121	.063	.85	8.19
100	.185	.120	.065	.88	8.06
150	.190	.118	.072	.89	7.49
200	.195	.116	.079	.93	7.15
300	.205	.112	.093	.94	6.94

contd.

Table-21

Electrochemical data for Cyclic Voltammetry of Dyes at modified (montmorillonite) GCE in the presence of 0.1M H_2SO_4

S.R. (mVs^{-1})	E_{pa}(V)	E_{pc}(V)	ΔE_p(V)	i_{pa}/i_{pc}	$i_{pc}v^{-1/2}$
		Azure A			
5	.085	.032	.053	.35	32.14
10	.090	.028	.062	.47	17.00
20	.095	.028	.067	.51	13.12
40	.100	.026	.074	.56	10.75
60	.105	.025	.080	.57	9.63
100	.110	.020	.090	.53	9.33
150	.112	.018	.094	.53	8.78
200	.118	.015	.103	.53	8.50
300	.125	.010	.124	.55	7.68
		Azure B			
5	.110	.055	.055	.42	15.00
10	.115	.052	.063	.48	11.50
20	.118	.050	.068	.44	9.57
40	.123	.048	.075	.53	7.50
60	.125	.042	.083	.53	6.96
100	.130	.040	.090	.50	6.96
150	.140	.035	.105	.52	6.20
200	.145	.030	.115	.54	5.81
300	.150	.027	.123	.55	5.66

contd.

Table-21

Electrochemical data for Cyclic Voltammetry of Dyes at modified (montmorillonite) GCE in the presence of 0.1M H_2SO_4

S.R. (mVs^{-1})	E_{pa}(V)	E_{pc}(V)	ΔE_p(V)	i_{pa}/i_{pc}	$i_{pc}v^{-1/2}$
		Methylene Blue			
5	.155	.110	.045	.50	3.57
10	.160	.108	.052	.50	3.00
20	.165	.106	.059	.50	2.48
40	.170	.104	.064	.69	2.00
60	.175	.102	.073	.72	1.84
100	.180	.100	.080	.75	1.89
150	.185	.098	.087	.61	3.36
200	.190	.096	.094	.64	3.13
300	.200	.092	.108	.70	3.10

Table-22

Electrochemical data for Cyclic Voltammetry of Dyes at modified (ZSM-5) GCE in the presence of 0.1M H_2SO_4

S.R. (mVs^{-1})	E_{pa}(V)	E_{pc}(V)	ΔE_p(V)	i_{pa}/i_{pc}	$i_{pc}v^{-1/2}$
		Thionine			
10	.215	.173	.042	0.93	16.0
20	.218	.172	.046	1.05	12.7
40	.220	.170	.050	1.04	11.5
60	.222	.170	.052	1.03	11.0
100	.225	.168	.057	0.94	11.0
150	.225	.168	.057	0.95	10.3
200	.229	.165	.064	0.93	10.0
300	.235	.160	.075	0.85	10.2
		Azure C			
10	.070	.030	.040	1.00	45.0
20	.075	.029	.046	1.11	35.4
40	.075	.029	.046	1.21	28.7
60	.078	.028	.050	1.14	28.5
100	.080	.028	.052	1.05	28.4
150	.082	.026	.056	1.02	27.7
200	.084	.025	.059	0.98	27.9
300	.085	.024	.061	0.93	27.3
		Azure A			
10	.058	.014	.044	0.91	23.0
20	.060	.015	.045	1.00	17.7
40	.062	.016	.046	1.03	16.0
60	.065	.016	.049	0.97	15.5
100	.066	.012	.054	0.92	15.8
150	.068	.010	.058	0.90	15.7
200	.070	.008	.062	0.87	15.8

contd.

Table-22

Electrochemical data for Cyclic Voltammetry of Dyes at modified (ZSM-5) GCE in the presence of 0.1M H_2SO_4

S.R. (mVs^{-1})	E_{pa}(V)	E_{pc}(V)	ΔE_p(V)	i_{pa}/i_{pc}	$i_{pc}v^{-1/2}$
		Azure B			
10	.060	.030	.030	0.57	52.5
20	.063	.030	.033	0.74	40.7
40	.068	.030	.038	0.88	32.5
60	.070	.031	.039	0.89	29.5
100	.072	.032	.040	0.86	29.2
150	.076	.030	.046	0.86	28.4
200	.078	.029	.049	0.85	27.3
300	.082	.026	.056	0.81	27.3
		Methylene Blue			
10	.094	.060	.034	0.72	55.0
20	.095	.060	.035	0.91	42.5
40	.096	.060	.036	1.00	33.7
60	.098	.058	.040	0.96	31.6
100	.100	.055	.045	0.95	30.8
150	.102	.054	.048	0.91	29.6
200	.105	.050	.055	0.90	29.6
300	.108	.048	.060	0.87	28.2

the order of 10^{-14} cm^2s^{-1}. The concentration of the dye within the film is taken as 0.17M. This concentration was estimated from the optimum dye intake capacity of montmorillonite as is shown in chapter 5 and measuring the amount of clay in the film (by gravimetric estimation). A rough estimate of thickness of the film was made (by density measurement and gravimetry) and found to be nearly 16 micron. No attempt was made to correct the errors introduced by film swelling due to hydration. In fact D_{app} for the dye is the sum of contributions from the actual physical diffusion of the dye and from electron exchange (hopping) between adjacent sites, as shown by the following equation,

$$D_{app} = D + (\pi/4) (k_{ex} d^2 C) \qquad (42)$$

D corresponds to physical diffusion and the second term corresponds to "diffusion" via electron hopping, where k_{ex} is the second order electron transfer rate constant and d is the distance between the electroactive centres of concentration C. The low value of D_{app} for the dye in clay suggests that diffusion occurs mainly via electron hopping. Physical diffusion seems unlikely at least for the fraction corresponding to the CEC, since the molecules can not be displaced from the clay binding sites to diffuse. Continuous potential cycling at 100 mVs^{-1} for several times shows a gradual decrease in the peak heights (Figs. 68-77) However, as the number of cycles increase, peak current differences between successive cycles become less and less

prominent. The differences in peak currents between the first and the second cycle is most prominent. Probably a high concentration of dye layer is formed at the vicinity of the modified electrode surfaces through ion exchange of comparatively loosely bound dye molecules by the background electrolyte. This layer is diffused away rapidly within the first cycle time. The process becomes less and less significant in subsequent cycles. This phenomenone is less significant in zeolite modified electrode. The values of $i_{pa}/i_{pc} < 1$, which is prominent in electrode processes of AzC, AzA, and AzB on montmorillonite modified electrode may stem from a coupled chemical reaction involving the Fe(III) ions in the lattice position of clay sample. This Fe(III) ions are shown to be active in various redox reactions on clay surface (136) and may compete with electrode reaction in oxidizing leucodyes to the corresponding thiazine dyes resulting in the decrease of anodic peak current.

4.3.3. Studies on the homogeneous reactions of the leucodyes With Fe(III) ions : Catalytic Regeneration Mechanism.

A cyclic voltammogram of azure C (5.0×10^{-5} M in 0.1 M H_2SO_4) is shown in fig. 83. Voltammograms of all other dyes are similar and consistent with reversible two electron transfer systems within the range of potential scan(v) of 5-100 $mV.s^{-1}$

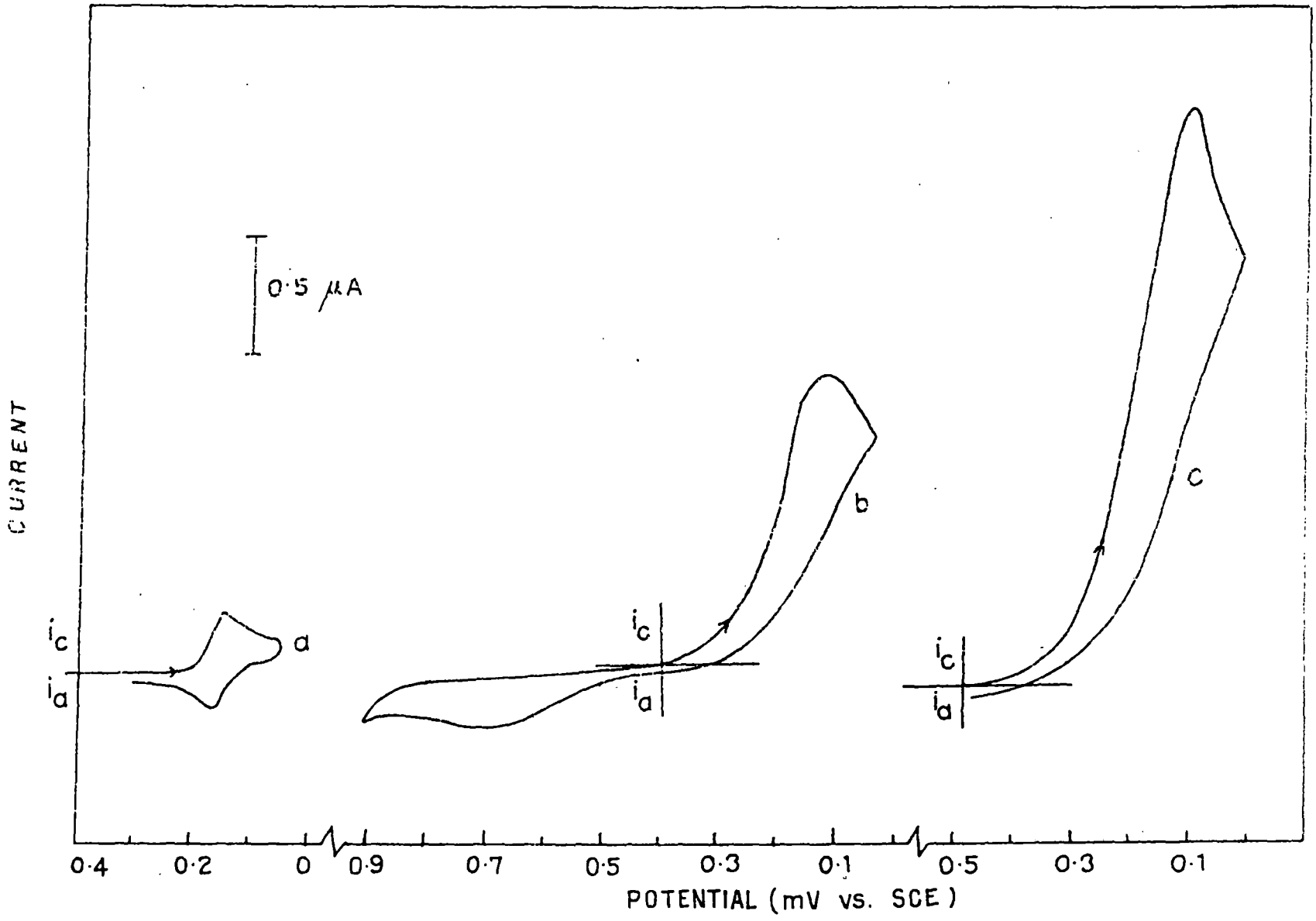

Fig. 83 : Cyclic Voltammograms of Azure C ($5x10^{-5}$M) in the presence of various concentration of Fe^{3+} : (a) 0, (b) $8x10^{-4}$ (c) $1.5x10^{-3}$M.

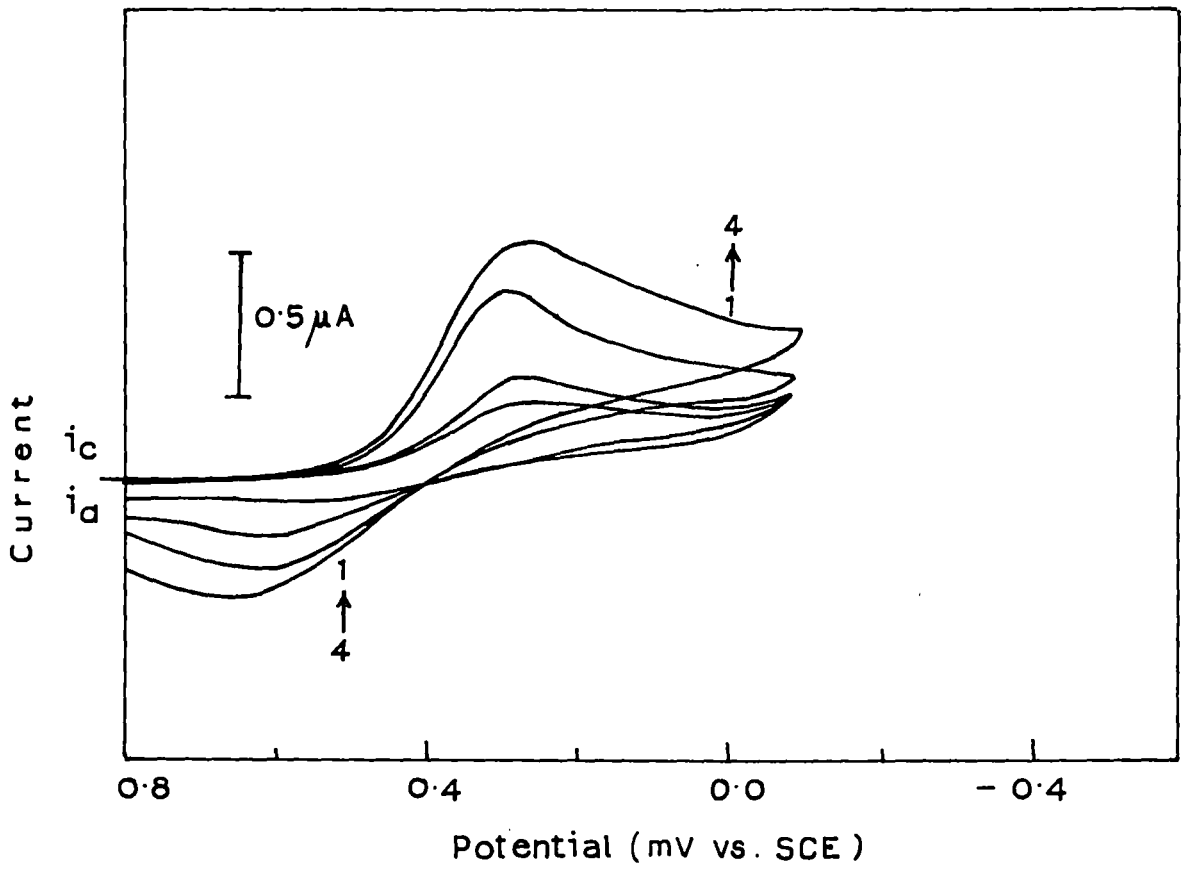

Fig. 84 : Cyclic Voltammograms of $FeCl_3$ in the presence of 0.1 M H_2SO_4 at GC electrode. Concentration of Fe(III) : (1) $2x10^{-4}$, (2) $4x10^{-4}$, (3) $6x10^{-4}$, (4) $8x10^{-4}$M. Scan rate : 5 mVs^{-1}.

(Discussed in section 4.3.1). Data pertaining to the position of peak potentials and current ratios, i_{pa}/i_{pc}, for the five thiazine dyes are shown in table 13-17 . Current vs. $v^{1/2}$ plots deviate from linearity above scan rates of 100 mVs^{-1} (table 13-17 ,figs. 55-59) The peak potentials (E_{pa} and E_{pc}) are not sensitive to scan rates and ΔE_p's do not vary appreciably up to a scan rate of 300 mVs^{-1} except for AzC. This shows that the electrode processes are very fast and the quasi-reversibility is apparent only above scan rate of 300 mVs^{-1}. Previous reports available for Th and MB were, however, consistent with the present observation (98,105,106,116). On the other hand, the Fe(II)/Fe(III) system exhibits slow electron transfer at the GC electrode in the potential range between 0.3 - 0.6V (fig 84). But the couple is no longer electrochemically active in the presence of thiazine dyes which of course have much higher heterogeneous kinetics (Table 20 ; k_s(Th)= 5×10^{-3} $cm.s^{-1}$, k_s(Fe)=3.1×10^{-5} $cm.s^{-1}$ on gold foil electrode (121)). On the other hand, voltammograms of thionine and its derivatives in the presence of varying amount of Fe(III) ions (5.0×10^{-5} - 1.0×10^{-3}M) show striking changes from those obtained in the absence of Fe(III) ions. The observed catalytic current results from the regeneration of dyes from the reduced leucodyes by reaction with Fe(III) ions (122,137). Representative voltammograms of AzC are shown in fig. 83. Alongwith the catalytic regeneration of thiazine dyes in the presence of Fe(III) ions, which of course is believed to be the

major process occurring in the system, some amount of semithiazines may also be present via a dismutation equilibrium (138). These semithiazines have been oxidized at the GC electrode to give the small anodic peak current at higher positive potential on the reversed scan (fig. 83b). Although Fe(II)/Fe(III) couple is electrochemically inactive at GC electrode in the presence of thiazine dyes, its adverse effect on the voltammograms of the latter by increasing the background current can not be ignored. To confirm that the experimental results conform to the theory of catalytically coupled reactions (EC') of the type shown in equation 40 as a major process, it is necessary to draw diagnostic plot of the current function against the potential scan rates.

This correlation can be seen by simply plotting $i_{pc}/v^{1/2}$ as a function of log v (139). Representative diagnostic plot for AzA and AzB are shown in fig. 85,86. In the absence of any Fe(III) ions, the plots for all the dyes are linear and parallel to the potential scan rate axis up to 100 $mV.s^{-1}$. This is expected for a diffusion controlled reversible electrode process. However, at higher scan rates the observed upward shift of the plot (not shown in figure, see table 13-17) is indeed the manifestation of positive deviation from linear relationship of i_{pc} with $v^{1/2}$ (fig. 55-59) for almost all the dyes. On the other hand, in the presence of Fe(III) ions ($5.0x10^{-5}$ - $1.0x10^{-3}$M), the diagnostic plots are similar for all dyes and are indicative of EC' type of coupled catalytic chemical reaction. The catalytic regeneration

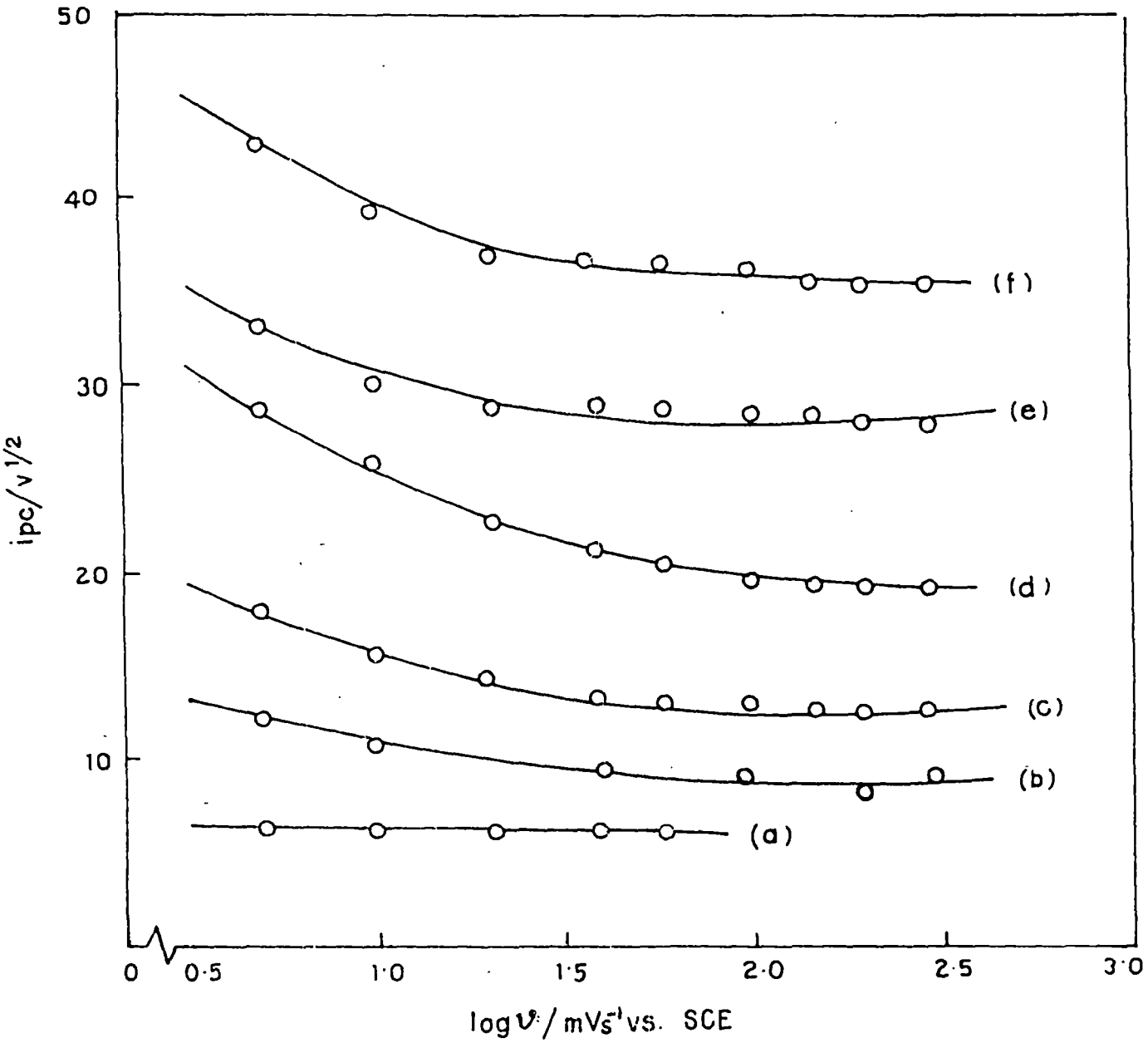

Fig. 85 : Diagnostic plots of current functions $i_{pc} / v^{\frac{1}{2}}$ VS. log v for Azure A ($5x10^{-5}$M) at various concentration of Fe^{3+} : (a-f) 0, $2x10^{-4}$, $4x10^{-4}$, $6x10^{-4}$, $8x10^{-4}$ and $1x10^{-3}$M.

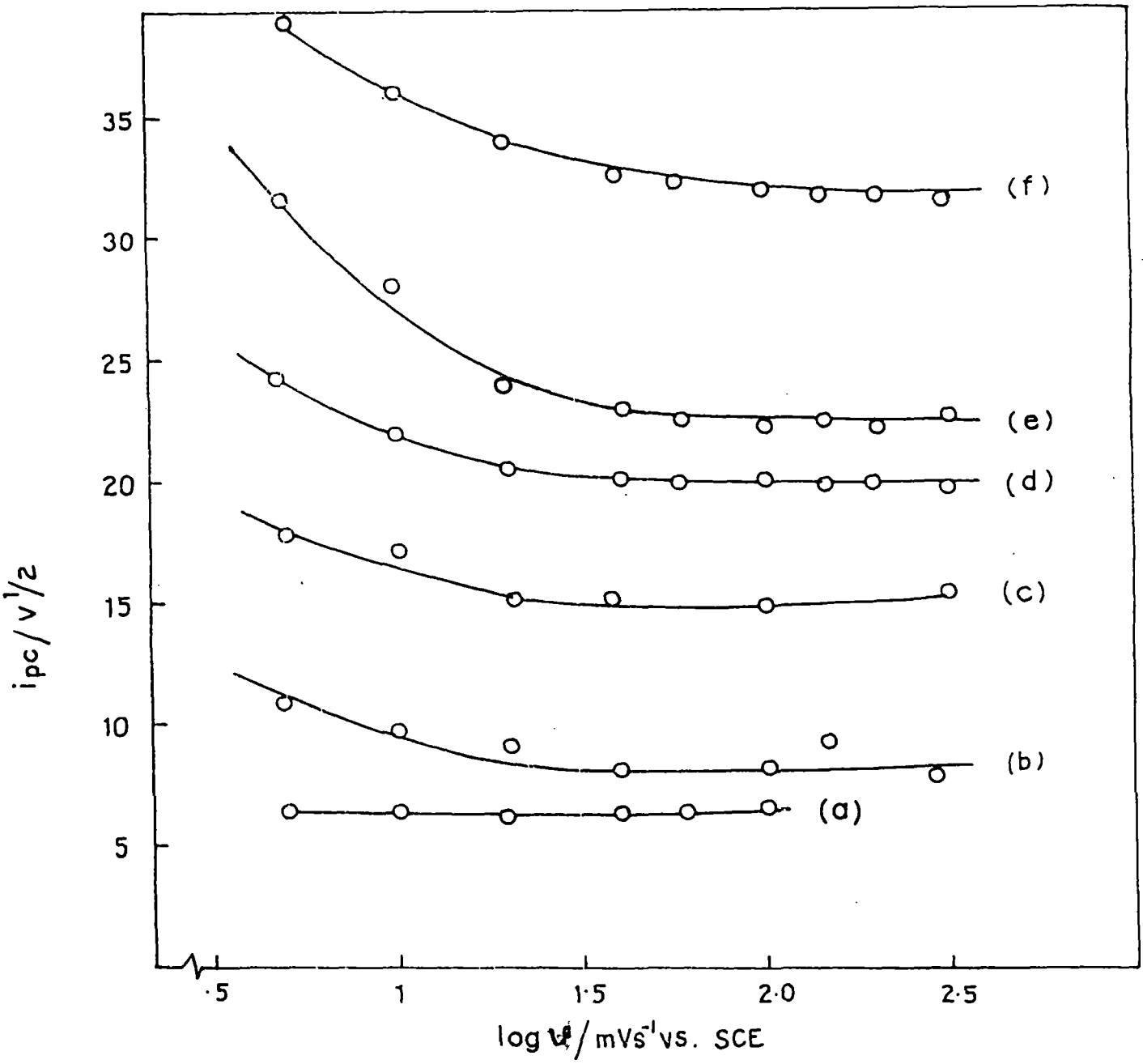

Fig. 86 : Diagnostic plots of current functions $i_{pc}/v^{\frac{1}{2}}$ VS. log v for Azure B ($5x10^{-5}$M) at various concentration of Fe^{3+} : (a-f) 0, $2x10^{-4}$, $4x10^{-4}$, $6x10^{-4}$, $8x10^{-4}$ and $1x10^{-3}$M.

of dyes as a major process is particularly apparent at lower scan rates as the reaction gets sufficient time for generation of dyes from the reduced leucoforms by reaction with Fe(III) ions, consistent with the theoretical model (140,141). However, when the scan rate increases, the ratio of kinetic current in the presence of Fe(III) to the cathodic peak current in the absence of Fe(III), i_d/i_{pc}, should tend towards unity. But this situation was not attained in the present study even at a sweep rate of 300 mVs^{-1} (Fig. 85-86). Similar results were also observed by previous workers for the intermolecular electron transfer of Cytochrome C in the presence of pseudomonas Cytochrome C551 (139) and for the homogeneous reaction of leucothionine with Fe(III) (108). Whereas we failed to identify any other mechanisms of coupled chemical reactions than EC' to be operative in the present systems, exact reason of the above is not certain.

Despite the simplified approach in view of the above and the complicated back reaction in the present systems, attempts have been made to derive kinetic information from the observed data. Using a working curve (Fig.14 of ref.140) of i_k/i_d vs. kinetic parameter, $(k_f/a)^{1/2}$, we have plotted the data of k_f/a (where a = nF/RT) against 1/V, which should be linear under first order conditions (figs. 87). The result shows marked deviation from the predicted linearity, at slower scan rates, which is consistent with loss of first order conditions. The reactant dye is not in sufficiently large excess and so is consumed to a

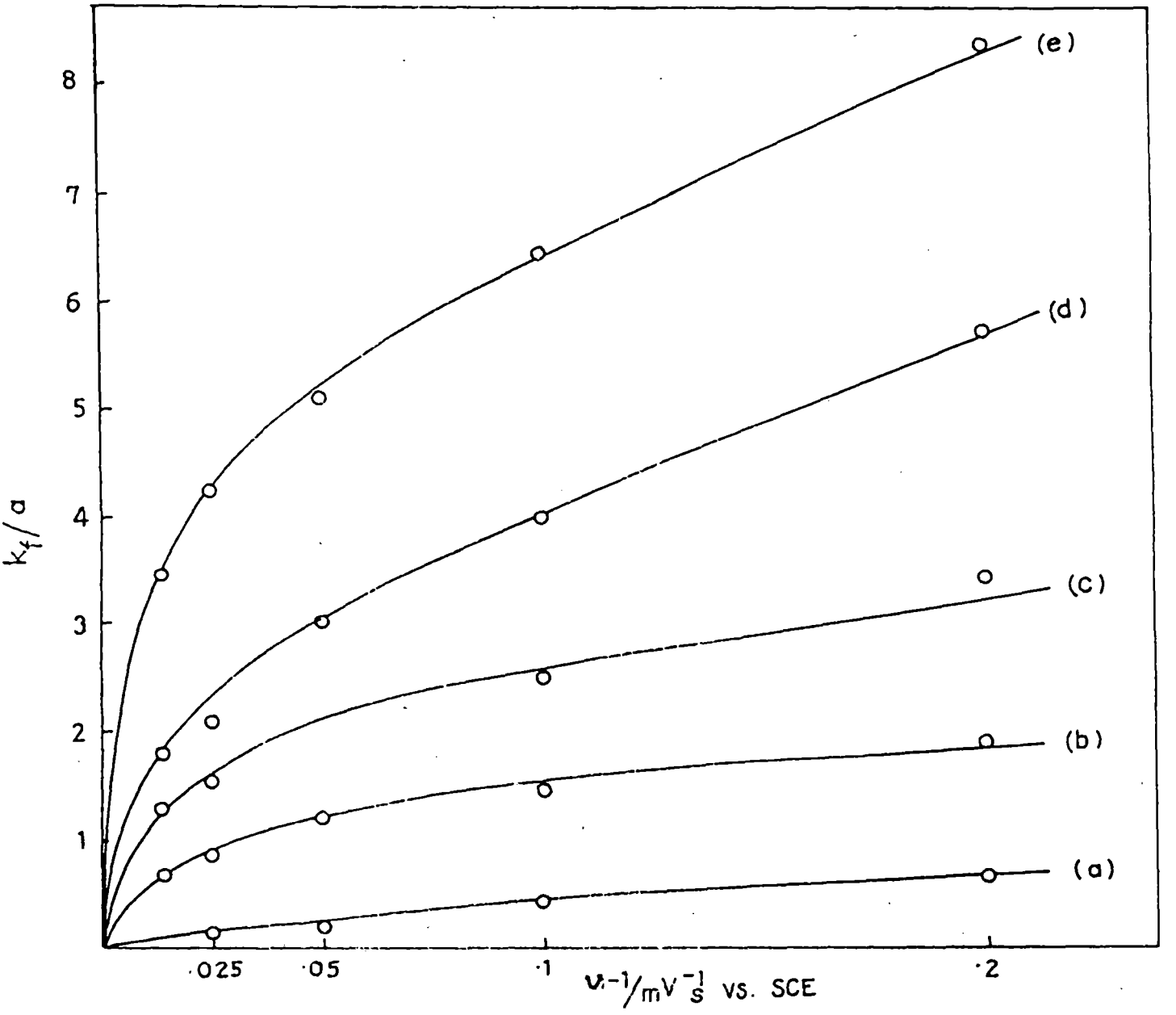

Fig. 87 : Plots of Kinetic paremeter, k_f/a, against 1/v for Azure A - Fe(III) system at various concentration of Fe^{3+} : (a-e) $2x10^{-4}$ $4x10^{-4}$, $4x10^{-4}$, $6x10^{-4}$, $8x10^{-4}$ and $1x10^{-3}$M.

considerable extent in the diffusion layer during the time period of a slower scan rate. Second order kinetics is probably followed and the situation is identical to one which occurred in intermolecular electron transfer of Cytrochrome C (139). Moreover, the initial slope of each curve (fig. 87) at infinite scan rates is proportional to the true pseudo-first order rate constant k_f^o,

$$k_f^o = (nF/RT)(\text{ initial slope }) .$$

Drawing tangents to the above curves at $1/v \longrightarrow 0$ yield values of k_f^o for each experiment. An alternative method of finding k_f^o is to calculate effective pseudo-first order rate constant k_f', from each k_f/a value at a given scan rate where,

$$k_f' = (F/RT).V.(k_f/a) \quad (\text{ Ref. 139})$$

Plotting k_f' as a function of 1/v and extrapolating to $1/v \longrightarrow 0$ one can evaluate the pseudo-first order rate constant, k_f^o, at infinite scan rate. This latter method seems to be more convenient and data for the five thiazine dyes are plotted in fig. 88-92. The nature of the plots are again similar for all the five dyes and also similar to those observed by Hill and Walton for intermolecular electron transfer in cytochrome C (139). Finally, k_f^o values at infinite scan rates and for varying

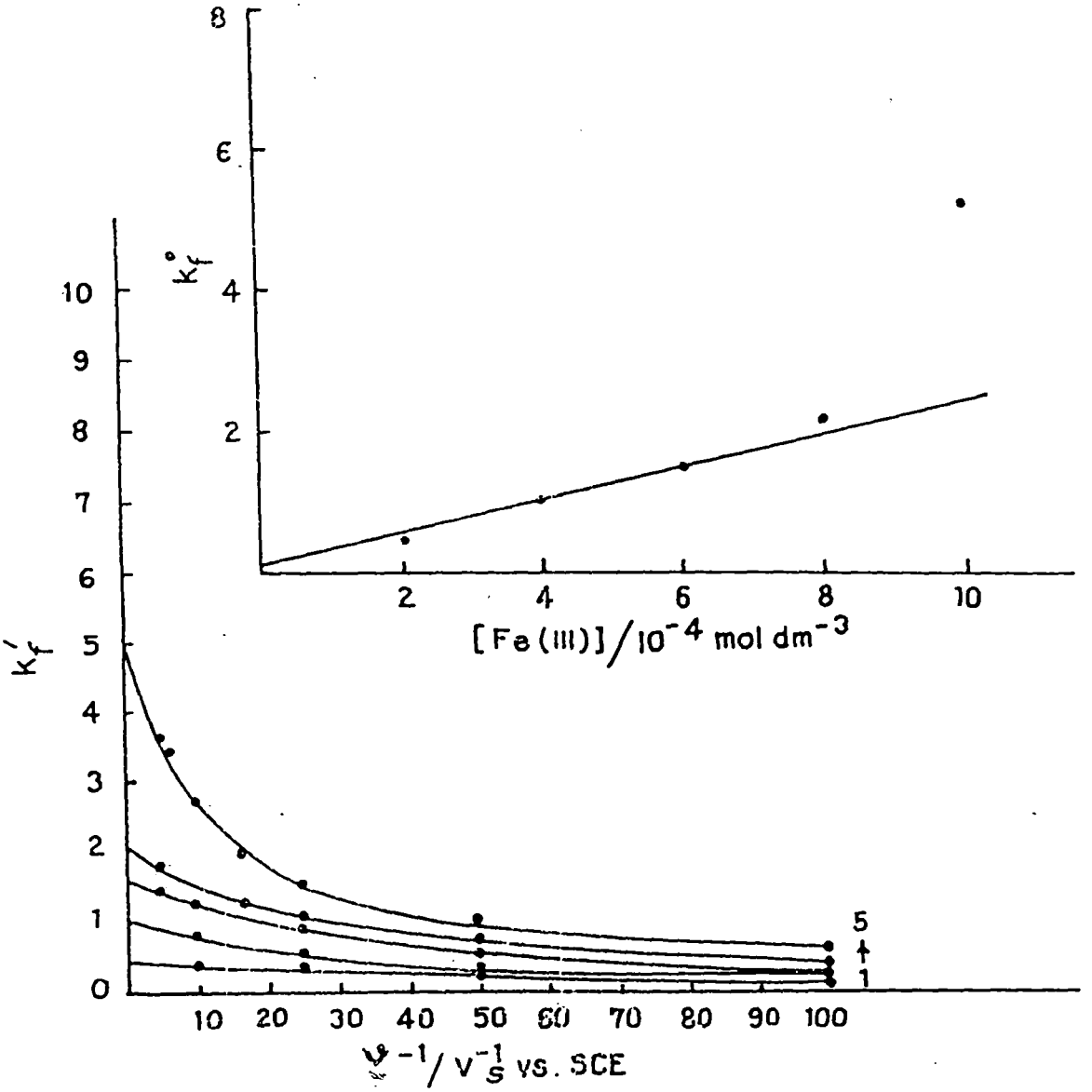

Fig. 88 : Effective pseudo - first order rate constant, k_f', as a function of reciprocal scan rate extrapolated to $1/v \to 0$ for Thionine with various concentration of Fe^{3+} (1-5) $2x10^{-4}$, $4x10^{-4}$, $6x10^{-4}$, $8x10^{-4}$ and $1x10^{-3}$M (lowerfig.) Pseudo - first order rate constant, k_f°, as a function of the concentrations of Fe^{3+} with the same system (upper fig.)

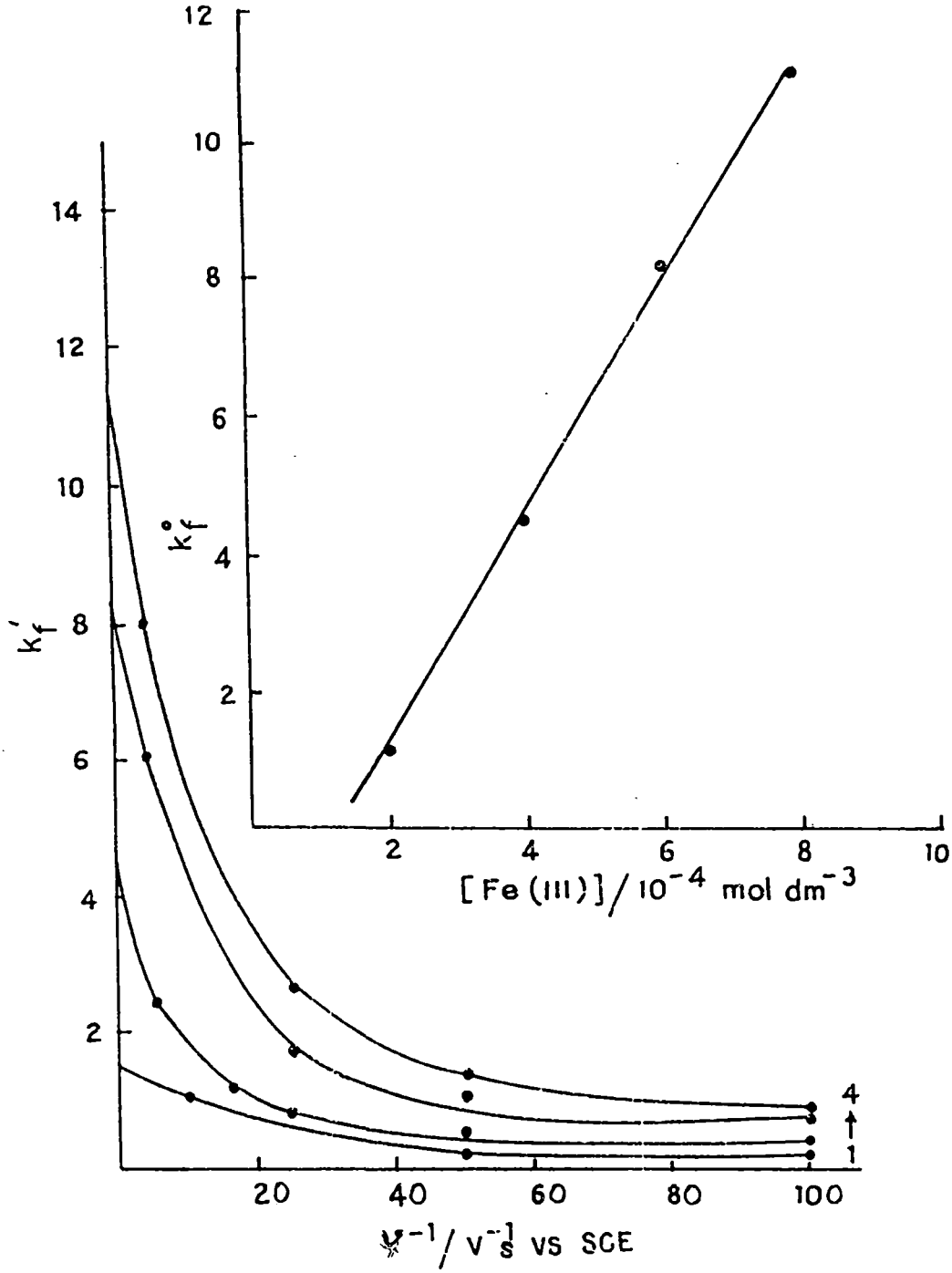

Fig. 89 : Effective pseudo - first order rate constant, k_f', as a function of reciprocal scan rate extrapolated to $1/v \rightarrow 0$ for Azure C with various concentration of Fe^{3+} : (1-4) : $2x10^{-4}$, $4x10^{-4}$, $6x10^{-4}$ $8x10^{-4}$M. (lower fig.). Pseudo - first order rate constant, k_f°, as a function of the concentration of Fe^{3+} with the same system (upper fig.)

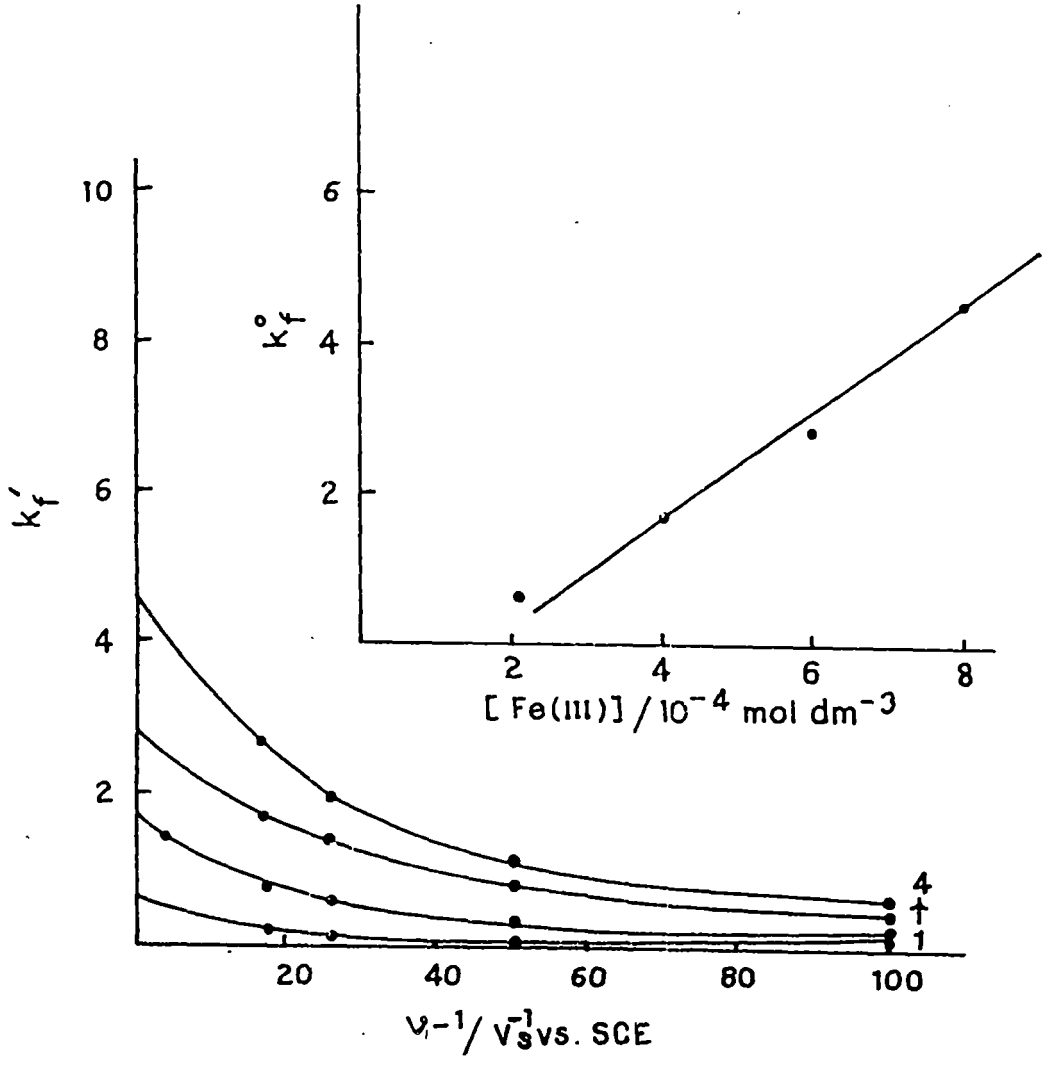

Fig. 90 : Effective pseudo - first order rate constant, k_f', as a function of reciprocal scan rate extrapolated to $1/v \rightarrow 0$, for Azure A with various concentration of Fe^{3+} : (1-4) $2x10^{-4}$, $4x10^{-4}$, $6x10^{-4}$ $8x10^{-4}$M. (Lower fig.). Pseudo first order rate constant, k_f°, as a function of the concentration of Fe^{3+} with the same system (upper fig.)

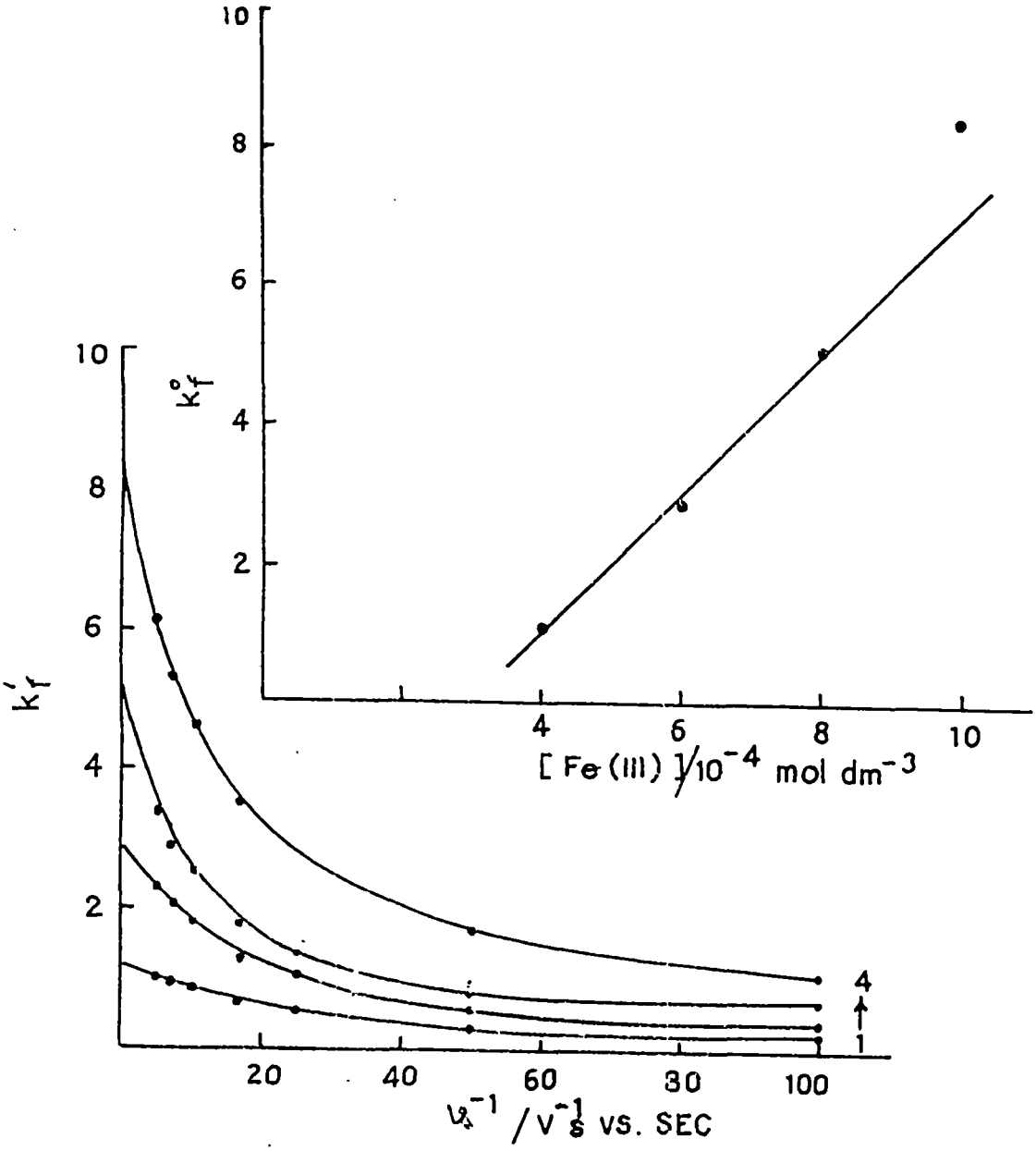

Fig. 91 : Effective pseudo - first order rate constant, k_f', as a function of reciprocal scan rate extrapolated to $1/v \rightarrow 0$, for Azure B with various concentration of Fe^{3+} : (1-4) $2x10^{-4}$, $4x10^{-4}$, $6x10^{-4}$ $8x10^{-4}$M. (Lower fig.). Pseudo first order rate constant, k_f°, as a function of the concentration of Fe^{3+} with the same system (upper fig.)

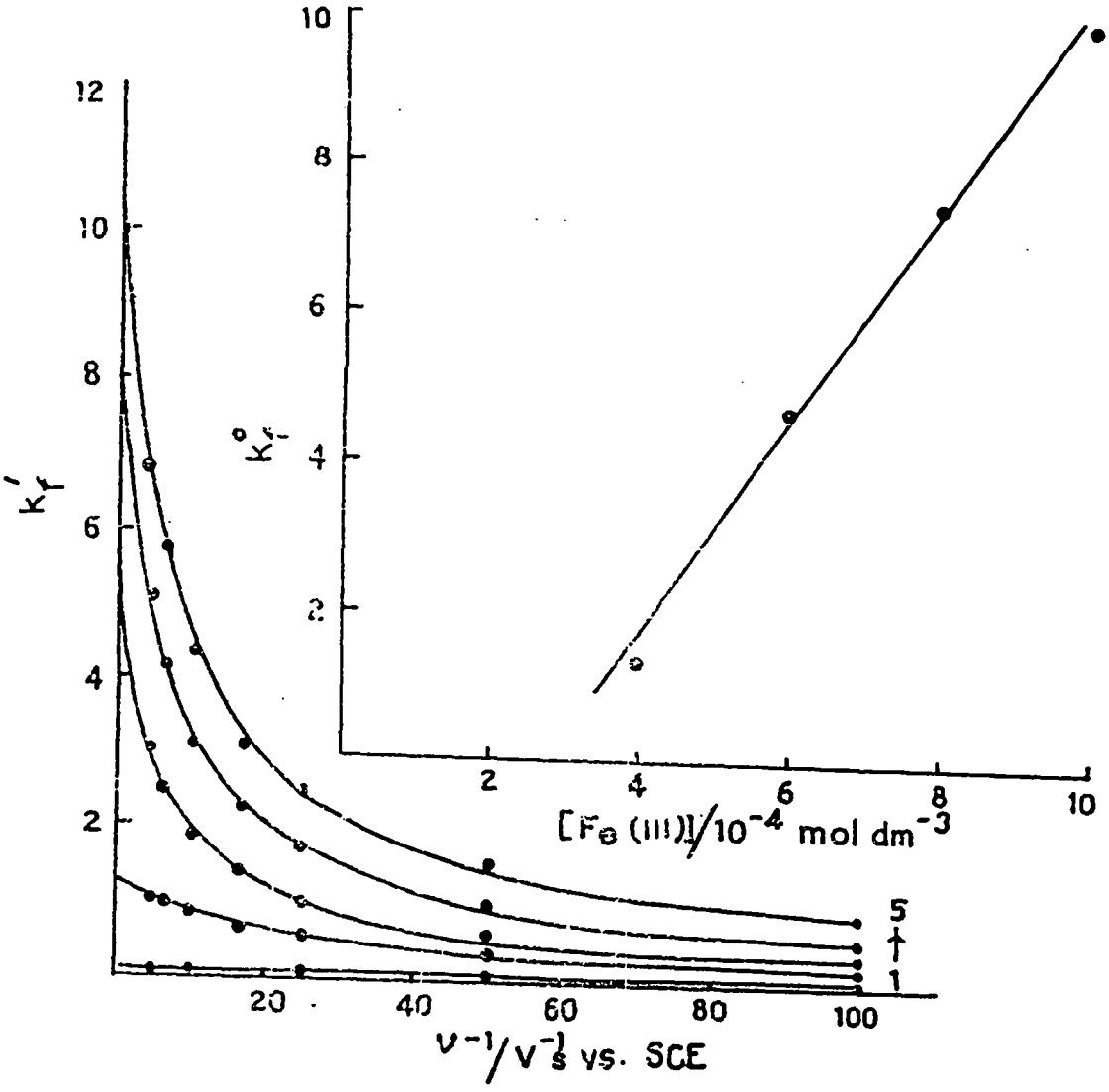

Fig. 92 : Effective pseudo - first order rate constant, k_f', as a function of reciprocal scan rate extrapolated to $1/v \rightarrow 0$, for Methylene Blue with various concentration of Fe^{3+} : (1-4) $2x10^{-4}$, $4x10^{-4}$ $6x10^{-4}$ and $8x10^{-4}$ M. (Lower fig.) . Pseudo - first order rate constant, k_f°, as a function of the concentration of Fe^{3+} with the same system (upper fig.).

concentrations of Fe(III), are plotted against the concentrations of Fe(III) ions in order to examine the second order rate constants, k_2's for the homogeneous reaction of Fe(III) with various leucodyes.

Table-23

Leucodyes	$k_2 \times 10^{-4}$/lit.mol^{-1}s^{-1}
Th	0.25
AzC	1.60
AzA	0.70
AzB	1.00
MB	1.40

These plots are linear indicating that the homogeneous reaction is first order with respect to Fe(III) ions and indeed the over all reaction is of second order (inset of fig. 88-92). However, a striking feature is that unlike Th, slopes of the plots for all other dyes decrease drastically at low Fe(III) concentrations (at $C_{Fe(III)} < 2.0 \times 10^{-4}$M for AzC, AzA and $C_{Fe(III)} < 4.0 \times 10^{-4}$M for AzB, MB), resulting in the deviation of the plots from linearity. This result suggests that at low Fe(III) concentrations the actual scheme of reaction should be

more complex than one shown in equation 40 and supports the hypothesis that the return of leucodyes to the corresponding thiazine dyes by Fe(III) ions occurs by two step process via the formation of semithiazine as an intermediate species. Conversion of semithiazines to the corresponding thiazine dyes may occur either by Fe(III) or through the dismutation equilibrium (as mentioned before) forming leuco dyes and the original dyes. The latter process is, however, more significant at low Fe(III) concentrations (138). Nevertheless, observed gradients of the straight lines are significant and the second order rate constants, k_2's derived from these data are depicted in Table 23. The table shows that k_2 value for thionine is 0.25×10^4 $lit.mol^{-1}s^{-1}$, which is the lowest among all the dyes used. Upon progressive alkylation of the dyes this value increases regularly with only exception for AzC which gives the highest value of 1.6×10^4 $lit.mol^{-1}s^{-1}$. Regular increase of k_2 with progressive alkylation of the dye molecule would indeed be expected from the electron donating nature of a methyl group. However, in the present systems, while the first methyl group brings about a six fold increase of the rate, the second one causes a two fold decrease and adding the third and the fourth has only a small effect (1.4 fold increase with each methyl). In fact, the leucodye with four methyl groups is oxidized more slowly than the dye with only one methyl group. It seems apparent that factors other than the electron donating effect of the methyl group are

involved. Substitution of hydrogens on the nitrogen of a dye molecule by methyl groups introduces hydrophobicity in the molecule as well. It has also been shown that hydrophobic environment in the presence of certain micelles delay back electron transfer in solution (137,142) while substitution with ionic or polar groups, for example disulfonated thionine, shows faster back electron transfer in PG cells (143,144). Thus, increased hydrophobicity due to alkylation of the present dyes may in turn slow down electron transfer reaction with Fe(III) ions in aqueous solution to some extent. These two mutually opposite effects of methyl group may thus be responsible for the observed variation of rates. It is also important to note in this context that the formal potential values ($E^{o'}$) for progressively methylated dyes are 0.205, 0.175, 0.207, 0.281 and 0.196 V (section 4.3.1.) respectively and the observed lowest value of $E^{o'}$ for AzC is consistent with the above results. However, one can infer from the foregoing result that, with the exception of AzC, the PG output will decrease continuously with alkyl substitution in the dye molecule. All previous reports showed that PG output for Fe(II)-MB cell is always less than that for Fe(II)-thionine cell. An earlier report of second order rate constants (measured by flash photolysis) ranged from 0.47×10^{3} $lit.mol^{-1}s^{-1}$ to 1.0×10^{3} $lit.mol^{-1}s^{-1}$ for various modified thiazine dyes (120).Ferreira and Harriman report a value of 9.0×10^{4} $lit.mol^{-1}s^{-1}$ for Fe(III)-thionine system by a similar

flash photolysis technique (138). On the other hand, with the help of an electrochemical method similar to one applied in the present study, Murthy and Srivastava estimated the value as 4.0×10^{5} lit.mol^{-1}s^{-1} for the reaction between Fe(III) ions and leucothionine (108). While a close comparison between data reported by different methods and under different conditions is not always valid, the general trend of the present result is satisfactory and specially the observed variation of k_2 due to progressive alkylation of dye molecule demonstrates the usefulness of a comparatively simpler electrochemical technique adopted here in the present investigation.

CHAPTER 5

INTERACTION OF DYES WITH MONTMORILLONITE AND ZEOLITE (ZSM-5) : SORPTION AND METACHROMASY

5.1 INTRODUCTION AND REVIEW OF THE PREVIOUS WORKS :

Interaction between organic matter and the clay minerals are important in many areas of geochemistry, agriculture and industry. Interests in the interaction of the dyes with clay minerals and zeolite are also stimulated in the present context due to the important role of such interactions in clay and zeolite modified electrodes as described in chapter 4. While sorption / ion exchange characteristics of these inorganic materials have direct implications on the physico-chemical nature of the electrodes, spectral changes observed in the above phenomena viz., metachromasy, gives some insight to the nature of bonding of dyes with the exchangers.

On the basis of crystal chemical approach, the correlation between the structures and the exchange properties of the clay minerals has been established from the important researches of Pauling (145), Bragg (146), Grauner (147), Brinddley (148), Hofmann (149), Marshal (150), Hendrics (151) and others (152-158). From these studies, clay minerals are recognised to consist essentially of two stuctural units. One is composed of two sheets of closely packed oxygens or hydroxyls in which aluminium or magnesium atoms are arranged in octahedral co-ordination so that they are equidistant from six oxygens or

hydroxyls, with aluminium in the octahedral position, only two-third of the possible positions are filled to balance the structure. The second unit is the tetrahedrally co-ordinated silica. A silicon atom being placed at the centre of a regular tetrahedron is equidistant from four oxygens or hydroxyls. The silica tetrahedra are joined together through oxygen to form a hexagonal network which is repeated indefinitely for forming a sheet composition $Si_4O_6(OH)_4$. The tips of all the tetrahedra are in the same direction and toward the centre of the unit. The structure of montmorillonite which is a member of the smectite class of minerals is shown in fig. 93. Montmorillonite is a 2:1 type or trimorphic layerd phyllosilicate in which the central octahedral aluminium sheet is surrounded by two tetrahedral silica sheets. Substitution by Fe^{+2}, Fe^{+3} or Mg^{+2} normally occurs in the octahedral position of aluminium (159).

The ion-exchange sorption of inorganic as well as organic ions are known to occur in clay minerals (160-164). The origin of the charge of the clay lattice are believed to be due to lattice imperfections, broken bonds at the edges of the particles and exposed structural hydroxyls in additon to the isomorphous substitution. The negative charge on the clay minerals is compensated by adsorption of cations. The counter-ions are held on the external surfaces of the aggregates and between the unit layers in clays which swell in aqueous suspension, whereas the sorption of counter-ions takes place onto the external surfaces

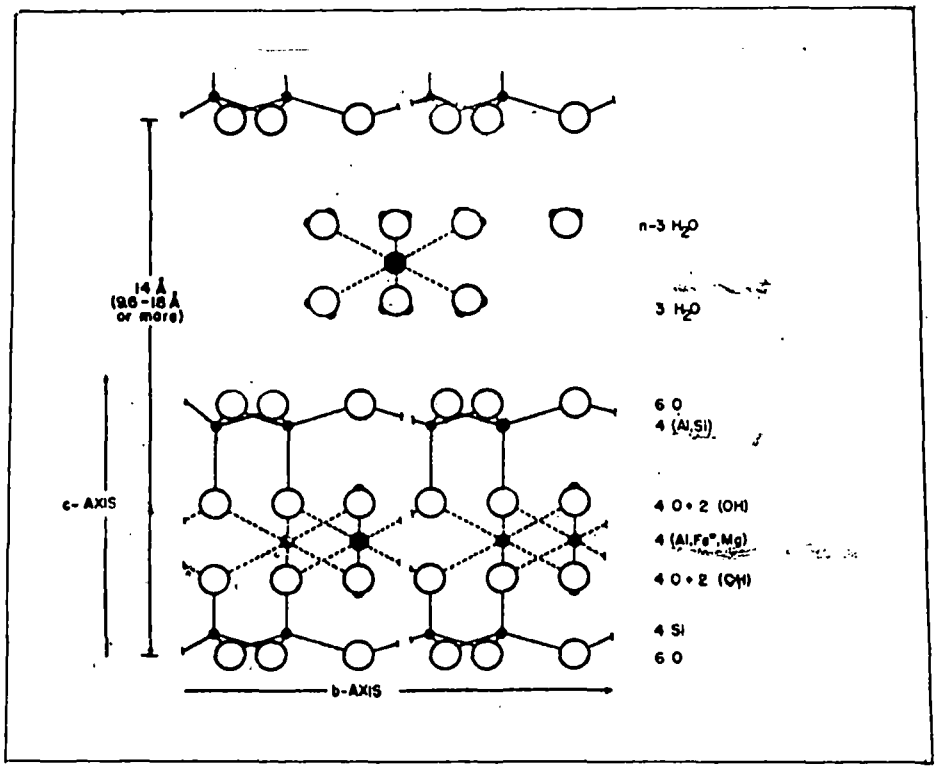

Fig. 93 : Structure of Montmorillonite

in non-swelling clays. In aqueous suspensions, some of these cations remain in a closet held stern layers, other diffuse away from the surface and thus form a diffused double layer. Provided that they are not fixed by engaging in strong, specific bonding with the clay or by being trapped between unit layers that have collapsed together irreversively (lattice collapse) the counter-ion can undergo ion exchange with other cations present in the system. The magnitude of the CEC of a clay depends largely on the type of the clay and to a lesser extent on the source of a particular sample. Systematic studies of cation exchange in pure clay minerals were carried out by Page and Baver (165), Bar and Tenderloo (166), Hendricks and Alexander (167), Schachtschabel (168), Mukherjee (169) and others. Most of the investigations were based on exchange reaction involving clay minerals with organic compounds have also been established by different scientists.

Adsorption studies of the dyes and large organic ions on different adsorbents, particularly on clays , have been made by many workers. Most of the studies were intended to measure the surface areas and CEC of the sorbents. As early as 1910 Mare (170) observed that dyes could be adsorbed by crystals up to a saturation value. Ramachandran and coworkers (171) measured the surface area by low temperature nitrogen adsorption of methylene blue, methyl violet and malacite green on the clay fraction of montmorillonite , kaolinite and illite. From the difference, the

actual extent of the area of contact was evaluated. This was found to be relatively small showing that while the surface is available for nitrogen adsorption, it is not accessible to dye molecules. The cation exchange capacity, found from methylene blue and methyl violet sorption on kaolinite and montmorillonite, was in close agreement with those found by standard methods. Brooks (172) adsorbed methylene blue on Na^{+} forms (Na^{22} and Na^{23}) of montmorillonite, kaolinite and silica sand flour and found the amount of dye adsorbed to be equivalent to the sodium displaced. The author believed that the dyes were adsorbed on the clay mineral surface through ion-exchange process. Plesch and Robertson (173) also proposed two distinct mechanisms to operate in sorption of dyes on surfaces of clay minerals; namely, the partly irreversible ion exchange and the fully reversible physical adsorption. Bergmann and O'Konski (42) reported that the adsorption of methylene blue on montmorillonite took place first through irreversible ion exchange mechanism and then by physical adsorption and verified the equation of Plesch and Robertson with their experimental results.

Ewingand Liu (174) estimated the cross-sectional areas of crystal violet and orange II assuming that the dye molecules were adsorbed flat on the surface of the clay minerals and they estimated the cross sectional area of crystal violet to be 160 A^{o}_{2} and 171A^{o}_{2} depending on whether the dye is adsorbed in the dehydrated or hydrated condition.

The surface area measured through dye adsorption, however, did not agree with those obtained by nitrogen adsorption in all cases. Kipling and Wilson (175) found discrepencies in specific surface areas of porous and non-porous active charcoal measured by methylene blue and nitrogen adsorption. Hofmann (176), on the basis of methylene blue and orange II adsorption on a wide variety of clays, showed that the surface area calculated was only 70% of the total surface area. Orr (177,178) found that the surface areas of two halloysite samples calculated by sorption of four dyes viz. malacite green oxalate, malacite green hydrocloride, amaranth and tetrazine, were apparently equal to 1/4 of the total surface. Similar discrepencies were also reported by Daran (179), Vander Grinter (180) and Bancelin (181) in their respective adsorption studies. Bancroff et al.(182) from adsorption of methylene blue on lead sulphate, Subrhamaya et al.(183) from crystal violet adsorption on glass and Doss and Singh (184) from thymol blue adsorption on active carbon, arrived at the similar unsatisfactory results.

Giles and coworkers (185) observed that the adsorption of basic dyes by silica from aqueous solution exceeded its monolayer coverage requirement. Association of the dye molecules in the adsorbed state has also been detected by electron micrography (186) that most of the dye molecules are associated in solution as micelles from 10 to 100 molecules units was reported by Lenhar and Smith (187,188), Vickerstaff and Lemin (189), Bergmann and

O'Konski (42), Mukherjee and Ghosh (35,190,191), Hertz et al. (192) and Hertz (193) also observed that dye molecules, of which the monovalent organocation are a sub-group, tend to aggregate into dimeric and polymeric species in aqueous solution. Kongonoviski (194) also observed the adsorption of dyes to take place through monolayer sorption of associated micelles. Brooks (172) advocated that the surface area and cation exchange capacity of the substrates, with methylene blue adsorption, could still be measured. To calculate CEC and surface areas he suggested addition of dye solution to a mineral suspension in small increaments till the equilibrium concentration was 1×10^{-6} M indicated by a slight blue colour of the supernatant.

Thi and Brindley (195) asserted that methylene blue can be used for the measurement of both suface areas and CEC of clay minerals such as montmorillonite. They attributed the cause of failure in measuring surface areas and exchange capacities by Faruki et al. (196) and Bodenheimer and Heller (197) to the insufficient replacement of Ca^{+2} ions by methylene blue from Ca-montmorillonite used in their studies. Using Na-clay instead of the Ca-clay these authors calculated the surface areas from the amount of methylene blue adsorbed when optimum flocculation occured. Fully exchanged values of methylene blue was used to calculate the CEC of montmorillonite. Methylene blue molecule was considered to possess approximately a rectangular volume of dimensions $17.0 \times 7.6 \times 3.25$ $\AA^3$. They believed that coating of clay

particles occured first and visualised a flat face-on orientation of methylene blue molecules (i.e. lying on the 17.0x7.6 $\overset{0}{A}^2$ face) for effective coverage of surfaces. Flat face-on orientation of the dye (i.e. 17.0x3.25 $\overset{0}{A}^2$) was assumed when full exchange takes place.

West, Carrol and Whitcomb (198) investigated systematically the adsorption characteristics of more than thirty dyes on photographic bromo-iodides and chloro-bromides suspensions in 70% aqueous gelatine solution in an attempt to correlate the sorption and optical sensitization. It was noticed in some cases that the dye adsorbed was very little at first but the rate of dye adsorption increased as more dye was adsorbed. They termed this as "co-operative adsorption". The intermolecular forces between the large dye molecules are so high that they polymerised when molecules came closer in the adsorbed state, giving rise to increased adsorption.

De and coworkers (199-205) made a series of studies on sorption of dyes onto clay minerals and their desorption from the clay-dye complexes by various inorganic and organic ions. They found Langmuir type of adsorption isotherms to operate in all cases. Surface area measurement, evaluation of CEC, determination of distribution coefficients and selectivity coefficient are the major part of their work. Narine and Guy (206) interacted thionine, methylene blue, new methylene blue, paraquat, diquat with bentonite in dilute aqueous systems. They noted that the dye

cations form aggregates on the clay surface and aggregation increases with ionic strength, raising the adsorption capacity by 25%. They also observed that changes in adsorption due to changes in temperature were small and the dyes were irreversibly bound by the clay matrix.

Yamagashi (207) recently studied the effect of alkyl chain length ($-CH_3$ to $C_{12}H_{29}$) for the adsorption of N-alkylated acridine orange cation on Na-montmorillonite. He observed that the length of the aliphatic tail had no appreciable effect on the binding constant and the rate of adsorption.

Zeolites are crystalline aluminosilicates with a great capacity of water and the ability to be completely hydrated and dehydrated without damage to the crystalline lattice. The intracrystalline architectured diversity of the natural zeolite minerals and their synthetic analouges and extensions results from the three dimensional network formed from conjoining SiO_4 and AlO_4 tetrahedral building blocks; the ensuing structure is an inorganic cross-linked and crystalline macromolecules. Fig. 94 illustrates the oxygen sharing, Al-O-Si Linkages in a two dimensional representation of the aluminosilicate zeolite structure (117).

The tetrahedral coordination of Si-O and Al-O (generally referred to as T-O) permits a variety of ringed structures to form, like the six T atom rings shown in fig. 94. These rings link to form the cage and the channel structures that give rise

to the molecular discriminatory nature of zeolite. In addition to showing the preliminary stages of the zeolite framework also displays two chemical features of the aluminosilicate zeolites that provide much of the chemical diversity of the system. For every Al atom in the lattice, with its AlO_2/SiO_2 stoichiometry, a fixed nagative charge results. These anionic sites are counter balanced by mobile cations typically alkali metal or alkaline earth metal cations, that easily ion exchange for other metal cations or organic cations of appropriately small dimensions.

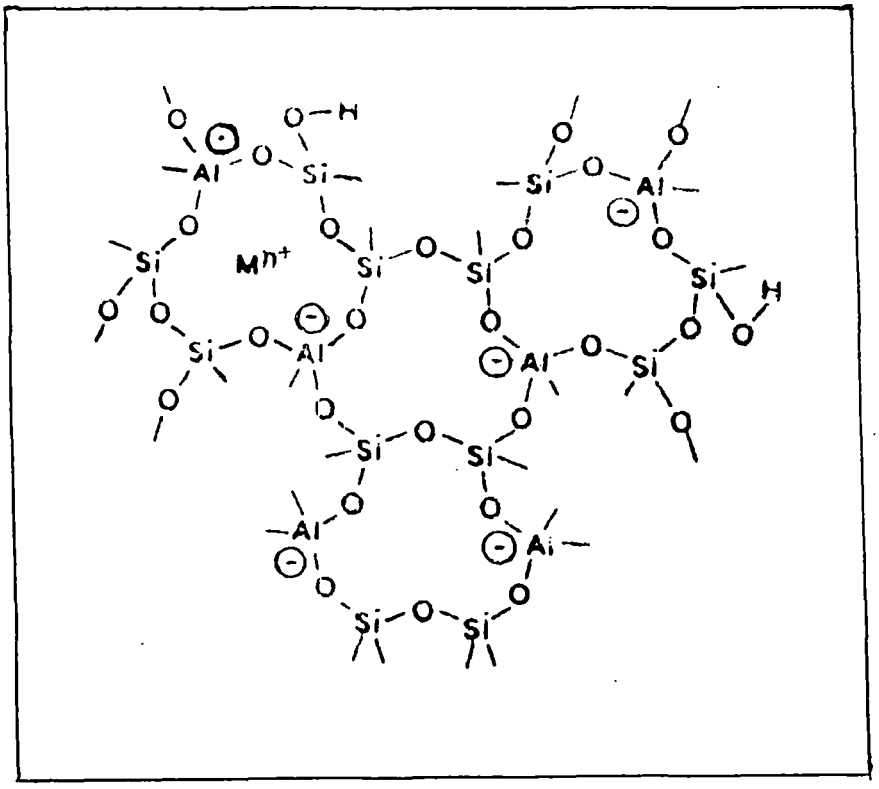

Fig. 94 : Structure of Zeolite

The second feature is the termination of bonding at the crystal faces with hydroxyl groups. Hydroxyls are the form in which protons are held in the zeolites and they are responsible for the strong acid nature of the aluminosilicate zeolite and their extensive use in acid catalysed reactions, not the least of which the cracking of petroleum. The incorporation of aluminium into the framework structure of the ZSM-5 type zeolite, which results in the occurence of acid sites, provide a good example of the progressive change from a zeolite silica polymorph, silicate 1 to a high silica zeolite, ZSM-5. The intracrystalline catalytic activity of zeolite Al-ZSM-5 is dominated by shape selective reactions which occur within its channel structure through the external surface, which is affected by the adsorption of bases. It is argued that the adsorption of cationic dyes such as methylkene blue by solid materials from aqueous solution is associated with the presence of acid sites and should provide a measure of their formation as a result of substitution on aluminium into the framework of silica polymorph (208,209,211).

METACHROMASY :

Adsorption of dyes by clay minerals often results in significant spectral changes specially in the electronic spectrum. The visible absorption spectrum is attributed to a

single electronic transition for each dye in the present investigation (chapter 3). The transition may be described interms of a single vibronic progression (chapter 3). Moreover it has been shown that the excitonic interaction results in splitting of dimer spectra into two band systems one at lower and the other at higher wavelengths of the corresponding monomer spectrum. However, the gradual replacement of the principal band (the so called α band) by a band with a shorter wavelength (the β band) as a result of interaction between dye molecules (dimer formation) or with due to the intercation of dye with inorganic exchangers (metachromasy) has been described in the literature in a qualitative manner in search of an insight knowledge regarding the type of intercation and bonding. In the present chapter a similar qualitative description of the metachromasy of the five thiazine dyes with montmorillonite are presented briefly.

Vadeneva observed metachromasy i.e. the appearance of a hypsochromatically shifted band in clay minerals (210) by studying adsorption of malacite green and brilliant green by montmorillonite and kaolinite. She concluded that formation of ionic bonds between clays and dye caused a bathochromic shift, while the intensification of the dipole bond was hypsochromic. A qualitative theory of metachromasy in solution was proposed by Schubert and Levine (37). They postulated that the metachromasy is produced as a result of selective and reversible binding within an anionic luster of a polymeric dye cation of highest

charge available.

Bergmann and O´Konski (42) described a spectroscopic study of methylene blue sorbed on montmorillonite. Spectral changes were found to follow changes in the amount of methylene blue sorbed on the clay surface. Due to the fact that these changes are similar to the spectral shifts accompanying dimerization and polymerization of methylene blue in aqueous solution these shifts were also attributed to dye-dye interaction on the surface of montmorillonite . According to these authors the dimer is held together by london dispersion forces and hydrophobic bonding.

Most researches on adsorption of organics by clays have focussed on smectite (212-215). Smectite clays have high adsorption capacities and generally form stable colloidal suspensions that can be investigated conveniently by various techniques suitable for suspensions. The high adsorption capacity make these clay-organics suitable for various thermal analysis investigations also.

The sorption of methylene blue by clay minerals was extensively applied by clay scientists in the determination of ion exchange capacity, surface area and for differentiation between various clay minerals. Since the publication of the paper by Bergmann and O´Konski (42) new knowledge has been gained, mainly from IR spectroscopy, on the mechanism of sorption of organic molecules by montmorollonite and on the nature of bonding occuring in the interlayer space (216).

The influence of solvent and concentration of aqueous solution on the spectrum of methylene blue was studied by Michaelis and coworkers. They found that Beer's law is obeyed in alcoholic solution but molar absorption depends on the concentration of the dye in aqueous solution. In alcoholic solution methylene blue shows a sharp and high peak with a maximum at 650 nm, due to $\pi-\pi^*$ transition (α band) (216). A shoulder at 590 nm is referred to as the β band. In very dilute aqueous solution the α band is displaced to 660 nm . As the concentration of methylene blue increases the α band intensity decreases and that of the β band increases considerably. Michealis states that the α band is the characteristics of monomeric cation and correspond to an electric oscillation along the X-axis of the molecule. The β band is the characteristics of the dimer and corresponds to an oscillator in the Y direction. Bergmann and O'Konski believe that β band is a transition moment which lies also along the long axis of the molecule but is perturbed due to an interaction between transition moments of the monomer units.

Schubert and Levine (211) differentiated between three bands α, β and γ at 665, 610 and 570 nm respectively. The γ band sometimes referred to as the "metachromatic band" is characteristics of polymeric cation. It is sometimes diffused and variable indicating that the observed peak is an envalope of overlapping bands (217). According to Schubert and Levine (211)

dimerization and polymerization lead to metachromasy due to interaction of some of the π electrons in level N/2, the most loosely bound electrons being responsible for the α band, and during polymerization a constraint is imposed.

Yariv and Lurie (216) studied the metachromasy of methylene blue in montmorillonite in terms of the knowledge about colloidal properties of clay suspensions and the mechanism of the peptization, aggregation and flocculation. They concluded that the metachromasy of methylene blue in montmorillonite is not connected with aggregation of the organic dye, but with the interactions of the oxygen sheet of silicate layer with the organic dye molecule (216). The intensity of the absorption bands of the sorbed methylene blue depends on the colloidal properties of the suspension. The effects are more the clay is peptized and less after coagulation. Three different modes of sorption of methylene blue were identified (a) hydrated form at the edges (b) metachromatic form almost to the oxygen sheet of the silicates and (c) possibly protonated form . Forms (a) and (c) are the first stages to occur during the sorption. The sorption takes place by a cation exchange mechanism.

Yamagishi and Soma (218) studied the adsorption of N-alkylated Acridine Orange (AO) by Na-montmorillonite. They showed that adsorption of the cationic dyes which belong to the AO family also results in metachromasy. They considerd the clay minerals as a poly electrolyte and believed that the interaction

between the negatively charged mineral and the dye cation is a pure electrostatic attraction and that metachromasy resulted from the electronic interaction between neighbouring adsorbed cations.

The idea of π interactions between the aluminosilicate layer and the aromatic entity was later supported comparing the adsorption of dibenzotropone and dibenzosuberone by montmorillonite (219). Only in the first molecule is aromacity induced, and its adsorption by montmorillonite results in π interactions between the organic molecule and the clay mineral. In rhodamine 6G the phenyl ring is sterically constrained to be roughly perpendicular to the planar xanthene group (220). Owing to this steric effect, π interactions between thr organic dye cation and the aluminosilicate layer can not occur. Thus no metachromasy is observed when rhodamine 6G penetrates into interlayer space of montmorillonite. It may therefore be concluded that metachromasy of cationic dyes in montmorillonite suspensions is expected only if there is no steric hindrance and when π interactions may occur between the aromatic ring and the oxygen plane of the aluminosilicate layer.

Grauer coworkers studied the adsorption of pyronine Y (PY) on montmorillonite to show that in the absence of the steric hindrance, π interactions between the dye cation and the aluminosilicate layer do occur (221). They showed that the adsorption of PY by montmorillonite results in metachromasy, namely a pronounced β band appears. In the presence of small

amount of clay (or a high degree of formal saturation) soluble PY contributes to the adsorption spectrum and the spectrum shows a high intensity of band α at 545 nm. with increasing clay concentrations (or decreasing formal degree of saturation) no PY remains in the aqueous phase and the β band increases. Adsorbed PY shows a bathochromic shift of α to 550 nm. The intensity of the shifted α band increases with the increase of clay concentration. They also showed the effect of clay concentrations in the suspension on the location of bands α and β in the absorption spectrum of the dye. From these spectroscopic studies they deduced the conclusions that (i) metachromasy in montmorillonite takes place even at very dilute solutions of the dye, which are not shown in the absence of the clay (ii) metachromasy in montmorillonite is observed at a very low formal degree of saturation, namely its occurance does not depend on the surface concentration of the dye (221).

Metachromasy in montmorillonite is attributed to the interaction of the lone pair electrons of the surface oxygens with the π electrons of the dye. This kind of interaction may occur only with clays having a tetrahedral substitution of Si by Al (222). Grauer and coworkers (221) compared the behaviour of laponite to that of montmorillonite and showed that the process which gives rise to metachromasy in laponite systems differs from that occuring in montmorillonite systems. In montmorillonite suspensions metachromasy occurs even with very low degree of

saturation, whereas in laponite suspensions metachromasy occur only when the degree of saturation is about the same as the cation exchange capacity of this mineral. They concluded that in the laponite system metachromasy is associated with the dimerization of the dye cation on the surface of this mineral. Cenens (223,224) coworkers also agreed with the above explanation of metachromasy in laponite.

5.2 EXPERIMENTAL :

The electroanalytical behaviour of the montmorillonite and ZSM-5 in the modified electrode makes it imperative for studying their sorption characteristics as an adsorbent.

various characteristics of the dyes, their structure and method of purification are presented in chapter 3. The characteristics of montmorillonite and ZSM-5 used in the present study are given below :

Sample	Description	CEC	Source
Montmorillonite	Light grey powder	80*	Evans medical Ltd. Liverpool England.
ZSM-5	White powder	47 (ref.208)	Dr.T.D.Smith Monas University Australia

* Determined by $BaCl_2$-$Ba(OH)_2$ method.

The clay fractions of montmorillonite clay minerals having size less than 2 mμ were isolated by the usual method of dispersion and sedimentation. The fraction thus collected were treated several times with dilute HCl, and after removal of the acid, warmed with 6% H_2O_2 in water bath to remove trace of any organic matter present. Excess H_2O_2 was decomposed by heating the samples in water bath. The iron present in the clay minerals was then removed by treating the clay samples with sodium metabisulphite and dithionate in acetate buffer solution at $60^{\circ}C$ followed by centrifugation, washing etc. as recommended by Bromfield (225). Finally the clay residues were washed to dispersion and dialysed. The clay suspension was then converted into the Na-form by stirring an approximately 2% suspension of the clay minerals with ion exchange resin (Dowex 50w x 80) in Na-form for about 4 hours. Na-clay ($_PH=7$) thus formed was used for the study. ZSM-5 sample, as received from the source, was used for the preparation of suspension.

Preparation of the suspension for adsorption study :

A certain amount of montmorillonite (7.4 g/lit.) and ZSM-5 (0.248 g/lit.) suspension were taken with the varying amount of dye solutions ($5x10^{-5}M$) and the final volume was made 20 ml by adding required amount of distilled water. ZSM-5 suspensions were found unstable above that concentration. The

suspensions (dye-mont. and dye-ZSM-5) were then shaken for 6 hours and kept at rest overnight for attaining the exchange equilibrium. The resulting exchanged residues were then cetrifugated (10,000 rpm) for 10 minutes and the supernatant solutions were analysed spectrophotometrically. From the differences between the initial concentration and the equilibrium concentration, the amount adsorbed was determined. The entire experiment was carried out at room temperature ($25\pm1^{0}C$)

Metachromasy :

A series of clay-dye suspensions with varying clay concentration (0.3×10^{-3} to 1.5×10^{-3} wt%) were prepared, keeping the concentration of the dyes in each sample at a fixed value of 9×10^{-6}M. The spectra of the clay-dye suspensions (montmorillonite) were recorded within 2 hours of preparation at room temperature ($25\pm1^{0}C$) using Shimadzu UV-240 model, in the range of 800-400 nm. The optical path length of the cell used was 1.0 cm.

5.3. RESULTS AND DISCUSSION :

5.3.1 Studies on Sorption :

The adsorption isotherm and the corresponding reciprocal

Langmuir plots of the dyes on montmorillonite and ZSM-5 are shown in the figs. 95-100. The adsorption isotherms are of H-type i.e., of high affinity class of Giles and coworkers (226) and is indicative of species adsorbed flat on the surface. and H-type curve is a special case of the L-type, caused by a very strong solute/substrate interaction.

The adsorption data are seen to fit the linear form of the Langmuir adsorption equation. Accordingly the plot of C/x vs C, where C is the equilibrium concentration of the dye and x is the amount adsorbed in mmol per 100 g of montmorillonite or ZSM-5 yields a good straight line (figs. 95-100). From the slope of the line, the value of x_m (the amount required to form a complete monolayer) is calculated in both the cases. The values are given in the table 24.

Table-24

Dye	Montmorillonite		ZSM-5	
	x_m (mmol/100g)	$kx10^{-5}$	x_m (mmol/100g)	$kx10^{-5}$
Th	93	4.6	44	3.1
AzC	94	5.0	42	3.7
AzA	95	5.3	42	3.9
AzB	100	6.5	43	4.4
MB	96	5.9	40	4.1

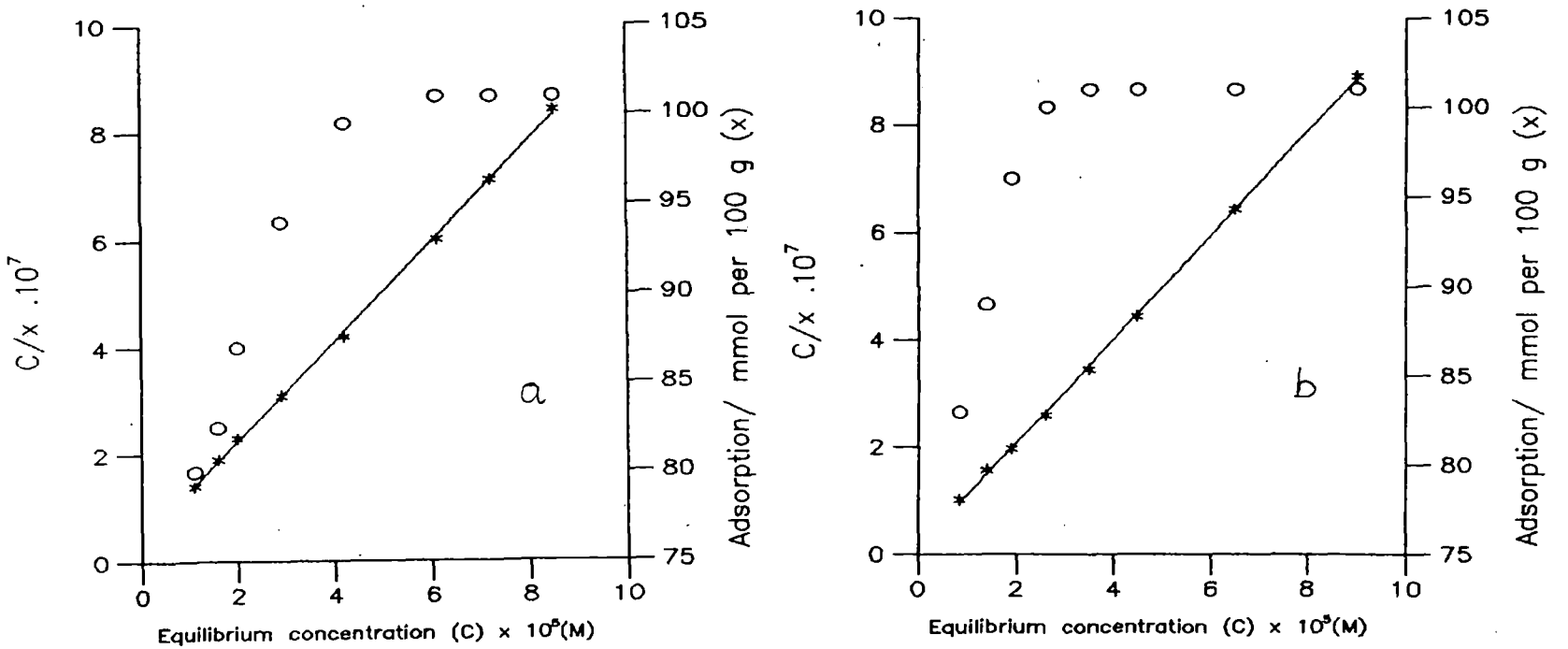

Fig. 95 : Adsorption isotherm and Langmuir plot of (a) Thionine and (b) Azure A in the presence of Montmorillonite.

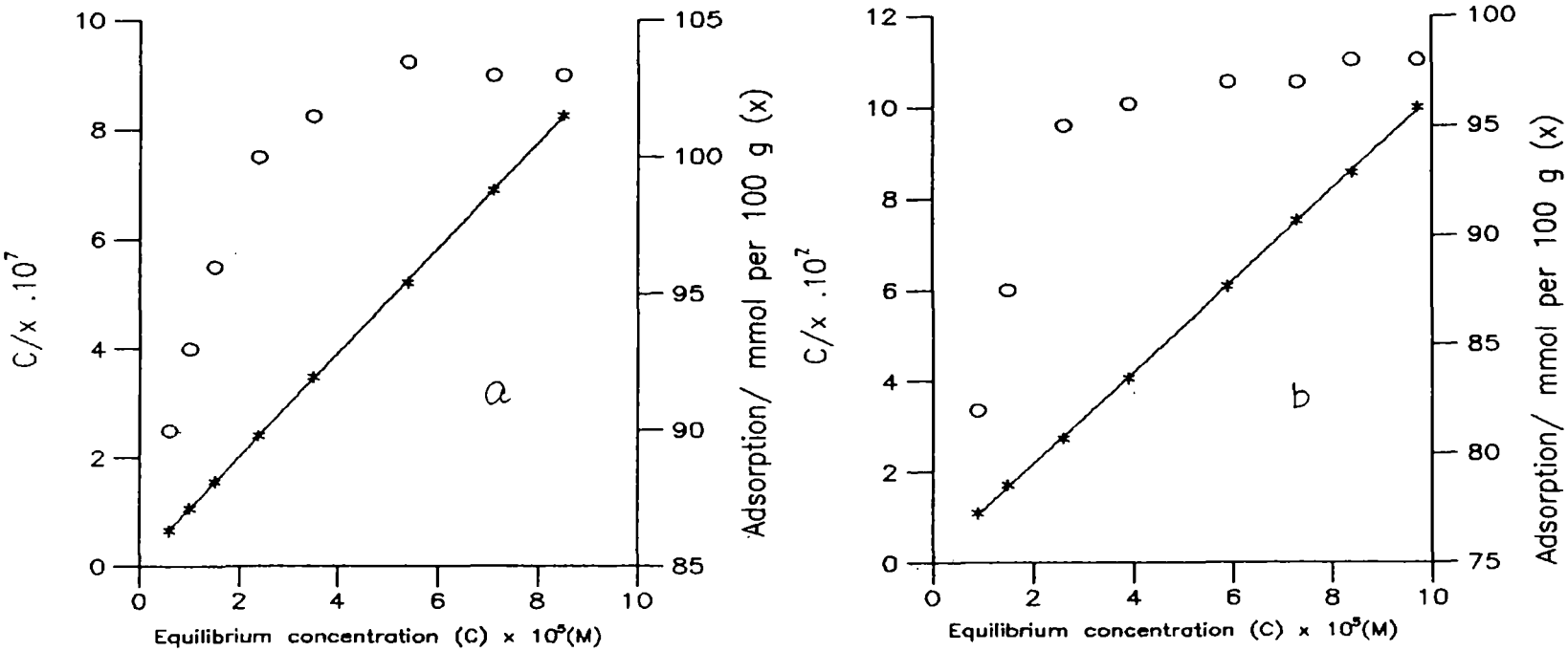

Fig. 96 : Adsorption isotherm and Languir plot of (a) Methylene Blue and (b) Azure C in the presence of Montmorillonite.

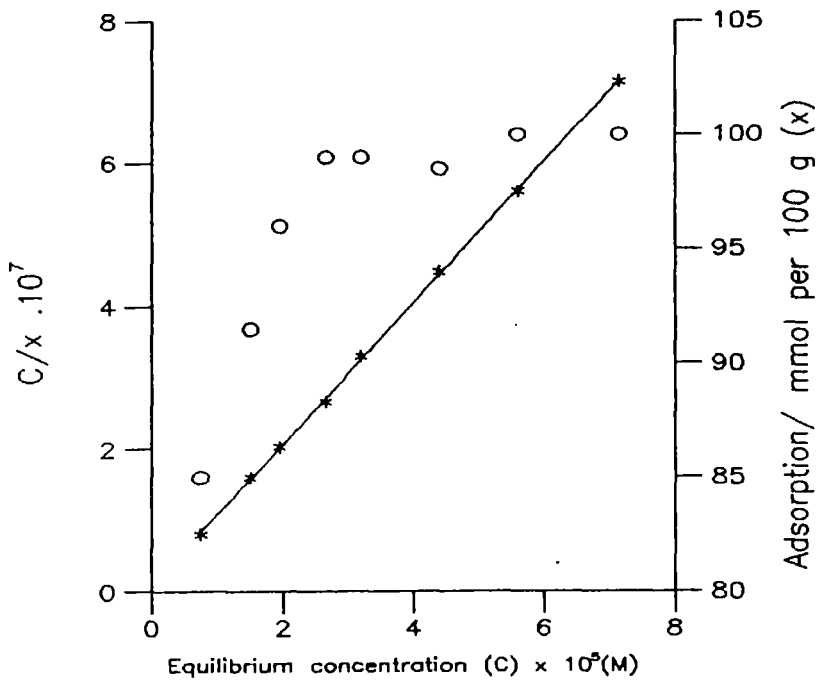

Fig. 97 : Adsorption isotherm and Langmuir plot of Azure B in the presence of Montmorillonite.

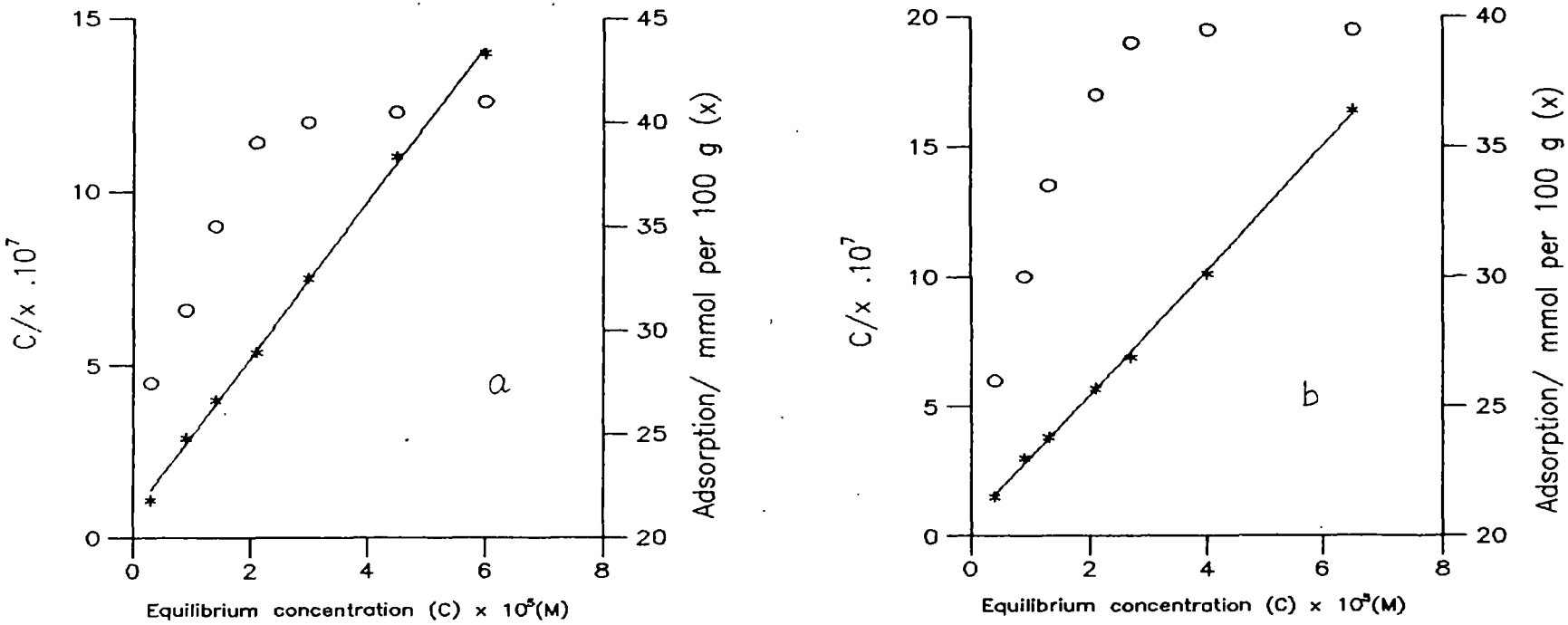

Fig. 98 : Adsorption isotherm and Langmuir plot of (a) Thionine and (b) Azure C in the presence of ZSM-5.

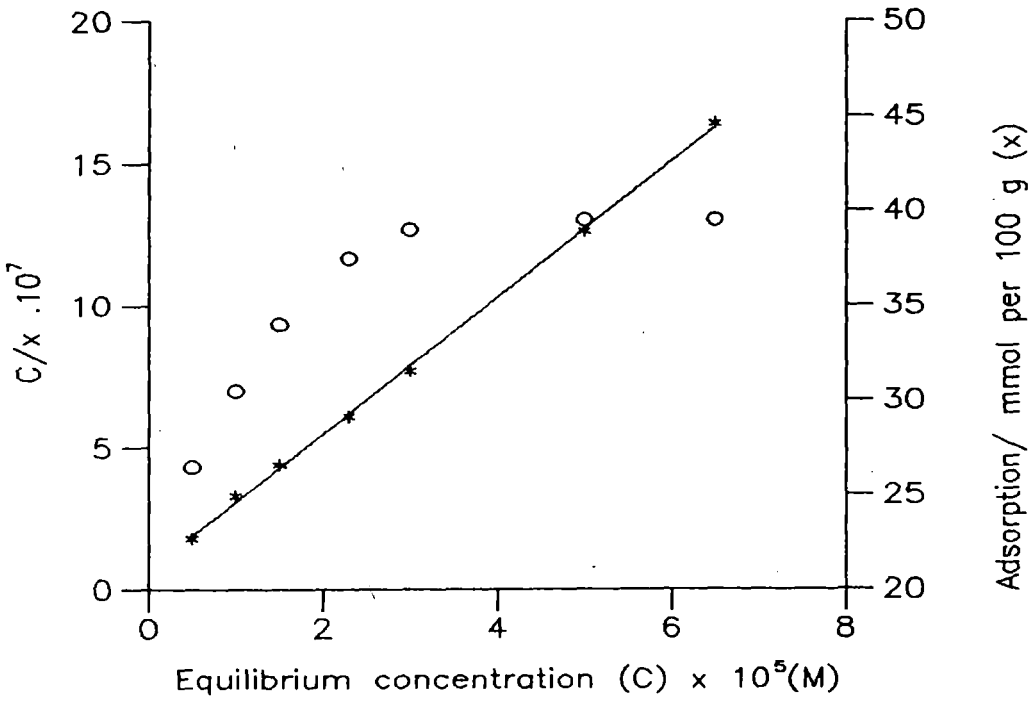

Fig. 99 : Adsorption isotherm and Langmuir plot of Azure A in the presence of ZSM - 5.

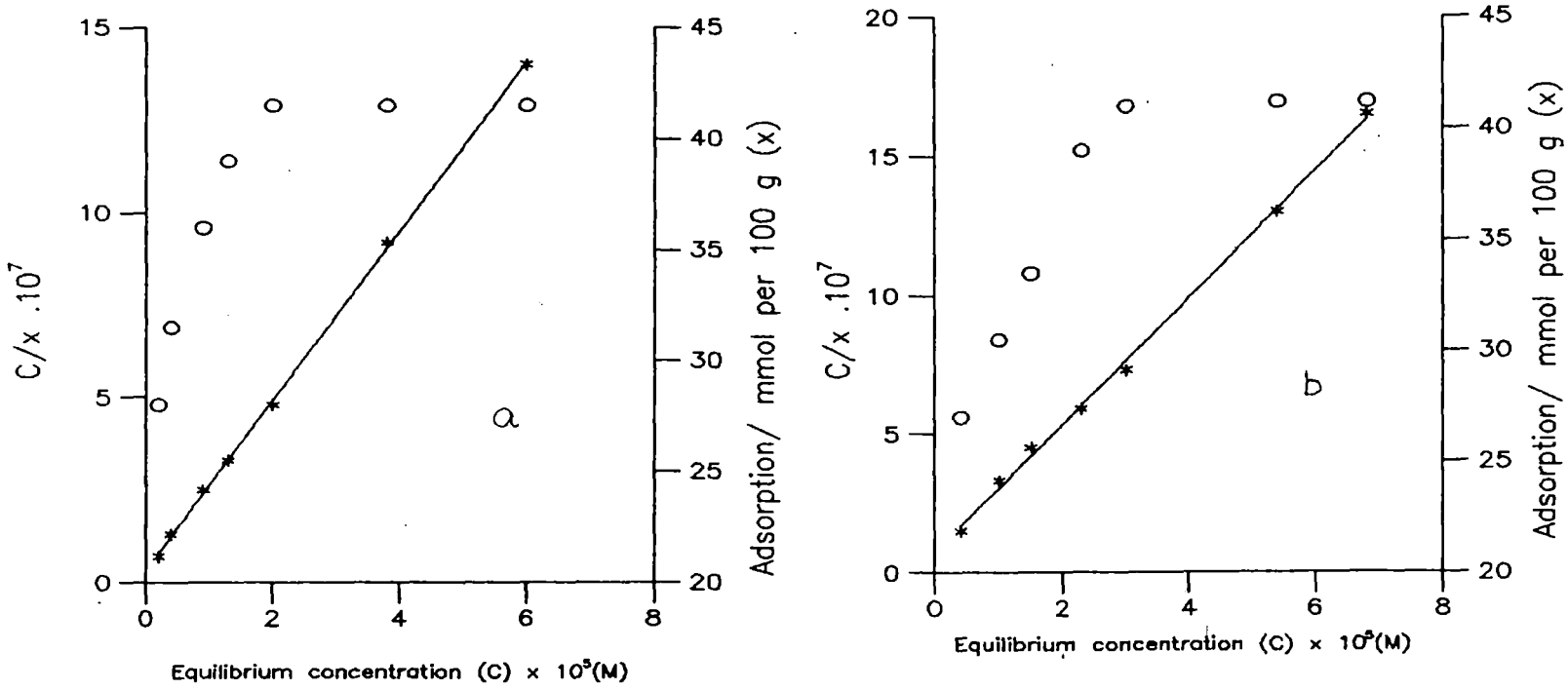

Fig.100 : Adsorption isotherm and Langmuir plot of (a) Azure B and (b) Methylene Blue in the presence of ZSM - 5.

There is a marked difference in the maximum amount dye adsorbed by montmorillonite and ZSM-5. In case of montmorillonite the value is high than that of ZSM-5. It is expected as the CEC of montmorillonite (80 mmol/100 g) is much higher than ZSM-5 (47 mmol/100 g) (208). Moreover, some dye molecules may enter into the interlayer space of the montmorillonite when the dye concentration in the suspension is increased. The possibility of entering the dye molecules into the interlayer space is evident from the metachromasy of the dyes in the presnce of montmorillonite (see section 5.3.2). But in the case of ZSM-5 the orientation of the dye molecules into the interlayer lattice is not possible as the dimension of the channels are not sufficient to accommodate the dye molecules having approximately a rectangular volume of 17.0x7.6x3.25 $\AA^3$. The maximum amount of dye molecules adsorbed onto the montmorillonite exceeds the CEC which may be explained by assuming multilayer formation of the adsorbed dye molecules due to dye-dye interaction and sorption of aggregated cations (42). Intercalation of dye molecules may also be taken into account for the sorption beyond CEC. A similar observation was also made by De and coworkers (227) in their work on methylene blue, crystal violet and malachite green. In the case of ZSM-5 the maximum amount of dye molecules adsorbed for the formation of complete monolayer is very close to its CEC (47 mmol/100 g). It indicates that multilayer formation and the sorption of aggregated dye cations is little in the case of

ZSM-5. Moreover, the strength of bonding of the dyes with ZSM-5 is probably weaker than that with montmorillonite. This is consistent with the observed electrochemical behaviour of the modified electrode where the cathodic current output was greater than that of montmorillonite modified electrode (table 21-22). In both the cases of montmorillonite and ZSM-5 the maximum amount of dye molecules adsorbed for the formation of monolayer onto the surfaces do not vary widely from dye to dye (table 24). The slight differences observed may be attributed to the structure, the mode of orientation and the hydrophobicity of the individual dye molecules. It is believed that the adsorption in the case of montmorillonite is mostly due to electrostatic and Vander waals forces up to the cation exchange capacity and due solely to Vander waals forces beyond it.

The values of the equilibrium constant (Langmuir bonding constants) of the dyes are calculated from the linear plots (Figs. 95-100) are given in table 24 .It should be pointed out that when adsorption is in excess of CEC due to sorption of aggregated dye species, the original meaning of the calculated values of x_m and the equilibrium constants is somewhat altered. Nevertheless, the latter parameter still gives some idea about the relative bonding strengths of adsorbents sorbed onto a particular substrate. It is seen from the table 24 that the variation of the values of equilibrium constants maintain a similar order in both the cases i.e.,the value increases from Th

to AzB and then decreases in MB and the values observed in montmorillonite and ZSM-5 for an individual dye are very close to each other. It is to be mentioned that the dimerization constants of Th, AzC, AzA, AzB and MB in aqueous medium are determined as 1.76×10^3, 2.35×10^3, 3.38×10^3, 6.25×10^3, and 3.68×10^3 lit mol^{-1} respectively at 30^0C (section 3.3.1). It is thus expected that when the sorption takes place from their solutions, AzB should be sorbed with larger fraction of the aggregates than that of other form of dyes. But the amount of maximum adsorption does not follow the order. It seems apparent that steric hindrance, hydrophobicity and the specific orientation of the dye molecules on the surfaces are operative simultaneously.

5.3.2. Studies on Metachromasy :

The spectrum of the dilute aqueous solutions (without clay) is shown in figs. 101-103. The prominent band at higher wavelength (α band) and the shoulder at lower wavelength (β band) of the dyes are recorded in table 25 .In case of AzC and AzA no shoulder appears in the spectrum in this dilution.

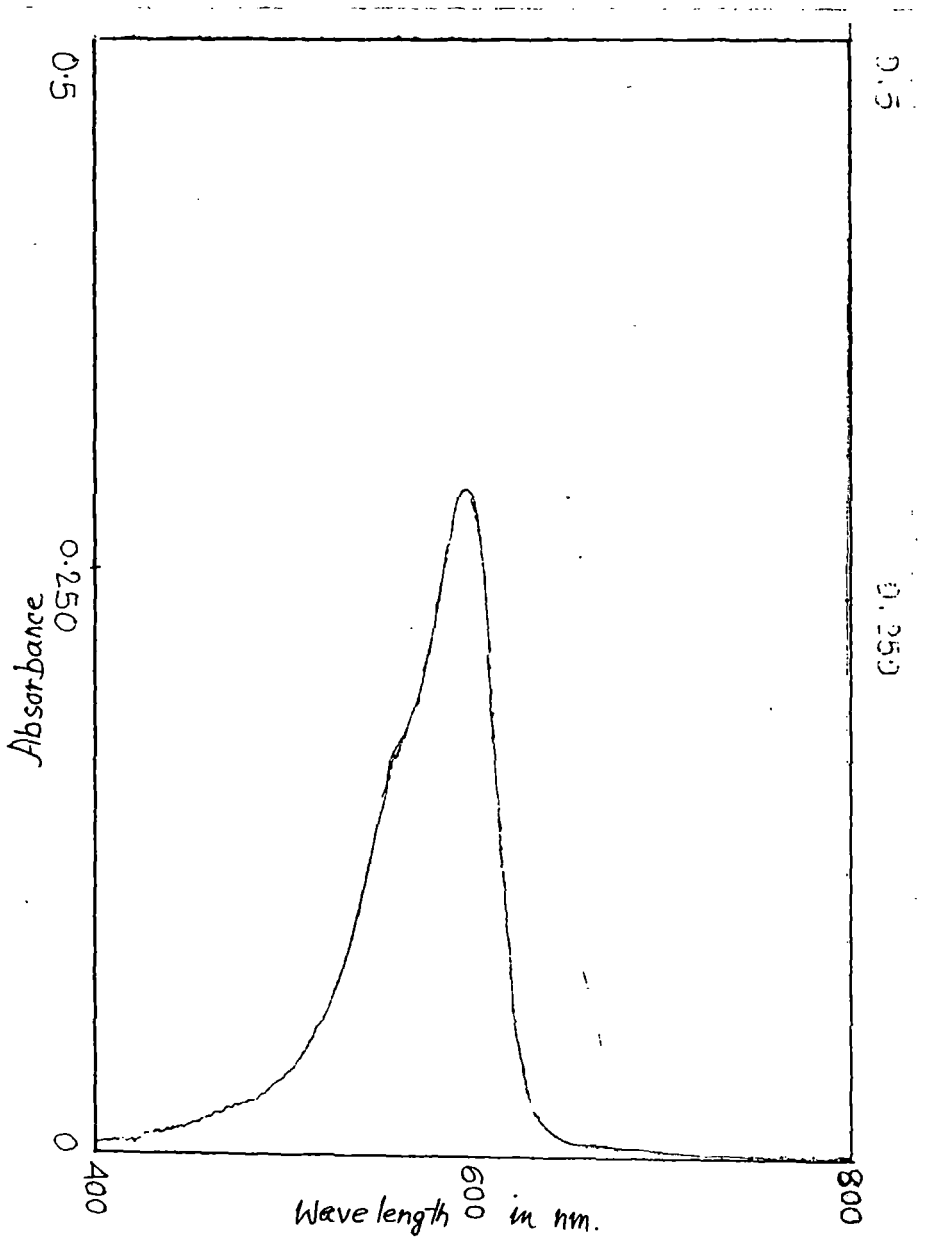

Fig. 101 : Visible absorption spectra of Thionine ($5x10^{-6}$M) in the absence of clay (montmorillonite)

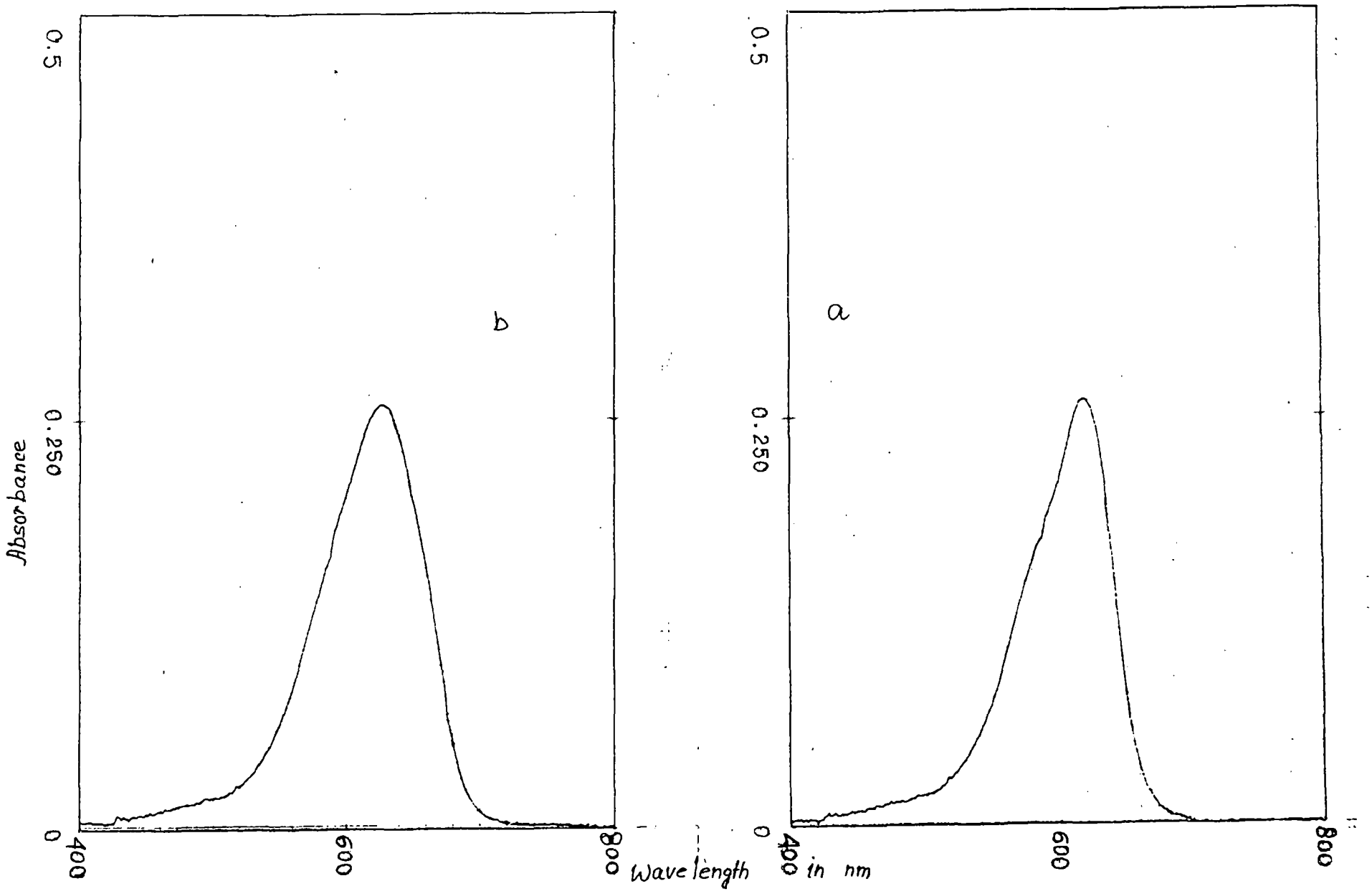

Fig. 102 : Visible adsorption spectra of (a) Azure C ($5x10^{-6}$M) and (b) Azure A ($5x10^{-6}$M) in the absence of clay (Montmorillonite).

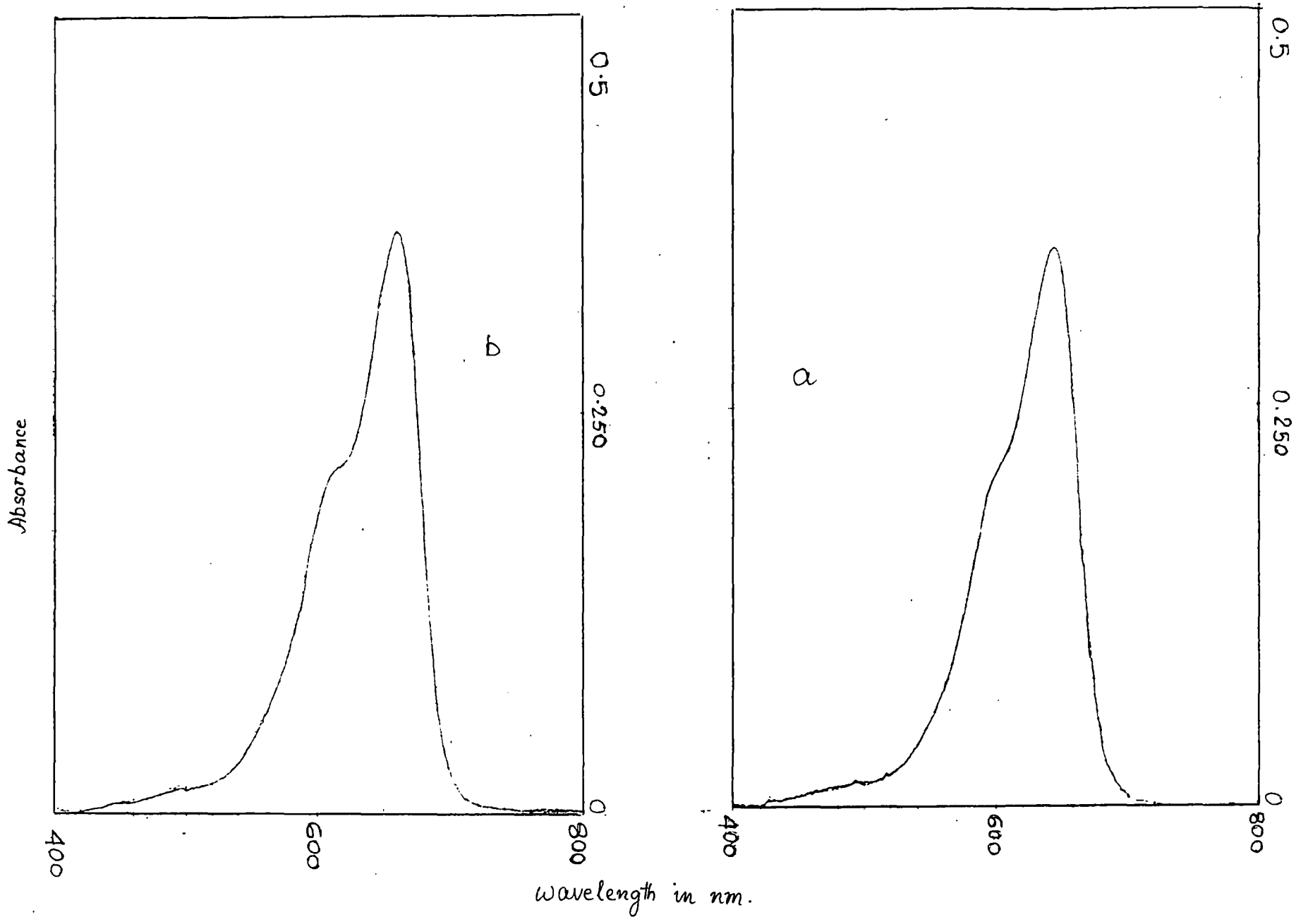

Fig. 103 : Visible Adsorption spectra of (a) Azure B ($5x10^{-6}M$) and (b) Methylene Blue ($5x10^{-6}M$) in the absence of clay (Montmorillonite).

Table-25

Dye	λ_{max} in nm. (α)	(β)
Th	596	564(s)
AzC	620	—
AzA	630	—
AzB	645	598(s)
MB	661	612(s)

(s)= Shoulder

The spectra of clay-dye suspensions show that the adsorption of the dye by montmorillonite results in metachromasy i.e., a gradual replacement of the principal α band by β band with a shorter wave length. In an aqueous dye solution the shift of the absorption peak in the visible region to shorter wave length occurs as the dye concentration increases and has been ascribed to the formation of dimers and higher aggregates. The α band is attributed to monomeric forms of the dye while the β band is attributed to dimeric forms. It is observed that when the concentration of the clay is very small (or a high formal degree of saturation) the spectrum is very similar to that of the corresponding aqueous solution of all the dyes. It is due to the fact that the adsorbed monomeric cations are in the environments in which the polarity is similar to that of the bulk solution. This environment is probably at the water clay interface, out side the interlayer space. This kind of adsorption or interaction

has been labelled as 'type A' (fig. 104, ref.230). As the concentration of the suspended clay increases (or decreasing formal degree of saturation) β band becomes more prominent. In the case of AzC at 12.0 mmol dye per 100 g clay, the α band becomes practically undetectable. With the larger concentration of clay the band α is shifted bathochromically (to longer wave length) followed by the hypsochromic shift (to shorter wave length) of the β bands. A bathochromic shift of α band due to adsorption by montmorillonite was observed previously by many workers (228,229). The shifting of the band maxima of the five dyes as a function of formal degree of saturation are shown in figs. 105-109. The shiftings from the lowest to the highest clay content of the suspensions are summerized in table 26.

Table-26

Dye	Bathochromic (λ in nm.)	Hypsochromic (λ in nm.)
Th	596-630	564-530
AzC	620- *	572-540
AzA	630-678	576-550
AzB	645-664	598-560
MB	661-675	612-568

* α band not detectable.

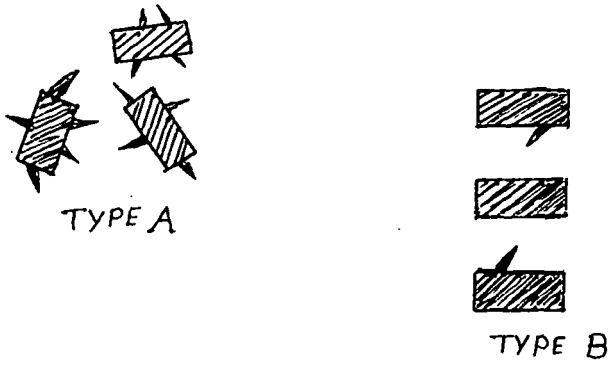

Fig. 104 : Schematic presentation of Adsorption.

The bathochromic shift is often due to an increase in environmental acidity. The interlayer water is also reported to be much more acidic than bulk water (231). and thus 'type B' (fig. 104, ref. 230) adsorption can be attributed to monomeric dye cations located inside the 'interlayer space' of the clay with electrostatic interaction of the positively charged dye ions with the negatively charged clay (229-232) being the principal binding force. An interlayer space is found between parallel layers which form a tactoid. The formation of tactoid increases with increase in clay concentration in the suspension and the type B adsorption also increases

It is assumed that metachromasy in montmorillonite is the consequence of π interaction between the oxygen plane of the aluminosilicate layers and the aromatic dye, then the hypsochromic shift is an indication of stronger π interactions. such strengthening trend is expected in the system owing to the increase in hydrophobic character of the interlayer space. This occurs because of the exchange of the inorganic hydrophilic cation with the organic cationic dye (213).

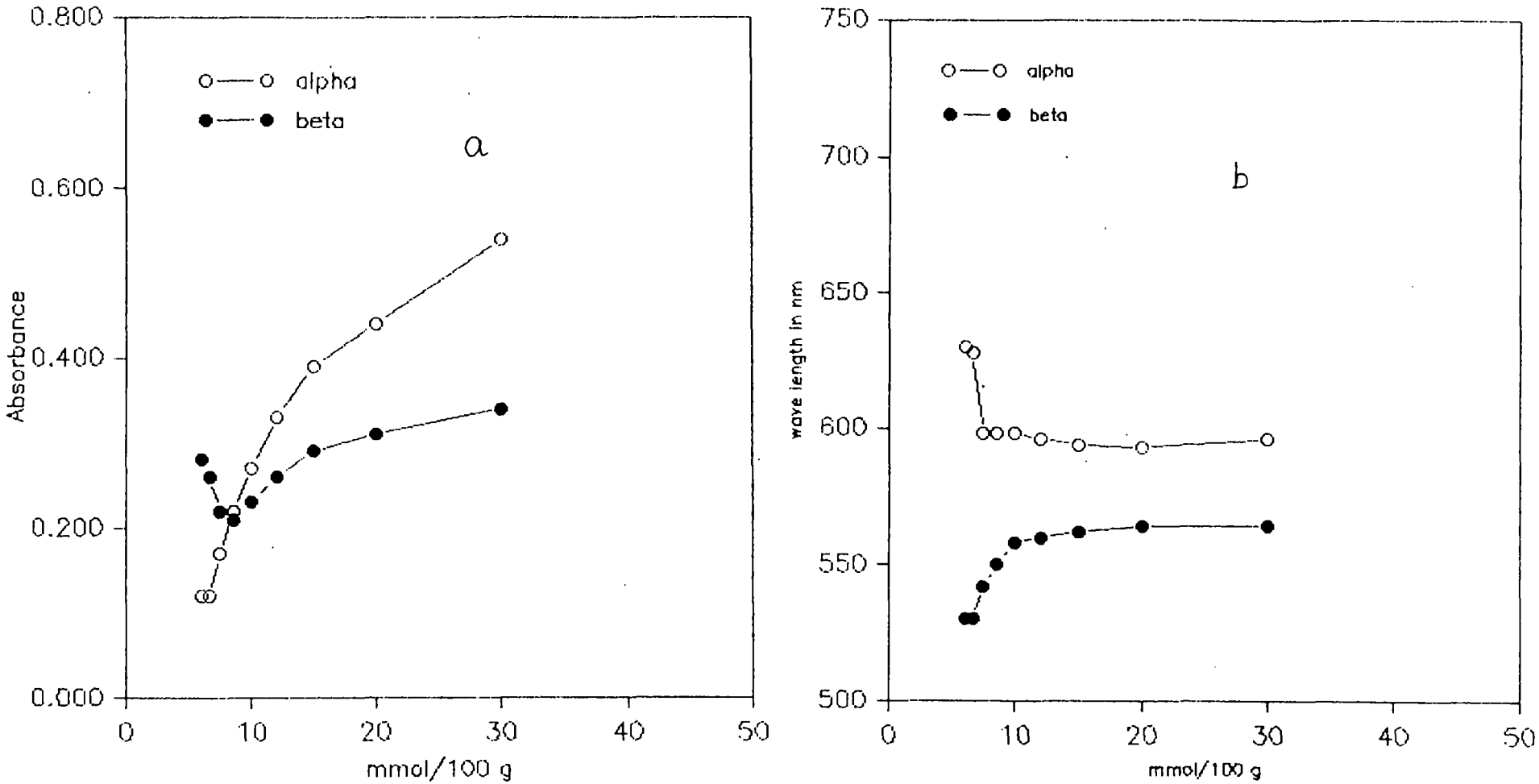

Fig. 105 : (a) Variation of absorbance and (b) shifting of band maxima as a function of Formal degree of saturation (mmol/100g) for Thionine in the presence of clay (Montmorillonite).

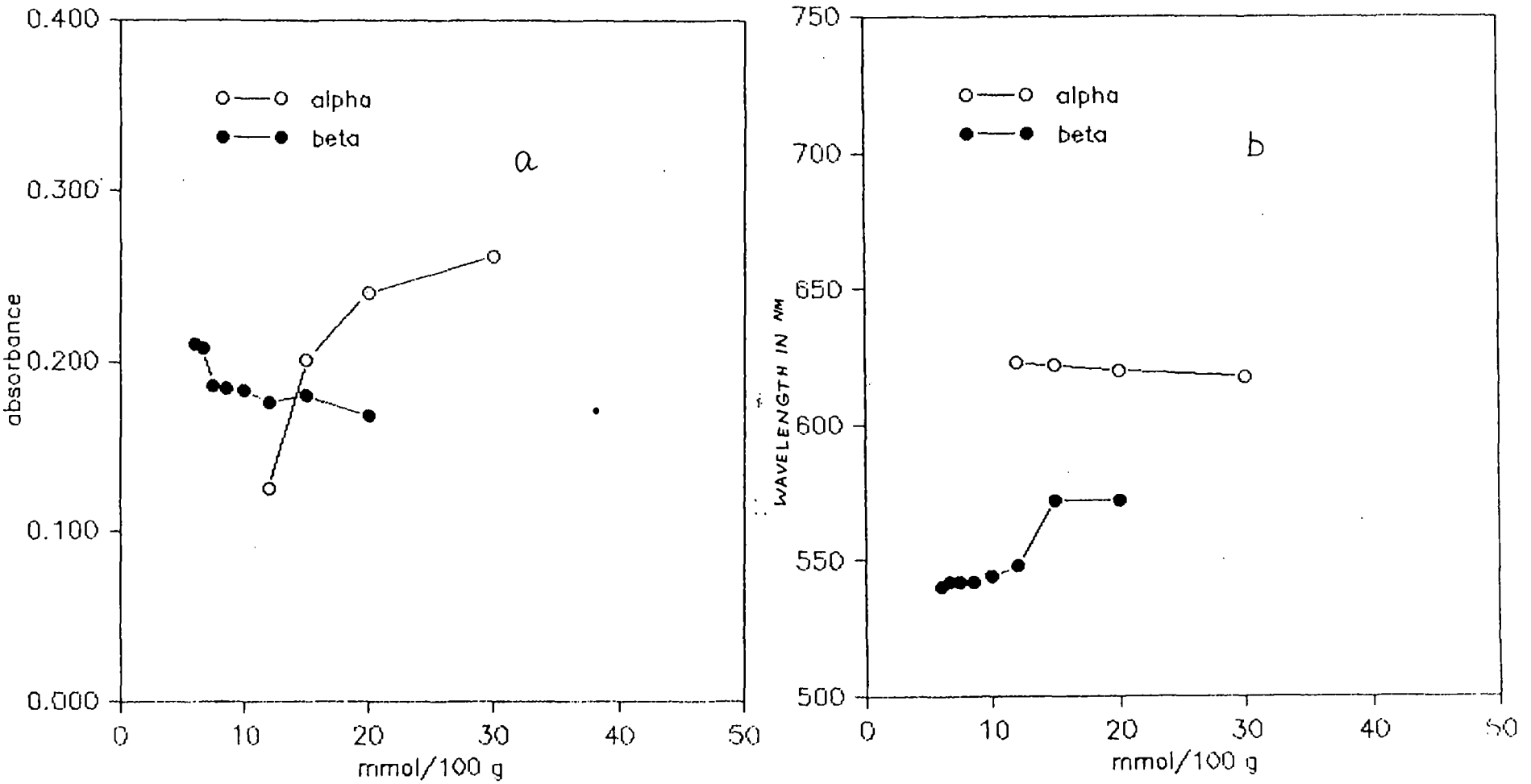

Fig. 106 : (a) Variation of absorbance and (b) shifting of band maxima as a function of Formal degree of saturation (mmol/100g) for Azure C in the presence of clay (Montmorillonite).

AA
107

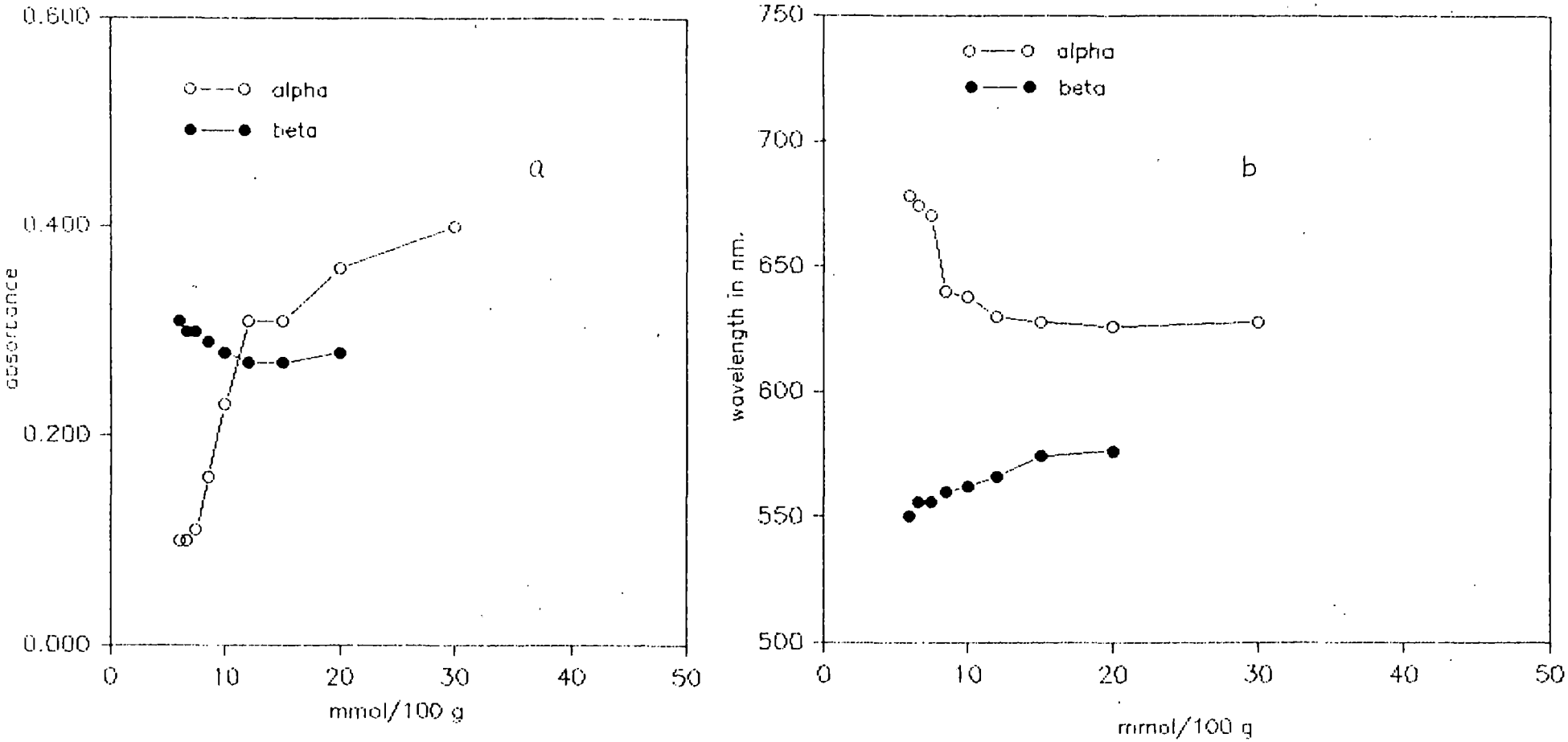

Fig. 107 : (a) Variation of absorbance and (b) shifting of band maxima as a function of Formal degree of saturation (mmol/100g) for Azure A in the presence of clay (Montmorillonite).

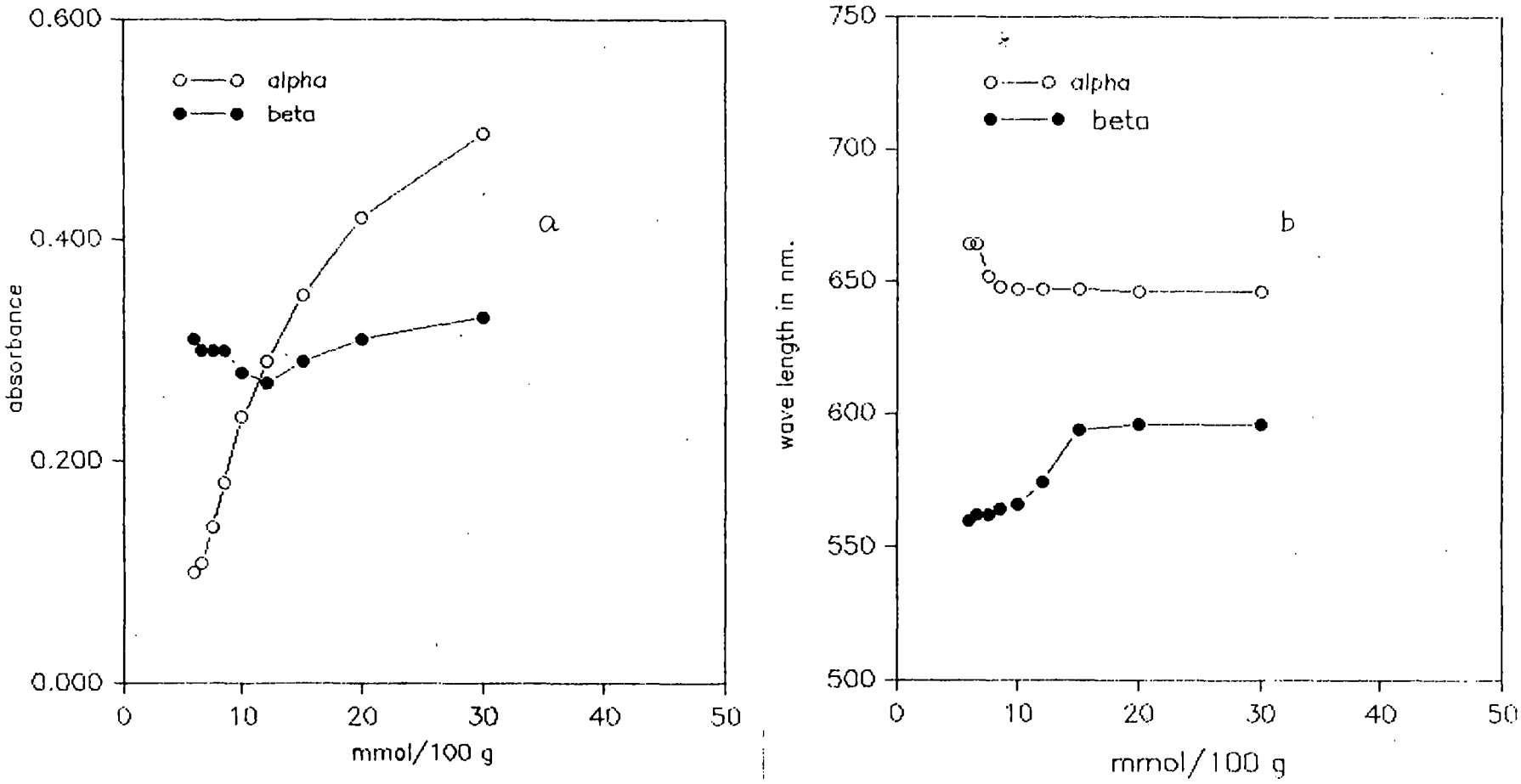

Fig. 108 : (a) Variation of absorbance and (b) shifting of band maxima as a function of Formal degree of saturation (mmol/100g) for Azure B in the presence of clay (Montmorillonite).

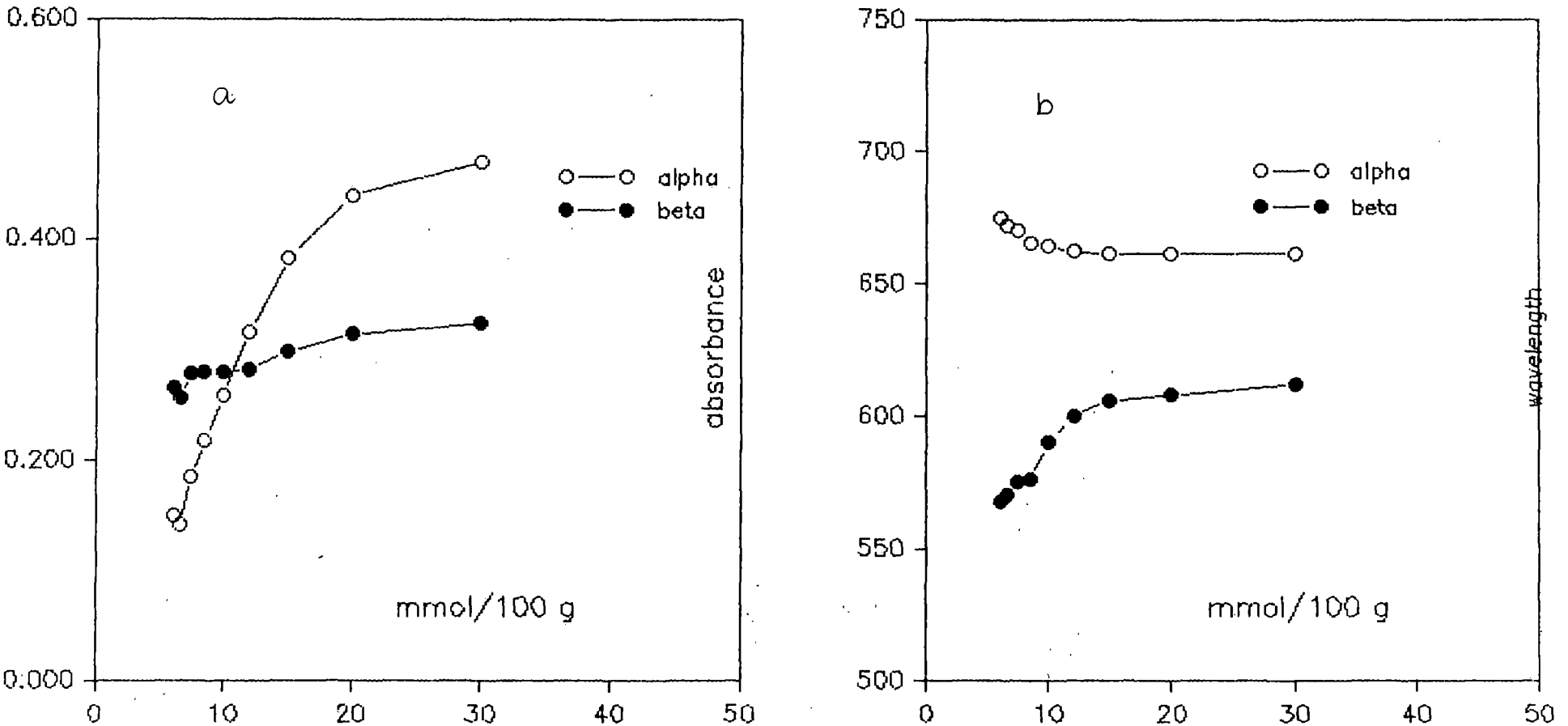

Fig. 109 : (a) Variation of absorbance and (b) shifting of band maxima as a function of Formal degree of saturation (mmol/100g) for Methylene Blue in the presence of clay (Montmorillonite).

Since the dye concentration was fixed in all the clay-dye suspensions in the present study, it was expected that the absorbance of band β would increase as α has decreased and *vice versa* (221). In the present study it is observed that the adsorption of the dye by montmorillonite resulted in considerable decrease in the intensities of α band in all the cases but the change in the intensity of the β band does not follow the order as expected. The changes in absorbance of the bands as a function of the formal degree of clay saturation are shown in Figs. 105-109. It is reported that the flocculation of montmorillonite affects the absorbance of bands α and β (230). Flocculation results in a decrease of absorbance, whereas with peptization the reverse process occurs. The absorbance intensity of the β band of MB follows the order of change as that of α band i.e.,decreases with increase in clay concentration in the suspension. In the case of AzB, AzA, AzC and Th the absorbance intensity of β band becomes minimum around 10 mmol dye per 100 g clay and the intensity increases further as the formal degree of saturation decreases. From the observation it may be inferred that the differences in the structures and hydrophobicities of the dye molecules influence the processes of flocculation and peptization of montmorillonite.

The Metachromatic behaviour of the thiazine dyes in the presence of ZSM-5 could not be studied precisely because of the excessive scattering of light by the zeolite particles.

CAPTER 6

SUMMARY AND CONCLUSIONS:

In chapter 1, a general introduction on photogalvanic effect of thiazine dye is presented. The improtance of electrode kinetics, self quenching phenomenon of photogalvanic solution, electrode selectivity, dye incorporated clay (montmorillonite) and zeolite (ZSM-5) modified electrode and quantitative ion-exchange parameters involving such a modified electrode are also mentioned briefly for these are brought to be pertinent with the objectives of the present investigation. Progressively alkylated thiazine dyes viz., thionine, azure C, azure A, azure B and methylene blue are selected not onlyfor their differences in solubilities and other physico-chemical characteristics pertaining to photogalvanic efficiencies but also because they provide an excellent opportunity for studing the effects of molecular size and shapes on various physico-chemical parameters incorporated in the thesis. (Page 1-14)

The scope and object of the present investigation has been incorporated in chapter 2. (Page 15-19)

In chapter 3, results of the investigations on the nature of dye-dye aggregation, the effect of increase of molecular size , temperature and solvent on aggregation, the probable structure of dye aggregates and the thermodynamics of dye aggregation in

aqueous and aqueous-ethanolic media are presented. Self aggregation of the dyes are important not only to understand the selfquenching phenomena occuring in photogalvanic cells, but also for some other important aspects viz. its possible application in understanding such phenomena as engergy transfer in biological systems, metachromasia, hypochromasia etc. and the binding processes of dyes by clay minerals which have been incorporated in the present thesis. In section 3.1.1., a brief review of previous studies on the general monomer- dimer equilibrium of dyes in the light of classical model is presented. Section 3.1.2., depicts the theoretical aspects of molecular exciton model. Section 3.1.3., contains a review on spectral properties of dimer in terms of exciton theory. Section 3.1.4., describes the vibronic exciton model for the interpretation of dimer spectra and includes some more recent development of molecular exciton theory. (page 20-50)

Various characteristics of this dyes, their structures and method of purification are presented in section 3.2. The experimental techniques for the study of dye aggregation is also presented in this section. (page 51-54)

Dimerization constants for the dyes at various temperature and solvents are determined applying an iterative technique by a computer program written in BASIC ianguage and presented in chapter 3.3.1. The dimerization constant decreases with the

increase in temperature and percentage of ethanol in the medium. At a particular temperature and solvent the value of dimerization constant increases upon methylation from thionine to azure B and decreases slightly in the case of methylene blue . At 20^{0}C in aqueous medium the values are 2.44×10^{3}, 2.95×10^{3}, 4.50×10^{3}, 8.98×10^{3} and 5.01×10^{3} lit./mol. for Th, AzC, AzA, AzB and MB respectively. Alkyl substitution effect is found to be significant and it is also evident that hydrophobic and Vander waals forces etc. in dimer formation are important and the steric hindrance caused by bulky substituents also plays an important role. (page 54-84)

Some important thermodynamic functions of dimerization process are determined in order to know the nature of bonding between the monomers in dimer. ΔH, and ΔG values are negative for the five thiazine dyes. ΔH and ΔG values do not differ very much upon progressive methylation. ΔS values, which are also negative, increase to much larger extent due to methylation. It suggests that aggregated dyes are more ordered than free monomer dyes. In general, the high values of ΔH and ΔS can be attributed to the role of hydrogen bonding in aggregate formation apart from hydrophobic and $\pi-\pi$ interactions. (page 84-87)

The dimer spectra have been interpreted by using Exciton theory, which predicts a splitting of the electronic transition in the dimer. The model offers a theoretical method for treating the resonance interaction of excited states of weakly coupled composite systems. The vibrational structure in spectra and vibronic interactions are neglected in this treatment. The decomposition of a dimer spectrum into two bands (monomer) show that the monomer visible spectrum corresponds to an electronic transition with two vibronic bands. Transition moments, oscillator strength and resonance interaction energies are determined from the dimer spectra. Using these values twist angle θ and the distances R_I' and R_{II}' (for two different models) between the monomer units in the dimer have been calculated for all the dyes. In view of the results of the previous as well as present study model I seems to be more appropriate.

The interdipole distance (R_I') varies from 5.59 to 6.76 $\overset{o}{A}$. The lowest value 5.59 $\overset{o}{A}$ is for the AzA. The twist angle θ varies from $28.4^{\emptyset}$ to $34.8^{\emptyset}$. The highest value is associated with thionine. No systemetic variation of the above parameters is observed on progressive methylation of the dye molecule. It seems apparent that apart from the steric effect hydrophobic as well as the electron donating nature of methyl groups are also involved in the process of dimerization. These are discussed in section 3.3.2. Although the exciton model as described in this section is a simplification of highly complecated problem, it offers

reasonable interpretation for the dimer spectra of present dye systems. (page 87-94)

In section 3.3.3., the dimer spectra of the five dyes are further analysed by vibronic exciton band model and the results of the analysis are given. The additional advantage of the model is that it allows one to analyse the dimer in further detail with respect to the strength of exciton coupling, the frequency and intensity of band origin, band width etc. The monmer spectra were fitted to a five parameter Gaussion equation, assuming that the spectra are due largly to a single harmonic vibronic progression, because some of the monomer fitting parameters are required to fit the dimer spectra. The dimer spectra were calculated and fitted to an adiabatic model using some monomer parameters and the spectra which refer to zero angle between the transition moments (i.e., the minimum series is zero in each spectrum) are shown. Although the monomer spectra fittings are satisfactiry, dimer spectra fittings are not always very well. The $\bar{\nu}_{00}$, which is the position of the (0,0) band of each of the two monomers in dimer, undergoes hypsochromic shift relative to that of the free monomer. The exciton interaction parameters (ε) are small (ε =0.9 to 1.15), which provides some supports for the model.

(page 95-100)

The electrochemical behaviour of the dyes on clean and modified (montmorillonite and ZSM-5) glassy carbon electrodes as well as the electrochemical processes involved therein in the presence of Fe(III) ions as an oxidant have been discussed in chapter 4. A brief review of the previous work on the redox properties of various dyes on clean and modified electrodes using cyclic voltammetric technique is presented in section 4.1.

(page 101-111)

The experimental procedure for electrochemical analysis using cyclic voltammograph is presented in section 4.2. The preparation of colloidal Pt, montmorillonite and ZSM-5 suspensions and the modification of electrode surface are also cited in this section (page 111-113)

The criteria related to the reversibility and the results thereof on a clean glassy carbon electrode (GCE) in different solvents are discussed in section 4.3.1. The formal potential values (average) for the five dyes are 0.205, 0.175, 0.207, 0.281 and 0.196V for Th, AzC, AzA, AzB and MB respectively in aqueous medium. Voltammetric measurements are consistent with two electron reversible redox couples of dye/leucodye pairs. The value of $0.058/\Delta E$ is rather low (<2) even at slow scan rates possibly due to the result of two successive one electron reversible charge transfer, with a fast protonation of the

intermediate to form a species which is more easily reduced than the dye molecule. The current ratio values, $i_{pa}/i_{pc}<1$, suggest that the electrogenerated leucodyes are involved in reactions which prevent their reoxidation upon scan reversal. Assuming reversibility of electrode reaction, the effective diffusion coefficients of the dyes in different solvents have been calculated at scan rate of $20mVs^{-1}$. The values for thionine are $3.05x10^{-6}$, $1.80 x10^{-6}$ and $1.10x10^{-6}$ cm^2s^{-1} in water, ethanol (50% v/v) and triton X-100 (0.001M) respectively. There is no systemetic change in the diffusion coefficient values with the progressive alkylation of dye molecule. But the effect of solvent is very prominent. The nature of the cyclic voltammograms obtained from concentrated dye solution ($1-2x10^{-4}$M) in the presence of 0.1M KCl and the effect of $_pH$'s therein have also been discussed specially in view of reactant and/or product adsorption on the electrode surface. The heterogeneous rate constant k for the quasi-reversible processes of the dyes is determined. The kinetic measurements are carried out within the range 300-1000 mVs^{-1} scan rates. All the values are found to be of the order of 10^{-3} $cm.s^{-1}$. (page 113-130)

A preliminary study of electrochemistry of dye incorporated montmorillonite and ZSM-5 modified electrode has been discussed in section 4.3.2. The presence of polyvinyl alcohol and Pt in the clay film is found to be critical in attaining better

electrochemical activity of the modified electrode. The modified electrodes exhibit quasi-reversible redox wave of the dyes. At slow scan rates the curves obtained from plotting of I_{pc} vs $v^{1/2}$ deviate from linearity significantly which suggests that the electrode processes are of diffusion type only at high scan rates. However, a rough estimation of apparent diffusion coefficient in montmorillonite film shows that the transport of the charge carriers in montmorillonite modified electrode occurs principally via electron hopping process within the film. Except thionine, the current output for all the dyes are substantially less in clay modified electrode than that in zeolite modified electrode. (page 131-139)

Although Fe(II)/Thionine cell is the most successful PG cell for solar energy conversion, dissipation of free energy due to thermal back reaction of leucodyes with Fe(III) ions constitutes a vital problem. In section 4.3.3., an electrochemical investigation of all the dyes in the presence of Fe(III) ions is reported. The theory of catalytic regeneration mechanism involving an electrode reaction followed by a coupled chemical reaction is applied to derive kinetic parameters of homogeneous reaction. The second order rate constants for the reaction of thiazine leucodyes with Fe(III) ions is found to increase from 0.25×10^4 to 1.6×10^4 lit/mol.s^{-1} upon monomethylation of thionine and to vary from 0.7×10^4 for the dimethyl derivative to 1.4×10^4

lit/mol.s^{-1} for tetramethyl one. The electron donating nature as well as hydrophobic characteristics of methyl group influence the kinetics of the homogeneous reaction. (page 139-147)

Since the nature of bonding of dyes on montmorillonite and ZSM-5 (zeolite) and the ion exchange characteristics of these substances have a vital role in the electrodic processes of modified electrodes, an investigation on the interaction of montmorillonite and ZSM-5 with the thiazine dyes has been discussed in terms of adsorption and metachromasy in chapter 5. The structure of montmorillonite and ZSM-5 is briefly discussed in the introductory part. A review of the earlier works on adsorption and metachromasy is included in section 5.1.

(page 148-164)

The method of preparation of pure Na-montmorillonite along with the experimental techniques of the study of adsorption and metachromasy are presented in section 5.2. (page 164-166)

The adsorption isotherms of the dyes on both the substances (montmorillonite and ZSM-5) are of H-type i.e., of high affinity class indicating a strong adsorbate-adsorbent interaction. From the structures of the thiazine dyes, it is clear that all the dyes can be involved into an ion exchange type of sorption through -S- or ->N- which become positive charge centres by

resonance. These structural considerations assign to the dyes a predominantly flat orientation onto the clay and zeolite surfaces, although other possibilities are not entirely excluded. The probability of distribution among the different orientations is conditioned by various factors such as the basicity of the nitrogen group, the number of resonating structures, the molecular geometry of the dye cations, the nature of the exchange sites, etc. It is, however, to be noted that the flat position is possibly attended with the minimum potential energy.

The adsorption data of all the dyes are found to fit with the Langmuir's equation. The equilibrium constant (Langmuir bonding constant) values in the case of montmorillonite are higher than that of ZSM-5. The variation of adsorption equilibrium constant values due to progressive methylation is found to be similar to that of the variation of dimerization constant values of the dyes. But the maximum adsorption capacity values of both (montmorillonite and ZSM-5) do not vary systematically on methylation of dye molecule. The results suggest that steric hindrance, hydrophobicity, electron donating nature of the methyl group and the specific orientation of the dye molecules on the surfaces are operative simultaneously. All these are discussed in section 5.3.1. (page 166-170)

In section 5.3.2., metachromasy of the dyes in montmorillonite has been described. All the dyes show

bathochromic shift of the α band followed by a hypsochromic shift of the β band as the clay content of suspensions increases. The absorbance intensities of both the bands α and β also changes with clay concentration. The α bands are attributed to monomeric forms of the dye and β band is to dimeric forms. It is assumed that metachromasy in montmorillonite is the consequence of π interaction between the oxygen plane of the aluminosilicate layers and the aromatic dye. (page 170-174)

The metachromasy of the dyes in the presence of ZSM-5 could not be studied precisely due to the excessive scattering of light by the zeolite particles

-: REFERENCES :-

1. Archer,M.D., J. Appl. Electrochem., 5, 17, 1975.
2. Quichenden,T.I. and Yim,G.K., Sol. Energy, 19, 283, 1977.
3. Memming,R. and KÖrsten,G., Ber-Bunsenges Phys. Chem., 76, 4, 1972.
4. Miller,L.J., "A Feasibility Study of a Thionine Photogalvanic Power Generation System", Final Report, Contract No.AF 33(616)- 7911, Sunstrand Aviation, ASTIA, Document No. 282876, 1962.
5. Becquerel,E., Hebd,C.R., Seances Acad. Sci., 9, 561, 1839.
6. Gomer,R., Electrochim. Acta., 20, 13, 1975.
7. Albery,W.J.and Archer,M.D., J. Electrochem. Soc., 124, 688, 1977.
8. Weber,K., Z. Physik. Chem., B15, 18, 1931.
9. Weiss,J., Nature, 136, 794, 1935.
10. Rabinowitch,E., J. Chem. Phys., 8, 551-560, 1940.
11. Wildes,P.D. and Lichtin,N.N., J. Am. Chem. Soc., 100, 6568, 1978
12. Clark,W.D.K. and Eckert,J.A., Sol. Energy, 17, 147, 1975.
13. Clark,W.D.K., Eckert,J.A.,Hall,D.E., Lichtin,N.N. and Wildes,P.D., Amer., Ceramic Soc.Bull.,56, 408, 1977.
14. Hall,D.E., Eckert,J.A., Lichtin,N.N. and Wildes,P.D., J. Electrochem.Soc., 123, 1705, 1976.
15. Wildes,P.D., Hoffman,M.Z., and Lichtin,N.N., in "Proceedings of the International Symposium of Solar Energy", Berkowitz, J. and Lesk,I. eds. The Electrochemical Soc., Princeton, New Jersy, P 128, 1976.

16. Wildes,P.D., Brown, K.T., Hoffman,M.Z., Hall,D.E. and Lichtin,N.N., Sol. Energy, 19, 579,1977.

17. Hall,D.E., Wildes,P.D. and Lichtin,N.N., J. Electrochem. Soc., 125, 1365, 1978.

18. Hall,D.E., J. Electrochem. Soc., 124, 804, 1977.

19. Kamat,P.V. and Lichtin,N.N., J.Phys. Chem. 85, 814, 1981.

20. Gronen,E.J.J., deGroot,M.S. and deRuiter,R., Electrochim. Acta., 30, 1199, 1985.

21. Albery,W.J., Foulds,A.W., Hall,K.J., Hillman,A.R., Egdell,R.G. and Orchard,A.F., Nature, 282, 793, 1979.

22. Murthy,A.S.N. and Reddy,K.S., Electrochim. Acta., 28, 473, 1983.

23. Murray,R.W., In Electroanalytical Chemistry, Bard,A.J. (Ed.) Marul Dekker, N.Y. 1984, Vol.13, p 191

24. Rolison,D.R., Chem. Rev., 90, 867, 1990.

25. Kamat,P.V., Electroanal. Chem., 163, 389, 1984.

26. Jost,W., Diffusion in Solids, Liquids and Gases : Acad. Press, New York, P 462.

27. Sheppard,S.E., Proc. Roy. Soc. (London), A82, 256, 1909.

28. Rohatgi-Mukherjee, Ind. J. Chem., 31, 500,1992.

29. McRay,E.G., and Kasha,M., J. Chem. Phys., 28, 721, 1958.

30. Robinowitch,E. and Epstein,L.F., J. Am. Chem. Soc.,64, 69, 1941.

31. Lennard-Jones, Proc. Roy. Soc. (london) A56, 463, 1924.

32. Burdett,B.C., in Aggregation Process in Solution , Eds. Jones,E.W. and Gormally,J. (Elsevier, Armsterdam, 1983) Chap.10, P 241.

33. Aquilera,O. and Neckers,D.C., Acc. Chem. Res., 171, 22, 1989.

34. Rohatgi,K.K. and Singhal,G.S., J. Phys. Chem. 70, 1695, 1960.

35. Mukherjee,P. and Ghosh,A.K., J.Am. Chem. Soc., 92, 6419, 1970.

36. Rabinson,B.H., Löffler,A. and Schawarz,G., J. Chem. Soc. Faraday Trans.I, 69, 56, 1973.

37. Schubert,M., Levine,A., J. Am. Chem. Soc., 77, 4197, 1955.

38. Turner,R. and Cowmann,M.K., Arch. Biochem. Bio. Phys., 237, 253, 1985.

39. Vitagliano,V., in Aggregation Processes in Solution , Eds. Jones,E.W. and Gormally,J. (Elsevier, Armsterdam, 1983) Cap. 11, P 271.

40. Shirai,M., Ohyabu,M., Ono,Y. and Tanaka,M., J. polym. Sci. Chem. Ed., 19, 555, 1982.

41. Newmann,M.G. and Hioka,N., J. Appl. Polym. Sci.,34, 2829, 1987.

42. Bergmann,K. and O'Konsky,C.T., J. Phys. Chem. 67, 2169, 1963.

43. West,W., and Pearce,S., J. Phys. Chem., 69, 1894, 1965.

44. Baranova,E.G. and Levshin,V.L., Optica i Spetrokopia, 10, 182, 1961.

45. Mataga,N., Bull. Chem. Soc. Japan, 30, 375, 1957.

46. Zanker,V., Z. Physik. Chem., 200, 250, 1952.

47. Hida,M. and Sanuki,T., Bull. Chem. Soc. Japan, 43, 2291, 1970.

48. Selwyn,J.E. and Steinfeld,J.I., J. Phys. Chem., 76, 762, 1972.

49. James,A.D. and Rabinson,B.H., Adv. Mol. Relax. Process, 8, 287, 1976.

50. Zadoroznnaya,E.M., Nabinvanets,B.I. and Maslei,N.N., Zh. Anal. Khim., 29, 993, 1974.

51. Arbeloa,I.L., J. Chem. Soc. Faraday Trans. 2,77, 1725, 1981.

52. Arbeloa,I.L. and Rohatgi-Mukherjee,K.K., Spectrochemica Acta., 44A, 423, 1988.

53. Newmann,M.G., Gessner,F. and Olivelra,V.A., J. Chem. Soc. Faraday Trans., 86, 3551, 1990.

54. McRae,E.G. and Kasha,M., Physical processes in Radiation Biology, Augenstein,L.,Rosenberg,B. and Mason,R., Ed.,Acad. press, N.Y., P 23, 1964.

55. Davydov,A.S., "Theory of Molecular Excitons" (Transtated by Kasha,M. and oppenheimer,M.Jr.) McGraw-Hill, N.Y., 1962.

56. Simpson,W.T., "Theory of Electrons in Molecules", Prentice-Hall, Englewood Cliffs, New Jersey, 1962.

57. McClure,D.S., Solid State Physics, 8, 1, 1959.

58. Kasha,M., Rev. Mod. Phys., 31, 162, 1959.

59. Kasha,M., Radiation Res., 20, 55, 1963.

60. Levinson,G.l., Simpson,W.T. and Curtis,W., J.Am. Chem. Soc., 79, 3414, 1957.

61. Kasha,M.,EL-Bayoumi,M.A. and Rhodes,W., J.Chem. Phys., 58, 916, 1961.

62. EL-Bayoumi,M.A., "Exciton Theory : Application to H-Bonded Complexes", Doctoral Thesis, Florida State University, Tallahssea, Florida (1961).

63. Hosoya,H., Tanaka,J. and Nagacura,S., J. Mol. Spectry. 8, 257, 1962.

64. Rohatgi,K.K. and Mukhopadhyay,A.K., J. Phys. Chem., 76, 3970, 1972.

65. Arbeloa.I.L., J.Chem. Soc. Faraday Trans.2, 77, 1735, 1981.

66. Jones,G.R., Duddell,D.A.,Murry,D. and Cundall,R.B.,J. Chem. Soc. Faraday trans.2, 80, 1181, 1984.

67. Basu,S., Rohatgi-Mukherjee,K.K, amd Arbeloa,I.L., Spectrochemica Acta., 42A, 1355, 1986.

68. Fulton,R.L. and Gautermann,M., J. Chem. Phys., 35, 1059, 1961.

69. Longuet-Higgins,H.C., Adv. Spectra., 2, 429, 1961.

70. Witkowski,A. and Moffit,W., J. Chem. PHys., 33, 872 1960.

71. Witkowski,A., Roczniki Chem., 35, 1409, 1961.

72. McRae,E.G., Ausrtal. J. Chem., 14, 344, 1961.

73. Merrifield,R.E., Radiation Res., 20, 154, 1963.

74. Siebrand,W., J. Chem. Phys., 40, 2223, 1964.

75. Fulton,R.L. and Gouterman,M., J. Chem. Phys., 41, 2280, 1964.

76. Förster,Th., Naturwiss, 50, 166, 1946.

77. Levinson,G.S., Simpson,W.T. and Curtis,W., J. Am. Chem. Soc. 79, 4314, 1957.

78. Simpson,W.T., and Petersen,D.L., J. Chem. Phys., 26, 588, 1957.

79. Kurucsev,T., J. Chem. Soc. Faraday Trans.2, 72, 2095, 1976.

80. Gál,M., Kelly,G.R. and Kurucsev,T., J. Chem. Soc. Faraday Trans. 2, 69, 395, 1973.

81. Gianneschi,L.P., Cant,A. and Kurucsev,T., J. Chem. Faraday Trans. 2, 73, 664, 1977.

82. MeCoy,E.F. and Ross,I.G., Aust. J. Chem., 15, 573, 1962.

83. Kurucsev,T., J. Chem. Educ., 55, 128, 1978.

84. Davydov,A.S., Quantum mechanics (Pergamon, Oxford, 1965), P. 522-524.

85. Weigang,O., J.Chem. Phys., 43, 71, 1965.

86. Joyee,D.E. and Kurucsev,T., Biopolymers, 12, 1459, 1973.

87. Kurucsev,T. and Strauss,U.P., J. Phys. Chem., 74, 3081, 1970.

88. Gál,M.E., Kelly,G.R., and Kurucsev,T., J.Chem. Soc. Faraday Trans. 2, 72, 2095, 1976.

89. Gianneschi,L.P. and Kurucsev,T., J. Chem. Faraday Trans. 2, 72, 2095, 1976.

90. Raju,K.V., Raju,G.R. and Sudhakar, G.D., Ind. J. Chem., 32, 85, 1993

91. Lavorel,J., J. Phys. Chem., 61, 1600, 1957.

92. Pant,D.D. and Pant,H.C., Indian J. Pure Appl. phys., 6, 239, 1968.

93. Rohatgi,K.K. and Singal,G.S., J. Phys. Chem., 69, 1894, 1965.

94. Di Benedetto,J.S. and Jones.J.A., J. Chem. Educ., 63, 1095, 1986.

95. Dye,J.L. and Nicely,V.A., J. Chem. Educ., 48, 443, 1971.

96. Klochkov,V.P. and Bogdanov,V.L., Opt. Spectrosc., 34, 25, 1973

97. Austin,J.M., Harrison,I.R. and Quichenden,T.I., J. Phys. Chem., 90, 1839, 1986.

98. Baulddreay,J.M., Archer,M.D., Electrochim. Acta. 28, 1515, 1983.

99. Quickenden,T.I.,Bassett,R.L., J. Phys. Chem., 85, 2232, 1981.

100. Bowen,W.R., Acta. Chem. Scand. Ser., A34, 437, 1980.

101. Cheng,H.Y., Sackett,P.H. and McCreery,R.L., J. Am. Chem. Soc., 100, 962, 1978.

102. Sackett,P.H., Mayansky,J.S., Smith,T., Kalus,S. and McCreery,R.L., J. Med. Chem., 24, 1342, 1981.

103. Sharma,L.R., Verma,R.S., Sharma,A. and Singh,G., Ind. J. Chem., 23A, 642, 1984.

104. Kamat,P.V., J. Chem. Soc. Faraday Trans.1, 81, 509, 1985.

105. Quickenden,T.I. and Harisson,I.R., J. Electrochem. Soc., 132, 81, 1985.

106. Albery,W.J., Foulds,A.W., Hall,K.J. and Hillman,A.R., J. Electrochem. Soc., 127, 654, 1980.

107. Wopschall,R.H. and Shain,I., Anal. Chem., 39, 1527, 1967.

108. Murthy,A.S.N. and Srivastava,T., J. Chem. Soc. Faraday Trans., 86, 105, 1990.

109. Ghosh,P.K. and Bard,A.J., J. Am. Chem. Soc., 105, 5691, 1983.

110. Fitch,A., Clay and Clay minerals, 38, 391,1990.

111. Inoue,H. and Yoneyama,H., J. Electroanal. Chem., 233, 291, 1987.

112. Rusling,J.F., Shi,C.N. and Suib,S.L., J. Electroanal. Chem.,245, 331, 1988.

113. Ghosh,P.K. and Bard,A.J., J. Phys. Chem., 88, 5519, 1984.

114. Yamagishi,A. and Aramata,A., J. Chem. Soc. Chem. Commun., 452, 1984.

115. Fitch,A. and Frausto,C.L., J. Anal. Chem., 257, 299, 1988.

116. Joo,P., Colloids and Surf., 49, 29, 1990.

117. Rolison,D.R., In Fundamental Aspects of Corrosion Protection by Surface modification; McCafferty, E.C.,Ouder,C.R., J,Eds., The Electrochemical Society: Pennington NJ, 1984, Vol.48-3.

118. Albery,W.1.,"Photovoltaic and Photoelectrochemical Solar Energy Conversion". Ed.by F.Cardon, W.P.Gomesand, and W.Dekeyser. Plenum Press, N.Y.(1981), p.313

119. Lodha,S., Khamesra,S., Sharma,B. and Ameta,S.C., Int.J.Energy Res. 15, 431, 1991

120. Albery,W.J. and Foulds,A.W., J.Photochem. 10, 41, 1979

121. Groenen,E.J.J.,deGroot,M.S., Ruiter,R.de. and Wit,N.de., J.Phys.Chem., 88, 1449, 1984.

122. Bard,A.J. and Faulkner,L.R., "Electrochemical Methods-Fundamentals and Applications". John Wiley & Sons, N.Y.(1980), p.429

123. Brokken-Zijp,J.C.M., and de Groot,M.S., Chem.Phys.Lett., 76, 1, 1980.

124..Hay,D.W., Martin,S.A., Ray,S. and Lichtin.N.N., J.Phys.Chem. 85, 1474, 1981.

125. Ferreira,M.I.C. and .Harriman,A., J.Chem.Soc.,Faraday Trans.I 173, 1085, 1977.

126. Hirai,H., Nakao,Y. and Toshima,H., J. Macromol. Sci. Chem., A13, 727, 1979.

127. Nicholson,R.S., Anal. Chem., 38, 1406, 1966.

128. Mabbott,G.A., J. Chem. Ednc., 60, 700, 1983.

129 Basu,J., Kundu,K.K. and Rohatgi-Mukherjee,K.K., Ind. J. Chem., 23A, 630, 1984.

130. Albery,W.J., Bowmen,W.R., Fisher,F.S, Fould,A.W. Hall,K.J, Hillman,A.R., Egdell,R.G. and Orchard,A.F. J. Electroanal. Chem., 86, 1, 1978.

131. Albery,W.J., Boutelle,M.G., Colby,P.J. and Hillman,A.R., ibid, 133 135,1982.

132. Bowmen,W.R., Acta Chem. Scandianaria, A34, 437,1980.

133. Quickenden,T.I., Herring,D.P., Yim,G.K., Electrochem. Acta., 25, 1397, 1980.

134. Kabasakalian,P., McGlotten, J. Anal.Chem., 31,431, 1959.

135. Nicholson,R.S., Anal.Chem., 37, 1351, 1965.

136. Bhattacharya,J., Saha,S.K. and Guhaniyogi,S.C., J.Polym.Sci. Part A: Polym. Chem. 28, 2249, 1990.

137. Galus,Z., Fundamentals of Electrochemical Analysis, E.Harwood Ltd. Chichester, !976, p 255-395.

138. Ferreira,M.I.C. and Harriman,A., J. Chem. Soc. Faraday Trans.I, 173, 1085, 1977.

139. Hill,H.A.O. and Walton,N.J., J. Am. Chem. Soc., 104, 6515, 1982

140. Nicholson,R.S. and Shain,I., Anal. Chem., 36, 706, 1964.

141. Nadjo,L. and Saviant,J.M., J. Electroanal. Chem, 48, 113, 1973.

142. Gratzel,M., Proc.Int.Conf.Photochem.Covers.Storage Soc.Energy 3rd, 1980,131,1981.

143. Albery,W.J., Bartlett,P.N., Davia,J.P., Foulds,A.W., Hillman,A.R and Souto-Bachiller,F.A., Faraday Discuss Chem.Soc. 70, 341, 1980.

144. Albery,W.J., Bartlett,P.N., Foulds,A.W., Souta-Bachiller,F.A. and Whiteside,R., J. Chem. Soc. Parkin Trans.2, 794, 1981.

145. Pauling,L., Proc.Natl.Acad.Sci. U.S., 16, 578,1930.

146. Bragg,W.L., Atomic Structure of Minerals, Cornell Univ.Press, Ithaca, 1937.

147. Gruner,J.W., Z.Krist., 83, 75, 1932.

148. Brindley,G.W. and Robinson,K., Mineralogy Mag., 27, 142,1946.

149. Hofmann,U., Endell,K. and Wilm,D., Z.Krist., 86, 340, 1933.

150. Marshall,C.E., Ibid, 91,433, 1935.

151. Hendricks,S.B., and Jefferson,M., Am. Miner., 24, 729,1939.

152. Mauguin,C.H., Bull.Soc.Franc.Min., 51, 285, 1982.

153. Jackson,W.W. and West,J., Z.Krist., 85, 160, 1933.

154. Mc Murchy, R.C., Ibid, 88, 420, 1934.

155. Barshad,I., Am.Miner., 34, 675, 1949.

156. Walker,G.F., Nature, 163, 726, 1949.

157. Grim,R.E., Bradley,W.F. and Brown,G, The Mica Clay Minerals, Chap.V.P. 138, Mineralogical Society of Great Britain Monograph, 1951.

158. Mac Ewan,D.M.C., J. Soil Sci., 1, 90, 1949.

159. Theng,B.K.G, The Chemistry of Clay-Organic Reactions, Adam Hilger Ltd, 1974.

160. Kelley,W.P., Cation Exchange in Soils, Reinhold, New York, 1948.

161. Weber,J.B., Adv. in Chem. Series, 111, 55, Am.Chem.Soc., 1972.

162. Phillen,O.D., Jr.,Weed,S.B. and Weber,J.B., Soil Sci.Soc. Am. Proc., 34, 527, 1970.

163. Marshall,C.E. and Krindbill,C.A., J.Phys.Chem., 46,1077,1942.

164. Weber,J.B., Perry,P.W. and Upchurch,R.P., Soil Sci. Soc. Am. Proc., 29, 678, 1965.

165. Page,J.B. and Baver,L.D., Proc. Soil Sci. Am., 4, 150, 1939.

166. Bar,A.L.S. and Tenderloo,H.J.E., Koll.Beih., 14, 97, 1936.

167. Hendricks,S.B. and Alexander,L.T., Proc. Soil Sco. Am., 5, 95, 1940.

168. Schachtschabel,P., Koll.Beih., 51, 199, 1940.

169. Mukherjee,S.K., Indian Soc. Soil Sci. Bull., 6, 67, 1951.

170. Mare,R., Z.Physik.Chem., 73, 685, 1910.

171. Ramchandran,W.S., Kacker,K.P. and Patwardhan,N.P., The American Mineralogists, 47, 165, 1962.

172. Brooks,C.S., Kolloid Zeitschrift Fur Polymere Band 199, Heft I Seite 31, 1964.

173. Plesch,P.H. and Liu,F.W.J., J. Colloid Sci., 8, 204, 1953.

174. Ewing,W.W. and Liu,F.W.J., J. Colloid Sci., 8, 204,1953.

175. Kipling,J.J. and Wilson,R.B., J. Appl. Chem., 10, 109, 1960.

176. Hofmann,U. Kottenhahn,H. and Morcos,H., Angew. Chem. Intern. Ed. Engl. 5, 242, 1966.

177. Orr,C., Special Rept. No. 1 Project, 143, 1950.
Jorgians Inst. of Technology, State Engineering Expt. Station, Atlanta.

178. Orr,C., Special Rept. No.2 Project, Ibid.

179. Darau,R., Z.Physik, 37, 419, 1926.

180. Van der Grinter,K., J. Chem. Phys., 23, 209, 1926.

181. Bancelin,F., Ibid, 22, 513,1925.

182. Bancroff,W.D. and Barnett,C.E., Colloid Symposium Monograph, 6, 73, 1928.

183. Subrahmanya,K.S., Rao,M.R.A. and Doss, K.S.G., Proc. Indian Acad. Sci., 34A, 324, 1951.

184. Doss,K.S.G. and Singh,A., J. Sci. Ind. Research (India), 12B, 79, 1953.

185. Margaret,M., Allingham, Cullen,J.W., Giles,G.H., Jain,S.K.and Wood,J.S., J. Appl. Chem., 8, 108, 1958.

186. Weissbein and Coven, Textile Res. J., 30, 58, 62, 1960.

187. Lenhar,S. and Smith,J.E., Ind. Eng. Chem., 27, 20, 1935.

188. Lenhar,S. and Smith,J.E., J. Am. Chem. Soc., 57,495,504,1935.

189. Vickerstaff,T. and Lemin,D.R., Nature, 157, 373, 1946.

190. Mukherjee,S. and Ghosh,A.K., J. Amer.Chem. Soc.,92,6403,1970.

191. Ghosh,A.K. and Mukherjee,P., Ibid, 92, 6408,1970.

192. Hertz,A.H., Danner,R.P. and Janusouis,G.A., Advances Chem. Ser. 79, Am. Chem. Soc., Washington D.C., 173, 1968.

193. Hertz,A.H., Adv. Colloid Interface Sci., 8, 237, 1977.

194. Kongonovoskii,A.M., Kolloidn zh. 28, 1966.

195. Pham Thi Hang and Brindley,G.W., Clays and Clay Minerals, 18, 203, 1970.

196. Faruki,F.A., Okuda,S. and Williumson,W.O., Clay Minerals, 7, 19, 1967.

197. Bodenheimer,W. and Heller,L., Israel J. Chem., 6, 307, 1968.

198. West.W., Carrol,B.H. and Whitcomb,D.H., J. Phys. Chem., 56, 1054, 1952.

199. De.D.K., Das Kanungo,J.L. and Chakravorty,S.K., Indian J. Chem., 11, 802, 1973.

200. Idem, Ibid, 12, 165, 1974.

201. Idem, Ibid, 12,1187,1974.

202. De,D.K., Das Kanungo,J.L. and Chakravorti,S.K.,J.Indian Chem. Soc., LVI, 608, 1979.

203. Idem, Ibid,L. 507, 1973.

204. Idem, J. Indian Soc. Soil Sci., 27, 85, 1979.

205. Idem, Ibid, 30, 369, 1982.

206. Narine,D.R. and Guy,R.D., Clays and Clay Minerals, 29,205, 1981.

207. Yamagashi,A., J. Phys. Chem., 85, 3090, 1981.

208. Handreck,G.P. and Smith,T.D., J. Chem. Soc. Faraday Trans. I. 84, 4191, 1988.

209. Handreck,G.P. and Smith,T.D., J. Chem. Soc. Faraday Trans I, 85, 645, 1989.

210. Vedeneva,J., J.Phy.Chem., U.S.S.R., 21, 881, 1947.

211. Richard,M.D.,Pop,C.G., J. Chem. Soc. Faraday Trans., 92, 317, 1996.

212. Theng,B.K.G., Clay and Clay Minerals, 30, 1, 1982.

213. Yariv,S and H.Cross, Geochemistry of Colloid Systems, Springer-Verlag, Berlin, 1979.

214. Yariv,S, Thermochem. Acta, 1985, 88, 49.

215. Grim,R.E., Clay Mineralogy, McGraw-Hill, New York, 1988.

216. Yariv,S and Lurie,D, Israel J. Chem., 9, 537, 1971.

217. BJerrum,J., Ballhausan,C.J. and Jorgensen,C.K., Acta. Chem. Scand., 8, 1275, 1954.

218. Yamagishi,A. and Soma,M., J. Phys. Chem., 85, 3090, 1981.

219. Grauer,Z., Yariv,S.,Heller-Kallai,L. and Avnir,D., J. Therm. Anal., 26, 49, 1983.; Grauer,Z., Yariv,S.,Heller-Kallai,L. Avnir,D.and Pelled,H., J. Colloid Interface Sci., 111, 261, 1986.

220. Arbeloa,F.L., Gonzales,I.L., Ojeda.R.P., and Arbeloa.I.L., J. Chem. Soc., Faraday Trans. 2, 78, 989, 1982.

221. Grauer,Z. Grauer,G.L., Avnir.D., and Yariv.S., J. Chem Soc., Faraday Trans.I, 83, 1685, 1987.

222. Yariv,S., Int. J. Trop., 6, 1, 1988.

223. Cenens,J., Vliers,D.S., Schoonheyot,R.A. and Schrijver,F.C.De., Proc. Int. Clay Conference, Denver, 1985 ed. Schultz,L.G., Olphen,V.H. and Mumpton,F.A. (The Clay Mineral Society, Bloomington, Indiana), p 352.

224. Cenens,J., and Schoonheyot,R.A., Clays Clay Minerals, 36, 214, 1988

225. Bromfield,S.M., Aust. J. Soil Res., 3, 31, 1965.

226. Giels,C.H., MacEwan,T.H., Nakhwa,S.N. and Smith,D., J. Chem. Soc., 3973, 1960.

227. De,D.K., Das Kanungo,J.L. and Chakravarti,S.K., J. Ind. Soc., Soil Sci., 27, 85,1979.

228. Cohen,R. and Yariv,S., J. Chem. Soc. Faraday Trans.I, 80, 1705, 1984.

229. Grauer,Z., Avnir,D. and Yariv,S., Can. J. Chem., 62, 1889, 1974.

230. Yariv,S., Nasser,A. and Baron,P., J. Chem. Soc.Faraday trans., 86, 1593, 1990.

231. Touillaux,R., Salvodor. P., Vandermeersche,C. and Fripial,J.J., Israel J. Chem., 6, 337, 1968.

232. Grauer,Z., Malter,A.B., Yariv,S. and Avnir,D., Colloids and Surfaces, 25, 41, 1987.

Canadian Journal of Chemistry / *Journal canadien de chimie*

DR. R. A. McCLELLAND, EDITOR
DEPARTMENT OF CHEMISTRY
UNIVERSITY OF TORONTO
80 ST. GEORGE STREET
TORONTO
ONTARIO M5S 1A1
FAX: 416-978-3592. E-Mail RMCCLELL@ALCHEMY.CHEM.UTORONTO.CA

Date: July 16, 1996 Control No. CHEM 96-021-M

Authors: S. Ahmed and S. K. Saha

Title: Electrochemical study of the reaction between progressivley alkylated thiazine leucodyes and Fe(III) on glassy carbon electrode

Dr. S. K. Saha
Department of Chemistry
University of Norht Bengal
Darjeeling 734430
India

Dear Dr. Saha:

The above manuscript has been accepted for publication and will appear in an early issue. Galley proofs will be sent to you for checking against the manuscript.

Yours sincerely

R.A McClelland

Robert A. McClelland

Electrochemical Study Of The Reaction Between Progressively Alkylated Thiazine Leucodyes And Fe(III) On Glassy Carbon Electrode

S. Ahmed and S. K. Saha*
Department of Chemistry
University of North Bengal
Darjeeling 734430, India

ABSTRACT

An electrochemical investigation on five progressively alkylated thiazine dyes in the presence of Fe(III) ions is reported. The theory of catalytic regeneration mechanism involving an electrode reaction followed by a coupled chemical reaction is applied to derive kinetic parameters of homogeneous reaction. The second order rate constant for the reaction of thiazine leucodyes with Fe(III) ions was found to increase from 0.25×10^4 to 1.6×10^4 $dm^3 mol^{-1} s^{-1}$ upon monomethylation and to vary from 0.7×10^4 for the dimethyl derivative to 1.4×10^4 $dm^3 mol^{-1} s^{-1}$ for the tetramethyl one. The electron donating nature as well as the hydrophobic characteristics of methyl group influence the kinetics of the homogeneous reaction.

Electrochemical Study Of The Reaction Between Progressively Alkylated Thiazine Leucodyes And Fe(III) On Glassy Carbon Electrode

S. Ahmed and S. K. Saha*
Department of Chemistry
University of North Bengal
Darjeeling 734430 , India

1. Introduction:

The most successful photogalvanic (PG) cell for solar energy conversion is the ferrous/thionine cell yet, this too is far from having ideal conversion efficiency (1,2). In this PG cell the photoreduction of thionine (Th) by Fe(II) ions produces semithionine (S) and Fe(III) ions. Semithionine rapidly disproportionates to Th and leucothionine (L).

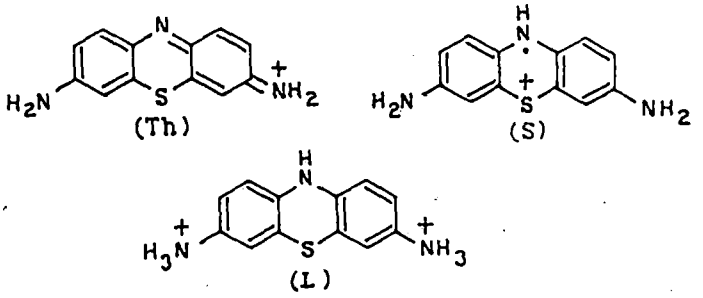

The advantage of the above system lies in achieving partial selectivity of charge carriers for appropriate electrodes. However, greatest efficiency would be obtained with a PG cell in which each electrode is perfectly selective for a different couple. Unfortunately, in homogeneous solution, thermal back reaction of electron transfer also takes place. This dissipation of free energy constitutes a considerable problem in the use of ferrous/thionine PG cell for any practical purposes (3).

The following reaction scheme adequately summarizes the whole process, including the relevant recombination reactions (pH 3) (4)

$$Th + Fe(II) + H^+ \xrightarrow{h\nu} S + Fe(III) \qquad (1)$$

$$2S + H^+ \rightleftharpoons Th + L \qquad (2)$$

Back Reaction :

$$S + Fe(III) \longrightarrow Th + Fe(II) + H^+ \qquad (3)$$

$$L + Fe(III) \longrightarrow S + Fe(II) + 2H^+ \qquad (4)$$

However, the homogeneous reaction scheme is very complicated and must be properly characterized. Solubility as well as aggregation characteristics of dyes are important criteria which control PG output. Alkyl substitution in dyes affect both these characteristics and, this prompted us to undertake some progressively alkylated thiazine dyes for a detail study on homogeneous reactions with Fe(III) ions. In view of this, an electrochemical technique has been adopted with the aid of dc voltammetry. Electrode reaction coupled with chemical reaction is an interesting subject of investigation for electrochemists (5). The electrochemical reduction of progressively alkylated thiazine dyes to corresponding leucodyes at the stationary electrode in the presence of Fe(III) ions may be described by what is called " catalytic regeneration mechanism", according to which an initial electroactive species is regenerated by the homogeneous chemical reaction. This mechanism can be represented by the following scheme (5):

$$O + ne \rightleftharpoons R \qquad \cdots \quad \cdots \quad (5)$$

$$R + Z \longrightarrow O + P \qquad \cdots \quad \cdots \quad (6)$$

If applied judiciously, this technique may yield kinetic parameters of the chemical reaction from a simple electrochemical experiment. Although thermal back reactions have been studied by flash photolysis technique in considerable detail (4, 6-8), the former technique has been applied only recently for the homogeneous reaction relevant to ferrous/thionine PG cell. Kinetic parameters were also determined using an indium doped SnO_2 electrode assuming a pseudo first order reaction condition to prevail even though the experimental result did not always conform with the theory (9). In view of the pivotal importance of the nature of the electrode surface in such a study and also to examine the role of hydrophobic interaction, if any, on the reaction kinetics, the present study has been undertaken. In this paper, we summarize the results of such an electrochemical study on the reaction between various alkyl derivatives of thiazine leucodyes with Fe(III) on a glassy carbon electrode which has been found to be well behaved in present set of systems.

2. Experimental:

Five progressively alkylated thiazine dyes viz., thionine, azure C, azure A, azure B and methylene blue which are used for the present study were supplied by Aldrich Chemical Co., U.K. All other chemicals were of analytical grade (Aldrich/B.D.H.) and used as received. The structures of the dyes are given below:

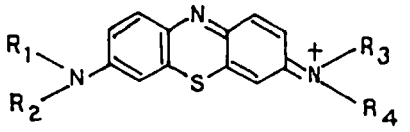

Thionine(Th): $R_1=R_2=R_3=R_4=H$

Azure C(AzC): $R_1=R_2=R_3=H$; $R_4=CH_3$

Azure A(AzA): $R_1=R_2=H$; $R_3=R_4=CH_3$

Azure B(AzB): $R_1=H$; $R_2=R_3=R_4=CH_3$

Methylene blue(MB): $R_1=R_2=R_3=R_4=CH_3$

All the dyes were found to contain coloured impurities and were purified over a chromatographic column of silica gel using chloroform-methanol mixture as eluent. Azure C was extracted efficiently with 8:2 chloroform-methanol mixture whereas, azure A was extracted with 7:3 solvent mixture. All other dyes were eluted by less polar solvent mixtures than that used for azure A. Finally, they were recrystallised and dried at 50°C under vacuum. Final purities of dye samples were checked by TLC using 8:2 water- acetic acid mixture as the mobile phase and the purities of all the dyes except AzC were found to be excellent. The commercial sample of AzC contained high percentage of insoluble materials in addition to other coloured impurities. Even after repeated chromatographic treatment, the sample gave a faint additional spot on the TLC plate indicating the presence of a small amount of impurity.

Although this dye could not be purified up to the level of other four dyes, various analyses (spectral and analytical) showed that final purity of the dye was satisfactory.

For electrochemical experiments, the supporting electrolyte was sulphuric acid. All solutions were purged with pure nitrogen before the experiment. Cyclic voltammetric experiments were carried out employing a BAS Cyclic voltammograph (CV-27, U.S.A.). The working electrode was a glassy carbon microelectrode (MF-2012, BAS, dia.3.2mm) with a platinum wire as an auxiliary electrode. Potentials were measured with respect to saturated calomel electrode. All measurements were done at constant pH of 2.0 and at room temperature of $25 \pm 1^{o}C$.

3. Results and Discussion:

A Cyclic voltammogram of azure C (5.0×10^{-5} mol.dm^{-3} in 0.1 mol.dm^{-3} H_2SO_4) is shown in fig.1a. Voltammograms of all other dyes are similar and consistent with reversible two electron transfer systems within the range of potential scan(ν) of 5-100 mv.s^{-1}. Data pertaining to the position of peak potentials and current ratios, i_{pc}/i_{pa}, for the five thiazine dyes are shown in table I. Current vs. (scan rate)$^{1/2}$ plots deviate from linearity above scan rates of 100 mv.s^{-1} (plots not shown, see table I).

The peak potentials (E_{pa} and E_{pc}) are not sensitive to scan rates and ΔE_p's do not vary up to a scan rate of 300 mvs^{-1} except for AzC. This shows that the electrode processes are very fast and the quasi-reversibility is apparent only in AzC. Previous reports available for Th and MB were, however, consistent with the present observation (9-12). Diffusion coefficient(D_0) values are determined from cyclic voltammetry measurements as 3.05×10^{-6}, 2.66×10^{-6}, 4.40×10^{-6}, 4.90×10^{-6} and $5.7\times10^{-6} cm^2 s^{-1}$ for Th, AzC, AzA, AzB and MB respectively (Determined from the slopes of i_{pc} vs. $\nu^{1/2}$ plots at slow scan rates, employing Randles - Seveik equation (5)).

Figs. 1 and 2 near here

Interestingly, the D_0 value increases regularly upon progressive alkylation of dye molecule with the only exception of AzC. On the other hand, the Fe(II)/Fe(III) system exhibits irreversible electron transfer at the GC electrode in the potential range between 0.3 - 0.6v (Fig.2). But the couple is no longer electrochemically active in presence of thiazine dyes which of course have much higher heterogeneous kinetics (k_s(Th)= $5\times10^{-3} cm.s^{-1}$, k_s(Fe)=$3.1\times10^{-5} cm.s^{-1}$ on gold foil electrode (4)).

TABLE - I

Dye	Scan rate (mvs^{-1})	E_{pa} (v)	E_{pc} (v)	ΔE_p (v)	i_{pa}/i_{pc}	$(E_{pc/2}-E_{pc})$ (v)	$i_{pc}v^{-1/2}$ ($\mu A.mv^{1/2}s^{1/2}$)	$0.058/\Delta E_p$
	5	0.225	0.195	0.030	0.870	0.025	5.93	1.93
	10	0.223	0.195	0.028	0.890	0.026	5.50	2.07
	20	0.220	0.193	0.027	0.900	0.027	5.32	2.14
Th	40	0.218	0.190	0.028	0.980	0.030	6.25	2.07
	60	0.215	0.185	0.030	0.930	0.032	6.15	1.93
	100	0.214	0.185	0.029	0.950	0.032	6.65	2.00
	200	0.210	0.182	0.028	0.970	0.033	7.72	2.07
	300	0.210	0.182	0.031	0.980	0.035	8.59	1.93
	5	0.198	0.165	0.033	0.800	0.035	5.00	1.75
	10	0.198	0.163	0.035	0.880	0.035	5.25	1.65
	20	0.196	0.160	0.036	0.800	0.037	4.96	1.61
AzC	40	0.195	0.158	0.037	0.760	0.038	5.50	1.56
	60	0.191	0.150	0.041	0.840	0.040	5.64	1.41
	100	0.185	0.145	0.040	0.830	0.042	6.33	1.45
	200	0.182	0.135	0.047	0.770	0.043	6.04	1.23
	300	0.180	0.130	0.050	0.770	0.045	7.31	1.16
	5	0.229	0.198	0.031	0.890	0.028	6.43	1.87
	10	0.226	0.195	0.031	0.880	0.028	6.25	1.87
	20	0.224	0.192	0.032	0.830	0.030	6.38	1.81
	40	0.222	0.191	0.031	0.790	0.032	6.75	1.87
AzA	60	0.220	0.188	0.032	0.730	0.035	6.97	1.81
	100	0.218	0.186	0.032	0.690	0.038	8.22	1.87
	200	0.214	0.180	0.034	0.610	0.043	8.05	1.70
	300	0.212	0.178	0.034	0.590	0.045	8.40	1.70
	5	0.300	0.270	0.030	0.870	0.028	5.54	1.93
	10	0.300	0.268	0.032	0.850	0.029	6.00	1.81
	20	0.298	0.265	0.033	0.840	0.030	6.17	1.76
AzB	40	0.297	0.262	0.035	0.840	0.035	6.93	1.66
	60	0.295	0.260	0.035	0.770	0.040	7.59	1.66
	100	0.294	0.260	0.034	0.730	0.042	8.01	1.70
	200	0.293	0.258	0.035	0.660	0.042	8.05	1.66
	300	0.293	0.257	0.036	0.580	0.045	8.04	1.61
	5	0.215	0.183	0.032	0.840	0.028	6.78	1.81
	10	0.215	0.182	0.033	0.810	0.030	6.75	1.76
	20	0.214	0.181	0.033	0.750	0.032	7.27	1.76
MB	40	0.212	0.180	0.032	0.610	0.032	7.75	1.81
	60	0.210	0.180	0.030	0.610	0.035	8.20	1.93
	100	0.205	0.175	0.030	0.630	0.036	9.01	1.93
	200	0.197	0.165	0.032	0.660	0.038	10.86	1.81
	300	0.195	0.160	0.035	0.650	0.040	10.97	1.66

On the other hand, voltammograms of thionine and its derivatives in the presence of varying amount of Fe(III) ions (5.0×10^{-5} - 1.0×10^{-3} moles dm^{-3}) show striking changes from those obtained in the absence of Fe(III) ions. The observed catalytic current results from the regeneration of dyes from the reduced leucodyes by reaction with Fe(III) ions. Representative voltammograms of AzC are shown in fig. 1b,c. Along with the catalytic regeneration of thiazine dyes in the presence of Fe(III) ions, which of course is believed to be the major process occurring in the system, some amount of semithiazines may also be present via a dismutation equilibrium (8). These semithiazines have been oxidised at the GC electrode to give the small anodic peak current at higher positive potential on the reversed scan (Fig. 1b.). Although Fe(II)/Fe(III) couple is electrochemically inactive at GC electrode in the presence of thiazine dyes, its adverse effect on the voltammograms of the latter by increasing the background current can not be ignored. To confirm that the experimental results conform to the theory of catalytically coupled reactions (EC') of the type shown in equation 5 and 6 as a major process, it is necessary to draw diagnostic plot of the current function against the potential scan rates.

Figs. 3 and 4 near here

This correlation can be seen by simply plotting $i_{pc}/\nu^{1/2}$ as a function of log ν (13). Representative diagnostic plot for AzB is shown in fig.3. In the absence of any Fe(III) ions, the plots for all the dyes are linear and parallel to the potential scan rate axis up to 100 $mv.s^{-1}$ (Fig.3a). This is expected for a diffusion controlled reversible electrode process. However, at higher scan rates the observed upward shift of the plot is indeed the manifestation of positive deviation from linear relationship of i_{pc} with $\nu^{1/2}$ (Table I) for almost all the dyes. On the other hand, in the presence of Fe(III) ions (5.0×10^{-5} - 1.0×10^{-3} $mol.dm^{-3}$), the diagnostic plots are similar for all dyes and are indicative of EC' type of coupled catalytic chemical reaction. The catalytic regeneration of dyes as a major process is particularly apparent at lower scan rates as the reaction gets sufficient time for generation of dyes from the reduced leucoforms by reaction with Fe(III) ions, consistent with the theoretical model (14,15). However, when the scan rate increases, the ratio of kinetic current in the presence of Fe(III) to the cathodic peak current in the absence of Fe(III), i_d/i_{pc}, should tend towards unity. But this situation was not attained in the present study even at a sweep rate of 300 mvs^{-1} (Fig.3). Similar results were also observed by previous workers for the intermolecular electron transfer of Cytochrome C in presence of pseudomonas Cytochrome C551 (13) and for the homogeneous reaction of leucothionine with Fe(III) (9).

Where as we failed to identify any other mechanisms of coupled chemical reactions than EC' to be operative in the present systems, exact reason of the above is not certain.

Despite the simplified approach in view of the above and the complicated back reaction in present systems, attempts have been made to derive kinetic information from the observed data. Using a working curve (Fig.14 of ref.14) of i_k/i_d vs. kinetic parameter, $(k_f/a)^{1/2}$, we have plotted the data of k_f/a (where a = nF/RT) against $1/\nu$, which should be linear under first order conditions (Fig.4). The result shows marked

Fig. 5 near here

deviation from the predicted linearity, at slower scan rates, which is consistent with loss of first order conditions. The reactant dye is not in sufficiently large excess and so is consumed to a considerable extent in the diffusion layer during the time period of a slower scan rate. Second order kinetics is probably followed and the situation is identical to one which occurred in intermolecular electron transfer of Cytrochrome C (13). Moreover, the initial slope of each curve (Fig.4) at infinite scan rates is proportional to the true pseudo-first order rate constant k_f^o,

$$k_f^o = (nF/RT)(\text{ initial slope }) .$$

Drawing tangents to the above curves at $1/\nu \rightarrow 0$ yield values of k_f^o for each experiment. An alternative method of finding k_f^o is to calculate effective pseudo-first order rate constant k_f', from each k_f/a value at a given scan rate where,

$$k_f' = (F/RT).\nu.(k_f/a) \quad \text{(Ref. 13)}$$

Plotting k_f' as a function of $1/\nu$ and extrapolating to $1/\nu \rightarrow 0$ one can evaluate the pseudo-first order rate constant, k_f^o, at infinite scan rate. This latter method seems to be more convenient and data for thionine is plotted in Fig.5. (Similar plots for all other dyes are submitted as supplementary material). The nature of the plots are again similar for all the five dyes and also similar to those observed by Hill and Walton for intermolecular electron transfer in cytochrome C (13). Finally, k_f^o values at infinite scan rates and for varying concentrations of Fe(III), are plotted against the concentrations of Fe(III) ions in order to examine the second order rate constants, k_2's for the homogeneous reaction of Fe(III) with various leucodyes.

Table II

Leucodyes	$k_2 \times 10^{-4}/dm^3 mol^{-1} s^{-1}$
Th	0.25
AzC	1.60
AzA	0.70
AzB	1.00
MB	1.40

These plots are linear indicating that the homogeneous reaction is first order with respect to Fe(III) ions and indeed the over all reaction is of second order (inset of fig.5). However, a striking feature is that unlike Th, slopes of the plots for all other dyes decrease drastically at low Fe(III) concentrations (at $C_{Fe(III)} < 2.0 \times 10^{-4}$ mol.dm^{-3} for AzC, AzA and $C_{Fe(III)} < 4.0 \times 10^{-4}$ mol.dm^{-3} for AzB, MB), resulting in the deviation of the plots from linearity. This result suggests that at low Fe(III) concentrations the actual scheme of reaction should be more complex than one shown in equation 5 and 6 and supports the hypothesis that the return of leucodyes to the corresponding thiazine dyes by Fe(III) ions occurs by two step process via the formation of semithiazine as an intermediate species. Conversion of semithiazines to the corresponding thiazine dyes may occur either by Fe(III) or through the dismutation equilibrium (as mentioned before) forming leuco dyes and the original dyes. The latter process is, however, more significant at low Fe(III) concentrations (8). Nevertheless, observed gradients of the straight lines are significant and the second order rate constants, k_2's derived from these data are depicted in Table II.

The table shows that k_2 value for thionine is 0.25×10^4 dm^{3}mol^{-1}s^{-1}, which is the lowest among all the dyes used.

Upon progressive alkylation of the dyes this value increases regularly with only exception for AzC which gives the highest value of 1.6×10^4 $dm^3 mol^{-1} s^{-1}$. Regular increase of k_2 with progressive alkylation of the dye molecule would indeed be expected from the electron donating nature of a methyl group. However, in the present systems, while the first methyl group brings about a six fold increase of the rate, the second one causes a two fold decrease and adding the third and the fourth has only a small effect (1.4 fold increase with each methyl). In fact, the leucodye with four methyl groups is oxidized more slowly than the dye with only one methyl group. It seems apparent that factors other than the electron donating effect of the methyl group are involved. Substitution of hydrogens on the nitrogen of a dye molecule by methyl groups introduces hydrophobicity in the molecule as well. It has also been shown that hydrophobic environment in presence of certain micelles delay back electron transfer in solution (4,16) while substitution with ionic or polar groups, for example disulfonated thionine, shows faster back electron transfer in PG cells (17,18). Thus, increased hydrophobicity due to alkylation of the present dyes may in turn slow down electron transfer reaction with Fe(III) ions in aqueous solution to some extent. These two mutually opposite effects of methyl group may thus be responsible for the observed variation of rates. It is also important to note in this context that the formal potential values ($E^{o'}$) for progressively

methylated dyes are 0.205, 0.175, 0.207, 0.281 and 0.196 v (average values for ν between 5-100 mVs^{-1}, Table I) respectively and the observed lowest value of $E^{o'}$ for AzC is consistent with the above results. However, one can infer from the foregoing result that, with the exception of AzC, the PG output will decrease continuously with alkyl substitution in the dye molecule. All previous reports showed that PG output for Fe(II)-MB cell is always less than that for Fe(II)-thionine cell. An earlier report of second order rate constants (measured by flash photolysis) ranged from 0.47×10^3 $dm^3 mol^{-1} s^{-1}$ to 1.0×10^3 $dm^3 mol^{-1} s^{-1}$ for various modified thiazine dyes (7). Ferreira and Harriman report a value of 9.0×10^4 $dm^3 mol^{-1} s^{-1}$ for Fe(III)-thionine system by a similar flash photolysis technique (8). On the other hand, with the help of an electrochemical method similar to one applied in the present study, Murthy and Srivastava estimated the value as $4.0 \times 10^5 dm^3 mol^{-1} s^{-1}$ for the reaction between Fe(III) ions and leucothionine (9). While a close comparison between data reported by different methods and under different conditions is not always valid, the general trend of the present result is satisfactory and specially the observed variation of k_2 due to progressive alkylation of dye molecule demonstrates the usefulness of a comparatively simpler electrochemical technique adopted here in the present investigation.

Acknowledgement: One of the authors (S.A.) wishes to thank the U.G.C., New Delhi for awarding a teacher fellowship.

4. References:

1. W.J.Albery. "Photovoltaic and Photoelectrochemical Solar Energy Conversion". Ed. by F.Cardon, W.P.Gomesand, and W.Dekeyser. Plenum Press, N.Y.(1981), p.313
2. S.Lodha, S.Khamesra, B.Sharma, and S.C.Ameta. Int.J.Energy Res. **15**, 431 (1991)
3. W.J.Albery, and A.W.Foulds. J.Photochem. **10**, 41 (1979)
4. E.J.J.Groenen, M.S.de Groot, R.de Ruiter, and N.de Wit. J.Phys.Chem. **88**, 1449 (1984)
5. A.J.Bard, and L.R.Faulkner. "Electrochemical Methods- Fundamentals and Applications". John Wiley & Sons, N.Y.(1980), p.429
6. J.C.M.Brokken-Zijp, and M.S.de Groot. Chem.Phys.Lett. **76**, 1 (1980)
7. D.W.Hay, S.A.Martin, S.Ray, and N.N.Lichtin. J.Phys.Chem. **85**, 1474 (1981)
8. M.I.C.Ferreira, and A.Harriman. J.Chem.Soc.,Faraday Trans.I **173**, 1085 (1977)
9. A.S.N.Murthy, and T.Srivastava. J.Chem.Soc.,Faraday Trans. **86**, 105 (1990)
10. T.I.Quickenden, and I.R.Harrison. J.Electrochem.Soc. **132**, 81 (1985)
11. P.Joo. Colloids and Surf. **49**, 29 (1990)
12. J.M.Bauldreay, and M.D.Archer. Electrochim.Acta. **28**, 1515 (1983)
13. H.A.O.Hill, and N.J.Walton. J.Am.Chem.Soc. **104**, 6515 (1982)

14. R.S.Nicholson, and I.Shain. Anal.Chem. 36, 706 (1964)

15. L.Nadjo, and J.M.Save'ant. J.Electroanal.Chem. 48, 113 (1973)

16. M.Gratzel. Proc.Int.Conf.Photochem.Convers.Storage Sol.Energy. 3rd 1980, 131 (1981)

17. W.J.Albery, P.N.Bartlett, J.P.Davies, A.W.Foulds, A.R.Hillman, and F.A.Souto-Bachiller. Faraday Discuss.Chem.Soc. 70, 341 (1980)

18. W.J.Albery, P.N.Bartlett, A.W.Foulds, F.A.Souto-Bachiller, and R.Whiteside. J.Chem.Soc. Perkin Trans. 2, 794 (1981)

Legends to figures

Fig.1. Cyclic voltammograms of AzC (5×10^{-5} mol.dm^{-3}) in presence of various concentrations of Fe^{3+}: (a) 0, (b) 8×10^{-4} (c) 1.5×10^{-3} mol.dm^{-3}. Supporting electrolyte: 0.1 mol.dm^{-3} H_2SO_4.

Fig.2. Cyclic voltammograms of $FeCl_3$ (in presence of 0.1 mol.dm^{-3} H_2SO_4) at GC electrode. Concentration of Fe(III): (1) 2×10^{-4}, (2) 4×10^{-4}, (3) 6×10^{-4}, (4) 8×10^{-4} mol.dm^{-3}. Scan rate: 5 mV.s^{-1}.

Fig.3. Diagnostic plots of current functions $i_{pc}/\nu^{1/2}$ vs. log ν for AzB (5×10^{-5}mol.dm^{-3} in 0.1 mol.dm^{-3} H_2SO_4) at various concentrations of Fe^{3+}: (a) 0, (b) 2×10^{-4}, (c) 4×10^{-4}, (d) 6×10^{-4}, (e) 8×10^{-4}, (f) 1×10^{-3} mol.dm^{-3}.

Fig.4. Plots of kinetic parameter , k_f/a, against $1/\nu$ for AzB-Fe(III) system at various concentrations of Fe^{3+}: (a) 2×10^{-4}, (b) 4×10^{-4}, (c) 6×10^{-4}, (d) 8×10^{-4}, (e) 1×10^{-3}mol.dm^{-3} (in presence of 0.1 mol.dm^{-3} H_2SO_4)

Fig.5. Effective pseudo-first order rate constant, k_f', as a function of reciprocal scan rate extrapolated to $1/\nu \rightarrow 0$, for experiment with Th-Fe(III) system: (1) 2×10^{-4}, (2) 4×10^{-4}, (3) 6×10^{-4}, (4) 8×10^{-4}, (5) 1×10^{-3}mol.dm^{-3} Fe^{3+} (in presence of 0.1 mol.dm^{-3} H_2SO_4)(Lower fig.). Pseudo-first order rate constant, k_f^0, as a function of the concentrations of Fe^{3+} with the same system (Upper fig.).

Headings of table

Table I : Electrochemical data from cyclic voltammetry of thiazine dyes (5×10^{-5} mol.dm^{-3} in 0.1 mol.dm^{-3} H_2SO_4)

Table II : Second order rate constant of the homogeneous reaction between thiazine dyes and Fe^{3+} ions.

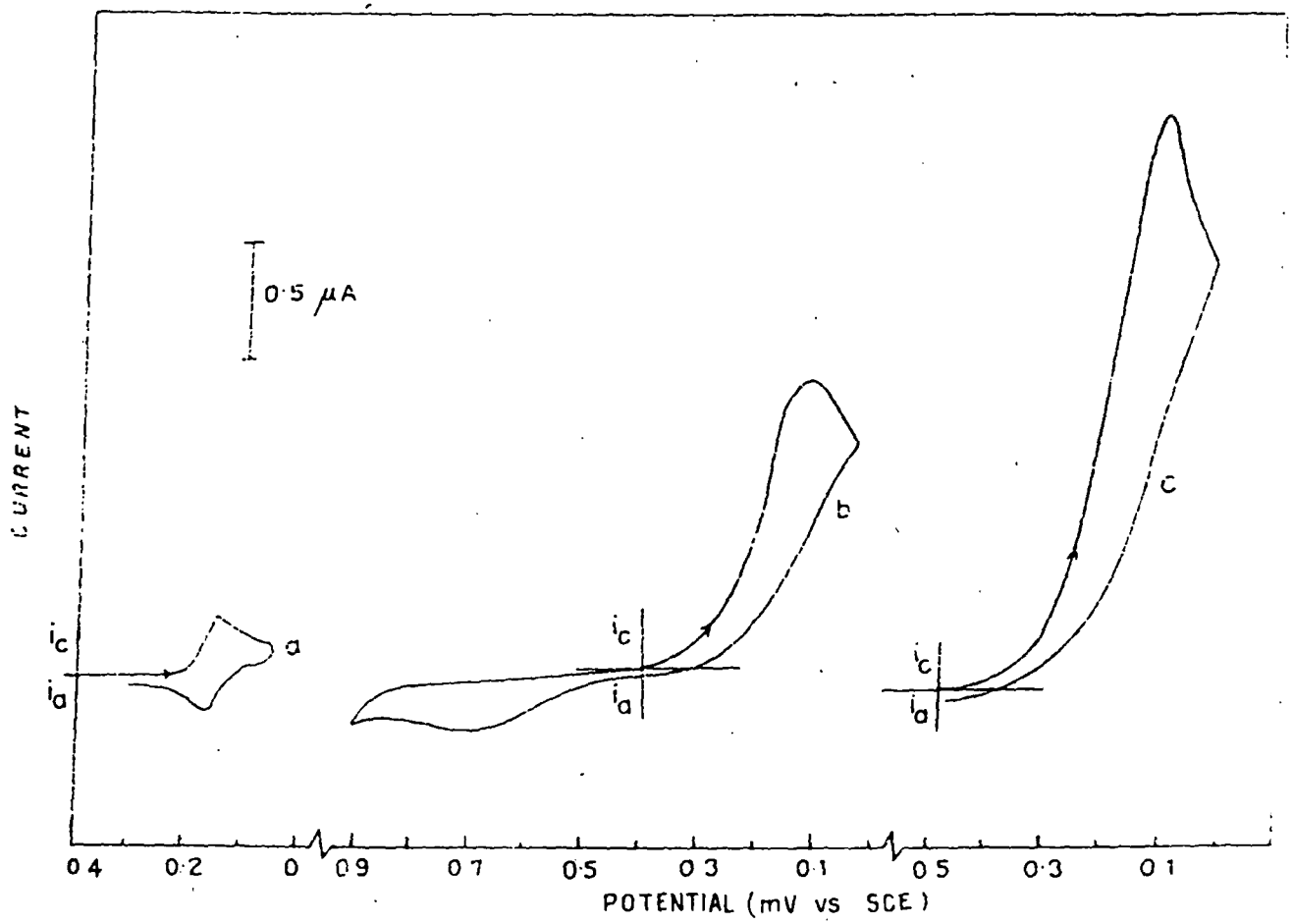
0·5 μA
CURRENT
a
b
c
i_c
i_a
0·4
0·2
0
0·9
0·7
0·5
0·3
0·1
0·5
0·3
0·1
POTENTIAL (mV vs SCE)

Fig 1

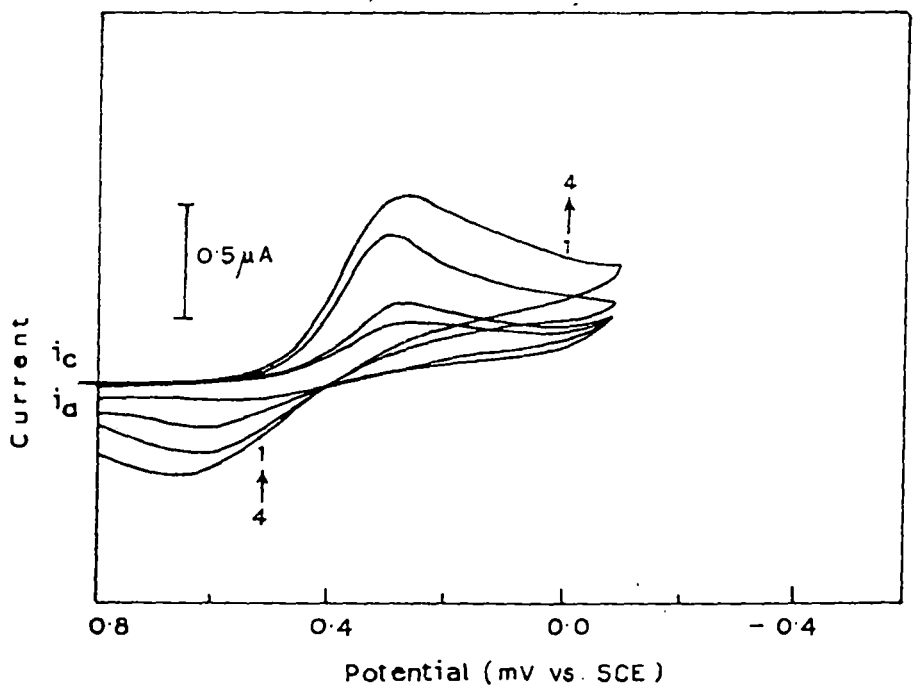

Fig. 2.

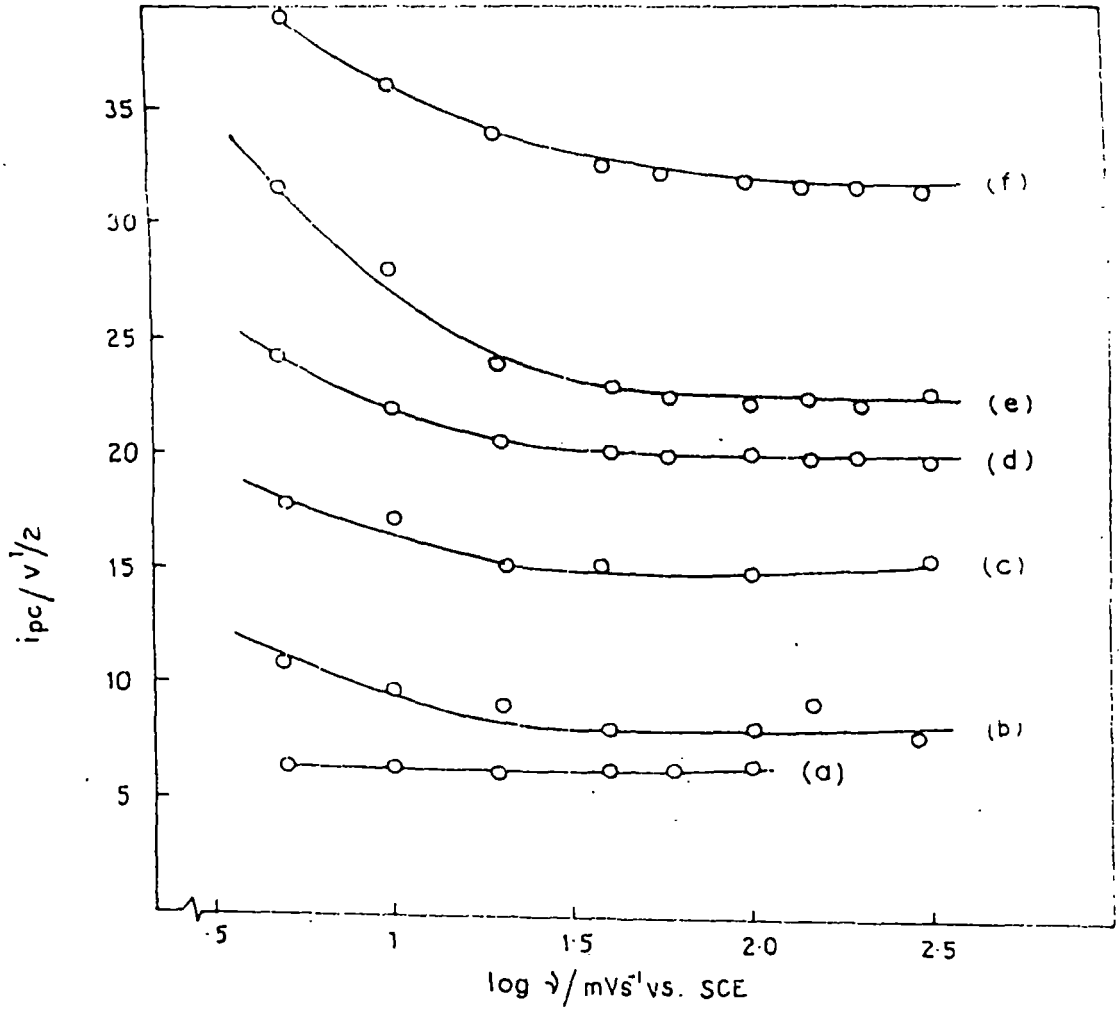

Fig . 3 .

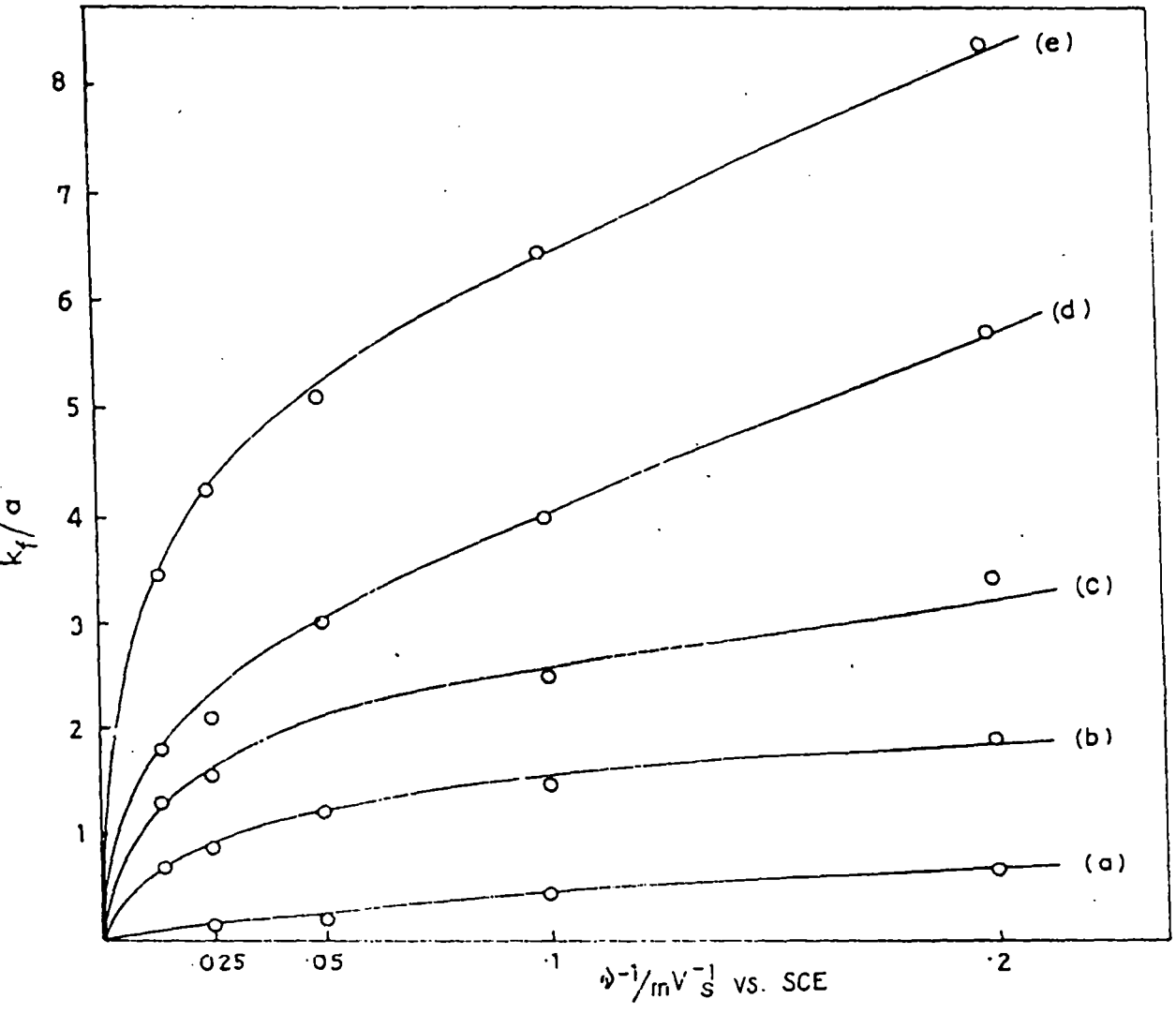

Fig.4.

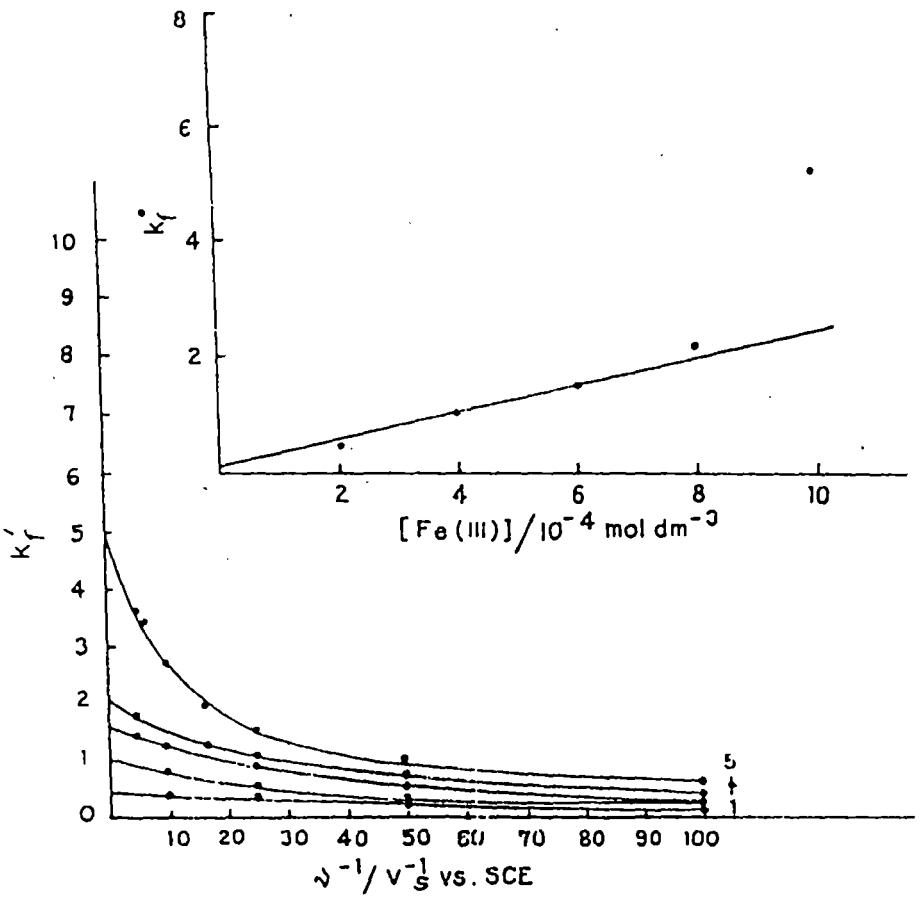
8
6
4
2
k_f^*
2
4
6
8
10
[Fe(III)]/10^{-4} mol dm^{-3}
10
9
8
7
6
5
4
3
2
1
0
k_f'
10 20 30 40 50 60 70 80 90 100
ν^{-1}/ V_S^{-1} vs. SCE
5
4
1

Fig. 5.